

TECHNISCHE UNIVERSITÄT MÜNCHEN

Lehrstuhl für Verfahrenstechnik disperser Systeme

Physical mechanisms involved in the transport of slugs  
during horizontal pneumatic conveying

Isabelle J. M. Lecreps

Vollständiger Abdruck der von der Fakultät Wissenschaftszentrum Weihenstephan für Ernährung, Landnutzung und Umwelt der Technischen Universität München zur Erlangung des akademischen Grades eines

Doktor–Ingenieurs

genehmigten Dissertation.

Vorsitzender: Univ.-Prof. Dr. U. M. Kulozik

Prüfer der Dissertation:

1. Univ.-Prof. Dr. K. Sommer (i.R.)
2. Univ.-Prof. Dr. K.-E. Wirth,  
Friedrich-Alexander-Universität Erlangen-Nürnberg
3. Univ.-Prof. Dr. H.-Chr. Langowski

Die Dissertation wurde am 16.05.2011 bei der Technischen Universität München eingereicht und durch die Fakultät Wissenschaftszentrum Weihenstephan für Ernährung, Landnutzung und Umwelt am 10.06.2011 angenommen.

*To my grand-mother Mauricette,  
for she is the only one  
who has always believed in me.*

-

*À ma grand-mère Mauricette,  
la seule qui m'ait toujours soutenu  
et ait cru en moi.*

Wer nicht fragt, bleibt dumm.

Norbert Zierer, 13 June 2009

-

Don't ever let someone tell you, you can't do something.

Not even me.

You got a dream, you got to protect it.

People can't do something themselves, they want to tell you you can't do it.

You want something, go get it. Period. All right?

From the film "The Pursuit of HappyNess", 2006

---

## Acknowledgements

For anyone who holds the final edition of their doctoral thesis in their hand for the very first time, they know that this is not only an achievement of their own. Much more than just a scientific and professional accomplishment, this is the result of many years of intellectual and personal development in which not only the supervisor and work colleagues but also friends and family have been largely involved. Now has come the point where I would like to thank all those who helped me achieve this work.

First of all, I would like to express my sincere thanks and warm gratitude to Univ.-Prof. Dr.-Ing. Karl Sommer. During the five years spent at the Lehrstuhl fuer Verfahrenstechnik disperser Systeme, he passed to me not only his passion for bulk solids technology and part of his valuable knowledge but also his rational way of thinking. The freedom he gave to me in my work and his way of valuing my ideas were the best encouragement one can have. He carried his title of “Doktorvater” (doctor’s father) for wellfounded reasons, always using the right words at the right time. However, I am happy he is no longer my boss. Now, I can call him a friend. I also wish to express my gratitude to both Univ.-Prof. Karl-Ernst Wirth and Univ.-Prof. Dr.-Ing. Langowski, whose opinions I value, for accepting to be examiners of my thesis. Finally, I would like to give thanks to Univ.-Prof. Dr.-Ing. Kulozik for taking the chair of the PhD examination.

The work presented in this thesis required a large amount of construction and experimental work. Without the kind help and exceptional efficiency of the workshop members, none of this would have been possible. I would like to thank in particular Peter Rauscher, Hans Wagner, Alfons Seitzl and Sebastian Rieger. They made the impossible become possible. Thank you also for teaching me a fourth useful language, which is Bavarian.

I would like to give my sincere thanks to Daniela Herold-Loibl who was the first one to welcome me warmly in the team. We had a great time sharing the “Damen-Buero” (ladies’ office). Also, I would like to thank Markus Hertel, Hans Scheuren and Johannes Tippmann for their ongoing support. You showed me that even if living in Bavaria can be very tough for a young French woman, some Bavarians have a very big heart. Thank you for always having an open ear, warm hugs and loving words for me, not forgetting the jokes and beers I probably refused over five hundred times.

My special thanks go to Helga Vogt who always ensured that everything went smoothly for me, whether I knew it or not. I also want to give many thanks to my predecessor Gerhard Niederreiter, who left me everything I needed to begin with my research, from well-organised documents to sound scientific principles as well as valuable contacts.

This report would not have existed in its current form without the prodigious help of all students who were involved in this research work. My deep gratitude goes in particular to Christine Haider, Stephan Speicher, Tolga Erden and Kai Wolz. I am so glad I had the chance to work with you. You did an extraordinary job and were the best team one can wish, both from a personal and professional point of view. I am very proud you all became respected engineers and my friends at the same time.

On no account would I forget to mention Malte Paes, Elsa Schreyer and Norbert Zierer. Merci for the good atmosphere created by your presence, for putting a smile on my face and giving to me motivation at all times.

I send my deep gratitude to Prof. Mark Jones who gave me the opportunity to both finalise my thesis and carry out further research in the area of pneumatic conveying as a member of his team. It makes me very proud. I would also like to express my gratitude to my new colleagues Ken Williams, Craig Wheeler and Tobias Krull for their support and help in correcting some important parts of my thesis. I would never have thought that so much kindness and competency could be combined within the same team.

I am grateful to all members of the bulk solids community I had the chance to meet during conferences for the interest, encouragements and kindness they provided me with. My most special acknowledgments go to Thomas Ittershagen, Sven Bensman, Harald Wilms, Marcel Droettboom, Ken Williams and Prof. Mark Jones.

As this section is coming to an end, I would like to deeply thank Anne-Claire Peroys, Mathilde Belin, Olivier Vandevair and Nicolas Le Brun for their support throughout my life and simply for making me become who I am. Je remercie également de tout cœur ma grand-mère Mauricette, la seule qui m'ait toujours soutenu et qui ait cru en moi. Ce mémoire n'existerait pas sans elle.

Finally, my last and most important thank you goes to my best colleague, best friend and fantastic husband Jan-Dirk for taking exceptional care of me, giving me so much energy and making everything always feel so easy.

---

## Kurzfassung

Bei der Dichtstromförderung wird der Feststoff bei geringem Fördergasbedarf und hoher Gutbeladung schonend transportiert. Um den hohen Druckverlust in der Leitung sowie das Verstopfen von Förderleitungen bei der Pfropfenförderung erklären zu können, wurden Untersuchungen an horizontal pneumatisch geförderten Schüttgutpfropfen durchgeführt. Die Ergebnisse liefern Informationen über die Geschwindigkeit, die Porositätsverteilung und die wirkenden Kräfte und ermöglichen damit Rückschlüsse auf die Pfropfenbildung sowie die Pfropfenstabilität. Die bisherigen theoretischen Modelle wurden ausführlich diskutiert und verglichen. Basierend auf den neu gewonnenen Kenntnissen konnte ein neuer theoretischer Ansatz entwickelt werden, der eine realitätsnahe Vorausberechnung des Druckverlustes ermöglicht.

## Abstract

In dense phase pneumatic conveying, only relatively small amounts of gas are used to transport large volumes of material. Because the complex physical mechanisms involved in the transport of high particle concentrations in a gas phase have still not been fully understood, the design of low velocity pneumatic conveying systems still remains a problem. This work focuses on the identification and description of the main physical mechanisms involved in horizontal slug flow pneumatic conveying. In particular, experimental investigations were carried out on slugs of granular material with respect to velocity, pressure profile, porosity and internal stress states. The results obtained lead to better comprehension of slug formation and stability. Besides, existing models for the prediction of the pressure loss in slug flow pneumatic conveying are reviewed and compared. Based on both experimental results and theoretical investigations, a new approach based on kinetic theory is proposed to predict the pressure loss and allow more reliable design of slug flow pneumatic conveying systems.

# Contents

<b>List of Symbols</b>	<b>11</b>
<b>1. Introduction</b>	<b>17</b>
<b>2. State of the art</b>	<b>21</b>
2.1. General definitions of pneumatic conveying . . . . .	21
2.1.1. Classification of pneumatic conveying . . . . .	21
2.1.2. State-diagram and types of flow . . . . .	21
2.1.3. Variations in pneumatic conveying terminology . . . . .	24
2.2. Factors influencing the conveying process . . . . .	25
2.2.1. Material properties . . . . .	25
2.2.2. Dimensional analysis . . . . .	26
2.2.2.1. Single phase flow: gas . . . . .	27
2.2.2.2. Two-phase-flow: particles and gas (dilute phase conveying) . . . . .	30
2.3. Different approaches to predict pressure loss and flow type in horizontal straight pipes . . . . .	32
2.3.1. Experimental determination of a particle friction factor . . . . .	32
2.3.2. Fluid flow through packed beds . . . . .	36
2.3.3. Bulk solids mechanics . . . . .	38
2.3.3.1. The Janssen theory . . . . .	38
2.3.3.2. In-plane stress analysis of cohesionless bulk materials . . . . .	39
2.3.4. State-diagram predictive approach of stable strand flow . . . . .	44
2.3.5. Numerical analysis to simulate dense-phase flow . . . . .	47
2.4. Thirty five years of research to understand slug flow . . . . .	48
2.4.1. Flow observation . . . . .	49
2.4.2. Particle, slug and gas velocity . . . . .	50
2.4.3. Slug length . . . . .	50
2.4.4. Prediction of the shape of the gas-particle interface . . . . .	51
2.4.5. Saltation, pick-up and optimal operating velocity . . . . .	51
2.4.6. Porosity distribution / Permeation through a slug . . . . .	52
2.4.7. Cross-sectional pressure profile, stress states and stress transmission coefficient . . . . .	53
<b>3. Relevant models to predict the pressure loss in horizontal slug flow pneumatic conveying</b>	<b>55</b>
3.1. Muschelknautz and Krambrock, 1969 . . . . .	55
3.2. Konrad, 1980 . . . . .	56
3.2.1. The Ergun packed bed model: mean particle velocity determination . . . . .	56
3.2.2. Bulk solids mechanics: pressure loss over a horizontal slug . . . . .	57
3.2.3. Application of a gas/liquid analogy to estimate the fraction $\alpha$ . . . . .	61
3.2.4. Overall pressure drop in a horizontal pipeline . . . . .	61

3.2.5. Limitations of the model . . . . .	62
3.3. Mi, 1994 . . . . .	63
3.4. Pan, 1995 . . . . .	66
3.5. Yi, 2001 . . . . .	68
3.6. Comparison and discussion of the models . . . . .	72
<b>4. Material and methods</b>	<b>85</b>
4.1. Test material . . . . .	85
4.2. Conveying rig . . . . .	85
4.3. Control of air supply . . . . .	87
4.4. Determination of slug velocity . . . . .	87
4.5. Measurement probe for the simultaneous detection of pressure, radial and wall shear stress	89
4.5.1. General description and measurement principle of the probe . . . . .	89
4.5.2. Investigations on the raw force signals and optimisation of measurement quality .	90
4.5.2.1. Determination of the natural frequency of the system . . . . .	91
4.5.2.2. Nyquist-frequency . . . . .	92
4.5.2.3. Determination of the optimal measurement frequency . . . . .	93
4.5.2.4. Is the force measurement plate suitable to detect impacts of single particles? . . . . .	97
4.5.3. Signal processing using LabVIEW . . . . .	100
4.5.4. Calibration of the force sensors . . . . .	100
4.5.4.1. Signal scaling . . . . .	101
4.5.4.2. Application of a Bessel low-pass filter . . . . .	102
4.5.4.3. Correction of electric discharge of the piezoelements . . . . .	104
4.5.4.4. Correction of pressure dependence of the force sensors . . . . .	105
4.5.4.5. Correction of interdependence between both sensors . . . . .	106
4.5.4.6. Influence of sampling frequency on the signal correction process . . . .	107
4.5.5. Determination of the slug porosity . . . . .	109
4.5.5.1. Calculation of the slug porosity by applying the Ergun equation . . . .	109
4.5.5.2. Determination of slug porosity using a slug-catcher . . . . .	115
<b>5. Results and Discussion</b>	<b>119</b>
5.1. General description of slug flow pneumatic conveying . . . . .	119
5.1.1. Pressure loss along the conveying pipeline . . . . .	119
5.1.2. Effect of the air velocity increase on slug flow characteristics . . . . .	121
5.1.3. Correlation between cross-section fraction $\alpha$ covered by settled particles and slug velocity . . . . .	124
5.1.4. General description of pressure, radial and wall shear stress induced by slugs . . .	128
5.2. Porosity within single slugs . . . . .	129
5.2.1. Porosity according to Ergun . . . . .	130
5.2.1.1. Porosity trend over moving slugs . . . . .	130



5.2.1.2.	Effect of the air supply velocity on slug porosity . . . . .	131
5.2.2.	Direct determination using a slug-catcher . . . . .	132
5.3.	Radial and wall shear stress during the transport of slugs . . . . .	134
5.3.1.	Stresses according to the circumferential pipe location . . . . .	134
5.3.1.1.	Stresses induced by slugs at the pipe bottom . . . . .	134
5.3.1.2.	Stresses induced by slugs at the side of the pipe . . . . .	136
5.3.1.3.	Stresses induced by slugs at the top of the pipe . . . . .	138
5.3.2.	Effect of the air supply velocity on the stresses induced by slugs . . . . .	139
5.3.3.	Discussion of the stresses induced by slugs during pneumatic conveying . . . . .	141
5.3.3.1.	Summary of the stresses measured during horizontal slug flow pneumatic conveying . . . . .	141
5.3.3.2.	Stresses induced at the pipe wall by pushing of a model-slug through the pipeline . . . . .	144
5.3.3.3.	Comparison between stresses induced by compressed moving slugs and slugs pneumatically conveyed . . . . .	146
5.4.	Application of the kinetic theory to explain the stresses induced by slugs . . . . .	147
5.4.1.	Mathematical model . . . . .	147
5.4.2.	Investigations on the velocity gradient . . . . .	148
5.4.3.	Application of the impulse theory to describe the stresses induced by slugs . . . . .	150
5.4.4.	Application of the kinetic theory to predict the pressure loss . . . . .	155
5.4.4.1.	Correlation between wall shear stress and pressure loss along a single slug . . . . .	155
5.4.4.2.	Prediction of the pressure loss over the conveying pipeline . . . . .	159
5.5.	Correlation between pressure, stresses, porosity and particle velocity . . . . .	163
5.5.1.	Investigation on single slugs in stable state . . . . .	163
5.5.1.1.	Slug 1: $v_f = 6.8$ m/s - Measurement position of the forces: pipe side	164
5.5.1.2.	Slug 2: $v_f = 6.8$ m/s - Measurement position of the forces: pipe top	165
5.5.1.3.	Slug 3: $v_f = 6.8$ m/s - Measurement position of the forces: pipe top	167
5.5.1.4.	Slug 4: $v_f = 8.5$ m/s - Measurement position of the forces: pipe side	169
5.5.2.	Investigation on a single slug that remained temporary blocked in the pipeline . . . . .	172
5.6.	The Bernoulli principle: part of the slug transport mechanism? . . . . .	175
5.6.1.	Presentation of Bernoulli's principle and application on slug flow pneumatic conveying . . . . .	175
5.6.2.	Calculation of the lifting force resulting from the Bernoulli principle . . . . .	177
5.6.2.1.	Specifications and assumptions for the parameters necessary to calculate the lifting force . . . . .	177
5.6.2.2.	Calculation of the percentage of lifted particles . . . . .	179
<b>6.</b>	<b>Conclusion</b>	<b>182</b>
<b>7.</b>	<b>Outlook</b>	<b>190</b>

---

<b>References</b>	<b>192</b>
<b>List of Figures</b>	<b>201</b>
<b>List of Tables</b>	<b>206</b>
<b>A. Annex</b>	<b>207</b>
A.1. Technical drawings of the slug-catcher . . . . .	207
A.2. Mathcad® calculation programs . . . . .	215

## List of Symbols

### Latin

$a$	Coefficient [-]
$a_f$	Part of the gas mass flow rate flowing through the layer of particles [-]
$A$	Pipe cross-section [m <sup>2</sup> ]
$A_1, A_2$	Points of intersection between wall yield locus and Mohr's circle
$A_{layer}$	Surface of the layer of particles [m <sup>2</sup> ]
$A_m$	Lateral surface of the pipe section on which the wall shear stress acts [m <sup>2</sup> ]
$A_{m\_total}$	Lateral surface of the pipe section considered [m <sup>2</sup> ]
$A_{plate}$	Surface of the stress measurement plate [m <sup>2</sup> ]
$A_{plate\_projection}$	Projection surface of the stress measurement plate [m <sup>2</sup> ]
$A_{sensor\_surface}$	Measurement surface of a force sensor [mm <sup>2</sup> ]
$A_{st}$	Cross-section area covered by a layer of particles [m <sup>2</sup> ]
$b$	Time constant [s]
$B_1, B_2$	Points of intersection between the wall yield locus and the biggest Mohr circle
$c$	Interparticle cohesion [-]
$c_k$	Coefficient in the model of Mi [-]
$c_1, c_2, c_3$	Coefficients in the model of Ergun [-]
$c_w$	Particle-wall cohesion [-]
$C$	Theoretical limiting state of stress at failure in the Mohr circle representation [-]
$d_{eq}$	Equivalent spherical diameter of a particle [m]
$d_p$	Particle diameter [m]
$d_{plate}$	Diameter of the stress measurement plate [m]
$D$	Pipe internal diameter [m]
$e$	Coefficient [-]
$Eu$	Euler number [-]
$f_g$	Cutoff frequency [Hz]
$f_N$	Natural frequency of a system [Hz]
$f_{Nyquist}$	Nyquist-frequency [Hz]
$f_r$	Friction factor in the frictional term of the Muschelknautz equation [-]
$f_s$	Particle-particle friction factor [-]
$f_{sampling}$	Sampling frequency [Hz]
$F$	Area of a quadratic profile [m <sup>2</sup> ]
$F_{axial}$	Axial force [N]
$F_{driving}$	Driving force due to the pressure [N]
$F_{friction\_lateral}$	Friction force due to the lateral stress [N]
$F_{friction\_weight}$	Friction force due to the weight of the slug [N]
$F_i, F_n$	Force value delivered by the force sensors at the time $i, n$ [N]
$F_{lift}$	Lifting force [N]

$F_{n,corrected}$	Actual force acting on the force measurement plate at the time n [N]
$F_{radial}$	Radial force [N]
$F_{retarding}$	Retarding force for the slug movement [N]
$F_R$	Friction force due to the weight of material [N]
$F_{total}$	Total resistance force against the slug movement [N]
$F_T$	Gas drag force [N]
$Fr$	Froude number for the gas [-]
$Fr_s$	Particle Froude number [-]
$Fr_i$	Friction number [-]
$g$	Gravitational acceleration [ $m/s^2$ ]
$h$	Filling height of the material in the Janssen model [m]
$H$	Height of the free cross-section over the stationary layer [m]
$I$	Impulse number on the measurement plate [1/s]
$k$	Constant in the model of Blake [-]
$k_0$	Constant in the model of Kozeny [-]
$k_1$	Constant in the model of Burke and Plummer [-]
$k_2$	Slope of the linear correlation of $M_i$ for the slug velocity [-]
$k_s$	Coefficient in the $M_i$ model for slug velocity [-]
$K$	Stress transmission coefficient as defined by Janssen [-]
$K_s$	Damping coefficient [Hz]
$K_w$	Stress transmission coefficient [-]
$K_w_{active/passive}$	Stress transmission coefficient for active, passive stress case [-]
$K_D$	Permeability of the porous medium in the Darcy equation [ $m^2$ ]
$l$	Length of a slug element [m]
$l_h$	Horizontal length of pipeline [m]
$l_v$	Vertical length of pipeline [m]
$l_w$	Width of the upper surface of the stationary layer of particles [m]
$L$	Pipe length [m]
$L_{bed}$	Depth or length of a bed of particles [m]
$L_e$	Length of the path taken by a fluid in traversing a given bed depth in the Kozeny's equation [m]
$L_{ex}$	Length of moving material associated to a plug [m]
$L_p$	Plug length [m]
$L_s$	Length of a single slug [m]
$L_{slug}$	Total length of slugs [m]
$L_T$	Total length of pipe [m]
$m$	Factor replacing $\varepsilon/S_p$ in the Kozeny model [-]
$m_{cal}$	Mass used for the calibration of the stress measurement probe [kg]
$\dot{m}_f$	Gas mass flow rate [kg/s]
$m_{particle}$	Mass of a single particle [kg]

$m_{particles}$	Mass of particles that can be lifted by the Bernoulli force [kg]
$m_{particles\_max}$	Mass of particles contained in a pipe section of defined length [kg]
$m_s$	Mass of particles in a slug [kg]
$\dot{m}_s$	Solids mass flow rate [kg/m <sup>3</sup> ]
$M_0, M_1, M_2$	Centres of Mohr's circles
$M_{air}$	Molar mass of the air [g/mol]
$N$	Particle number density [/m <sup>3</sup> ]
$N_p$	Number of particles in contact with the measurement plate [-]
$p$	Vertical pressure of the material in the model of Janssen [Pa]
$p_{atm}$	Atmospheric pressure [Pa]
$p_{dyn}$	Dynamic pressure [Pa]
$p_m$	Amount of momentum [kg.m/s]
$p_s$	Horizontal pressure of the material in the model of Janssen [Pa]
$p_{s,max}$	Maximum wall pressure in the model of Janssen [Pa]
$P$	Pressure [Pa]
$P_f$	Gas pressure [Pa]
$P_{inlet}$	Pressure at the pipe inlet [Pa]
$P_n$	Pressure at location n [Pa]
$P_{outlet}$	Pressure at the pipe outlet [Pa]
$P_s$	Normal pressure at the wall due to hydrostatic pressure [Pa]
$P_{stat}$	Static pressure [Pa]
$P_{total}$	Total pressure [Pa]
$P_{st\_dyn}$	Dynamic pressure in the strand [Pa]
$P_{st\_stat}$	Static pressure in the strand [Pa]
$P_{su\_dyn}$	Dynamic pressure in the suspension [Pa]
$P_{su\_stat}$	Static pressure in the suspension [Pa]
$P_N$	Standard condition of pressure [Pa]
$r$	Pipe radius [m]
$r_b$	Bend radius [m]
$r_{eq}$	Equivalent spherical radius of a particle [m]
$R$	Friction force between strand and stationary layer [N]
$R_a$	Gas constant [J/K.mol]
$R_p$	Radius of pipe as defined in Fig. 3.2 [°]
$Re$	Reynolds number [-]
$s$	Side of the quadratic cell profile used by Janssen [m]
$S$	Shear stress between suspension and strand [Pa]
$S_p$	Area of particle surface per unit volume of packed bed [1/cm]
$t$	Time [s]
$T_0$	Temperature [K]
$T_g$	Period of oscillation [s]

$T_N$	Standard condition of temperature [K]
$u$	Circumference of the cell in the model of Janssen [m]
$v_{back}$	Velocity at the back of a slug [m/s]
$v_f$	Superficial gas velocity [m/s]
$v_{f_i}$	Gas velocity at location $i$ [m/s]
$v_{f\_atm}$	Superficial gas velocity in atmospherical conditions [m/s]
$v_{f\_min}$	Minimum gas velocity for horizontal flow [m/s]
$v_{f\_st}$	Gas velocity in the strand [m/s]
$v_{f\_su}$	Gas velocity in the suspension [m/s]
$v_{fm}$	Mean gas velocity [m/s]
$v_{front}$	Velocity at the front of a slug [m/s]
$v_{inst}$	Interstitial gas velocity [m/s]
$v_{normal}$	Particle velocity normal to the wall [m/s]
$v_p$	Particle velocity in axial direction [m/s]
$\bar{v}_p$	Mean particle velocity in axial direction [m/s]
$\bar{v}_{p\_int}$	Interstitial mean particle velocity [m/s]
$v_{p_i(333)}$	Particle velocity measured at point $i$ [m/s]
$v_{rel}$	Slip velocity between gas and particles [m/s]
$v_{rel_i}$	Slip velocity between gas and particles at point $i$ [m/s]
$v_{rel\_int}$	Interstitial slip velocity [m/s]
$v_s$	Solids velocity [m/s]
$v_{s\_int}$	Interstitial solids velocity [m/s]
$v_{slug}$	Slug velocity [m/s]
$v_{st}$	Strand velocity [m/s]
$v_{su}$	Suspension velocity [m/s]
$\dot{V}_{atm}$	Gas volume flow rate in atmospherical condition of pressure [m <sup>3</sup> /s]
$\dot{V}_f$	Gas volume flow rate [m <sup>3</sup> /s]
$\dot{V}_{f\_Ergun}$	Gas volume flow rate through an ideal packed columns [m <sup>3</sup> /s]
$V_p$	Equivalent spherical volume of a particle [m <sup>3</sup> ]
$V_{p_{total}}$	Volume over the plate corresponding to one layer of particles [m <sup>3</sup> ]
$\dot{V}_N$	Gas volume flow rate for standard conditions of temperature and pressure [m <sup>3</sup> /s]
$w_s$	Sedimentation velocity [m/s]
$x$	Axial coordinate
$\bar{x}$	Summary statistic in the Rumpf model [-]
$y$	Radial coordinate

## Greek

$\alpha$	Fraction of the pipe area covered by the stationary layer [-]
$\alpha_p$	Pipeline angle to the horizontal axis [ $^\circ$ ]
$\beta$	Friction coefficient in the Muschelknautz model [-]
$\gamma$	Specific weight of the material in Janssen's model [ $\text{kg}/\text{m}^2 \cdot \text{s}^2$ ]
$\gamma_b$	Specific weight of the material [ $\text{N}/\text{m}^3$ ]
$\gamma_s$	Friction coefficient in the model of Segler [-]
$\varepsilon$	Porosity [-]
$\varepsilon_{bulk}$	Bulk porosity [-]
$\varepsilon_i$	Porosity at point i [-]
$\varepsilon_{st}$	Strand porosity [-]
$\zeta$	Damping ratio [-]
$\eta$	Velocity ratio [-]
$\eta_f$	Dynamic viscosity of the gas [ $\text{Pa} \cdot \text{s}$ ]
$\eta_{fi}$	Dynamic viscosity of the gas at point i [ $\text{Pa} \cdot \text{s}$ ]
$\eta_{slug}$	Viscosity of a slug [ $\text{Pa} \cdot \text{s}$ ]
$\theta$	Angle as defined in Fig. 3.2 [ $^\circ$ ]
$\lambda$	Mean free path [m]
$\lambda_f$	Friction factor for the transport of gas [-]
$\lambda_w$	Strand's momentum coefficient [-]
$\lambda_Z$	Particle friction factor [-]
$\lambda_Z^*$	Modified particle friction factor introduced by Muschelknautz [-]
$\mu$	Mass flow ratio [-]
$\mu_{st}$	Mass flow ratio in the strand [-]
$\mu_w$	Wall friction coefficient [-]
$\xi_P$	Friction coefficient of the material [-]
$\rho_b$	Bulk density [ $\text{kg}/\text{m}^3$ ]
$\rho_f$	Gas density [ $\text{kg}/\text{m}^3$ ]
$\rho_{f\_inlet}$	Gas density at the pipe inlet [ $\text{kg}/\text{m}^3$ ]
$\rho_{f\_outlet}$	Gas density at the pipe outlet [ $\text{kg}/\text{m}^3$ ]
$\rho_{fm}$	Average gas density [ $\text{kg}/\text{m}^3$ ]
$\rho_s$	Particle density [ $\text{kg}/\text{m}^3$ ]
$\sigma_1, \sigma_2, \sigma_3$	Principal stresses normal to the principal planes [ $\text{N}/\text{mm}^2$ ]
$\sigma_{axial}$	Axial stress [Pa]
$\sigma_b$	Axial stress at the slug back [Pa]
$\sigma_{bst}$	Bulk density of solids in the stationary layer [ $\text{kg}/\text{m}^3$ ]
$\sigma_f$	Axial stress at the front of the slug [Pa]
$\sigma_{f1}, \sigma_{f2}$	Parts of the axial stress at the front of the slug [Pa]
$\sigma_n$	Abcissa of a point located on a Mohr circle [ $\text{N}/\text{mm}^2$ ]
$\sigma_r$	Radial compression stress [Pa]

$\sigma_{r/w}$	Stress in radial direction at the wall [Pa]
$\sigma_{radial}$	Radial stress [Pa]
$\sigma_x$	Axial compression stress [Pa]
$\sigma_{x/w}$	Stress in axial direction at the wall [Pa]
$\sigma_y$	Compressive stress in the $y$ -direction [N/mm <sup>2</sup> ]
$\tau$	Shear stress [Pa]
$\tau_{cal}$	Calculated shear stress [Pa]
$\tau_{exp}$	Experimental wall shear stress [Pa]
$\tau_n$	Ordinate of a point located on the Mohr's circle [N/mm <sup>2</sup> ]
$\tau_w$	Wall shear stress [Pa]
$\tau_{xy}, \tau_{yx}$	Shear stresses in a $x$ - $y$ -two-dimensional-plane [N/mm <sup>2</sup> ]
$\phi$	Internal friction angle [°]
$\phi_s$	Static friction angle [°]
$\phi_w$	Angle of wall friction [°]
$\Phi$	Fraction of the pipe cross-section not covered by particles [-]
$\omega$	Angle as defined in Fig. 2.11 [°]
$\omega_0$	Undamped angular frequency [Hz]
$\Delta p, \Delta p_1, \Delta p_2$	Pressure gradient [Pa/m]
$\Delta F_i$	Error due to the discharge of the piezoelements [N]
$\Delta P$	Total pressure loss [Pa]
$\Delta P_{cal}$	Predicted pressure loss [Pa]
$\Delta P_{exp}$	Experimental pressure loss [Pa]
$\Delta P_f$	Pressure loss due to the transport of gas [Pa]
$\Delta P_h$	Pressure loss in horizontal pipeline [Pa]
$\Delta P_p$	Additional pressure gradient due to the material [Pa]
$\Delta P_s$	Pressure loss due to the transport of material [Pa]
$\Delta P_{stat}$	Difference in the static pressure [Pa]
$\Delta P_v$	Pressure loss in vertical pipeline [Pa]
$\Delta P_Z$	Non-dimensional pressure loss [-]
$\Pi_1, \Pi_2, \Pi_3$	Dimensionless number [-]



# 1. Introduction

Pneumatic conveying of particulate solids is one of the innovations that characterise industry of the 19<sup>th</sup> century. The first documented pneumatic conveying system can be attributed to the Peugeot plant at Valentigney, France. This system served since 1847 for the exhaustion of dust from fourteen grindstones [55]. However, if the definition of pneumatic conveying is confined to the transport of particulate matter from location A to B, then the first pneumatic conveying lines transported grains into silos in 1878. Nowadays, due to their versatility, such systems are found in a wide variety of industries whose processes involve the transfer and storage of bulk materials including agriculture, mining, food, chemical, pharmaceutical, metal refining and processing.

Pneumatic conveying systems are often preferred to mechanical conveying systems. This choice may be attributed to their simplicity and suitability for the transport of powdered and granular materials in both in-plant and external applications. The system requires a source of compressed gas, a feed device, a conveying pipeline and a material and gas separation system at the end of the process. Since the system is totally enclosed, both the product transported and the environment are protected. The carrier gas employed is usually air but if required, dry air or inert gas such as nitrogen can be used for hygroscopic or potentially explosive materials. The flexibility in both plant layout and operation adds to the attractiveness of such systems. The combination of horizontal sections, vertical sections and bends facilitates flexible routing, leading to better utilisation of floor space and the ability to avoid existing equipment or structures. Moreover, most systems can be arranged for completely automatic operation [53].

Pneumatic conveying is typically categorised as either one of two modes. If the material is transported with high velocity in the form of a suspension in the air, it is referred to as dilute phase conveying. If the material is conveyed at low velocity in a non-suspension mode, it is referred to as dense phase conveying. Furthermore, dense phase conveying is usually divided into various flow types from which strand flow and slug flow are the most common. The choice of the most suitable type of flow to transport a bulk material depends not only on the production requirements but also on the physical characteristics of the product to convey. The first systems that have been developed are the still most commonly used high velocity pneumatic conveyors. In high velocity systems, particles are generally in a turbulent suspension and collide frequently with the pipe wall. These high velocity collisions result in considerable wear of the pipe and may lead to a high rate of particle breakage in the case of friable products. To overcome these difficulties, commercial systems for low velocity dense phase pneumatic transport and particularly for slug flow pneumatic conveying have been developed. In slug flow pneumatic conveying, particles are conveyed in the form of slugs that fill the entire pipe cross-section. The slugs, separated by gas pockets, move gently along the pipeline. This type of flow has the advantage that it only needs a small amount of gas to transport high capacities. Moreover, pipe wear, dust generation and product attrition generated by dilute phase conveying can be significantly reduced. In the early days of dense phase pneumatic conveying, slug flow was undesirable and additional technologies such as by-pass systems were integrated in the conveying system to avoid the formation of slugs [58]. Later, as the many advantages of slug flow were recognised, additional techniques necessary to realise a smooth slug

transport were developed like the injection of secondary air at different locations over the conveying line or the intermittent supply of material or air to the conveying line. Slug flow is sometimes the only way to transport friable and valuable materials whose initial properties must be maintained, like food products or pharmaceuticals.

Even though there has been increased interest in dense phase conveying since the seventies and the development of special dense phase conveying systems, the real establishment of such systems for industrial applications has been somewhat slow. The resistance typically comes from practitioners for whom the random performances of the conveying system results in too higher risk. In fact, even if operating a pneumatic conveying system constitutes a relatively easy task, the design of such a system is often problematic. After World War II, research teams in both industry and academia worked actively to assist designers of pneumatic conveying systems. From the beginning, work has focused on developing design guidelines for the selection of system parameters like pressure, mass flow rate and velocity of both the gas and solid phase in order to furnish equipment manufacturers design tables, diagrams and equations to aid in the design of new conveying systems. While this has been satisfactorily achieved in the field of high velocity pneumatic conveying by integrating friction factors as in the transport of gas alone, the design of low velocity pneumatic conveying systems and particularly slug flow conveying systems still remains a problem. This is because the complex physical mechanisms involved in the transport of high particle concentrations in a gas phase have still not been fully understood. In fact, in dense phase, the flow phenomena occurring in the pipeline are not only influenced by the gas velocity, solid properties, pipeline direction and configuration and solid feeding devices, but also the particle-particle and particle-wall interactions are of great importance and should be taken into account. In addition, the transport of solids by a gas stream can cause some unique phenomena that often are not seen in gas-liquid flows or single-phase flows, like the production of electrostatic charges, which make it even more difficult to describe physically. Because of the high number of factors influencing the flow, it is acknowledged that a certain empiricism may always be present in the prediction methods.

If energy expenditure, wear of conveying pipe and particle attrition were not of any concern, the designer of a pneumatic conveying system would be prudent to avoid both the minimum conveying velocity and the minimum pressure drop regions altogether where conveying disturbances or failure due to pipe blockage occur more frequently. However, these considerations are exactly what the designer must fulfil. Therefore, the prediction of the key operating parameters, i.e. pressure loss along the system and minimum and optimal conveying velocity as well as the prediction of the flow boundaries, particularly for slug flow, still interest systems designers and continue to be areas of active research. In fact, conveying close to the lower boundary of slug flow is particularly gentle whereas lower pressure drop can be achieved for operations close to the upper boundary.

In the last hundreds years, research has adapted itself to the needs of the industry and many new research topics arose, including the calculation of energy consumption, the investigation of electrostatic charges and the determination of abrasion behaviour during pneumatic transport. However, a survey of the past and current literature shows than the main research topics in dense phase pneumatic conveying still focus on the fundamental understanding of the physical mechanisms involved in the transport itself.

Even if investigations on the formation, transport characteristics and stability of slugs represent a large and active research area on its own, the basic physics involved in slug flow has not yet been fully understood to enable accurate prediction models for reliable design of slug flow pneumatic conveying systems. In a recent article, Sanchez reviewed existing models and correlations for dense-phase conveying and compared the various predicted results with his experiments, showing one more time the lack of precision of the models available in the literature [70]. For slug flow conveying, the design of industrial plants is generally based on expensive pilot plant tests, mostly using a 1:1 scale where correlation of pressure loss, transport gas velocity and mass flow rate are generated each time for a specific material conveyed in a predetermined pilot plant. Pressure drop prediction by slug flow conveying remains a problem and in practice, the results of experimental investigations are used to minimise the risk of pipeline blockage.

The development of a reliable model to predict the pressure loss by slug flow pneumatic conveying firstly requires a fundamental understanding of the physical mechanisms involved in this mode of transport followed by their mathematical description. Some investigations have approached the slug flow mode of transport using basic principles, which presents the advantage that the correlations developed apply for all products and all conveying systems. However, this kind of approach is particularly difficult since many parameters have an influence and cross correlations are difficult to recognise. Other work has used experimental investigations in an attempt to systematise the process characteristics and with the correlations developed mostly succeeded in performing accurate design for a defined system. However, in most cases the results are not transferable to other kinds of products and systems other than those for which the investigations were carried out. Moreover, experiments are usually carried out in laboratory or small-scale pilot-plants and no guarantee exists that the knowledge gained can be extrapolated to larger scale systems with success. Many investigators have chosen to apply soil mechanics / bulk solids mechanics whereas others determine the pressure loss by applying fluid mechanics i.e. two-phase flow models. However, the theories used are not correlated at all, which is accentuated by the lack of communication between research teams having similar goals, but whose theoretical approaches or application fields are quite different. More recently, new approaches based on computational simulations have been developed, which combine both fluid dynamics and particle physics to simulate the transport of discrete particles or whole slugs in a gas flow considered as continuous medium. However, computational limitations do not allow calculations to be carried out for a whole system.

Due to the complexity of the calculation methods and the contradictions between the different theories and results obtained, the existing prediction procedures are seldom used in practice and manufacturers rather use costly and time intensive but more reliable experimental trials to perform the design for a dense-phase pneumatic conveying system. This statement gave rise in 2006 to the work of Niederreiter who investigated the behaviour of single slugs in vertical pipes and gained important knowledge of the internal stress state and porosity within moving slugs of cohesionless materials [60]. In the vertical condition, gravitation and conveying forces act in the same direction so that slug characteristics like porosity, particle and interstitial gas velocity or radial and wall shear stress can be considered a constant over the pipe cross-section. However, this assumption is not applicable for horizontal conveying. The present work deals with the investigation of the physical mechanisms involved in the transport of slugs

in horizontal pipes with focus on pressure, porosity and internal stress state. The objectives are the identification of the main physical mechanisms playing a role in the formation and the transport of slugs and the subsequent establishment of mathematical models to describe the pressure loss. In particular, the focus is on a better understanding of how the particles inside the slugs move and transmit stresses to the wall so that the mechanisms driving the instabilities and leading to pipe blockage can be identified. In fact, in many theoretical studies, slugs are regarded as compact porous solid columns that are able to transfer axial stresses into radial stresses. This transmission of stress is usually held responsible for the high pressure loss taking place by slug flow pneumatic conveying and the occurrence of pipe blockage. However, up to now, experimental investigations failed to determine the coefficient of stress transmission and assumptions have to be used in calculation models. To depict the state of the art in the field of slug flow modelling, a full chapter is dedicated to the significant calculation procedures for pressure loss existing in the literature. The basic concepts of these models are detailed and compared to emphasise the evolution in the theories used. Besides, calculations are carried out to illustrate quantitatively the differences between the predicted results.

To verify that the assumptions made in the prediction models are physically grounded, experimental investigations were carried out on horizontal single slugs of granular material with respect to particle velocity, pressure profile, porosity and internal stress states. In particular, a special measurement probe has been used to measure in-situ both the radial and wall shear stresses induced by slugs at different locations around the pipe circumference. This probe, which was initially developed by Niederreiter to investigate the stress state of vertical moving slugs has been optimised to allow accurate detection of the stresses at a sampling frequency of 10,000 Hz. Additionally, a slug-catcher was specially designed to investigate the porosity within a slug and particularly the density profile over slug height. Based on the experimental results, a new approach is proposed to describe physically the relation between porosity, wall shear stress, particle velocity, solids loading, and pressure loss along the pipeline.

## 2. State of the art

Basically, pneumatic conveying is characterised by three physical parameters: the solids charge depending on the mass flow rate of material to convey, the gas velocity required to transport this given mass flow rate and the resulting pressure loss occurring in the pipeline. Depending on the combination of these three variables, different types of flow take place in the conveying pipe. The occurrence of a given type of flow is also influenced by the properties of the material to transport. Each mode of flow is characterised by specific physical mechanisms governed by particular physical laws. Therefore, great importance has to be attached to the accurate definition and description of each flow mode. Over the time, the many factors influencing the flow and the complexity of the mechanisms involved in pneumatic transport gave rise to very different theories and calculation procedures to predict the pressure loss occurring in the conveying pipe. In the last decades, since high velocity pneumatic conveying has been well investigated and understood, research has rather focused on dense phase and particularly on slug flow pneumatic conveying. After a description of the various types of flow existing and the factors influencing the conveying process, the approaches usually employed to predict the pressure loss are detailed. Afterwards, the significant work that has been done on slug flow pneumatic conveying in the last thirty-five years is shortly reviewed to serve as basis for subsequent discussion.

### 2.1. General definitions of pneumatic conveying

#### 2.1.1. Classification of pneumatic conveying

Because of the wide application field of pneumatic conveying, practitioners described and classified this transport process very early. A widely used classification, particularly in industry, considers the mode of production of the pressure necessary for the transport and differentiates between vacuum and positive pressure conveying systems. Since the pressure gradient covers a very wide range of values, it is usually differentiated between low-pressure ( $< 0.2$  bar), middle-pressure (pressure gradient between 0.2 and 0.7 bar) and high-pressure systems ( $> 0.7$  bar). Another classification consists in differentiating between horizontal and vertical pipeline sections and further between upward and downward direction. The classification that is mostly applied in research considers the flow mode occurring during conveying. Basically, there are two types of flow in pneumatic transport, namely dilute phase flow and dense phase flow, which are characterised by the air supply velocity set up and the pressure loss and solids loading occurring in the pipeline. In order to identify the flow mode boundaries and be able to identify the operating points, a state-diagram is usually developed for a specific product conveyed in a given pipeline system.

#### 2.1.2. State-diagram and types of flow

To consolidate the theory in pneumatic transport, a number of practitioners explored the phase-diagram approach. The most common diagram is the one of Zenz who proposed a pressure drop/gas velocity

analysis [101]. According to the solids mass flow rate, the gas supply velocity, the particle size and density and the pipe diameter, very different flow patterns occur in the conveying pipeline (Fig. 2.1).

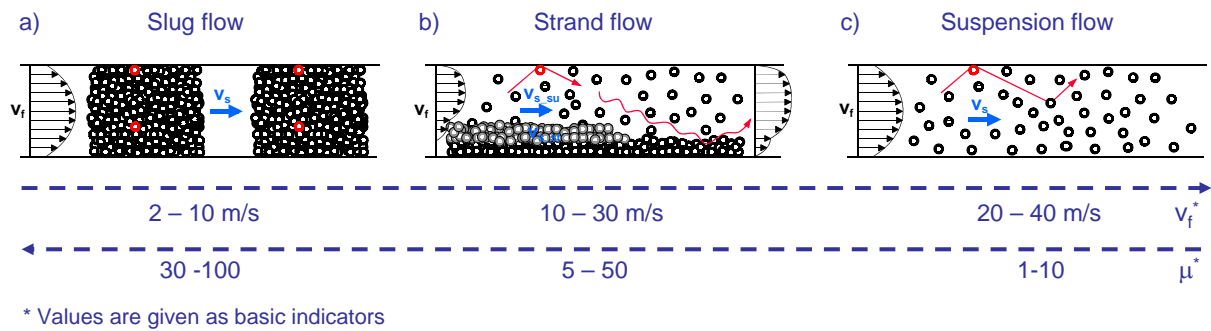


Figure 2.1: The three basic flow types in pneumatic conveying

For a specific product conveyed in a pipe with a given diameter, the different types of flow are generally described by decreasing fluid velocity at a constant solids mass flow rate. At high air velocities, the particles are assumed to fly with a uniform distribution over the pipe cross-section (Fig. 2.1c). This state is referred to as fully suspended flow, which is located on the right hand side of boundary D in Fig. 2.2 representing a typical Zenz plot.

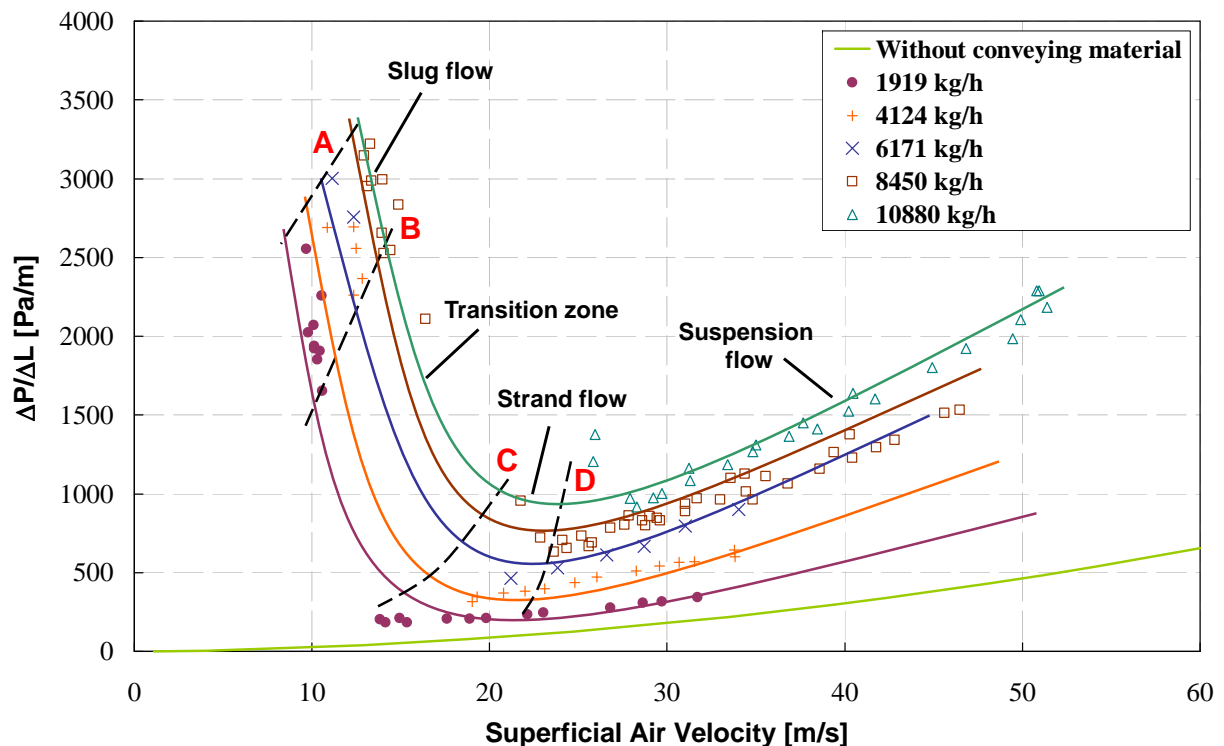


Figure 2.2: State-diagram for pneumatic conveying of Polypropylene granules ( $d_{eq} = 3.0$  mm) in a 50 mm i.d. pipeline [60]

The gas-solid flow systems are multi-particle and as such present a myriad of wall collisions as well as particle-particle collisions where momentum is transferred. The flying particles hit on the pipe wall,

lose velocity, and have to be reaccelerated by the transported gas. These repeated short but numerous reaccelerations are responsible for the additional pressure gradient. This type of flow is characterised by a high transport gas velocity and a very low solids charge.

At low air velocities, because the gas velocity is not high enough to maintain all particles in suspension, segregation of the suspended particles occurs and the state of strand type conveying is achieved (Fig. 2.1b). In this conveying state, under conditions of constant solid mass flow rate, the pressure drop increases with decreasing air velocity. There is no sharp transition from fully suspended flow to strand type conveying but the transition is gradual. The main part of the solids mass flow rate results from the particles transported in a strand sliding at the pipeline bottom. A small fraction of the particles is transported in the suspension above it. If the gas velocity is decreased further, the shear force at the strand surface may be lower than the resistance force between the layer of particles and the pipeline wall. In this case, a stationary bed of particles forms at the pipeline bottom, while particles are transported almost only in form of a layer sliding over it.

If the gas velocity is reduced further, a transition from strand type conveying to slug flow occurs for solids of large particle sizes whereas, in the case of fine particles, blockage of the system mainly develops. Particles are conveyed in the form of slugs, which fill the entire cross-section of the pipeline. The slugs, separated by gas pockets, move gently along the pipeline. Slug flow is generally schemed according to an ideal approach as in Fig. 2.1a. In the real case, slug flow can be better described as a wave motion: a moving slug picks up the material of the stationary particles layer in front of it and deposits a similar quantity of material at the rear (Fig. 2.3).



Figure 2.3: Schematical representation of slug flow as it usually occurs in the reality

Slug flow pneumatic conveying is gaining importance in industry because it needs only a small amount of gas to transport high capacities. Less product and pipeline damages, lower energy consumption and smaller dust-separating equipment are further advantages. In conveying granular materials, a transition regime between strand flow and slug flow is observed for a small velocity range. Blockage, instability or even failure in conveying may take place in this transition region due to the high pressure fluctuations resulting from the flow mode alteration between strand flow and slug flow. Since no stable pressure drop occurs in conjunction with this type of conveying, the pressure drop in state-diagram is commonly represented in the form of a broken curve (Fig. 2.2). However, a lower pressure drop can be achieved for operations close to its boundaries, which explains that these boundaries are still investigated. Although the upper boundary of the transition zone has been a popular research topic, its lower boundary, i.e. the maximum conveying velocity of slug flow conveying was more rarely investigated [99].

Each type of flow reacts differently to changes occurring in the operating parameters. For instance, according to the flow, a small decrease of the gas supply velocity may result in the increase of the pressure gradient (slug flow), in its decrease (suspension flow), in almost insignificant changes (near the

point of minimum pressure loss) or in sudden high pressure fluctuations if the operating point reaches the instable zone. This explains that the prediction of the type of flow and the boundaries of the state-diagram still represent one of the first priorities of theoretical consideration.

### 2.1.3. Variations in pneumatic conveying terminology

Even if the definition of pneumatic conveying as being the transport of a material in a gas flow can be considered as universal, it is not the case for many terms characterising this process. The lack of uniformity in terminology adds to the confusion of understanding the physical phenomena [36]. Because products behave very differently according to their physical characteristics, pneumatic conveying of coarse and fine particles are commonly treated separately. The next separation in this field consists in differentiating between dilute-phase and dense-phase whose concept is often discussed in the literature. Nevertheless, confusion still exists concerning what exactly is meant by dense-phase since sometimes it represents high solids loading with 20/1 values or greater, sometimes it defines conveying with low velocity while sometimes it is used to define conveying when the velocity is lower than the sedimentation velocity. Finally, in other cases, it means a piston flow. Consequently, according to the definition, strand flow sometimes belongs to dense-phase and sometimes to dilute-phase. Other authors set the boundary between dilute and dense-phase in the transition area where conveying is unstable (Fig. 2.2).

A second example illustrating the disparities in definitions is given by the term minimum conveying condition. The minimum conveying condition means for some authors the point of minimum pressure loss (boundary D in Fig. 2.2) whereas it means the minimum gas velocity where conveying is possible, i.e. boundary A for others. This disagreement is probably due to the fact that in a first time, slug flow was considered as undesired by the practitioners and has become later more and more interesting. A last example of variation in the pneumatic conveying terminology is given by plug flow, or slug flow, which is also termed dense phase flow [38] or pulse-piston flow since it can be considered as the movement of alternated solids and gas slugs.

In this work, the term dense-phase pneumatic conveying is used to describe the flow pattern from the point where the gas velocity is not sufficient anymore to maintain all particles in suspension, with the exclusion of the unstable zone. Dense-phase includes strand flow, slug flow and moving bed. Fig. 2.4 shows the terminology used in this study. Only granular materials are considered in this study. Therefore, the theories, the results and the discussion presented are valid for the transport of coarse granular matter but not necessarily for the transport of fine powder. The only term of slug flow is used to define the conveying of particles by air along a pipe that is filled with particles at one or more cross-sections. The term of plug as used by Konrad is employed to describe a length of bulk solids that occupies the full cross-section of the pipeline, i.e. a slug without the front and the rear parts where associated particles are moving but the cross-section is not entirely filled with particles.



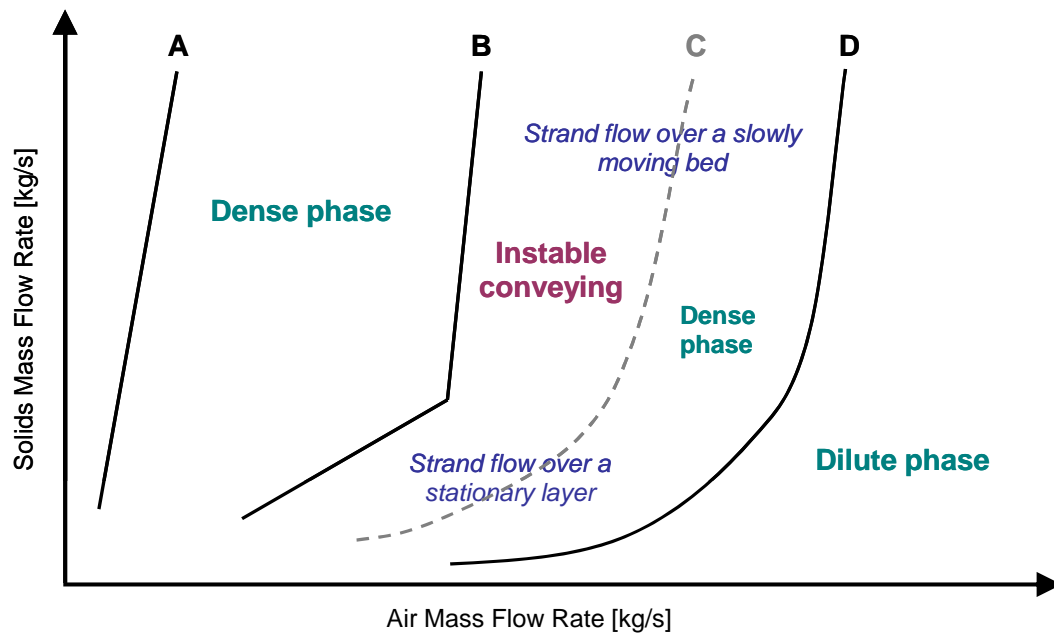


Figure 2.4: Schematical state-diagram and terminology as used in this work

## 2.2. Factors influencing the conveying process

### 2.2.1. Material properties

The physical properties of the product transported influences significantly the transport feasibility, so that system designers often rather carry out experiments in a pilot-plant, mostly using a 1:1 scale, before dimensioning a conveying system. Siegel cited the wall friction factor, the internal friction factor, the fluidisation behaviour and the particle size distribution as major factors making slug flow pneumatic conveying more or less easy or even impossible [78]. According to Klinzing, the properties of the solids ranging from granular to fine powders are the controlling parameters for the behaviour of the slugs in pipelines [21]. Therefore, these properties must be carefully considered in any attempt to analysis or to predict the slug flow mode.

Dense phase pneumatic conveying is not suitable to transport all types of products. For example, material strongly aspherical, presenting a wider particle size distribution, a heterogeneous composition, a high humidity or a high density are particularly difficult to transport. Furthermore, the ability of slugging is not observed with all materials. However, based on the existing literature, naturally occurring slug flow was always obtained with coarse plastic pellets for a wide range of velocities. In fact, Polypropylene and Polyethylene pellets exhibit high permeability and de-aeration rates, which make those materials particularly suitable for dense-phase transport.

Many experimental investigations were carried out to develop a numerical criterion that would predict the behaviour of bulk material fluidised by gas. Geldart established a classification diagram in which particulate materials are classified into four different groups from A to D, characterised by density difference, i.e.  $(\rho_s - \rho_f)$  and mean particle size [29]. This classification has been well established

to predict the material ability to fluidise. Later, Mainwaring and Reed measured the permeability factor and the de-aeration of particles to estimate the potential of material to be conveyed [44]. Dixon developed theoretical “slugging diagrams” for systems with different pipe diameters based on the Geldart classification diagram. These diagrams can be used to determine whether a bulk material has a natural slugging tendency and whether dunes or full diameter slugs are likely to form [20]. Jones and Mills [33] developed a fluidisation test that can be used to classify bulk materials according to the modes of flow they can achieve in the conveying pipeline [42]. A detailed review and comparison of the work of various researchers who established correlations between the principal properties of the materials that can be used to predict the feasibility of conveying particles in the dense phase mode was published by Sanchez [69]. He found that the best correlation was obtained using the dimensionless numbers that are a function of permeability factor, de-aeration factor and minimum fluidisation velocity.

### 2.2.2. Dimensional analysis

The most accurate method to dimension an industrial pneumatic conveying system for a given product mostly consists in carrying out experimental trials during which the pressure loss occurring for a defined gas velocity and product mass flow rate is measured. The experimental investigations generally take place in pilot plants with internal diameters of 25 mm, 50 mm or 80 mm so that a scale-up or scale-down is often required. However, the physical properties of the material to convey, the transporting gas but also the characteristics of the conveying system influence the flow and the physical mechanisms occurring in the pipeline. To transfer the data measured experimentally and realise a scale-up, the similitude model, which considers the similarities in the geometry, dynamic and mass flow ratio must be respected. This can be achieved by using dimensionless numbers. Moreover, to reduce the experimental effort to determine empirical values characterising the transport but also to simplify the physical and mathematical correlations developed, one method consists in reducing the number of influence parameters by interrelating single factors. This is also achieved by using dimensionless quantities whose advantage is to be universally valid. By carrying out a dimensional analysis, the number of influence parameters can be reduced without losing any information. The goal is to find a general expression for the pressure loss  $\Delta P$  valid for all types of products conveyed in all systems and for all types of flows. The first step to establish such an expression is to list all physical parameters that may have an influence on the pressure loss. From a general point of view, the pressure loss depends on the characteristics of the conveying gas, the product properties and the mass flow rates of both gas and material conveyed:

$$\Delta P = f(\text{Gas}, \text{Product}, \text{MassFlowRate})$$

Because of the high number of physical parameters that may have an influence on the pressure loss, the conveying of gas alone will be first considered. Then the particles will be added to the flow of gas. Further, straight lines and bends will be considered separately.

**2.2.2.1. Single phase flow: gas** From theoretical and experimental considerations, the pressure depends on the pipeline characteristics, i.e. pipe diameter  $D$ , pipe horizontal length  $l_h$  and vertical length  $l_v$ , bend radius  $r_b$  as well as on the physical characteristics of the conveying gas, i.e. gas velocity  $v_f$ , gas dynamic viscosity  $\eta_f$  and gas density  $\rho_f$ . Therefore, the expression for  $\Delta P$  will have the form:

$$\Delta P_f = f(v_f, D, l_h, l_v, r_b, \eta_f, \rho_f)$$

Since the pressure loss resulting from the transport of gas alone depends on seven factors, interrelations between the variables have to be found to reduce the number of factors. The transport of gas is a dynamic process and the expression for the dynamic pressure is known under the form:

$$P_{dyn} = \frac{1}{2} \cdot \rho_f \cdot v_f^2$$

Therefore, the expression for the pressure loss can be written in the following form:

$$\Delta P_f = f_1(v_f, D, l_h, l_v, r_b, \eta_f, \rho_f) \cdot \frac{1}{2} \cdot \rho_f \cdot v_f^2$$

However, because the function  $f_1$  still depends on the gas velocity that is unknown, this form does not permit to reduce the number of variables. Since the pressure losses along the pipeline correspond to the addition of the pressure losses in defined sections, the dimensional analysis can be carried out by dividing the pipe into several pipe sections, i.e. the different sections horizontal, vertical and bends can be investigated separately.

### Horizontal and vertical straight pipes

Since the force of gravity does not affect the gas transport, horizontal and vertical pipes can be treated similarly. The total length of straight pipe  $L$  can be considered instead of vertical length  $l_v$  and horizontal length  $l_h$ . Therefore, the pressure loss in straight pipes depends on five variables:

$$\Delta P_f = f(v_f, D, L, \eta_f, \rho_f) \cdot \frac{1}{2} \cdot \rho_f \cdot v_f^2$$

The resistance force to the gas transport can be written in form of the friction coefficient  $\lambda_f$ , so that:

$$\Delta P_f = \lambda_f(v_f, D, L, \eta_f, \rho_f) \cdot \frac{1}{2} \cdot \rho_f \cdot v_f^2$$

This expression contains a total of  $p = 6$  variables. All these parameters can be expressed using only three base quantities and base units, i.e. length  $l$ , masse  $m$  and time  $t$ . Therefore  $r = 3$ .

The number of dimensionless numbers  $q$  should be

$$q = p - r = 3$$

By applying the Buckingham's principle ( $\Pi$ -principle), all units of the influence parameters can be unformed to let appear the base units. A first dimensionless number is formed by relating the two variables having the same units, i.e. the length  $L$  and the diameter  $D$ . From the geometrical point of view, pressure loss is inversely proportional to pipe diameter. Hence, the dimensionless number  $\Pi_3$  is formed as following:

$$\Pi_3 = \frac{L}{D}$$

The units of the three remaining factors, i.e. viscosity, density and pressure loss are unformed to let appear the three base units  $l$ ,  $m$ , and  $t$ .

– Viscosity  $\eta_f$  in  $Pa \cdot s = \frac{m}{l \cdot t}$

– Density  $\rho_f$  in  $\frac{m}{V} = \frac{m}{l^3}$

– Pressure loss  $\Delta P$  in  $Pa = \frac{m}{l \cdot t^2}$

The units of all parameters can be written in a matrix:

$$\begin{array}{c} \eta_f \quad \rho_f \quad v_f \quad D \quad \Delta P \\ \text{m} \begin{pmatrix} 1 & 1 & 0 & 0 & 1 \\ -1 & -3 & 1 & -1 & -1 \\ -1 & 0 & -1 & 0 & -2 \end{pmatrix} \\ \text{l} \\ \text{t} \end{array}$$

The goal is to reach a matrix of the form:

$$\begin{array}{c} \eta_f \quad \rho_f \quad v_f \quad D \quad \Delta P \\ \text{m} \begin{pmatrix} 1 & 0 & 0 & p_{11} & p_{12} \\ 0 & 1 & 0 & p_{21} & p_{22} \\ 0 & 0 & 1 & p_{31} & p_{32} \end{pmatrix} \\ \text{l} \\ \text{t} \end{array}$$

and hence dimensionless numbers of the form:

$$\Pi_1 = D \cdot (\eta_f^{-p_{11}} \cdot \rho_f^{-p_{21}} \cdot v_f^{-p_{31}})$$

$$\Pi_2 = \Delta P \cdot (\eta_f^{-p_{12}} \cdot \rho_f^{-p_{22}} \cdot v_f^{-p_{32}})$$

The original matrix has to be rearranged to reach the desired matrix:

$$\begin{array}{c}
 \text{Original matrix} \\
 \left( \begin{array}{ccccc} 1 & 1 & 0 & 0 & 1 \\ -1 & -3 & 1 & -1 & -1 \\ -1 & 0 & -1 & 0 & -2 \end{array} \right) = \left( \begin{array}{ccccc} 1 & 1 & 0 & 0 & 1 \\ 0 & -2 & 1 & 1 & 0 \\ 0 & 1 & -1 & 0 & -1 \end{array} \right) = \left( \begin{array}{ccccc} 1 & 1 & 0 & 0 & 1 \\ 0 & 1 & -1 & 0 & -1 \\ 0 & -2 & 1 & 1 & 0 \end{array} \right) = \left( \begin{array}{ccccc} 1 & 1 & 0 & 0 & 1 \\ 0 & 1 & -1 & 0 & -1 \\ 0 & 0 & -1 & 1 & -2 \end{array} \right) \\
 \begin{array}{ccc} L_2 = L_2 + L_1 & L_2 = L_3 & L_3 = L_3 + 2L_2 \\ L_3 = L_3 + L_1 & L_3 = L_2 & \\ & & \end{array} \\
 \\
 \text{Rearranged matrix} \\
 = \left( \begin{array}{ccccc} 1 & 1 & 0 & 0 & 1 \\ 0 & 1 & -1 & 0 & -1 \\ 0 & 0 & 1 & -1 & 2 \end{array} \right) = \left( \begin{array}{ccccc} 1 & 1 & 0 & 0 & 1 \\ 0 & 1 & 0 & -1 & 1 \\ 0 & 0 & 1 & -1 & 2 \end{array} \right) = \left( \begin{array}{ccccc} 1 & 0 & 0 & 1 & 0 \\ 0 & 1 & 0 & -1 & 1 \\ 0 & 0 & 1 & -1 & 2 \end{array} \right) \\
 \begin{array}{ccc} L_3 = L_3 \times (-1) & L_2 = L_2 + L_3 & L_1 = L_1 - L_2 \\ & & \end{array}
 \end{array}$$

This leads to:

$$\Pi_1 = D \cdot \eta_f^{-1} \cdot \rho_f^1 \cdot v_f^1 = \frac{D \cdot v_f \cdot \rho_f}{\eta_f} = \frac{D \cdot v_f}{\nu_f} = Re$$

$$\Pi_2 = \Delta P \cdot \eta_f^0 \cdot \rho_f^{-1} \cdot v_f^{-2} = \frac{\Delta P}{\rho_f \cdot v_f^2} = Eu$$

The Euler-number  $\Pi_2$  can be expressed according to the two other dimensionless numbers, i.e.

$$\Pi_1 = Re \text{ and } \Pi_3 = \frac{L}{D}:$$

$$Eu = f \left( Re, \frac{L}{D} \right)$$

Therefore, the friction coefficient  $\lambda_f$  is a function of only two variables and the expression for  $\Delta P_f$  can be simplified:

$$\Delta P_f = \lambda_f \left( Re, \frac{L}{D} \right) \cdot \frac{1}{2} \cdot \rho_f \cdot v_f^2$$

Under isotherm conditions, since the pressure losses along the conveying pipeline can be added, the relation between the total pressure loss and the pipe length is linear. Moreover, the pressure loss is inversely proportional to the pipe diameter. Consequently, the length  $L$  and the pipe diameter  $D$  can be taken out of the function and the expression becomes:

$$\Delta P_f = \lambda_f (Re) \cdot \frac{L}{D} \cdot \frac{1}{2} \cdot \rho_f \cdot v_f^2 \quad (2.1)$$

However, it should be pointed out that the friction coefficient still depends on the pipe diameter that is included is the Reynolds-number.

Although the number of influence parameters could be reduced, values for the friction coefficient  $\lambda_f$  and the mathematic correlations with  $Re$  still have to be determined experimentally.

For horizontal pipeline sections:

$$\Delta P_h = \lambda_f(Re) \cdot \frac{l_h}{D} \cdot \frac{1}{2} \cdot \rho_f \cdot v_f^2$$

For vertical pipeline sections:

$$\Delta P_v = \lambda_f(Re) \cdot \frac{l_v}{D} \cdot \frac{1}{2} \cdot \rho_f \cdot v_f^2$$

## Bends

The dimensions analysis in bends is the same as for straight pipes except that the friction coefficient  $\xi$  is used to describe the friction in this area. Therefore:

$$\Delta P_f = \xi \left( Re, \frac{L}{D} \right) \cdot \frac{1}{2} \cdot \rho_f \cdot v_f^2$$

As for the friction coefficient  $\lambda_f$  in straight pipes, values for the friction coefficient  $\xi$  have to be determined experimentally.

### 2.2.2.2. Two-phase-flow: particles and gas (dilute phase conveying)

The total pressure loss occurring during the transport of a solid material in a gas flow results from the sum of the pressure gradients due to the gas flow  $\Delta P_f$  on the one hand and to the material on the other hand. The pressure loss due to the material is known as additional pressure gradient  $\Delta P_P$ .

$$\Delta P = \Delta P_f + \Delta P_P$$

To express the total pressure loss, an additional friction coefficient  $\xi_P$  is inserted in Eq. 2.1 to describe the friction resulting from the material transport:

$$\Delta P = (\lambda_f + \xi_P) \cdot \frac{L}{D} \cdot \frac{1}{2} \cdot \rho_f \cdot v_f^2$$

The friction coefficient  $\xi_P$  of the material is a function of pipe diameter, gas properties, i.e. density and velocity as well as material properties, i.e. density  $\rho_s$ , mass flow rate  $\dot{m}_s$  and sedimentation velocity  $w_s$ . Furthermore, the force of gravity has a significant effect on the material transport:

$$\Delta P_P = \xi_P(v_f, \rho_f, w_s, \rho_s, \dot{m}_s, g, D) \cdot \frac{L}{D} \cdot \frac{1}{2} \cdot \rho_f \cdot v_f^2$$

The solids mass flow rate  $\dot{m}_s$  can be expressed in form of the dimensionless mass flow ratio  $\mu = \frac{\dot{m}_s}{\dot{m}_f}$ . Barth [4] showed that  $\Delta P_P$  is a linear function of  $\mu$ , which leads to:

$$\Delta P_P = \xi_P(v_f, \rho_f, w_s, \rho_s, g, D) \cdot \mu \cdot \frac{L}{D} \cdot \frac{1}{2} \cdot \rho_f \cdot v_f^2$$

The friction coefficient  $\xi_P$  depends on a total of  $p = 6$  variables. Like previously done for the flow of gas alone, those variables can be described using solely the three base units for length  $l$ , masse  $m$  and time  $t$ . Therefore, three dimensionless numbers that define the interrelations between the factors have to be found to reduce the number of parameters.

A first dimensionless number results from the ratio of solids to gas velocity:

$$\Pi_3 = \frac{w_s}{v_f} = \eta$$

Following a similar procedure as the one carried out for the gas alone, the Euler-number can be found:

$$\Pi_2 = \frac{\Delta P}{\rho_f \cdot v_f^2} = Eu$$

The remaining variables can be combined to form the Froude number:

$$\Pi_1 = \frac{v_f^2}{g \cdot D} = Fr$$

Therefore, the expression for  $\Delta P_P$  can be simplified and written as following:

$$\Delta P_P = \xi_P(Fr, Eu, \eta) \cdot \mu \cdot \frac{L}{D} \cdot \frac{1}{2} \cdot \rho_f \cdot v_f^2$$

The gas velocity  $v_f$  is contained in the three process dimensionless numbers  $Fr$ ,  $Eu$  and  $\eta$ . In addition, the solids mass flow rate  $\dot{m}_s$  is also a function of the gas velocity. Therefore,  $\mu = f(v_f)$ .

As shown previously,  $Eu = f(Re, \frac{L}{D})$ , so that:

$$\Delta P = \left( \lambda_f \left( Re, \frac{L}{D} \right) + \xi_P \left( Fr, Re, \frac{L}{D}, \eta \right) \right) \cdot \mu \cdot \frac{L}{D} \cdot \frac{1}{2} \cdot \rho_f \cdot v_f^2 \quad (2.2)$$

By applying the Buckingham's principle, the number of influence parameters for the transport of a solid material in a gas stream could be significantly reduced. However, Eq. 2.2 illustrates the necessity of finding further correlations between the influence factors. Significant work has already been done to establish experimental correlations between the key parameters. However, the correlations result from

experimental investigations carried out for specific materials in a defined system and the extrapolation of the results gained to other materials or pipe geometries has not been proven right. Designers of pneumatic conveying equipment generally use diagrams that illustrate the pressure loss as function of a certain parameter. However, the high number of influence parameters makes the establishment of universal diagrams impossible.

### 2.3. Different approaches to predict pressure loss and flow type in horizontal straight pipes

The main objective of research on pneumatic conveying has always been the accurate prediction of the pressure loss expected in the conveying system. Over the time, very different approaches have been used to achieve this goal. Early investigations on dilute phase pneumatic conveying resulted in the development of calculation methods involving a particle friction factor. Later, as research began to focus on dense-phase pneumatic conveying, new approaches involving bulk solids mechanics, theories for fluid flow through packed beds or state-diagrams arose. Lately, the application of numerical analysis opened new possibilities. The objective of this section is to detail the different basic approaches on which the main prediction models are grounded in order to provide a basis to facilitate the physical comprehension of the existing models for slug flow.

#### 2.3.1. Experimental determination of a particle friction factor

According to Barth, the total pressure drop  $\Delta P$  is basically given as the sum of the pressure  $\Delta P_f$  due to the fluid and the additional pressure drop  $\Delta P_p$  due to the transport of particles [4] as shown in Fig. 2.5.

$$\Delta P = \Delta P_f + \Delta P_p \quad (2.3)$$

The pressure drop for the transport of the gas alone  $\Delta P_f$  is usually given by an expression for single-phase flows such as the phenomenological equation of Darcy-Weisbach [16]:

$$\Delta P_f = \lambda_f \cdot \frac{L_T}{D} \cdot \frac{1}{2} \cdot \rho_f \cdot v_f^2 \quad (2.4)$$

where the gas friction factor is determined by using a mathematical expression such as the Blasius equation, which describes the velocity distribution in the laminar boundary layer close to the wall [7]. The additional pressure drop  $\Delta P_p$  is balanced with the fluid drag force and is given by the momentum theorem:

$$\Delta P_p \cdot A = F_T \quad (2.5)$$



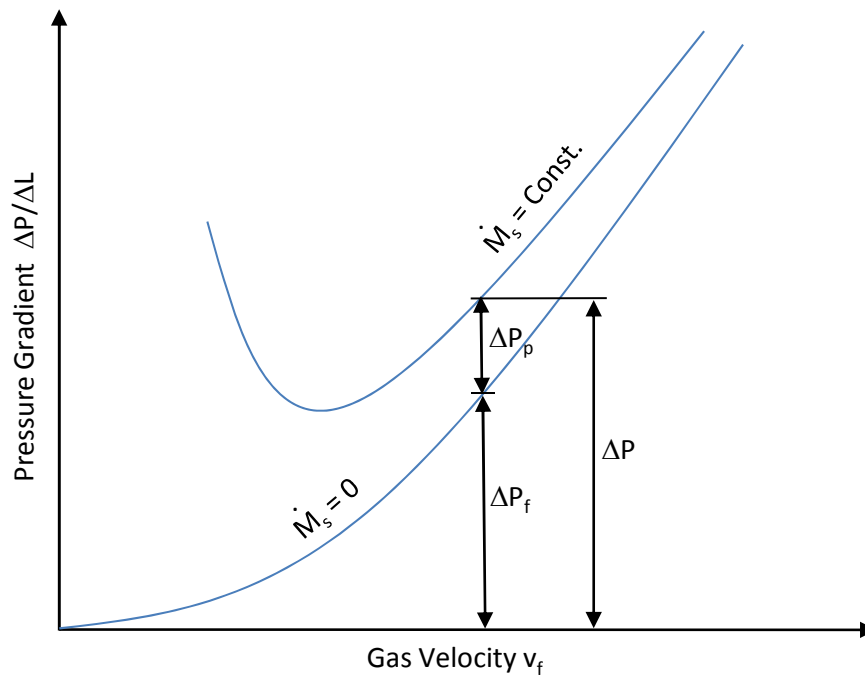


Figure 2.5: Pressure loss in gas-particles flow

Since during a long time pneumatic conveying systems were largely confined to transport systems at rather high gas velocities, the prediction procedures started with this type of flow. Gasterstädt published the first scientific work in this field in 1924. He investigated the relationship between the terminal falling velocity of a wheat grain and its velocity in a horizontal pneumatic conveyor [28]. The second relevant work was published by Segler [73] who studied the horizontal transport of wheat and oats in pipes of different diameter and reported his results as the friction coefficient  $\gamma_s$  defined by the equation:

$$\Delta P = \gamma_s \cdot \frac{L_T}{D} \cdot \frac{1}{g} \cdot \frac{1}{2} \cdot \rho_f \cdot v_f^2 \quad (2.6)$$

Segler showed that for a constant air flow rate, the coefficient  $\gamma_s$  is proportional to the solid flow rate. Eq. 2.6 results from an analogy to the Darcy-Weisbach friction factor equation, where the pressure drop due to the solids transport is expressed as following [16]:

$$\Delta P_p = \lambda_Z \cdot \frac{L_T}{D} \cdot \frac{1}{2} \cdot \rho_b \cdot v_s^2 \quad (2.7)$$

Barth relaunched scientific investigations and proposed in 1954 an equation for the dimensionless pressure gradient valid for flow free of acceleration. The pressure gradient is expressed in form of a particle friction factor based on the power required for particle transport associated with a solid mass flow rate  $\dot{m}_s$  and a pipe length  $\Delta L$  [55].

$$\lambda_Z = \frac{\Delta P_p}{\Delta L} \cdot \frac{2 \cdot D}{\mu \cdot \rho_f \cdot v_f^2} \quad (2.8)$$

Barth correlated the dimensionless pressure gradient given by Eq. 2.8 with the dimensionless Froude number:

$$Fr = \frac{v_f^2}{D \cdot g} \quad (2.9)$$

$$\lambda_Z = \lambda_Z(Fr) \quad (2.10)$$

Eq. 2.10 suggests that for one type of particulate material the dimensionless pressure gradient  $\lambda_Z$  should fit one single curve independently of the pipe diameter. Nevertheless, experimental measurements disagree with this theoretical statement, as underlined by Molerus [55, 56]. Muschelknautz and Krambrock showed that this expression is valid only for high gas velocities [58]. Attempting to improve the basic statement given in Eq. 2.10, Muschelknautz considered a force balance between the driving force  $\Delta P_p \cdot A$  and a resistance force  $F_T$  and introduced a modified particle friction factor in his equation:

$$\lambda_Z^* = \lambda_Z \cdot \frac{1}{\eta} \quad (2.11)$$

Muschelknautz assumed the additional specific energy required in the gas stream to be equal to the sum of the specific energy due to the wall friction of the sliding material on the one hand and to the particle/wall impacts on the other hand. Therefore, he sub-divided the dimensionless pressure gradient into two components, namely a frictional term including the friction factor  $f_R$  and a particle impact term involving the impact factor  $\lambda_Z^*$ :

$$\frac{\Delta P_p}{\Delta L} = \left( \frac{2 \cdot f_R}{\eta \cdot Fr^2} + \lambda_Z^* \cdot \eta \right) \cdot \frac{\mu \cdot \rho_f \cdot v_f^2}{2 \cdot D} \quad (2.12)$$

The first extreme corresponds to all particles being suspended and flying evenly distributed over the pipe cross-section at rather high gas velocity whereas the second extreme corresponds to all particles sliding along the bottom of the pipe at rather low gas velocities [55]. However, Eq. 2.12 requires the accurate prediction of the velocity ratio  $\eta$ , which has been an active area of research in the last forty years but still remains difficult, particularly because it involves both bulk solids and fluid mechanics. Muschelknautz [57] and Bohnet [8] largely investigated both theoretically and experimentally the determination of  $\lambda_Z^*$  and  $f_R$  and determined values of  $\lambda_Z^*$  for many products, particularly coarse materials. However, these values are strongly dependent on the system material transported / pipe wall material [97]. Nevertheless, the method proposed by Muschelknautz still finds application in industry and is detailed in the VDI WärmAtlas [86].

According to the particle diameter, Weber established two correlations for  $\lambda_Z$  involving both the Froude number and the particle Froude number [88]:

for  $d < 0.5$  mm:

$$\lambda_Z = \frac{2.1 \cdot Fr_s^{0.25} \cdot \left(\frac{D}{d_p}\right)^{0.1}}{\mu^{0.3} \cdot Fr} \quad (2.13)$$

for  $d > 0.5$  mm:

$$\lambda_Z = \frac{0.082 \cdot Fr_s^{0.25} \cdot \left(\frac{D}{d_p}\right)^{0.1}}{\mu^{0.3} \cdot Fr^{0.86}} \quad (2.14)$$

The first motivations in the field of research was to furnish planers and designers of conveying equipment the key parameters and intercorrelations necessary to perform the design. These values were obtained empirically. When experiments were well planed and the data analysis showed a certain similarity, an accurate basis for the calculations could be obtained for the area over and above the area experimentally investigated. Siegel [78], Welschof [90], Segler [73] and Gasterstädt [28] did significant work to measure the pressure loss during conveying of numerous coarse products in various pipelines with the hope that theirs results could be extrapolated to other materials conveyed in other pipes.

Wen and Simons [92] presented an empirical correlation for the pressure gradient in the pipeline in terms of pipe, particle properties and solids and air mass flow rates (Eq. 2.15):

$$\frac{\Delta P}{\Delta L} = 41.846 \cdot 10^{-3} \cdot \rho_b \cdot \left(\frac{d_p}{D}\right)^{0.25} \cdot v_s^{0.45} \quad (2.15)$$

However, this correlation was found to systematically underpredict the pressure drop data for long pipes [91], probably because the authors neglected the effect of air compressibility. Moreover, as pointed out by Klinzing, the Wen and Simon model was developed mainly for what is considered a wave like dense-phase flow, i.e. heavily loaded solids flow, not for slug flow [70].

First motivated by the considerable energy savings possible and later by the desire to reduce dust generation and maintain product quality, industry slowly began to focus on low velocity systems. As a consequence, research in the field of pneumatic conveying reoriented and dense-phase flow became an area of active research. In a first time, slug flow was not desired and components like by-pass were integrated in the conveying system to avoid the formation of slugs [58].

The real development of slug flow pneumatic conveying occurred in the mid seventies. Beside Muschelknautz and Krambrock who developed a model using a force balance for a moving packed bed that shows an exponential representation of the pressure drop with slug length, Legel and Schwedes [41] and Lippert [43] are further pioneers in the field of slug flow research. Their investigations involved a variety of materials, both cohesive and non cohesive in nature.

### 2.3.2. Fluid flow through packed beds

One approach to handling a gas-solid flow system is to make an analogy with a single-fluid system. This concept has proceeded many times of which the fluidised bed analysis is the most common. In this approach, slugs are considered as permeable structures through which the leakage of gas during the transport process is permitted. A survey of the literature revealed various mathematical expressions, which describe the pressure loss through such permeable structures. The existing models result from the correlation between different assumptions suggested by the authors and experimental data. Some of these correlations are applicable for the whole range of gas velocity while others are to be used at low or high fluid flow rates only.

The fundamental equation of permeability is the empirical equation developed by D'Arcy [16] who measured the flow of water through sands and sandstones and proposed the following expression:

$$v_f = K_D \cdot \frac{\Delta P}{L_{bed}} \quad (2.16)$$

where  $K_D$  is the permeability for the porous medium.

Later, the method of Blake [6, 14] gave rise to the following form of the D'Arcy equation valid for viscous flow:

$$v_f = \frac{\varepsilon^3}{k \cdot \eta_f \cdot S_p^2} \cdot \frac{\Delta P \cdot g}{L_{bed}} \quad (2.17)$$

where  $k = 5$  and  $S_p$  is the area of particle surface per unit volume of packed space.

This equation was developed further by Kozeny. Kozeny assumed the granular bed as equivalent to a group of parallel, similar channels, so that the total internal surface and the total internal volume are equal to the particle surface and the pores volume, respectively, in the bed itself. Kozeny also used the statement of Dupuit-Forchheimer [27] who realised that the apparent velocity must be less than the true velocity in the pores, i.e.  $v_{inst} = \frac{v_f}{\varepsilon}$  and assumed that the interstitial velocity is a constant from cross-section to cross-section of the bed. Based on these assumptions, he derived Eq. 2.18, in which he replaced the expression  $\frac{\varepsilon}{S_p}$  by the value  $m$  and  $k$  by the expression  $k_0 \cdot \left(\frac{L_e}{L_{bed}}\right)$ :

$$v_f = \frac{\varepsilon \cdot m^2}{k_0 \cdot \eta_f} \cdot \frac{\Delta P \cdot g}{L_{bed}} \cdot \left(\frac{L_{bed}}{L_e}\right)^2 \quad (2.18)$$

$L_e$  is the actual length of path taken by the fluid in traversing the depth  $L_{bed}$ . Kozeny determined from experimental investigations that the value for the expression  $k_0 \cdot \left(\frac{L_e}{L_{bed}}\right)$  is about 5. The Kozeny equation is identical to a dimensional analysis, which uses as parameter besides  $\Delta P$  the material properties and the characteristic length of the pores system.

Carman verified the equation proposed by Kozeny experimentally and showed that it provides very good agreement for a relatively homogeneous size of particles contained in the mixture. However,

contrary to Kozeny, other authors did not accept the Dupuit assumption and developed other expressions. For example, instead of regarding the bed as being equivalent to a group of parallel channels, Burke and Plummer considered the total resistance of the bed as the result of the sum of the separate resistances due to the individual particles composing it, as measured from the rate of free fall [11]. For a bed of spheres, the resulting equation for streamline flow was found to be:

$$v_f = \frac{d_p^2}{k_1 \cdot \eta_f} \cdot \frac{\varepsilon^2}{36 \cdot (1 - \varepsilon)} \cdot \frac{\Delta P \cdot g}{L_{bed}} \quad (2.19)$$

where  $k_1 = 0.5$ . However, since it has been shown by Blake that  $v_f$  is proportional to  $\frac{\varepsilon^3}{(1-\varepsilon)^2}$  and not to  $\frac{\varepsilon^2}{(1-\varepsilon)}$ , this equation had to be abandoned [14].

Based on theoretical and experimental investigations, Ergun found that the total energy losses in fixed beds are caused by simultaneous kinetic and viscous energy losses. The viscous energy losses are proportional to  $(1 - \varepsilon)^2 / \varepsilon^3$  and the kinetic energy losses to  $(1 - \varepsilon) / \varepsilon^3$ . Based on this concept, Ergun developed a general equation for pressure drop through fixed beds given by Eq. 4.21. The numerical coefficients 150 and 1.75 result from empirical investigations.

$$\frac{\Delta P}{L_{slug}} = 150 \cdot \frac{\eta \cdot (1 - \varepsilon)^2}{d_p^2 \cdot \varepsilon^3} \cdot v_{rel} + 1.75 \cdot \frac{\rho_b \cdot (1 - \varepsilon)}{d_p \cdot \varepsilon^3} \cdot v_{rel}^2 \quad (2.20)$$

Ergun examined this equation from the point of view of its dependence upon flow rate, fluid properties, fractional void volume and orientation, size, shape and surface of the granular solids. He found it to fit data for spheres, cylinders and crushed solids over a wide range of flow rates. However, some workers do not recommend the use of this model for slug flow, mainly because they consider that slugs do not behave as moving packed beds but have a certain amount of internal fluidisation, which is difficult to predict [70]. To determine the pressure loss by applying the Ergun equation, the fractional void volume within a slug has to be estimated. On the inspection of the form of Eq. 2.20, it becomes obvious that an accurate estimation of the voidage is required to determine the pressure loss since  $\varepsilon$  enters to second- and third-power terms. However, because slug flow is a dynamic process and the total weight of the granular material filling a given volume is not known, the porosity of a slug is difficult to measure directly. Therefore, slugs are mainly considered as displaying porosity equal to the porosity of the bulk material itself.

Rumpf criticised the various porosity functions based on experimental investigations presented in the literature [68]. Rumpf suggested that to determine a porosity function accurately, the porosity must be independent upon other parameters so that it can be varied without changing any other physical parameter, which is rarely the case. He also criticised the fact that some authors like Batel [5] introduced new parameters, which are not proved to represent real physical parameters. Therefore, he investigated the flow through pores independently from all existing models but using dimensional analysis.

He found that the resistance law for flow through packed columns is given by:

$$\frac{\Delta P}{\rho_f \cdot v_f^2} \cdot \frac{\bar{x}}{L_{bed}} = Const \cdot f(Re, \varepsilon) \quad (2.21)$$

where  $\bar{x}$  is a summary statistic that considers the porosity of the package, the mean particle size as well as the dispersion and form parameters.

Rumpf pointed out that the mainly used mathematical equations of Carman and Kozeny, Ergun and other authors are variants from this equation. In addition, Rumpf investigated porosity functions with porosity as single parameter. For this purpose, he prepared beds of polystyrene granules with different porosities by mixing the granules with different quantities of sugar. He sealed the contact points by treating the whole mixture with carbon tetrachloride and drying it and finally rinsed the sugar. Using this method, he was able to obtain some solid nets with a porosity varying from 0.35 to 0.68. He showed that the power function  $\varepsilon^{-5.5}$  or the function  $4 \cdot (1 - \varepsilon) \cdot \varepsilon^{-4.55}$  describes the porosity more accurately than the porosity function  $\frac{(1-\varepsilon)^2}{\varepsilon^3}$ . Nemeč suggested that the range of porosities investigated by Rumpf includes higher porosities than normally encountered in beds composed of spherical particles, which could lead to non-uniform packed beds, which, in turn, could affect the results [59].

### 2.3.3. Bulk solids mechanics

**2.3.3.1. The Janssen theory** As early as 1895, the German engineer Janssen published a paper on the behaviour of grains in storage silos [32]. He noticed that contrary to fluids that exert hydrostatic pressure, corns contained in a quadratic silo exert a bottom pressure which is much smaller than the weight of the cell content. He recognized the existence of friction between corn and container wall and determined a wall friction coefficient  $f_w$  that he assumed to be a constant over the filling height, i.e. for variable wall pressure. The wall friction increases with increasing filling height, leading to the increase of the wall pressure up to a certain value where a further increase is no more noticeable. At this point, the friction between material and wall is equal to the weight of the material above and the pressure on the walls reaches its maximum. The maximum wall pressure  $p_{s,max}$  was expressed by:

$$p_{s,max} = \frac{\gamma \cdot s^2}{4 \cdot \mu_w} \quad (2.22)$$

Assuming that vertical and horizontal pressure are proportional, Janssen performed a force balance on a bulk element (Eq. 2.23) to derive an expression for the vertical pressure given by Eq. 2.24.

$$F((p + dp) - p) = \gamma \cdot F \cdot dx - \mu_w \cdot p_s \cdot u \cdot dh \quad (2.23)$$

$$p = \frac{s \cdot \gamma}{4K} \cdot \left( 1 - \exp\left(-4K \cdot \frac{h}{s}\right) \right) \quad (2.24)$$

where

$$K = \frac{p_s \cdot \mu_w}{p} \quad (2.25)$$

Eq. 2.23 and 2.24 constitute a major concept in the determination of the stress granular materials exert on the walls of containers, silos and pipes. The relevance of the Janssen work is proved by the recent publication of Sperl who translated the original paper from German to English and added comments to allow better understanding of the original work [81].

**2.3.3.2. In-plane stress analysis of cohesionless bulk materials** Under flow conditions and due to the pressure gradient between the front and the back of a slug, external forces acting in the conveying direction are commonly assumed to compress the particles inside the slug in the axial  $x$ -direction. Because the pipe wall prevents the particles from moving in the radial direction, the axial compression stress  $\sigma_x$  causes a radial compression stress  $\sigma_r$  perpendicular to the pipe wall. Fig 2.6 shows the stresses acting on a compressed horizontal slug. At the boundary between particles and pipe wall, failure occurs and the Coulomb failure criterion applies. Hence, the shear stress at the wall  $\tau_w$  is related to the normal stress by:

$$\tau_w = \sigma_{r/w} \cdot \tan \phi_w + c_w \quad (2.26)$$

where  $\sigma_{r/w}$  is the radial compression stress at the wall and  $c_w = 0$  for a cohesionless material. The expression for  $\sigma_{r/w}$  can be derived from the analysis of Mohr's circle diagram.

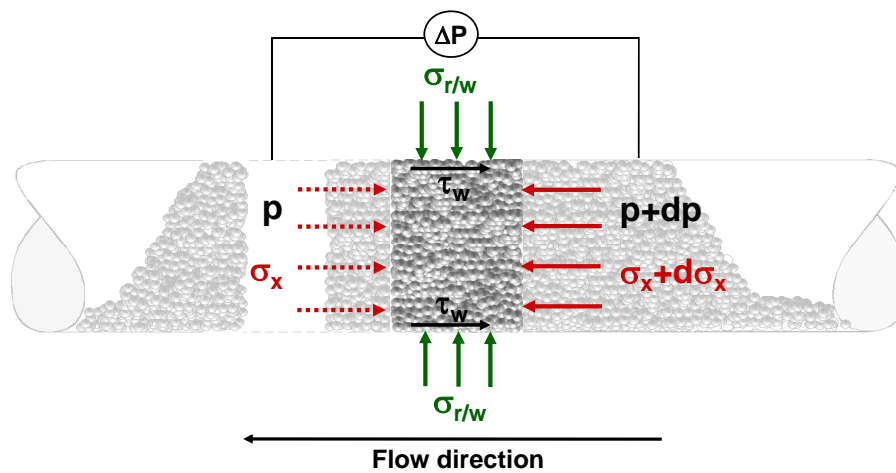


Figure 2.6: Stresses acting on a compressed slug horizontally conveyed

Mohr's circle is a two-dimensional graphical representation of the state of stress of an element P within an infinite homogeneous particulate medium that is commonly used to describe the strength of a bulk material already submitted to a given consolidation degree. The strength is represented on a shear-compressive stress diagram where abscissa  $\sigma_n$  and ordinate  $\tau_n$  of each point located on a Mohr

circle are the normal stress and shear stress components, respectively, acting on a particular cutting plane with a unit vector  $\vec{n}$  with components  $(n_1, n_2, n_3)$  (Fig. 2.7). In other words, the circumference of the circle is the locus of points that represent the states of stress on individual planes at all their orientations. To construct the Mohr circle for a general three-dimensional case of stresses at a point, the values of the principal stresses must be evaluated. It is assumed that  $\sigma_1 > \sigma_3 > \sigma_2$ . For many applications in bulk solids technology, it is sufficient to consider only one plane. As a rule, the plane considered is the one in which the smallest minor and largest major principal stresses and hence the greatest shear stress that is responsible for the movement of particles relative to each other, i.e. the flow of bulk solid are acting [71]. In this case, one refers to a two-dimensional state of stress where the third principal stress  $\sigma_3$  is neglected.

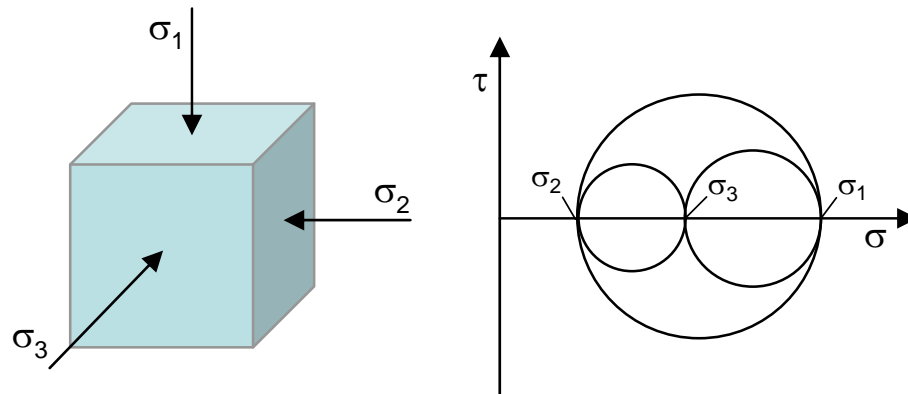


Figure 2.7: Volume element with the three principal stresses acting perpendicular to each other (on the left hand side); Stress circles corresponding to the three principal stress planes (on the right hand side)

In a general state of stress, the infinitesimal volume element considered (Fig. 2.8) is subjected to compressive stresses  $\sigma_x$  and  $\sigma_y$  as well as to shear stresses  $\tau_{xy}$  and  $\tau_{yx}$ .

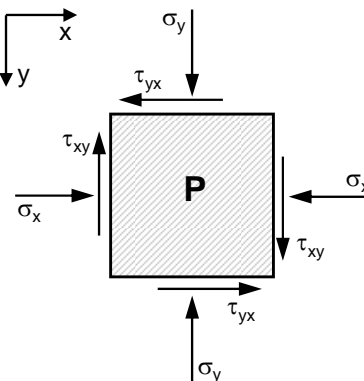


Figure 2.8: Two-dimensional stress state on a volume element

Fig. 2.9 shows the possible states of stress on an element P, represented by a series of Mohr circles. Basically, this element P can display three different states represented in Fig. 2.9 by the Mohr circles with the centres  $M_0$ ,  $M_1$  and  $M_2$ . The yield locus (YL), also named Mohr circle envelope, and the wall yield



locus (WYL) are boundaries defining in which state of flow an element of a particulate medium is. The wall yield locus is defined by the friction angle  $\phi_w$  between particulate medium and wall plane whereas the yield locus is defined by the internal friction angle  $\phi$  that is the friction angle between particles. When the Mohr circle lies completely under the WYL (Mohr circle  $M_0$ ), the particulate medium is in a static state, which means that all the particles composing the bulk are stationary. This is the case when the supply gas velocity is not high enough to transport the material along the conveying pipeline. The second state of the particulate medium is represented by the Mohr circle  $M_1$  that intersects the WYL but still lies completely under the YL. In this state, shearing occurs at the boundary between bulk material and wall but the particles are still fixed relative to each other. This state is used to describe slug flow where slugs are usually considered as a rigid body slipping along the wall plane. The points representing the plane of the wall lie at  $A_1$  and  $A_2$ . The third state of the bulk material is represented by the Mohr circle  $M_2$  that is tangent to the Mohr failure envelope YL. In this state, relative movement exists between the particles. The particles adjacent to the wall plane slip along the wall and  $B_1$  or  $B_2$  represent the plane of the wall. The state of stress acting at point  $C$  is the theoretical limiting state of stress on the failure plane at failure. Consequently, no state of stress and hence no Mohr's circle can exist above the Mohr circle envelope since failure occurs in the bulk material [52].

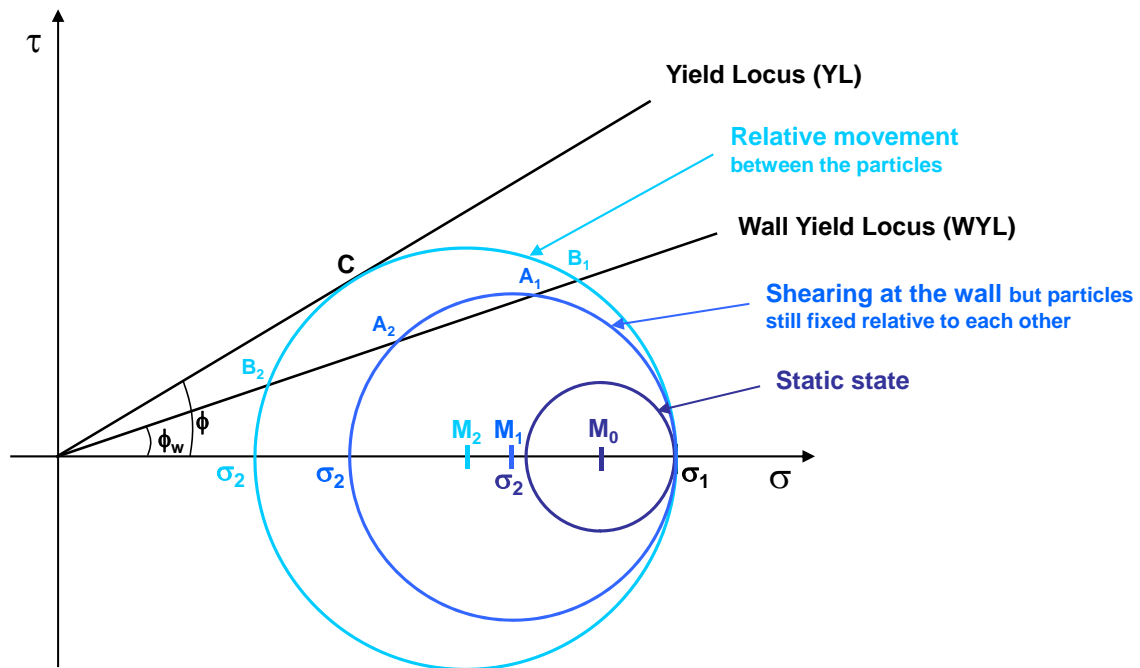


Figure 2.9: Possible states of stress on an element P, represented by a series of Mohr's circles

Therefore, the greatest stress states are given by the Mohr circle  $M_2$  tangent to the yield locus. In this case, the Coulomb failure criterion given by Eq. 2.26 applies and for a cohesionless material ( $c_w = 0$ ), the ratio between the wall shear stress and the radial stress is equal to the wall friction factor given by  $\mu_w = \tan(\phi_w)$ .

Since granular materials are frictional, it is almost impossible to calculate  $\sigma_{r/w}$  exactly. As shown in Fig. 2.10, even for a defined principal stress  $\sigma_1$ , there are an infinite number of possible Mohr circles

representing the stress state of a moving slug. Those Mohr circles are located between the YL and the WYL of the material, i.e. they satisfy the criterion that the slug slips along the pipe wall but there is no relative motion between the slug particles. However, a unique Mohr circle exists that represents the actual stress state of the slug. Even if the actual stress state and the corresponding static friction angle  $\phi_s$  are difficult to predict accurately, it is possible to predict the range within which the stresses must lie whose boundaries are given by failure occurrence. The two extremes are known as active and passive failures, which correspond to pulling and pushing failure of the slug. The active failure occurs at the active stress state that is when the axial stress is greater than the radial stress. The passive failure occurs at the other possible stress state that is when the radial stress is greater than the axial stress. Fig. 2.11 shows for a given stress state measured at pipe wall, i.e. for a given couple of values  $\tau_w / \sigma_{r/w}$  the two Mohr circles corresponding to active and passive case.

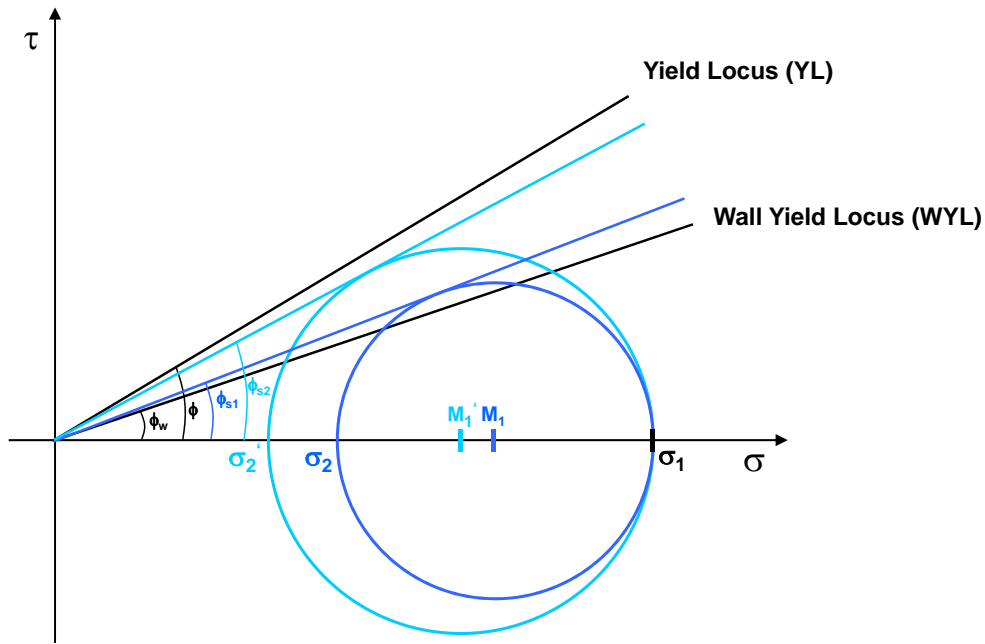


Figure 2.10: Examples of Mohr circles corresponding to the stress state occurring by slug flow

The stress transmission coefficient  $K_w$ , which relates radial and axial stress is commonly used to describe the stress state in an element of particulate medium :

$$K_w = \frac{\sigma_r}{\sigma_x} \quad (2.27)$$

Using trigonometry, the stress transmission coefficient can be determined as follows [38, 51]:

For active stress state:

$$K_{w\_active} = \frac{1 - \sin \phi \cdot \cos (\omega - \phi_w)}{1 + \sin \phi \cdot \cos (\omega - \phi_w)} \quad (2.28)$$

where  $\omega$  is the angle as defined in Fig. 2.11 and

$$\sin \omega = \frac{\sin \phi_w}{\sin \phi_s} \quad (2.29)$$

For passive stress state:

$$K_{w\_passive} = \frac{1 + \sin \phi \cdot \cos (\omega + \phi_w)}{1 - \sin \phi \cdot \cos (\omega + \phi_w)} \quad (2.30)$$

During conveying, as the bulk material slips along the pipeline wall,  $\phi_w \leq \phi_s \leq \phi$ . For the two extremes, i.e. when failure occurs,  $\phi_s = \phi$ .

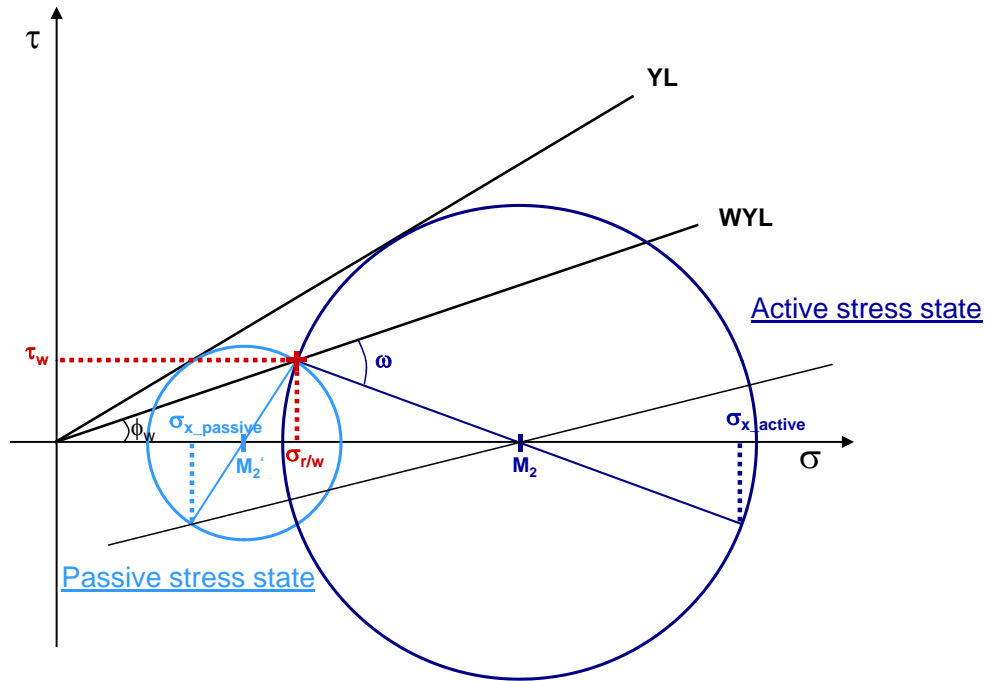


Figure 2.11: The two Mohr circles corresponding to active and passive stress state for a given couple of values  $\tau_w / \sigma_{r/w}$

The stress transmission coefficient  $K_w$  can be found in all predictive models for the pressure loss based on a bulk solids mechanics approach. Hence, the determination of  $K_w$  is key to achieve accurate pressure loss prediction by applying those models. This explains why the determination of the stress state within a moving slug is an area of ongoing research that involves both theoretical and experimental investigations. Konrad was one of the first researcher to investigate the behaviour of slugs by applying the common stress relationships seen in bulk solids and soil analysis in conjunction with the basic force balances [38]. Konrad assumed that passive failure occurs in horizontal slug flow pneumatic conveying. Klinzing stated that the pressure drop in horizontal pipes is governed by the wall shear stress and assumed the failure to be passive as well [2]. On the other hand, after having developed an expression to calculate the static internal friction angle  $\phi_s$  based on values of wall friction angle  $\phi_w$ , Mi calculated values for the stress transmission coefficient and found that all values for the materials tested were less

than 1. This led him to the conclusion that the stress state in slugs should be in the active stress case during slug flow.

### 2.3.4. State-diagram predictive approach of stable strand flow

The pressure drop required for solids transport is usually described using dimensionless groups such as  $\lambda_z = \lambda_z(Fr)$ . However, Wirth pointed out that the variation of pipe diameter results in a different representation  $\lambda_z = \lambda_z(Fr)$  so that such a correlation does not permit to realise the scale-up of a conveying system. Hence, Wirth proposed a new concept to predict the pressure drop in form of a state-diagram where the dimensionless pressure loss is represented as a function of the Froude number, which contains both particle fall velocity and pipe diameter [97]. Wirth's motivation to formulate a prediction procedure in form of a state-diagram was also to keep a certain clearness in the results of the prediction procedure.

Wirth's approach is based on the momentum transfer of particles moving with different velocities. To realise the balance of the forces acting in horizontal pneumatic conveying, he divided the pipe cross-section into two regions. The first region is a moving strand, the second region is a suspension of particles flowing evenly above it. Wirth described the stresses acting on the strand surface in stable strand flow and developed a state-diagram to predict the flow type based on the momentum transfer of the particles hitting the strand surface.

Later, in the case of horizontal granular material conveying, Wypych identified across the pipeline section a three-layer flow structure consisting of a suspension flow over a strand flow over a stationary layer or slowly moving bed (Fig. 2.12). Based on this observation, he extended the 2-layer-model proposed by Wirth to a 3-layer-model [99].

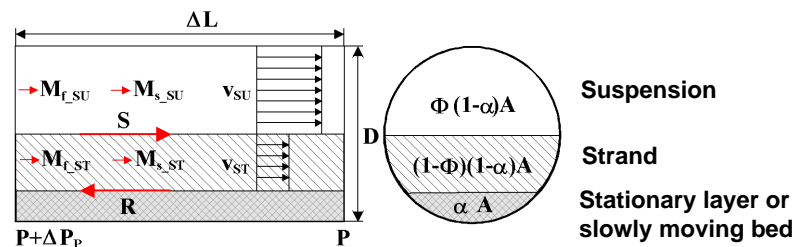


Figure 2.12: 3-layer-model proposed by Wypych [99]

The approach of Wypych to establish the 3-layer-model is based on the physical and mathematical concepts derived by Wirth. Three basic assumptions were taken into account: all the particles transported in the suspension above the strand are moving at the velocity of the air, all the particles transported in the strand are moving at the velocity of the air in the strand and the velocity of the slowly moving bed is negligible.

From a force balance involving the additional pressure gradient  $\Delta P$ , the shear stress  $S$  between suspension and strand resulting from particles of the suspension hitting the strand surface and the

friction force  $R$  between the strand and the stationary layer that acts in the opposite direction (Fig. 2.12), the dimensionless pressure loss can be expressed as following:

$$\Delta P_Z = \frac{\Delta P}{f_s \cdot \rho_s \cdot \left(1 - \frac{\rho_f}{\rho_s}\right) \cdot (1 - \varepsilon_{st}) \cdot g \cdot l_h} \quad (2.31)$$

where  $\Delta P$  is the pressure gradient that can be predicted for example by applying the iterative method proposed by Yi [100] (see Section 3.5) and  $\varepsilon_{st}$  is the strand porosity, which is approximately equal to the bulk porosity.

Besides, the non-dimensional pressure loss is correlated to the fraction of the pipe cross-section over the stationary layer or slowly moving bed  $\Phi$  (Fig. 2.12) as following:

$$\Delta P_Z = (1 - \Phi) \quad (2.32)$$

Therefore, in stable strand flow, the cross-section fraction of the pipe covered by the stationary or slowly moving layer  $\alpha$  is provided if the pressure gradient is known.

The number of particles transported in the suspension is very small and the velocity of the lower layer can be neglected. Hence, the material can be assumed to be transported within the strand only. With similar considerations, the mass of air is assumed to be transported within the suspension only. From the combination of mass of gas and solids balances, the following equation for the velocity ratio  $\eta$  between particles and conveying gas is obtained:

$$\eta(\Phi) = \frac{v_{st}(\Phi)}{v_{su}(\Phi)} = \frac{\Phi}{1 - \Phi} \cdot \left[ \frac{\rho_s \cdot (1 - \varepsilon_{st})}{\rho_f \cdot \mu_{st}} - \varepsilon_{st} \right]^{-1} \quad (2.33)$$

Using Eq. 2.32 and Eq. 2.33, the dimensionless pressure loss can be expressed according to the mass flow ratio  $\mu$  and the velocity ratio  $\eta$ :

$$\Delta P_Z(\eta, \mu) = \frac{1}{1 + \left( \frac{\rho_s}{\rho_f} \cdot \frac{1 - \varepsilon}{\mu} - \varepsilon \right) \cdot \eta} \quad (2.34)$$

The shear stress  $S$  acting on the interface strand/suspension (Fig. 2.12) is caused by the exchange of moving particles with different velocities. Through their impulse with the strand, particles of the suspension are slowed down to the velocity of the strand. For each of those particles, a particle of the strand is striped out and accelerated at the velocity of the suspension. From this assumption and the combination of mass and force balances, the gas velocity can be expressed in the form of the dimensionless friction number  $Fr_i^2$ :

$$Fr_i^2 = \frac{v_f^2}{f_s \cdot \frac{\rho_s}{\rho_f} \cdot \left(1 - \frac{\rho_f}{\rho_s}\right) \cdot (1 - \varepsilon_{st}) \cdot D \cdot g} \quad (2.35)$$

Moreover, the friction number depends of both the mass flow ratio  $\mu$  and the velocity ratio  $\eta$  and can be expressed as following:

$$Fri^2(\eta, \mu) = \sqrt{\frac{1}{\lambda} \cdot \frac{\pi}{4} \cdot \frac{1}{1 - \frac{\rho_f}{\rho_s} \cdot \frac{\mu \cdot \varepsilon}{1 - \varepsilon}} \cdot \frac{1}{1 - \eta} \cdot \frac{\phi(\eta, \mu)^3 \cdot (1 - \phi(\eta, \mu)) \cdot (1 - \alpha(\eta, \mu))}{[4 \cdot (1 - \alpha(\eta, \mu)) \cdot \phi(\eta, \mu) \cdot [1 - (1 - \alpha(\eta, \mu)) \cdot \phi(\eta, \mu)]]^{\frac{1}{3}}}} \quad (2.36)$$

where  $\alpha$  is the maximum thickness of the slowly moving layer that can be driven by the friction  $R$  between the strand and the stationary layer:

$$\alpha(\eta, \mu) = \frac{\Delta P(\eta, \mu) \cdot (f_s - f_w)}{f_s \cdot \Delta P(\eta, \mu) + f_w \cdot (1 - \Delta P(\eta, \mu))} \quad (2.37)$$

and  $\lambda$  is the strand momentum coefficient, which was approximated experimentally by Wirth with  $\lambda_w = 0.0826$  [96].

As a consequence, using the dimensionless expressions for the pressure loss and gas velocity given by Eq. 2.34 and Eq. 2.36, respectively, the characteristic curves for a specific installation can be depicted in a dimensionless state-diagram for dense-phase pneumatic conveying. In addition, based on the balances of mass, forces and momentum and the unstable flow forming mechanism, Wirth and Wypych described mathematically the boundaries of the transition zone between strand flow and slug flow. According to these boundaries, three different types of operating points are discerned, which are located in the dimensionless state-diagram in separate areas corresponding to the different dense-phase flow types: strand flow, slug flow and unstable flow (Fig. 2.13).

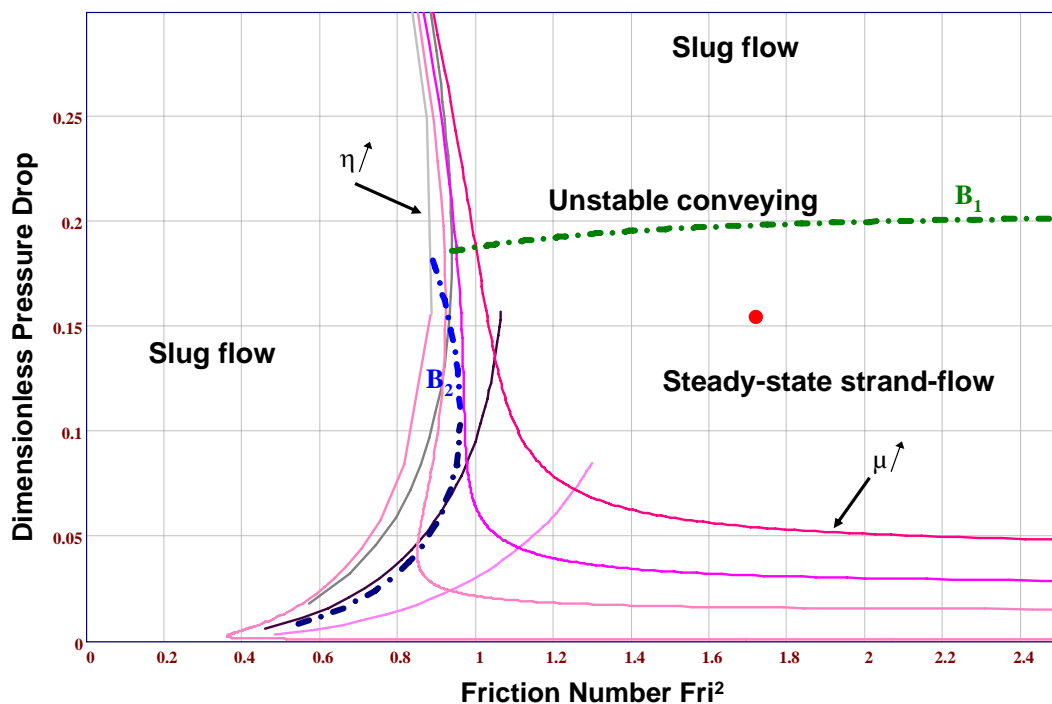


Figure 2.13: Example of dimensionless state-diagram for dense-phase pneumatic conveying

From a physical point of view, the boundaries separate operating points whose response to changes occurring in the process differs. From a mathematical point of view, the first boundary of steady-state strand flow, called first limit of stable saltation conveying, separates the points having a positive slope of the curves  $\eta = Const.$  from that having a negative slope (boundary  $B_1$  in Fig. 2.13):

$$B_1(\eta, \mu) \text{ for } \frac{\frac{d}{d\mu} Fri(\eta, \mu)}{\frac{d}{d\mu} \Delta P(\eta, \mu)} = 0$$

The second limit of stable saltation conveying separates the points having a positive slope of the curves  $\mu = Const.$  from that having a negative slope (boundary  $B_2$  in Fig. 2.13) :

$$B_2(\eta, \mu) \text{ for } \frac{\frac{d}{d\eta} Fri(\eta, \mu)}{\frac{d}{d\eta} \Delta P(\eta, \mu)} = 0$$

According to the gas velocity, one or two values of  $\eta$  are found to solve  $B_2(\eta, \mu) = 0$ . From these solutions, the whole boundary line  $B_2$  can be depicted. In the area close to the boundaries, little modifications of the operating parameters lead to significant changes of the flow-type. Therefore, the flow is particularly unstable in those operating areas. Above the horizontal boundary  $B_1$  and on the left hand side of boundary  $B_2$ , slug flow takes place. Below boundary  $B_1$  and on the right hand side of boundary  $B_2$ , steady-state strand flow happens.

Using Eq. 2.34 and Eq. 2.36 as well an experimental or predicted value for the pressure loss, the operating point for a given gas and solids mass flow rate can be located in the dimensionless state-diagram and the flow-type occurring in the pipeline system can be determined. For example, the red point in Fig. 2.13 shows an operating point where steady-state strand flow occurs.

### 2.3.5. Numerical analysis to simulate dense-phase flow

Some authors took up the challenge to model dense-phase gas-particle flow using exclusively computer tools. Different methods are used according to the scale in which the phases are considered, i.e. macro or micro-scale. Both phases, i.e. solids and gas phase are treated as well as their interactions. One method consists in combining Computer Fluid Dynamics (CFD) to simulate the fluid flow with Discrete Element Method (DEM) to simulate the behaviour of the single particles or the plug as unity. The main difficulty is that the phases are affected by each other and due to the high solids concentration, in addition to the two-way coupling, the particle-particle interactions have to be taken into account. Dense-phase pneumatic conveying corresponds in the field of numerical analysis to a typical example of contact-dominated flows in multiphase flows. Many papers have been reported on this topic in the last twenty years. Tsuji and Sommerfeld belong to the small circle of authors who performed relevant work in the area of numerical simulation of dense-phase pneumatic conveying. A summarise of the most important studies of particle-laden gas flows in pipes or channels is given by Sommerfeld who classified

the works into two tables according to whether the investigations were mainly experimental oriented or concern modelling and numerical analysis [79].

Three theoretical approaches can be used for modelling dense-phase flow numerically: the two-fluid theory, the Eulerian granular approach and the discrete element method. The two first one are based on macroscopical balance equations of mass, momentum and energy for both the gas and the solids phases. In the DEMs and the Eulerian-Lagrangian approach, the gas phase is considered as the continuous phase in which the particles are dispersed. Even if significant improvements have been made in the last years, DEM still does not allow the calculation of full-scale cases because of computation limitations.

To describe numerically the particle motion in a horizontal pipe, the calculation of wall collisions and inter-particle collisions is of great importance. Inter-particle collisions can be described by deterministic, i.e. randomness as well as stochastic models. Among the stochastic approaches, the application of a stochastic model in the frame of the Euler/Lagrange approach can be cited [80, 61] where the occurrence of a collision is decided based on the collision probability according to kinetic theory of gases. The occurrence of collisions and the fluid turbulences lead to random velocity fluctuations of the particles that cause momentum and energy transfers. They, in turn, give rise to macroscopic phase properties such as fluid viscosity and thermal conductivity. This is the concept used by the Eulerian granular method, which employs the kinetic theory of rare gases to model the granular phase properties such as pressure, temperature and viscosity.

When the particles composing a slug constitute a packed bed, contacts between particles can be considered of long duration and frictional. This results in the existence of a frictional stress. On the other hand, when a certain amount of free volume exists inside of a slug, the contacts between particles can be considered as temporary and collisional. This part of the stress consists of kinetic and collisional stresses. Therefore, an analogy between particles and molecules can be drawn. However, when the particle concentration is so high as to be close to the packed state, where the frictional contact may play a decisive role in the transport of the particle phase, this analogy is not valid anymore. At a packed state, the bed is crammed with particles, and hence the frictional mechanism of particle-quantity transfer that may prevail over the other forces should be considered as well. For this reason, according to Wang, the total stress should be approximated as the sum of frictional and kinetic-collisional contributions as if each of them would act alone [87].

The use of numerical analysis to simulate dense-phase flow and particularly slug flow presents advantage in that slug flow does not have to be considered as steady-state flow but as the dynamic process that it actually is.

## **2.4. Thirty five years of research to understand slug flow**

The basic concepts that are still used to describe slug flow were originally based on flow observations coupled with pressure measurements. It has been early recognised that many parameters characterising the air flow, the material transported and the conveying pipeline itself significantly influence slug flow. However, the influence of the key parameters such as slug velocity is mostly difficult to predict.



Therefore, while experimental work is still carried out to investigate the influence and relationship of the key parameters, the number of numerical studies in the field of slug flow pneumatic conveying keeps increasing. This section aims to give a brief overview of the key results that can be found in the literature with respect to slug flow characterisation. However, it should be pointed out that this list is not exhaustive but focuses on relevant results that can be correlated with the experimental results obtained in this work and described in Section 5.

### 2.4.1. Flow observation

Ramachandran was possibly the first to study the flow of solid-gas mixtures using long transparent pipes to enable flow observation in large pipe diameters [63]. He concluded that many modes exist by which solids-gas mixtures flow in the transport line and differentiated between dunes flow over a thick or thin layer of stationary solids and slug flow. Ramachandran noticed that the ease of movement is better in the case of coarser particles due to lower compaction of the mass. He also noticed that the material follows different modes of flow along the pipeline and cited three possible reasons to explain the high pressure drop and low velocity in the initial regions, which gradually change to low pressure drop and higher velocity at the end of the pipeline. According to Ramachandran, the difference may result from different resistance for the movement of solids according to the type of flow, the resistance by slug flow being lower than the resistance by dune flow. The high pressure drop at the pipeline inlet may be due to the energy losses initially required to accelerate the solids. Or the expansion of the air from higher to lower pressures may lead to the increase of the size of the interstices between particles, i.e. to the decrease of the compaction degree which, in turn, leads to the increase of the particle velocity.

Between the slugs, the upper part of the pipe contains moving air with some dispersed particles while the lower part of the pipe is filled with stationary particles. Observations of the flow pattern led Konrad to the premise that the material is conveyed only in the slugs and in the regions just in front of and behind them [38]. The material is picked up from the stationary layer by the moving slug, transported along the pipe and then dropped off the back of the slug to form a stationary layer of the same thickness further along the pipe. For this reason, slug flow should not be considered as a steady state transport, i.e. the transport is not characterised by constant pressure, air and solids flow with respect to cycle time. The fluctuations in the pressure profile are principally due to the variation in the number of slugs present in the pipeline. By applying a gas-solid analogy, Konrad described the cross-sectional area ratio of stationary bed to pipe  $\alpha$  as a function of the particle velocity:

$$\alpha = \frac{1}{1 + \frac{v_p}{0.542\sqrt{g \cdot D}}} \quad (2.38)$$

Later, Mi investigated experimentally the thickness of the stationary bed and found that the equation proposed by Konrad shows good agreement [51]. However, Krull reported that the analogy gas/liquid appears to underestimate the area occupied by the stationary layer across the range of slug velocities he tested [39]. Kuang traced numerically the process of particle exchange between settled layer and

slug that occurs in horizontal slug flow [40]. He found that the particles in the centre of a settled layer move into the upper part of a slug while the particles initially located in the lower part of a settled layer move into the lower area of the slug.

Besides the wave transport, many workers including Konrad assumed that plugs are like moving packed beds, so that all particles within each plug move with the same velocity and are fixed relative to each other [37].

#### 2.4.2. Particle, slug and gas velocity

Tomita investigated slug flow pneumatic conveying in horizontal pipeline numerically [83]. He used the method of characteristics to solve one-dimensional unsteady equations for the isothermal gas flow coupled with equations of motion for the slugs. He found that the gas velocity increases preceding the slug arrival and mentioned that this would explain the jump of particles in front of the slug that is frequently observed. He also found that the slug velocity is not always constant but changes sinusously. Mi [51] investigated experimentally the slug velocity by calculating the cross-correlation function of wall pressure signals. He found that for a given material, the values of slug velocity are independent of the solids mass flow rate and appear to be described by a linear correlation of the form

$$v_{slug} = k_s \cdot (v_f - v_{f\_min}) \quad (2.39)$$

where  $v_{f\_min}$  is the minimum air velocity for horizontal flow. Krull also found a reasonable linear trend between slug velocity and superficial air velocity for the materials he tested [39]. Klinzing suggested as a rough estimate of slug velocity that it achieves about 70% of the air velocity in horizontal pipe [2].

Using numerical analysis of horizontal slug flow of Polyethylene granules, Kuang described the profile of gas velocity qualitatively [40]. He reported that the gas mainly flows in the empty part of the pipe over a settled layer before encountering a slug, then redistributes itself to cover the entire cross-sectional area at the rear of a slug and finally becomes a partial flow again after passing through the slug. When the gas flow rate is low and the particles in a settled layer are stationary, he sometimes observed a backflow of gas inside the settled layer before and after a slug. The results of the numerical investigations carried out by Levy indicated that slugs are continuously created and destructed so that the determination of slug velocity by the method of cross-correlation between various locations of radial or axial pressure measurement that have large separation between them is not suitable, even if it has been widely used [42].

#### 2.4.3. Slug length

Daoud and Guigon investigated slugs of Polyethylene pellets and noticed that the plug length decreases with the gas flow rate while for a given mass flow rate, the plug length increases along the pipe. They explained the changes of plug length and velocity along the pipe by establishing relationships based on

mass balances at the front face and rear of the plug. For this purpose, they defined the velocity of the front and rear as the sum of the solids velocity in the plug and the velocity of the particles being picked up at the front or deposited at the rear, respectively. They explained the increase in the plug length along the pipe by the velocity difference between the front and rear of the plug [15]. Hitt achieved similar results [31]. By investigating the transport of Polyethylene pellets, Hitt found that the waves increase in length along the pipeline. Mason identified the same phenomenon and observed further over the pipeline short waves close together with a long gap before another series of waves [45]. This implies that the waves increase in length and then break up. Krull could not establish any direct correlation between the individual slug length and the air mass flow rate set and suggested that factors such as the pressure gradient and the slug velocity largely influence the length of a slug [39]. The numerical simulations carried out by Levy [42] revealed that both the shape and the length of the slugs change along the pipe.

#### 2.4.4. Prediction of the shape of the gas-particle interface

Slugs of particulate material are separated by what are frequently called gas slugs. Konrad [37] investigated the shape of the gas-particle interface between two slugs of cohesionless particles pneumatically conveyed through a horizontal pipeline. He predicted the shape of the particle free surface between two slugs by assuming that the interfacial slope is not affected by the air pressure between two slugs but only by the air pressure distribution within the bulk solids, which is governed by Laplace's equation. Using both prediction and experimental observations, he showed that the back surface of a slug is steeper than the front surface and gets progressively less steep from the top to the bottom. On the contrary, the front surface is steeper at the bottom than at the top, which may lead to instabilities. As a further result, he showed that an increase in voidage is often observed at the front surface, which is rather diffuse than sharp. For his prediction, he neglected the effect of the pipe wall on the air velocity profile and suggested that the retard of the air flow due to the wall effect may lead the front slope to be steeper close to the pipe wall than his prediction would suggest. Levy cited several working groups including Konrad, Tsuji, Mason and Ramakrishnan that also have described the shape of the slugs with the slope at the rear steeper than at the front face [42].

#### 2.4.5. Saltation, pick-up and optimal operating velocity

Many authors have been interested in the determination of pick-up or saltation velocities. Zenz determined experimentally the saltation velocity of single particles and proposed a graphic representation that involves the particle Reynolds-number  $Re_p$  and the drag coefficient  $C_D$ . Matsumoto developed experimentally a correlation for the minimum transport velocity in horizontal pneumatic conveying with respect to solids loading ratio, pipe diameter and material characteristics [48]. Cabrejos and Klinzing also developed a technique for finding the pick-up velocity of solid particles in horizontal pneumatic conveying [12]. As the free cross-section area increases, the air velocity over the layer decreases and so does the capacity of the stream to pick up more particles. By describing the interaction between the

forces acting on a particle, they developed a model for the incipient motion of a single sphere initially at rest on the bottom of a horizontal pipe and subjected to a steady fully developed turbulent flow of air. They used the term of saltation velocity to define the velocity in a horizontal line at which the particles start to drop out of the suspension and settle on the bottom of the pipe. Furthermore, they defined the pick-up velocity as the fluid velocity required to resuspend a particle initially at rest on the bottom of a line. They found as expected that the pick-up velocity is higher than the saltation velocity. In addition, they emphasised that the pick-up velocity is difficult to predict because this parameter is influenced by a multitude of variables including the physical characteristics of the material, the coefficient of sliding friction and the interactions between particles. In another approach, Davies suggested the theoretical calculation of critical velocities to maintain solids in suspension in horizontal pipes by applying the turbulence theory [18].

Since the definition given to the saltation velocity varies from one worker to the other, the comparison between the various results published in the literature is difficult. For instance, Meyers [49] defined the saltation velocity for coarse particles as the optimal operating condition of a horizontal pneumatic conveying system (pressure minimum point) whereas Matsumoto [48] defined it as the minimum superficial velocity required for the transport of solids without the formation of a stationary bed on the bottom of the horizontal pipe [12]. The saltation velocity is frequently defined as the gas velocity where the minimum pressure drop occurs. This saltation point coincides with the point at which the particles are observed to drop out of suspension and either remain in a stationary layer on the bottom of the pipe or travel along the pipe by rolling or sliding [98].

Other investigators like Kano have been interested in the optimisation of the conveying process from an energetic point of view [35, 34]. By investigating the optimum conditions for slug flow pneumatic conveying of granular material, Kano showed that the power required to convey a slug is lower by using a low air pressure and a pipe with a large internal diameter. He reported that a shorter length of slug leads to a greater transport efficiency. The prediction of the pressure minimum curve has also been a topic of active research for Rizk [66].

#### **2.4.6. Porosity distribution / Permeation through a slug**

Aziz and Klinzing investigated the pressure loss variation across a plug according to the possibility for the gas to permeate through the plug [3]. For this purpose, they conveyed plugs of fine powder whose front or back section had been previously consolidated to block the throughput of transport gas either into the plug or out from it. They concluded that the pressure drop across the plug varies either linearly if the permeation of the transport gas into the plug is allowed or in an exponential fashion if the plug is consolidated at its back and its initial dense state solid packing is maintained. They emphasised that the consolidation states of a plug determine what control the wall friction. The wall friction results either from the classical physics wall shear given as standard product of the plug weight and coefficient of wall sliding friction or from the powder mechanics wall friction that results from the Mohr circle diagram. The first one has been used in the derivation of pressure drop models like the Weber pressure drop equation whereas the second one has found application primarily in the theory of Konrad and later

in the theories that emerged from it. Therefore, they concluded that the transport of material is made easier, if a certain amount of permeation is possible.

A direct method to estimate the filling degree over the pipe cross-section consists in measuring capacitance. This method was employed by Mason who used sound and capacitance techniques to measure the average value of the quantity at a pipe cross-section [46]. Williams also used Electrical Capacitance Tomography analysis to investigate the internal flow structure of the transient material pulses of fine powders within a pneumatic conveyor. This method re-enforces the current limitations of steady-state approaches [93]. Kuang investigated the porosity distribution within a slug of Polyethylene pellets by means of discrete particle simulation and found that in axial direction, a lower solid concentration emerges on the front and tail of a slug whereas in radial direction, the solid concentration is denser in the centre of a slug than close to the wall [40]. In addition, he observed a region with high solid concentration at the bottom of a settled layer in front of a slug and suggested that it is caused by the compression of the slug. He also observed that although the distribution of solid concentration in the pipe is not uniform, the average solid concentration of a slug across the pipe cross-section fluctuates around a constant that is lower than the bulk density.

#### **2.4.7. Cross-sectional pressure profile, stress states and stress transmission coefficient**

To investigate the pressure profile across the pipe cross-section, Mason designed a special conveying system where the superficial velocity of the transport gas can be varied whilst the mass flow rates of gas and solid can be closely controlled and are kept a constant [47]. He recorded the pressure difference in cross-section and found that the pressure difference is caused by the distorted gas flow structure in the pipe cross-section as gas flows from the gap above a stationary layer into a slug and then out through the front end of the slug. He observed a pressure peak occurring at the back of the slug.

Cairns [13] investigated experimentally slug flow in horizontal pipe. He reported that the pressure difference in a cross-section is negligible before the arrival of a slug, the pressure in the top area of the cross-section increases as the slug approaches and the pressure reaches a maximum at the rear of the slug and finally decays to the pre-slug level after the slug has passed.

Levy developed a three-dimensional model to simulate plug flow using the two-fluid theory and found that both the radial and the axial pressure drop are functions of the particle concentration [42]. He clearly observed that the plugs caused a pressure jump at the top of the pipe cross-section and as a result, the axial pressure drop became positive. The highest pressure drop value was obtained when the particle concentration achieved its highest value at the top of the pipe cross-section. He reported that the lowest amplitude of the radial pressure drop was obtained at the front face of the slug. He suggested that this is probably due to the presence of high solids concentration and stress at that point, i.e. the highest friction force appeared at the front end of each plug.

All theoreticians who developed models for pressure drop prediction in slug flow pneumatic conveying that involve a stress transmission from axial into radial direction had to deal with the determination of a stress transmission coefficient. This determination occurred mainly purely theoretically or semi-

empirically, sometimes experimentally. Among others, Yi developed an apparatus to measure directly the stress transmission coefficient in which a bulk solids sample retained between two porous plates was pulled upward along the test rig pipe [100]. The distance between the plates was varied so that different compression states of the slug were achieved. Both the acting axial stress and resulting radial stress were measured. For the two pipe diameters and the diverse slug lengths he tested, he found that once the axial stress exceeded a limiting value, the stress transmission coefficient appeared to be a constant. However, the measurements were carried out on a very short non-aerated slug so that the results probably do not reflect what actually occurs during pneumatic conveying. Mi investigated experimentally wall pressure whose values he obtained by subtracting the static air pressure from the total air pressure. He reported that the wall pressure is higher at the bottom of the pipe than at the top due to the weight of the slug [52]. He also calculated semi-empirical values for the stress transmission coefficient by assuming that axial and frontal stress are equal. As a result, he suggested that since all stress transmission values obtained are less than 1, the interparticle stresses in a horizontal moving slug are in the active state. However, the substitution of the axial stress by the frontal stress was proved later to be false, as mentioned by Yi [100].

Vasquez investigated the wall friction during slug flow pneumatic conveying by means of pressure transducers for both the total pressure and air pressure and used a bending type transducer to measure the total radial stress [85]. He found values for the stress transmission coefficient lower or higher than 1 according to the material investigated. Krull criticised the measurement technique used by Vasquez and assumed that the values of stress transmission coefficient obtained are not true [39]. Krull developed a test rig himself with whom the radial stress within a slug of granular material can be measured directly without obstructing the flow by using what he described as a large-scale static pressure transducer. This test chamber provides an averaged radial stress around the circumference of the slug. Therefore, this device is particularly suitable to measure the radial stress by vertical pneumatic conveying where the stress can be assumed to be homogeneously distributed around the pipe circumference. Krull reported that a linear relationship exists between the pressure gradient through a slug and the radial wall pressure measured. In addition, he developed a new model to calculate the stress transmission coefficient that requires among others knowledge of depth of stationary layer  $\alpha$ , slug velocity, average pressure gradient across a slug and average radial wall pressure. By applying this model, he could establish a linear decreasing correlation between stress transmission coefficient and ratio slug velocity/air mass flow rate he called air loading factor.

### 3. Relevant models to predict the pressure loss in horizontal slug flow pneumatic conveying

In this Chapter, the relevant models existing for pressure loss prediction in horizontal slug flow pneumatic conveying are summarised. The aim is to emphasise the evolution of the theories, clarify the assumptions drawn by the authors and compare the calculation results. While one single model based on the determination of a friction coefficient has been chosen, i.e. the model proposed by Muschelknautz and Krambrock, four models developed on bulk solids mechanics are described. The model of Muschelknautz and Krambrock is detailed in the VDI-Wärmeatlas, which shows its relevance [86]. Not only for this reason but also because this model is relatively easy to handle, it has been widely used by constructors who want to perform the design of a slug flow pneumatic conveying system. The four other models are the approaches of Konrad [38], Mi [51], Pan [62] and Yi [100]. Konrad published in 1989 an extensive paper in which he clearly explained all assumptions he made and derived all mathematical equations in detail. Most of the papers published later refer to Konrad's paper. Whereas Mi incorporated semi-empirical equations in his model to facilitate the calculation of the pressure loss, the calculation models of Konrad, Pan and Yi involve each at least two equations describing the pressure loss that are required to calculate two unknown quantities, mainly the pressure loss and slug velocity.

To facilitate the comparison between the models, the nomenclature used by the different authors has been unified. With the intention of presenting some models easy to understand, only the basis equations as well as the equations necessary for the comprehension are presented. Moreover, physical explanations are given rather than mathematical derivations. Finally, calculations are performed to compare and discuss the results given by the five models from a physical and practical point of views.

#### 3.1. Muschelknautz and Krambrock, 1969

Since the gas pressure decreases gradually along the length of the pipe, the effects of the gas compressibility are usually considered by using a stepwise correction of the gas density  $\rho_f$ , i.e. local incompressibility is assumed. In small-scale conveying equipments, the pressure drop is usually found to be a linear function of the pipe length. However, this approximation is no longer valid in the case of industrial conveying pipes, which reach a few hundred metres in length. The expansion of the gas down the pipe can no longer be ignored. Consequently, gas compressibility has to be taken into account in the derivation of the equation for pressure drop. One of the first attempts to consider gas compressibility was the approach of Muschelknautz and Krambrock [58] who suggested that the main resistance force in dense-phase conveying is due to the friction force between material and pipe wall caused by the weight of the particles:

$$F_R = \frac{\dot{m}_s \cdot g \cdot dL}{v_s} \cdot \beta \quad (3.1)$$

where  $\beta = \sin \alpha_p + f_w \cdot \cos \alpha_p$ , i.e.  $\beta = f_w = \tan \phi_w$  in horizontal pipeline.

After having inserted the solids charge  $\mu$  in the equation so that  $\dot{m}_s$  disappears and assuming that the expansion of the gas is isothermal, the authors proposed the following correlation, which suggests that the overall conveying pressure difference increases exponentially with the pipeline length:

$$P_1 = P_2 \exp\left(\frac{\mu \cdot g \cdot \tan \phi_w \cdot L}{R_a \cdot T \cdot \eta}\right) \quad (3.2)$$

Muschelknautz gives tables and diagrams derived from experimental results which whom the velocity ratio  $\eta$  or the ratio  $\frac{\beta}{\eta}$  can be determined. The authors suggest that if the pressure value at pipeline inlet is more than 2.2 times the pressure at pipeline outlet, the design of the pipeline system should be realised stepwise.

It should be pointed out that this correlation does not consider the effect of the pipeline diameter.

### 3.2. Konrad, 1980

Konrad developed a model to predict the pressure drop in horizontal slug flow by applying the principles of powder mechanics on the one hand and the Ergun equation on the other hand. He used the former to calculate the pressure loss through a slug he assumed to be a packed bed. Konrad also developed a calculation method to estimate the mean velocity of the particles contained in a slug.

The model was developed on the basis of:

- the packed bed model, to relate the overall pressure drop to the slip velocity between the gas and the solids
- the powder mechanics, to calculate the pressure drop required to move a single slug
- a gas-liquid analogy, to predict the velocity of the interface at the front end and rear of the slug.

#### 3.2.1. The Ergun packed bed model: mean particle velocity determination

Konrad assumed slugs as moving packed beds with a density similar to the bulk density of the granular material. He chose to apply the equation of Ergun to describe the pressure gradient through a horizontal slug:

$$\frac{\Delta P}{L_s} = 150 \cdot \frac{\eta_f \cdot (1 - \varepsilon)^2}{d_p^2 \cdot \varepsilon^3} \cdot v_{rel} + 1.75 \cdot \frac{\rho_b \cdot (1 - \varepsilon)}{d_p \cdot \varepsilon^3} \cdot v_{rel}^2 \quad (3.3)$$

Contrary to the packed beds of Ergun that were fixed, slugs are moving. Therefore, the superficial slip velocity  $v_{rel}$  must be used instead of the superficial air velocity  $v_f$ . The superficial slip velocity, i.e. the slip velocity for a free cross-section can be expressed as following:

$$v_{rel} = v_f + v_s - \bar{v}_p \quad (3.4)$$



and results from the interstitial slip velocity:

$$v_{rel\_int} = \frac{(v_{f\_int} + v_{s\_int} - \bar{v}_{p\_int})}{\varepsilon} \quad (3.5)$$

The mass flow rate  $\dot{m}_s$  corresponds to the mass of moving solids divided by the time taken to travel through the pipe. Hence, an expression for the total length of slugs is found:

$$L_{slug} = \frac{\dot{m}_s \cdot L_T}{A \cdot \rho_b \cdot \bar{v}_p} \quad (3.6)$$

By inserting Eq. 3.6 into the Ergun equation, a quadratic expression for the mean particle velocity  $\bar{v}_p$  is found where  $v_f + v_s$  has been replaced by  $\frac{\dot{m}_s}{A} \cdot \left( \frac{1}{\rho_f \cdot \mu} + \frac{1}{\rho_s} \right)$ :

$$\begin{aligned} \bar{v}_p - \bar{v}_p \cdot \left[ \frac{150 \cdot \eta_f \cdot (1 - \varepsilon)}{1.75 \cdot \rho_f \cdot d_p} + \frac{\Delta P \cdot A \cdot \rho_s \cdot \varepsilon^3 \cdot d_p}{1.75 \cdot L_T \cdot \bar{m}_s \cdot \rho_f} + \frac{2\bar{m}_s}{A} \cdot \left( \frac{1}{\rho_f \cdot \mu} + \frac{1}{\rho_s} \right) \right] \\ + \left[ \frac{150 \cdot \eta_f \cdot (1 - \varepsilon) \cdot \bar{m}_s}{1.75 \cdot \rho_f \cdot d_p \cdot A} \cdot \left( \frac{1}{\rho_f \cdot \mu} + \frac{1}{\rho_s} \right) + \frac{\bar{m}_s^2}{A^2} \cdot \left( \frac{1}{\rho_f \cdot \mu} + \frac{1}{\rho_s} \right)^2 \right] = 0 \end{aligned} \quad (3.7)$$

### 3.2.2. Bulk solids mechanics: pressure loss over a horizontal slug

Konrad suggested that the particles within a slug exert forces on each other in a manner similar to that of particles that are in a discharging hopper. Therefore, he adapted the method used by Janssen [32] to analyse the vertical stress in granular media to horizontal flow. Fig. 3.1 shows the balance of forces in a moving slug.

The basic differential equation is very similar to that of Janssen except that the term due to gravity is omitted:

$$\frac{dP}{dx} + \frac{d\sigma_x}{dx} + \frac{4\tau_w}{D} = 0 \quad (3.8)$$

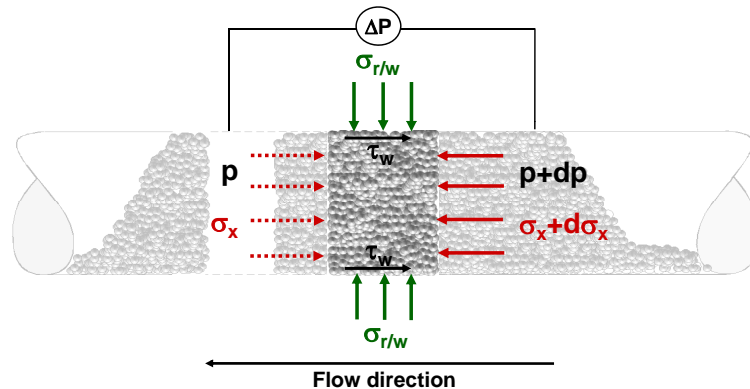


Figure 3.1: Force balance on a moving slug

To evaluate the wall shear stress  $\tau_w$ , Konrad assumed that the material obeys the Coulomb failure criterion:

$$\tau_w = \mu_w \cdot \sigma_{r/w} + c_w \quad (3.9)$$

However, since granular materials are frictional, the stress distribution is difficult to predict accurately. Nevertheless, the range within which the stresses must lie, whose extremes are known as the active and passive solutions, can be determined using the Mohr circle (see Section 2.3.3.2).

Therefore, Konrad derived the following expressions for the radial stress at the wall.

For passive failure, that he assumed to occur in horizontal slug flow pneumatic conveying:

$$\sigma_{r/w\_passive} = K_w \cdot \sigma_{x/w} + (K_w + 1) \cdot c \cdot \cos \phi \cdot \cos(\omega + \phi_w) \quad (3.10)$$

where the coefficient of internal friction at the wall  $K_w$  is:

$$K_{w\_passive} = \frac{1 + \sin \phi \cdot \cos(\omega + \phi_w)}{1 - \sin \phi \cdot \cos(\omega + \phi_w)} \quad (3.11)$$

For active failure:

$$\sigma_{r/w\_active} = K_w \cdot \sigma_{x/w} - (K_w + 1) \cdot c \cdot \cos \phi \cdot \cos(\omega - \phi_w) \quad (3.12)$$

where

$$K_{w\_active} = \frac{1 - \sin \phi \cdot \cos(\omega - \phi_w)}{1 + \sin \phi \cdot \cos(\omega - \phi_w)} \quad (3.13)$$

For a cohesionless material,  $\sin \omega = \frac{\sin \phi_w}{\sin \phi}$

Besides, Konrad assumed the stress distribution due to the gravity as hydrostatic and used a method based on that due to Wilson [94] to express the normal stress  $P_s$  at the wall resulting from hydrostatic pressure (Fig. 3.2).

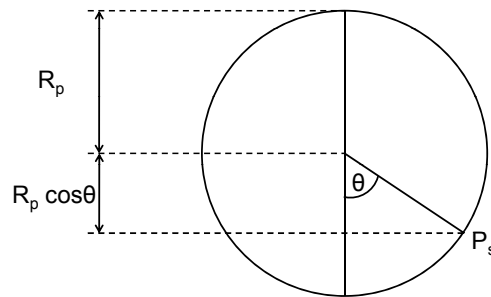


Figure 3.2: Section of the pipe illustrating the hydrostatic pressure

Konrad expressed the normal stress at the wall as following:

$$P_s = (1 + \cos \theta) \cdot R_p \cdot \rho_b \cdot g \quad (3.14)$$

He assumed that this vertical stress distribution could be added to that for the Janssen analysis and expressed the normal stress at the wall according to the angle  $\theta$ :

$$\sigma_{r/w\_passive} = K_w \cdot \sigma_{x/w} + (K_w + 1) \cdot c \cdot \cos \phi \cdot \cos(\omega + \phi_w) + (1 + \cos \theta) \cdot R_p \cdot \rho_b \cdot g \quad (3.15)$$

The normal stress  $\sigma_{r/w}$  is assumed hydrostatic and hence independent of  $\theta$  so that the average normal stress at the wall is:

$$\sigma_{r/w\_passive} = K_w \cdot \sigma_{x/w} + (K_w + 1) \cdot c \cdot \cos \phi \cdot \cos(\omega + \phi_w) + R_p \cdot \rho_b \cdot g \quad (3.16)$$

Combining Eq. 3.9 with Eq. 3.16, an equation for the average wall shear stress  $\tau_w$  is found:

$$\tau_w = \mu_w \cdot K_w \cdot \sigma_{x/w} + \mu_w \cdot (K_w + 1) \cdot c \cdot \cos \phi \cdot \cos(\omega + \phi_w) + \mu_w \cdot R_p \cdot \rho_b \cdot g + c_w$$

The value  $\sigma_b$  is given to the axial stress at the slug rear. The value  $\sigma_f$  is given to the axial stress at the front face of the slug. Konrad demonstrated that the error is negligible if the stress at the front and rear are assumed to be equal, i.e.  $\sigma_f = \sigma_b$ .

With the assumption that the pressure gradient is a constant, i.e. for incompressible fluid or for a compressible fluid over a short distance over which the gas expansion can be neglected, and taking into account all previous assumptions proven by Konrad as making sense, Eq. 3.8 can be integrated. For passive case, this yields:

$$\frac{\Delta P}{L_p} = \frac{4\mu_w \cdot K_w \cdot \sigma_f}{D} + \frac{4\mu_w \cdot (K_w + 1) \cdot c \cdot \cos \phi \cdot \cos(\omega + \phi_w)}{D} + 2\mu_w \cdot \rho_b \cdot g + \frac{4c_w}{D} \quad (3.17)$$

For a cohesionless material,  $c = c_w = 0$ . Therefore, Eq. 3.17 can be simplified:

$$\frac{\Delta P}{L_p} = \frac{4\mu_w \cdot K_w \cdot \sigma_f}{D} + 2\mu_w \cdot \rho_b \cdot g \quad (3.18)$$

The stress transmission coefficient  $K_w$  in Eq. 3.17 can be calculated using Eq. 3.11 or Eq. 3.13 according to the stress case considered. An expression is needed for the stress  $\sigma_f$  on the front end of a horizontal slug. Konrad estimated the stress  $\sigma_f$  by performing a momentum balance at the front of a horizontal moving slug (Fig. 3.3).

$$A \cdot \sigma_f = \rho_b \cdot A \cdot (v_{front} - v_p) \cdot (v_{front} - (v_{front} - v_p))$$

$$\sigma_f = \rho_b \cdot (v_{front} - v_p) \cdot v_p \quad (3.19)$$

The velocity  $v_{front}$  of the front surface of the slug is now needed to obtain an expression for  $F$  where all parameters are known. Konrad performed a particle balance over the region located at the front of the slug (enclosed by the dashed circle in Fig. 3.3) by giving the system a velocity  $-v_{front}$ .

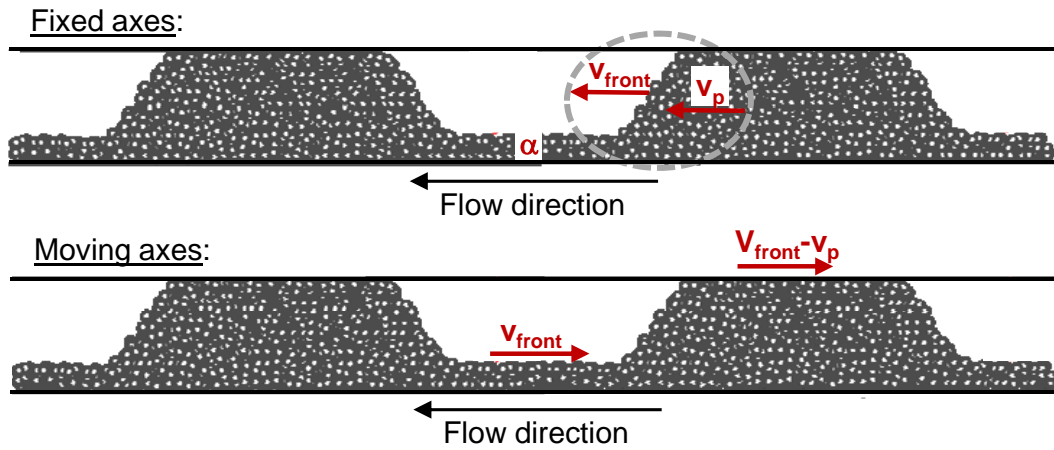


Figure 3.3: Particle balance at the front end of a slug as proposed by Konrad [38]

$$\begin{aligned} v_{front} \cdot \alpha \cdot (1 - \varepsilon) \cdot \rho_s &= (v_{front} - v_p) \cdot (1 - \varepsilon) \cdot \rho_s \\ v_{front} &= \frac{v_p}{1 - \alpha} \end{aligned} \quad (3.20)$$

The same result is obtained for the velocity  $v_{back}$  at the back surface of the slug:

$$v_{back} = \frac{v_p}{1 - \alpha} \quad (3.21)$$

By combining Eq. 3.19 and 3.20, an expression for  $\sigma_f$  is obtained:

$$\sigma_f = \frac{\rho_b \cdot \alpha \cdot v_p^2}{1 - \alpha} \quad (3.22)$$

A similar method is applied to obtain the stress at the back end of a slug:

$$\sigma_b = \frac{\rho_b \cdot \alpha \cdot v_p^2}{1 - \alpha} \quad (3.23)$$

Since the height of the deposited layer is the same at each point of the cross-section between two slugs, it results that  $\sigma_f = \sigma_b$ .

However, the calculation of the stress  $\sigma_f$  at the slug front and the stress  $\sigma_b$  at the slug back require the determination of the fraction  $\alpha$  of the pipe area occupied by material at a cross section between two slugs. The fraction  $\alpha$  is estimated by using a gas/liquid analogy.

### 3.2.3. Application of a gas/liquid analogy to estimate the fraction $\alpha$

Based on observations of the slug flow pattern, Konrad suggested that dense-phase pneumatic conveying can be treated analogue to a two-phase gas/liquid flow. This analogy is well-established for fluidised beds. According to the two-phase theory of fluidisation proposed by Toomey [84] and developed by Davidson [17], all gas in excess of that needed for minimum fluidisation passes through the bed as bubbles, i.e. gas slugs, which are essentially free of particles. The particulate phase remains at minimum fluidising conditions, which means that the voidage, not counting the bubbles, remains practically unchanged. The propagation velocity of a single slug in a horizontal system is assumed to be similar to the propagation velocity of a single gas cavity, i.e. gas slug in liquid, which has been already investigated by Brooke Benjamin [10] and Zukoski [102]. Therefore, Konrad carried over their results and took the propagation velocity of a single slug in a horizontal system to be  $0.542\sqrt{g \cdot D}$ .

The slug velocity is assumed equal to the particle velocity ahead of the slug + the single slug velocity:

$$v_{slug} = v_p + 0.542\sqrt{g \cdot D} \quad (3.24)$$

By combining Eq. 3.21 and Eq. 3.24, an expression for  $\alpha$  is obtained:

$$\alpha = \frac{1}{1 + \frac{v_p}{0.542\sqrt{g \cdot D}}} \quad (3.25)$$

It should be pointed out that the gas/liquid analogy suggests that  $\alpha$  is not a function of any material specific parameters.

### 3.2.4. Overall pressure drop in a horizontal pipeline

By inserting the expressions for the front stress  $\sigma_f$  (Eq. 3.22) and for the fraction of the cross-section area covered by material  $\alpha$  (Eq. 3.25) in the general expression for the pressure loss over a slug of cohesionless material (Eq. 3.18), the following equation is obtained:

$$\frac{\Delta P}{L_p} = \frac{4 \cdot \mu_w \cdot K_w \cdot 0.542 \cdot \sqrt{g} \cdot \rho_b \cdot v_p}{\sqrt{D}} + 2\mu_w \cdot \rho_b \cdot g \quad (3.26)$$

If steady-state flow and constant mass flow rates are assumed, the superficial gas velocity must increase along the pipe, which may result in a change of the mode of flow.  $L_p$  corresponds to the

length of pipeline where the cross-section is totally filled with material that Konrad named the total length of plug. However, the slugs consist not only in those plugs but also in a length corresponding to a volume of material that is moving but not within a plug, i.e. a length of associated moving material located at the front end and at the rear. Therefore, the total pressure loss should be expressed as function of the total length of slugs  $L_{slug}$ . Since the transmission of stress suggested by Konrad from axial into radial direction occurs only in the sections corresponding to the plugs, Eq. 3.26 becomes:

$$\frac{\Delta P}{L_{slug}} = \frac{2.168 \cdot \mu_w \cdot K_w \cdot \sqrt{g} \cdot \rho_b \cdot v_p \cdot L_p}{\sqrt{D} \cdot L_{slug}} + 2\mu_w \cdot \rho_b \cdot g \quad (3.27)$$

Eq. 3.27 can be transformed so that only  $L_{slug}$  but not  $L_p$  appears in the expression. By applying the two-phase theory of dense-phase pneumatic conveying to express the gas volume passing through as slugs:  $A \cdot (v_f + v_s - v_{slip}) = A \cdot \bar{v}_p$  and by considering the total volume of the pipeline filled with gas, the total length of plugs  $L_p$  and the total length of moving material  $L_{ex}$  associated to it (i.e. material at front end and rear of a slug), an expression for  $\frac{v_p \cdot L_p}{L_{slug}}$  can be found. This expression can be inserted in Eq. 3.27, which becomes:

$$\frac{\Delta P}{L_{slug}} = 2.168 \cdot \mu_w \cdot \rho_b \cdot K_w \cdot \frac{\sqrt{g}}{\sqrt{D}} \cdot \bar{v}_p \cdot \frac{1 - 2 \cdot \frac{\dot{m}_s}{\rho_b \cdot A \cdot \bar{v}_p}}{1 - \frac{\dot{m}_s}{\rho_b \cdot A \cdot \bar{v}_p}} + 2\mu_w \cdot \rho_b \cdot g \quad (3.28)$$

Therefore, a system of two equations exists with whom the two unknown quantities, namely the pressure over the entire length of slug  $\Delta P$  and the mean particle velocity  $\bar{v}_p$  can be calculated. The first equation (Eq. 3.29) results from the packed bed theory of Ergun while the second equation (3.30) results from the bulk solids mechanics.

$$\frac{\Delta P}{L_{slug}} = 150 \cdot \frac{\eta \cdot (1 - \varepsilon)^2}{d_p^2 \cdot \varepsilon^3} \cdot (v_f - \bar{v}_p) + 1.75 \cdot \frac{\rho_b \cdot (1 - \varepsilon)}{d_p \cdot \varepsilon^3} \cdot (v_f - \bar{v}_p)^2 \quad (3.29)$$

$$\frac{\Delta P}{L_{slug}} = 2.168 \cdot \mu_w \cdot \rho_b \cdot K_w \cdot \frac{\sqrt{g}}{\sqrt{D}} \cdot \bar{v}_p \cdot \frac{1 - 2 \cdot \frac{\dot{m}_s}{\rho_b \cdot A \cdot \bar{v}_p}}{1 - \frac{\dot{m}_s}{\rho_b \cdot A \cdot \bar{v}_p}} + 2\mu_w \cdot \rho_b \cdot g \quad (3.30)$$

### 3.2.5. Limitations of the model

To develop his model, Konrad did not consider the gas expansion along the pipe. However, slug flow is characterised by a significant pressure gradient, which leads to the significant increase of gas velocity along the pipe. Hence, Konrad recommended to apply this calculation model only for short pipe sections. The slugs have been assumed by Konrad as packed beds so that the bulk porosity was used in the Ergun equation to calculate the pressure loss through the slugs. However, slugs have often been proved to be aerated beds. In this case, Ergun's equation is still applicable if the voidage does not exceed a certain value but the slug internal porosity has to be known. Furthermore, Konrad determined theoretically the stress transmission from axial into radial direction by using the Mohr circle for passive stress case.

However, it has not been proved experimentally that the application of the Mohr circle to describe the stress state inside of a slug is correct or that slugs are in a passive stress state.

### 3.3. Mi, 1994

Mi and Wypych developed a semi-empirical expression for the pressure gradient in horizontal slug flow pneumatic conveying of cohesionless bulk solids ( $c_w = 0$ ) by establishing a theoretical force balance of the moving slug. In addition, they extrapolated the results of experimental investigations to determine values for the stress transmission coefficient and the slug velocity [51].

Mi chose to apply the principles of powder mechanics to a moving slug to establish a theoretical relationship for the pressure gradient in a slug. The force balance on a single slug is the same than the force balance proposed by Konrad (Fig. 3.1). The external forces in the flow direction compress the particles inside a slug, which result in the axial stress  $\sigma_x$  and its increment in axial direction  $d\sigma_x$ . The normal stress  $\sigma_{rt}$  acting perpendicularly to the pipe wall is due to two components, namely the stress  $P_s$  resulting from the material weight, which varies according to the location over the pipe cross-section and the stress  $\sigma_{r/w}$  caused by the pipe wall reacting against the axial compression  $\sigma_x$  that is described by means of the stress transmission coefficient  $K_w$ . The stress  $\sigma_{r/w}$  is assumed as a constant over the pipe cross-section. Therefore:

$$\sigma_{rt} = P_s + \sigma_{r/w} \quad (3.31)$$

with

$$P_s = (1 + \cos \theta) \cdot \rho_b \cdot g \cdot R_p \quad (3.32)$$

and

$$\sigma_{r/w} = K_w \cdot \sigma_{x/w} \quad (3.33)$$

where  $K_w$  is determined by applying the Mohr circle. Contrary to Konrad, the authors suggested from experimental investigations that moving slugs are in an active stress state.

The material is cohesionless and assumed to obey the Coulomb failure criterion so that the shear stress at the wall  $\tau_w$  for a cohesionless material is expressed as following:

$$\tau_w = \mu_w \cdot \sigma_{x/w} \quad (3.34)$$

The equilibrium between the driving force and the resistance forces takes place when a moving slug reaches steady state, which leads to:

$$\frac{dP}{dx} + \frac{d\sigma_x}{dx} + \frac{\int_0^{2\pi} \tau_w \cdot R_p \cdot d\theta}{A} = 0 \quad (3.35)$$

The pressure gradient is assumed a constant, so that  $\frac{dp}{dx} = -\frac{\Delta P}{L_s}$  and the solution to Eq. 3.35 becomes:

$$\sigma_x = c_k \cdot \exp\left(-\frac{2\mu_w \cdot K_w}{R} \cdot x\right) + \left(-2\rho_b \cdot g \cdot \mu_w + \frac{\Delta P}{L_s}\right) \cdot \frac{D}{4\mu_w \cdot K_w} \quad (3.36)$$

By applying the boundary conditions for  $\sigma_x$  at the front end ( $\sigma_f$ ) and the rear ( $\sigma_b$ ) of a slug as Konrad did and assuming that  $L_s \gg D$ , an equation for the pressure gradient of a single horizontal slug is determined:

$$\frac{\Delta P}{L_s} = \frac{4\mu_w \cdot K_w}{D} \cdot \sigma_f + 2\rho_b \cdot g \cdot \mu_w \quad (3.37)$$

The stress at the front end of a slug  $\sigma_f$  is due to the particles of the stationary layer that have to be picked up by the slug. Therefore,  $\sigma_f$  is estimated by establishing a momentum balance in the front area:

$$\sigma_f = \alpha \cdot \rho_{bst} \cdot v_{slug}^2 \quad (3.38)$$

where  $\rho_{bst}$  is the bulk density of solids in the stationary layer, which is equal to  $\rho_b$  and  $v_{slug}$  is the slug velocity, which is assumed to be equal to the mean velocity of the particles in the slug.

The slug velocity was experimentally found to be described by a linear correlation of the form:

$$v_{slug} = k_2 \cdot (v_{fm} - v_{f\_min}) \quad (3.39)$$

A correlation for  $v_{f\_min}$  resulting from previous investigations is used [50]:

$$v_{f\_min} = \frac{\rho_s \cdot g \cdot \tan(\phi_w) \cdot \varepsilon^3 \cdot d_p^2}{180 \cdot (1 - \varepsilon) \cdot \eta} \quad (3.40)$$

Furthermore, Mi showed experimentally that the slope  $k_2$  can be determined by using Eq. 3.41.

$$k_2 = 105 \cdot \frac{\varepsilon \cdot d_p}{D} \cdot \left(\frac{\tan \phi_w}{\tan \phi}\right)^{\frac{1}{3}} \quad (3.41)$$

where  $\phi$  is the internal friction angle.

The determination of the fraction of the cross-section area covered by the stationary layer is required to estimate  $\sigma_f$ . Mi proposed to use the equation developed by Konrad that he proved to be in agreement with the results of his experimental investigations:



$$\alpha = \frac{1}{1 + \frac{v_p}{0.542\sqrt{g \cdot D}}} \quad (3.42)$$

It should be pointed out that even though the equation proposed by Konrad [38] and the one used by Mi [51] to predict the thickness of the stationary layer  $\alpha$  are the same, the meaning is different. While Mi considers the slug velocity  $v_{slug}$  as equal to the particle velocity  $v_p$ , Konrad took the slug velocity as equal to the mean particle velocity + the propagation velocity of a slug similar to the propagation of a gas bubble in a liquid [100].

Eq. 3.37 expresses the pressure loss along a single slug. Similar to Konrad, Mi treated the sum of the length of all individual slugs as one long slug of length  $L_{slug}$ . The material is considered to be transported only in the cross-section fraction  $(1 - \alpha)$  not covered by the stationary layer. From a mass flow rate balance over the time, Eq. 3.43 is obtained:

$$L_{slug} = \frac{\dot{m}_s \cdot L_T}{A \cdot (1 - \alpha) \cdot \rho_b \cdot v_{slug}} \quad (3.43)$$

Therefore, by inserting Eq. 3.38 for  $\sigma_f$  and Eq. 3.43 for  $L_{slug}$  in Eq. 3.37, the following expression is obtained to calculate the overall pressure loss over the horizontal pipe:

$$\Delta P = \left(1 + 1.084 \cdot K_w \cdot Fr_s^{0.5} + 0.542 \cdot Fr_s^{-0.5}\right) \cdot \frac{2g \cdot \mu_w \cdot \dot{m}_s \cdot L_T}{A \cdot v_{slug}} \quad (3.44)$$

where

$$Fr_s = \frac{v_{slug}^2}{g \cdot D}$$

Mi's model considers the air expansion by taking into account the average air velocity over the entire pipeline  $v_{fm}$  in the calculation of the slug velocity (Eq. 3.39). The average air velocity is a function of both the superficial air velocity at the pipe inlet  $v_f$  and the average air density  $\rho_{fm}$ :

$$v_{fm} = \frac{v_f \cdot P_{atm}}{\frac{\rho_{fm} \cdot R_a \cdot T_0}{M_{air}}} \quad (3.45)$$

The conservation law is used to determine the average air density over the entire pipe:

$$\Delta P = \frac{2 \cdot P_{outlet} \cdot \rho_{fm}}{\rho_{f\_outlet}} - 2 \cdot P_{outlet} \quad (3.46)$$

Like the Konrad model, the approach of Mi requires the determination or the assumption of a value for the stress transmission coefficient  $K_w$ . Based on measurements of radial stress and calculations of axial stress, Mi proposed a semi-empirical equation to calculate  $K_w$ . This method is discussed further in Section 3.6.

### 3.4. Pan, 1995

Pan presented a predictive method for the pressure drop in horizontal single-slug pneumatic conveying [62]. In particular, he simplified and modified the Konrad model [38] so that the value of the particle velocity is no further required for the calculation. Pan made the same assumptions as Konrad with respect to the flow pattern.

Similar to the theoretical approach of Konrad, a balance of the forces acting on a slice of material of length  $dx$  was established (Eq. 3.8). However, Pan disagreed with Konrad who assumed that the vertical stress distribution due to the force of gravity is hydrostatic and can be added to that for the Janssen analysis, so that

$$\sigma_{r/w} = \sigma_{r/w\_Janssen} + R_p \cdot \rho_b \cdot g \quad (3.47)$$

Instead, Pan pointed out that the assumption of a hydrostatic pressure variation for the gravity term would only be correct if the material is fully fluidised and expanded. Hence, he inserted the gravity term  $\rho_b \cdot g \cdot \mu_w$  directly in the balance of forces:

$$\frac{dP}{dx} + \frac{d\sigma_x}{dx} + \frac{4\tau_w}{D} + \rho_b \cdot g \cdot \mu_w = 0 \quad (3.48)$$

Following the assumptions of Konrad, Pan applied the Mohr circle representation to determine the wall shear stress  $\tau_w$  for the material, which he assumed to obey the Coulomb failure criterion. Therefore, he was able to express the range of values within which the stresses must occur, i.e. the passive and active solutions (see Eq. 3.9, 3.10 and 3.12 given by Konrad).

The derivation of the expression for the pressure loss is similar to the derivation detailed by Konrad. However, since Pan considered the friction force due to the weight of the material in a different way, the importance given to this term in the final expression for the total pressure loss is also different from the one in the Konrad equation. While Konrad used the term  $2 \cdot \mu_w \cdot \rho_b \cdot g$  as part of the addition, Pan considers only half of it, i.e.  $\mu_w \cdot \rho_b \cdot g$ . This leads to the following expression for passive case:

$$\frac{\Delta P}{L_p} = \frac{4\mu_w \cdot K_w \cdot \sigma_f}{D} + \frac{4\mu_w \cdot (K_w + 1) \cdot c \cdot \cos \phi \cdot \cos(\omega + \phi_w)}{D} + \mu_w \cdot \rho_b \cdot g + \frac{4c_w}{D} \quad (3.49)$$

Instead of developing mathematical correlations to express all parameters required for the pressure loss calculation using Eq. 3.49, i.e. fraction of the pipe area  $\alpha$  covered by the stationary layer of particles, particle velocity  $v_p$  and total plug length  $L_p$ , Pan proposed to use the equations proposed by Konrad for the front stress  $\sigma_f$  (Eq. 3.19) and the slug velocity  $v_{slug}$ . In addition, he assumed the slug velocity as equal to the velocity of the front end  $v_{front}$  (Eq. 3.20). Both  $\sigma_f$  and  $v_{slug}$  are a function of the particle velocity  $v_p$ . Therefore, the combination of those two parameters permits to obtain an expression for  $\sigma_f$ , in which the particle velocity is eliminated. As a consequence, the theoretical determination of the

particle velocity is no further required. By substituting the expression for  $\sigma_f$  (Eq. 3.50) in Eq. 3.49, an expression for the pressure loss is obtained.

$$\sigma_f = 0.542 \cdot \sqrt{g \cdot D} \cdot \rho_b \cdot \left( v_{front} - 0.542 \cdot \sqrt{g \cdot D} \right) \quad (3.50)$$

$$\begin{aligned} \frac{\Delta P}{L_p} &= 4 \cdot \mu_w \cdot \rho_b \cdot K_w \cdot 0.542 \cdot \sqrt{g \cdot D} \cdot v_{slug} + \rho_b \cdot g \cdot \mu_w \cdot (1 - 1.175 \cdot K_w) \\ &\pm \frac{4\mu_w \cdot (K_w + 1) \cdot c \cdot \cos \phi \cdot \cos(\omega + \phi_w)}{D} + \frac{4c_w}{D} \end{aligned} \quad (3.51)$$

And therefore for cohesionless material where  $c = c_w = 0$ :

$$\frac{\Delta P}{L_p} = 4 \cdot \mu_w \cdot \rho_b \cdot K_w \cdot 0.542 \cdot \sqrt{g \cdot D} \cdot v_{slug} + \rho_b \cdot g \cdot \mu_w \cdot (1 - 1.175 \cdot K_w) \quad (3.52)$$

Eq. 3.52 requires the determination of the slug velocity  $v_{slug}$ . Similarly to Konrad, Pan proposed to use the Ergun equation, which contains the both unknown quantities pressure loss and slug velocity. Therefore, a system of two equations is used to determine the two unknown quantities pressure gradient  $\frac{\Delta P}{L_p}$  and slug velocity  $v_{slug}$ :

$$\frac{\Delta P}{L_p} = 4 \cdot \mu_w \cdot \rho_b \cdot K_w \cdot 0.542 \cdot \sqrt{g \cdot D} \cdot v_{slug} + \rho_b \cdot g \cdot \mu_w \cdot (1 - 1.175 \cdot K_w) \quad (3.53)$$

$$\frac{\Delta P}{L_p} = 150 \cdot \frac{\eta_f \cdot (1 - \varepsilon)^2}{d_p^2 \cdot \varepsilon^3} \cdot (v_{fm} - v_{slug}) + 1.75 \cdot \frac{\rho_b \cdot (1 - \varepsilon)}{d_p \cdot \varepsilon^3} \cdot (v_{fm} - v_{slug})^2 \quad (3.54)$$

It should be pointed out that while Konrad defined the slip velocity in the Ergun equation as the difference between gas velocity and mean particle velocity within a slug, Pan considered the slip velocity as the difference between the gas velocity and the slug velocity. Moreover, the pressure gradient in the Ergun equation refers to the total length of plug whereas Konrad referred it to the total length of slug. Pan pointed out that this method avoids the need to estimate the mean particle velocity  $\bar{v}_p$ , which was necessary for the calculation method of Konrad.

Since the method was developed for single-slug conveying, the total length of the plug is defined regarding the total mass of conveyed solids and the cross-section area not covered by the stationary layer through which the material is conveyed. The total length of slug is assumed equal to the total length of plug:

$$L_p = L_s = \frac{m_s}{A \cdot (1 - \alpha) \cdot \rho_b} \quad (3.55)$$

However, the method can be adapted to multi-slug conveying. By neglecting the volume of particle transported at the front end and the rear of a slug where the pipe cross-section is not full, the total length of plug can be obtained as following (see Section 3.2):

$$L_p = L_{slug} = \frac{\dot{m}_s \cdot L_T}{A \cdot (1 - \alpha) \cdot \rho_b \cdot \bar{v}_p} \quad (3.56)$$

To take the effects of the gas expansion into account, the calculations are carried out with the average gas velocity  $v_{fm}$ , which is a function of the superficial air velocity  $v_f$  at the pipe inlet and average air density  $\rho_{fm}$ :

$$v_{fm} = \frac{v_f \cdot P_{atm}}{\frac{\rho_{fm} \cdot R_a \cdot T_0}{M_{air}}} \quad (3.57)$$

Therefore, a third equation is required to calculate the mean gas velocity. This equation is based on the conservation law:

$$\Delta P = \frac{2 \cdot P_{outlet} \cdot \rho_{fm}}{\rho_{f\_outlet}} - 2 \cdot P_{outlet} \quad (3.58)$$

It should be pointed out that the variation of the pressure gradient with the gas expansion is considered as linear. Therefore, the pressure loss calculation should be performed only for a short pipe section. Furthermore, like the models of Konrad (see Section 3.2) and Mi (see Section 3.3), the method proposed by Pan requires the determination of the stress transmission coefficient  $K_w$ .

### 3.5. Yi, 2001

To predict the pressure loss in horizontal pipes, Yi proposed an iteration method involving a balance of forces for a moving slug on the one hand and the equation of Ergun for packed beds (see Section 2.3.2) on the other hand [99]. By means of a two-equations-system, the unknowns quantities pressure loss  $\Delta P$  and slug velocity  $v_{slug}$  can be calculated.

Yi established a force balance for a moving slug (3.4) by considering that during slug flow conveying, the movement of a single slug is balanced by a resistance force comprising three components (Eq. 3.59):

- a friction force between particles and pipeline wall  $F_{friction\_weight}$  caused by the weight of the slug
- a force  $F_{axial}$  resulting from the front stress  $\sigma_f$  caused by the stationary layer in front of the slug: particles of the stationary layer are picked up by the slug and accelerated at the velocity of the slug particles
- a wall friction force  $F_{friction\_lateral}$  resulting from the lateral stress transmitted from the axial stress along the slug, similar to Janssen silo's theory.

$$F_{total} = F_{friction\_weight} + F_{axial} + F_{friction\_lateral} \quad (3.59)$$

The friction force resulting from the weight of the slug sliding on the pipe wall can be expressed by Eq. 3.60:

$$F_{friction\_weight} = \frac{\pi}{4} \cdot f_w \cdot \rho_b \cdot g \cdot L_s \cdot D^2 \quad (3.60)$$

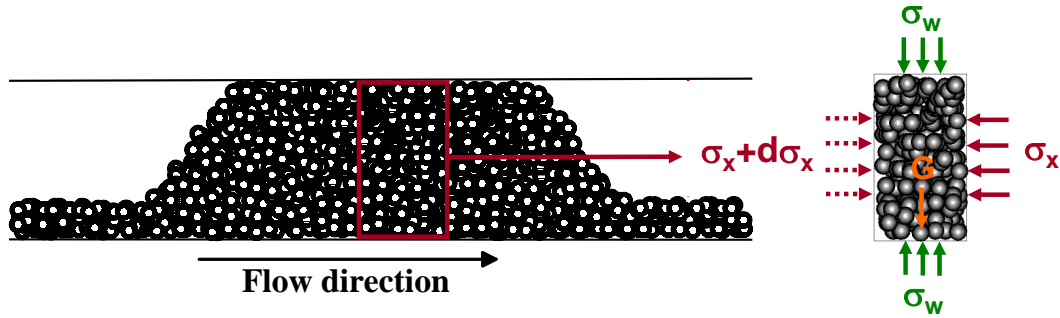


Figure 3.4: Slug element and acting stresses [100]

In slug flow, the layer of particles lying at the pipe bottom creates a resistance force to the movement of the slugs. The transport of slugs is wave-like. Hence, a slug picks up granules at the front and deposits a similar amount of product at the rear. This mechanism leads to the existence of a stress that Yi assumed to result from the stress  $\sigma_{f1}$  due to the raising of particles from the stationary layer onto the moving slug and the stress  $\sigma_{f2}$  caused by the acceleration of those particles to the velocity of the moving slug:

$$\sigma_f = \sigma_{f1} + \sigma_{f2} \quad (3.61)$$

By establishing a momentum balance between the particles of the moving slug and the particles of the stationary layer in front of the slug, an expression is obtained for the stress  $\sigma_{f2}$ , in which the slug velocity is a key parameter:

$$\sigma_{f2}(v_{slug}) = \alpha \cdot (1 - \alpha) \cdot \rho_b \cdot v_{slug}^2 \quad (3.62)$$

Whereas the stress  $\sigma_{f2}$  appears in other models as well, Yi added the stress  $\sigma_{f1}$ , which is due to the force required to lift the particles located at the surface of the settled layer over the height  $H$  (Fig. 3.5). The height  $H$  is a function of the pipe area fraction  $\alpha$  covered by the settled particles, which in turn is a function of the slug velocity.

$$\sigma_{f1}(v_{slug}) = \frac{\rho_b \cdot g \cdot H(v_{slug})}{K_w} \quad (3.63)$$

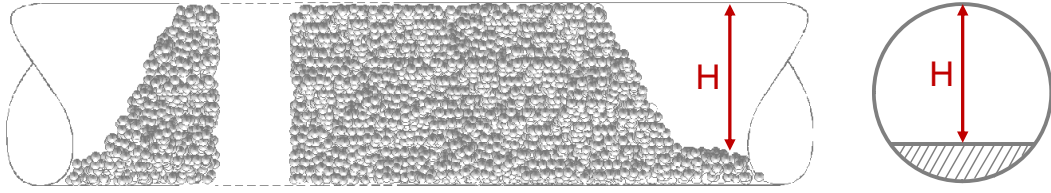


Figure 3.5: Height  $H$  over which particles of the stationary layer have to be lifted [100]

The height  $H$  of the suspension over the strand is determined as following:

For  $v_{slug} \geq 2 \cdot 0.542 \cdot \sqrt{g \cdot D}$ :

$$H(v_{slug}) = 0.5 \cdot \left( D + \sqrt{D^2 - l_w(v_{slug})^2} \right)$$

whereas for  $v_{slug} < 2 \cdot 0.542 \cdot \sqrt{g \cdot D}$ :

$$H(v_{slug}) = 0.5 \cdot \left( D - \sqrt{D^2 - l_w(v_{slug})^2} \right)$$

where the width  $l_w$  of the upper surface of the stationary layer between two slugs can be geometrically approximated :

$$l_w(v_{slug}) = [4 \cdot \alpha(v_{slug}) \cdot (1 - \alpha(v_{slug}))]^{1/3} \cdot D$$

The fraction  $\alpha$  of the pipe area covered by the layer of particles is calculated as following:

$$\alpha(v_{slug}) = \frac{0.542 \cdot \sqrt{g \cdot D}}{v_{slug}} \quad (3.64)$$

Eq. 3.64 is similar to the equation proposed by Konrad (Eq. 3.25) who applied a gas/liquid analogy to estimate the fraction  $\alpha$ . However, Konrad assumed the slug velocity to be equal to the sum of the particle velocity  $v_p$  ahead of the slug and the single slug propagation velocity  $0.542 \cdot \sqrt{g \cdot D}$ . Hence, he expressed  $\alpha$  as a function of  $v_p$  and not of  $v_{slug}$  (see Section 3.2).

The third resistance component to slug movement is the friction force  $F_{friction\_lateral}$  due to the fraction  $K_w$  of axial stress  $\sigma_f$  transmitted into radial direction. To derivate Eq. 3.65, Yi applied the theory of Janssen who described the normal stress inside of a silo filled with a bulk material:

$$F_{friction\_lateral}(v_{slug}) = \pi \cdot D \cdot f_w \cdot K_w \cdot \sigma_f(v_{slug}) \cdot \left( L_{slug} - \frac{D}{4 \cdot f_w \cdot K_w} \right) \quad (3.65)$$

By inserting Eq.3.60, Eq. 3.61 and Eq. 3.65 into Eq. 3.59, the total resistance force for a moving slug is obtained. Therefore, an expression for the pressure gradient can be derived (Eq. 3.67) by applying Eq. 3.66:

$$\Delta p \cdot L_{slug} = \frac{F_{total}}{A} \quad (3.66)$$

$$\Delta p_1 = \frac{4 \cdot f_w}{D} \cdot [\rho_s \cdot g \cdot H + K_w \cdot \alpha \cdot (1 - \alpha) \cdot \rho_s \cdot v_{slug}^2] + \rho_s \cdot f_w \cdot g \quad (3.67)$$

To obtain an expression of the form  $\Delta p_1 = f(v_{slug})$ , a value for the stress transmission coefficient  $K_w$  has to be determined or assumed, depending on whether an active or passive stress case is considered.

Since both the pressure gradient and the slug velocity are unknown, a second equation in which the pressure loss is expressed as a function of the slug velocity is required. Yi adopted the assumptions of Konrad and proposed to use the semi-empirical equation of Ergun as well:

$$\Delta p_2 = 150 \cdot \frac{\eta_f \cdot (1 - \varepsilon)^2}{d_p^2 \cdot \varepsilon^3} \cdot (v_f - v_{slug}) + 1.75 \cdot \frac{\rho_b \cdot (1 - \varepsilon)}{d_p \cdot \varepsilon^3} \cdot (v_f - v_{slug})^2 \quad (3.68)$$

However, while Konrad considered the slip velocity as equal to the difference between gas velocity  $v_f$  and mean particle velocity  $\bar{v}_p$ , Yi considered the slip velocity as equal to the difference between gas and slug velocity  $v_{slug}$ . Furthermore, similar to Konrad, Yi assumed slugs to be like moving packed beds, which display the bulk density. Therefore, he used the bulk porosity  $\varepsilon$  of the conveyed material to calculate the pressure loss according to the Ergun model.

By using an iterative procedure involving both Eq. 3.67 and Eq. 3.68, the slug velocity  $v_{slug}$  and the pressure gradient  $\Delta p$  can be determined for horizontal slug flow. Yi assumed the pressure loss between two slugs as negligible and the total pressure drop along the pipeline as equal to the pressure drop through the total length of slug. Hence, to calculate the total pressure loss for the entire pipeline, the total length of slugs is required. Following the method of Mi [51], Yi considered the solids material as being transported only through the fraction of the cross-section area  $(1 - \alpha)$  not covered by the stationary layer. Therefore, by performing a balance for the mass flow rate over the time, Yi obtained the same equation as Mi earlier:

$$L_{slug} = \frac{\dot{m}_s \cdot L_T}{A \cdot (1 - \alpha) \cdot \rho_b \cdot v_{slug}} \quad (3.69)$$

Therefore, the total pressure loss over the pipeline can be calculated as following:

$$\Delta P = \Delta p \cdot L_{slug} \quad (3.70)$$

where

$$\Delta p = \Delta p_1 = \Delta p_2 \quad (3.71)$$

It should be pointed out that similar to Konrad and Mi, Yi treated the sum of the length of all individual slugs as one long slug of length  $L_{slug}$ . Hence, the front stress  $\sigma_f$  resulting from both the raise and acceleration of the particles is considered only one time, although this stress actually occurs at the front of each slug. The total stress at the front should depend on the number of slugs present in the pipeline at a given time  $t$ . However, the prediction of the slug number would require the additional prediction of the length of all single slugs.

### 3.6. Comparison and discussion of the models

While discussion about the validity of empirically developed models mainly focus on the suitability to use them for the pressure drop prediction during the transport of a material for which the model has not been specifically developed, discussion about theoretically developed models mainly lead to a wider range of critics. Not only the fundamentals of the models but also the disagreements between the diverse authors and even the inconsistency between the various publications of the same author lead to extended discussion. However, only the relevant differences and discussion items about the models detailed in this work are presented shortly in this section. The models were applied to predict the pressure loss during horizontal transport of Polypropylene pellets in a pipeline of 80 mm internal diameter. The physical characteristics of the material conveyed are presented in Table 4.1. All calculations were performed for a solids mass flow rate of 5,300 kg/h.

Most of the theoretical models are based on the calculation of a stress  $\sigma_f$  at the front end of the slug. In fact, the presence of the stationary layer of particles generates a stress on the front end of the slug that is usually calculated by estimating the momentum exchange between the moving slug and the particles of the stationary layer lying in front of it. Various researchers have proposed and derived an equation for the frontal stress of the slug that they included either in the Konrad model or in their own one. However, authors like Klinzing reported that the stress on the front end of the slug is zero and added that this assumption is supported by the experimental observation that when the slug breaks into smaller parts without collapse, there are insignificant changes in the pressure drop [2]. Yi considered the stress at the front end of a slug in the calculation of the total pressure loss but took it only one time into account and not for each slug. Fig. 3.6 shows that according to the force balance Yi carried out on a slug element, the axial stress, i.e. the stress at the front end of a slug is low in comparison to the other stresses.

Therefore, the Yi model could be simplified by neglecting this stress without influencing significantly the results of the calculation. However, the frontal stress is assumed to be transmitted through the slug of packed particles, by interparticle stresses, to the pipe wall where it generates a shear stress, in addition to that due to the weight of the particles. Fig. 3.6 shows that even for a stress transmission coefficient  $K_w = 1$ , the radial stress corresponds to the main part of the total stress. Hence, even



though the axial stress at the front has little direct impact on the total pressure loss, the calculation of the front stress is still required to calculate the radial stress and further the total stress.

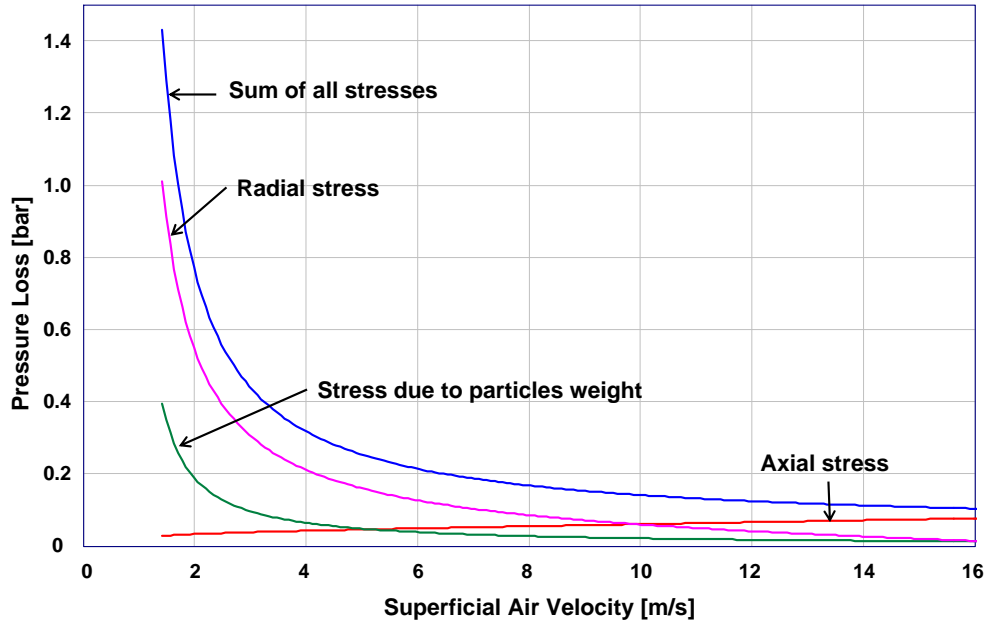


Figure 3.6: Part of each stress in the total pressure loss according to Yi for  $K_w = 1$

The momentum transfer that takes place at the front face of a slug depends principally on the slug velocity, i.e. particle velocity and the height of the layer of stationary particles, i.e.  $\alpha$ . However, disagreements can be found in the literature concerning the prediction of both parameters.  $\alpha$  is sometimes calculated using Eq. 3.72 and sometimes using Eq. 3.73. Fig. 3.7 permits to compare  $\alpha$  calculated with the two equations. The lower is the particle velocity, the more significant is the difference between  $\alpha$ -values.

$$\alpha_1 = \frac{0.542 \cdot \sqrt{g \cdot D}}{v_{slug}} \quad (3.72)$$

$$\alpha_2 = \frac{1}{1 + \frac{v_{slug}}{0.542 \cdot \sqrt{g \cdot D}}} \quad (3.73)$$

The calculation of  $\alpha$  is not only required to estimate the stress at the front end of a slug but is also used for the calculation of the total length of slug in the pipeline. Fig. 3.8 shows both the stress at the front end of a slug calculated by applying Eq. 3.38 and the total length of slug calculated by applying Eq. 3.43 for the two expressions available for  $\alpha$ .

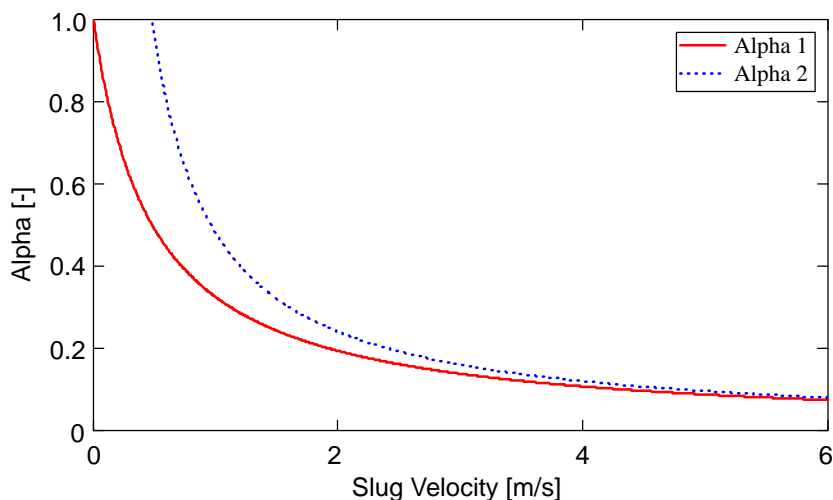


Figure 3.7:  $\alpha$  calculated according to the two equations found in the literature

The  $\alpha$ -calculations carried out with both expressions show significant differences for low values of slug velocity. However, the choice of the expression for  $\alpha$  influences the values of the stress at the front end of the slug and the total length of slug only slightly in the range of air velocity where stable slug flow pneumatic conveying occurs for the material considered, i.e.  $6.5 < v_f < 8.5$  m/s. This is due to the fact that the two expressions for  $\alpha$  yield significantly different values only for a slug velocity lower than 3 m/s. However, as shown in Fig. 3.9, the calculation models yield theoretical values of slug velocity lower than 3 m/s only for a very low gas velocity where slug flow is not achieved in the reality.

In addition, experimental investigations were carried out to determine the slug velocity during horizontal slug flow pneumatic conveying of Polypropylene pellets (see Section 5.1). The results showed that the maximum slug velocity reached 3.5 m/s for a range of gas velocity between 6.5 m/s and 8.5 m/s. Hence, all calculation models appear to overpredict this key parameter.

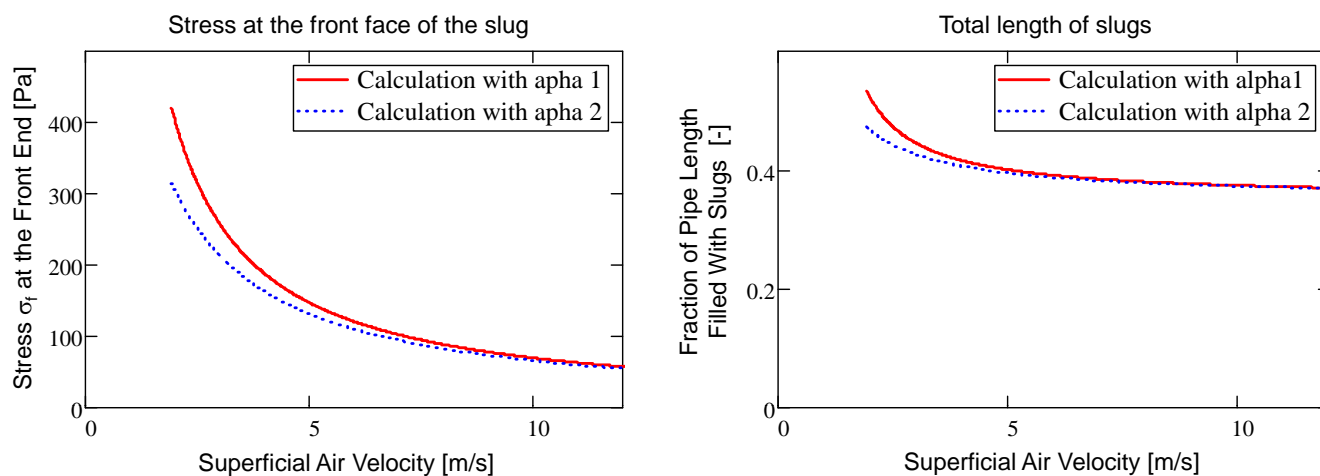


Figure 3.8: Effect of the choice of the expression of  $\alpha$  on the calculation of the front stress (on the left hand side) and the total length of slug (on the right hand side)

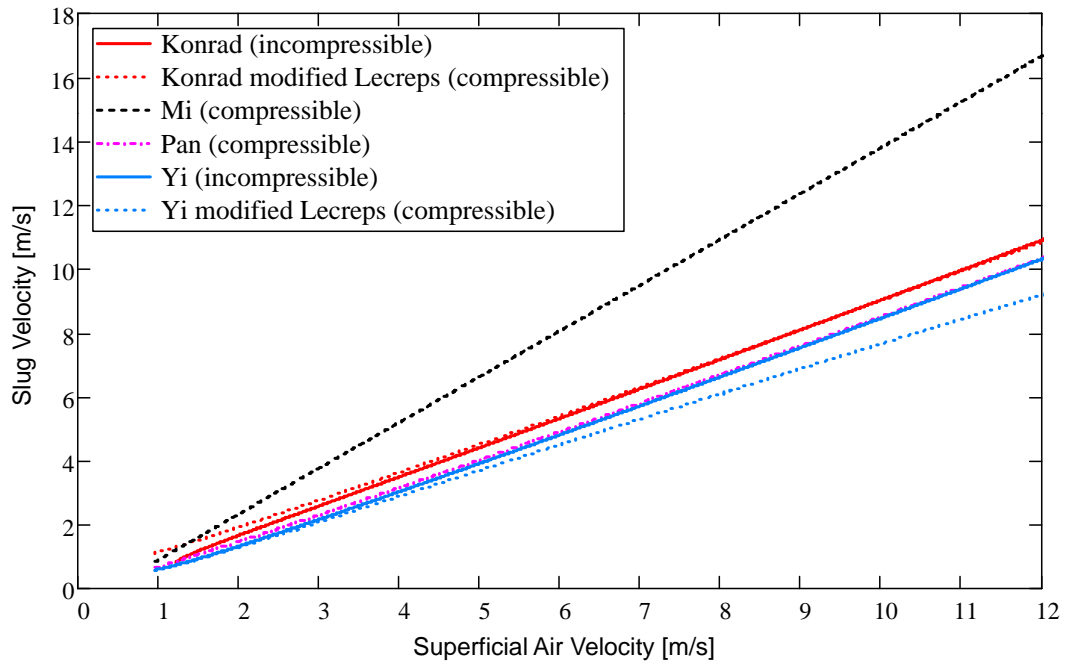


Figure 3.9: Comparison of the slug velocity obtained by applying different models for slug flow pneumatic conveying

Furthermore, authors who use the same expression for  $\alpha$  do not necessarily use it under the same mean. In fact, the slug velocity  $v_{slug}$  involved in the calculation is sometimes taken to be equal to the particle velocity in the middle of a slug (Eq. 3.74) and sometimes considered as equal to the particle velocity at the front of a slug in addition to the propagation velocity of a single slug (Eq. 3.75). This variation in the definition affects the result of the pressure loss calculation as well.

$$v_{slug_1} = \bar{v}_p \quad (3.74)$$

$$v_{slug_2} = v_p + 0.542 \cdot \sqrt{g \cdot D} \quad (3.75)$$

The part of the axial stress transmitted into radial direction similarly to the silo theory of Janssen is influenced by the stress transmission coefficient  $K_w$ . Fig. 3.6 showed that the radial stress corresponds to the most important stress fraction, i.e. the efficiency of the pressure loss prediction by applying the Yi model depends principally on the accurate determination of  $K_w$ . Fig. 3.10 shows the direct influence of the  $K_w$ -value on the pressure loss predicted by applying the models of Konrad, Mi, Pan and Yi. The effect of the  $K_w$ -value is similar for all prediction models. The increase of the stress transmission coefficient leads to the increase of the part of axial stress transmitted into radial direction, which in turn leads to a higher pressure loss. For each models, the pressure loss calculated by using a common  $K_w$ -value for active case, i.e.  $K_w = 0.5$  is about twice the pressure loss obtained when calculations are carried out with a common value for passive case, i.e.  $K_w = 1.3$ . Hence, the accurate determination of the stress transmission coefficient is a key requirement to predict the pressure loss by using a predictive approach based on bulk solids mechanics.

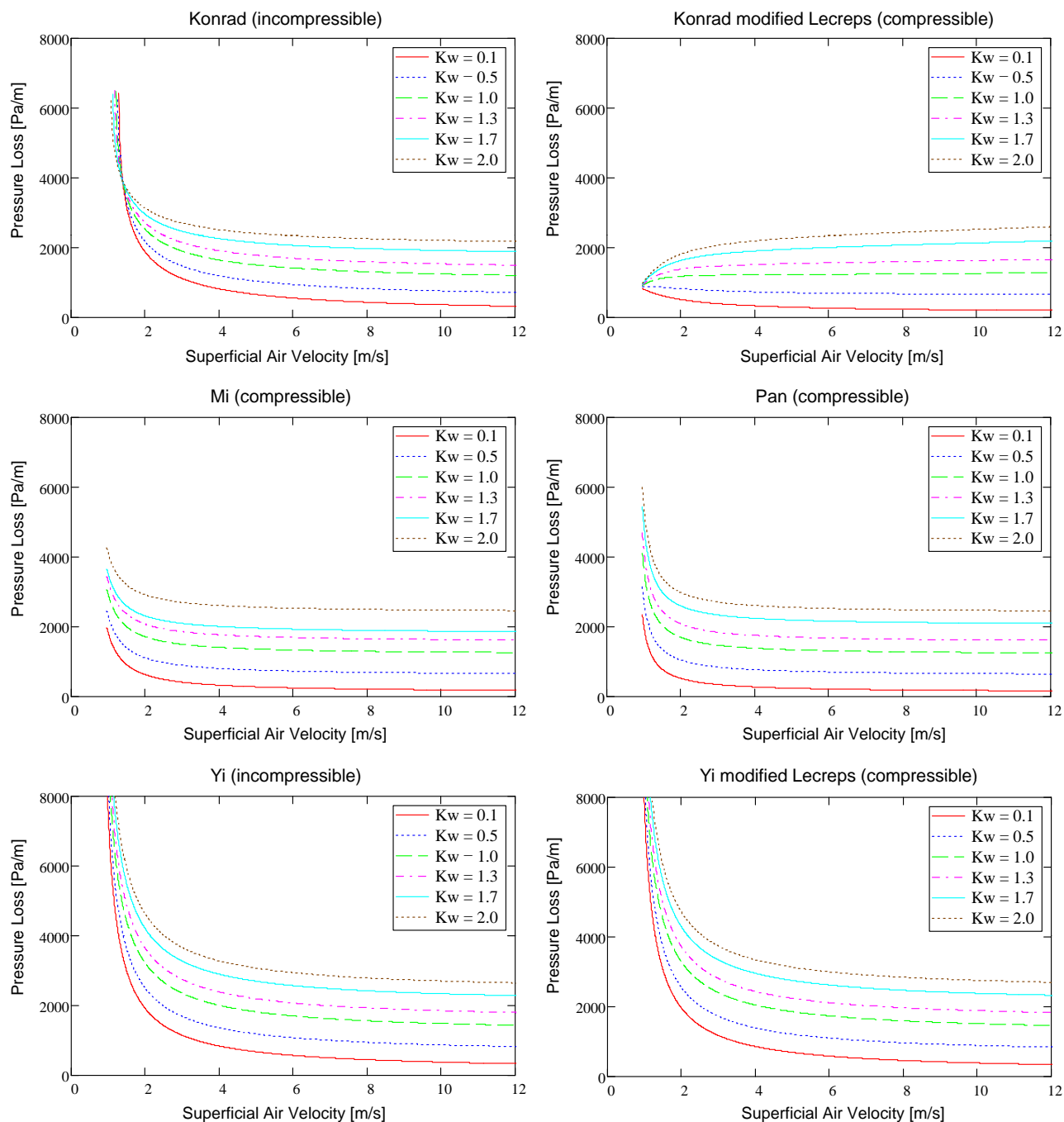


Figure 3.10: Effect of the  $K_w$ -value on the pressure loss predicted by applying the models of Konrad, Mi, Pan and Yi

When the stress transmission coefficient is calculated by using the Mohr circle representation, since the actual stress state is unknown, it has to be assumed that either an active or passive stress case exists, i.e. pulling or pushing failure occurs. Then the static internal friction angle  $\phi_s$  is assumed as equal to the internal friction angle  $\phi$  and by applying Eq. 3.76 or Eq. 3.77, the stress transmission coefficient is calculated. Hence, only the angles of wall friction  $\phi_w$  and internal friction  $\phi$  have to be determined experimentally. Sanchez reported that the calculation of  $K_w$  in the passive model underpredicts the data while in the active case it overpredicts the pressure drop [70]. Most authors disagree on the failure that

takes place in the pipeline during horizontal slug flow pneumatic conveying so that the determination of the stress transmission coefficient is an area of ongoing research.

$$K_{w\_passive} = \frac{1 + \sin \phi \cdot \cos (\omega + \phi_w)}{1 - \sin \phi \cdot \cos (\omega + \phi_w)} \quad (3.76)$$

$$K_{w\_active} = \frac{1 - \sin \phi \cdot \cos (\omega - \phi_w)}{1 + \sin \phi \cdot \cos (\omega - \phi_w)} \quad (3.77)$$

where

$$\sin \omega = \frac{\sin \phi_w}{\sin \phi}$$

To simplify the determination of  $K_w$ , Mi established a semi-empirical correlation between wall friction angle  $\phi_w$  and static internal friction angle  $\phi_s$  [51]. Based on measurements of radial stress and calculations of axial stress, Mi proposed the following correlation:

$$\phi_s = \frac{4}{3} \cdot \phi_w \cdot \gamma_b^{\frac{1}{3}} \quad (3.78)$$

with  $\gamma_b = \frac{\rho_b}{\rho_w}$  where  $\rho_w$  is the density of water at 4°C.

Mi described slug flow as an active stress case and applied Eq. 3.77 to calculate  $K_w$ . Eq. 3.78 presents great advantage in that the stress transmission coefficient can be calculated using only measurements of wall friction angle. In his review, Sanchez [70] showed that the correlation of Mi gives good results when used to predict the pressure drop.

From a general point of view, the problem related to the accurate determination of the stress transmission coefficient remains unsolved. The stress transmission coefficient has rarely been measured successfully by experiments. In some cases accurate stress measurement devices were available, but in the experiments the authors failed to reproduce the actual transport conditions that occur during slug flow pneumatic conveying or in other studies the measurements took place directly in the conveying pipe but the results were not reliable due to inadequate measuring devices (see Section 2.4.7).

Due to the high pressure gradient that characterises slug flow pneumatic conveying, the conveying gas expands significantly between the pipe inlet and outlet. If steady-state flow and constant mass flow rates are assumed, the decrease of the gas density leads to the proportional increase of the conveying gas velocity along the pipe. Consequently, the transport mechanisms and the slug properties like slug length and velocity or even the mode of flow may change over the pipeline. Furthermore, in the operating area of slug flow, because the operating curves are particularly steep, a slight increase or decrease in the gas velocity leads to high variations of the pressure gradient, i.e. the pressure gradient at the beginning of the pipeline is higher than the pressure gradient in further pipe sections located downstream.

However, the gas expansion is not always considered in the predictive approaches. For example, Konrad developed his predictive method by assuming gas incompressibility and indicated that the predicted

results show good agreement in a pipe of one meter length. Other authors recommend performing the calculation for a pipe no longer than ten meters or the pipe should be separated into successive sections, where the gas velocity at the entrance of the pipe  $n + 1$  is calculated regarding the pressure decrease in the pipe  $n$  by applying the conservation law.

Calculations were carried out by applying the models of Konrad, Mi, Pan, Yi and Muschelknautz presented previously. The observation that the overall conveying pressure difference increases exponentially with the pipeline length led Muschelknautz to develop a model that considers the air expansion. The models of Mi and Pan also consider the air expansion. Both predictive methods were developed for an average air density over the pipe length. The models of Konrad and Yi initially developed for a constant air density were modified to take into account the air expansion. Calculations were also carried out with the original models to allow comparison between the results of the pressure loss prediction with and without consideration of the air expansion. All calculation sheets are presented in Annex A.2.

Similarly to other existing models that consider the changes in the air density along the pipeline, the air expansion was taken into account by considering the average air density over the pipe instead of the air density in standard conditions of pressure. Since an additional equation was needed to determine the average air density, the conservation law was applied:

$$P_{inlet} \cdot \rho_{f\_inlet} = P_{outlet} \cdot \rho_{f\_outlet} \quad (3.79)$$

The conveying process was considered isothermal and the pressure at the pipe outlet  $P_{outlet}$  equal to the atmospheric pressure. Therefore, an additional equation could be obtained to express the pressure loss as a function of the average air density:

$$\Delta P = \frac{2 \cdot P_{outlet} \cdot \rho_{fm}}{\rho_{f\_outlet}} - 2 \cdot P_{outlet} \quad (3.80)$$

As a result, the three unknown dimensions pressure loss, slug velocity and average density could be predicted using an iterative procedure based on a system of three equations. In addition, the average air velocity could be calculated as following:

$$v_{fm} = \frac{v_{f\_atm} \cdot p_{atm}}{\frac{\rho_{fm} \cdot R_a \cdot T_0}{M_{air}}} \quad (3.81)$$

Fig. 3.11 shows that according to the Muschelknautz model, a decrease in the air velocity leads to an exponential increase of the pressure gradient. Therefore, the model reproduces correctly the trend of the pressure gradient observed in dense phase pneumatic conveying. The key parameters of the model are the friction factor  $f_w$  and the ratio solids velocity to gas velocity  $\eta$ . Fig. 3.11 indicates that the choice of the velocity ratio influences significantly the predicted pressure gradient. Muschelknautz recommended a value of  $\eta = 0.2$  for the transport of plastic pellets [86]. However, a velocity ratio between  $\eta = 0.6$  and  $\eta = 0.8$  is usually observed during the transport of coarse particles.

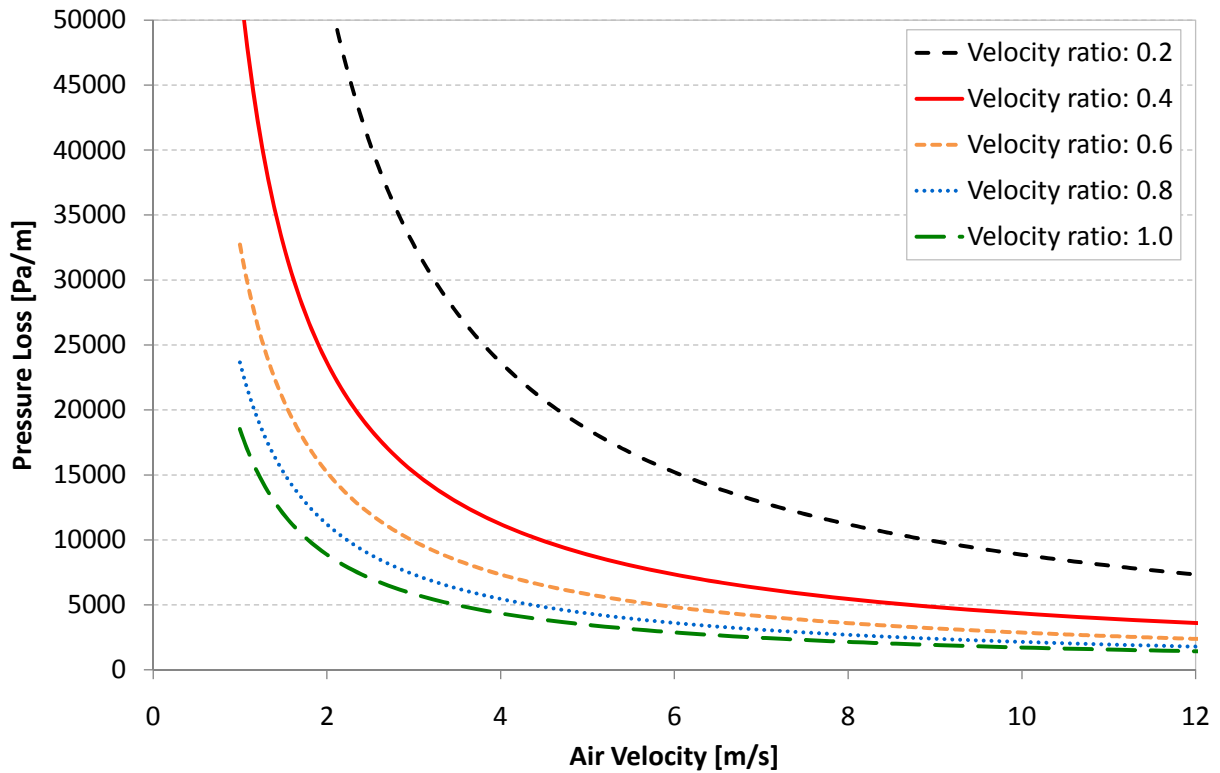


Figure 3.11: Pressure drop prediction by applying the Muschelknautz model

Fig. 3.12 to 3.15 allow a comparison between the pressure losses predicted by applying the models of Konrad, Mi, Pan and Yi. The predicted results are presented for different values of stress transmission coefficient. The calculations were carried out for a pipe of one meter length and different values of stress transmission coefficient, i.e. for active stress case ( $K_w = 0.4$ ), passive stress case ( $K_w = 2.3$ ),  $K_w = 1$  and for the  $K_w$ -value calculated by applying the model of Mi ( $K_w = 0.8$ ). The solids mass flow rate was kept constant and set to 5300 kg/h. In Fig. 3.12 to Fig. 3.15, the experimental pressure gradient obtained for this given mass flow rate is also depicted.

The best agreements between the experimental and predicted pressure gradient are obtained for the calculations with  $K_w = 1.0$  and  $K_w = 0.8$  (according to Mi's model). The calculations based on the assumption of a passive stress case overpredict the pressure gradient (Fig. 3.13) while the pressure gradient is underpredicted when an active stress case is assumed (Fig. 3.12). This contradicts the results of Sanchez [70].

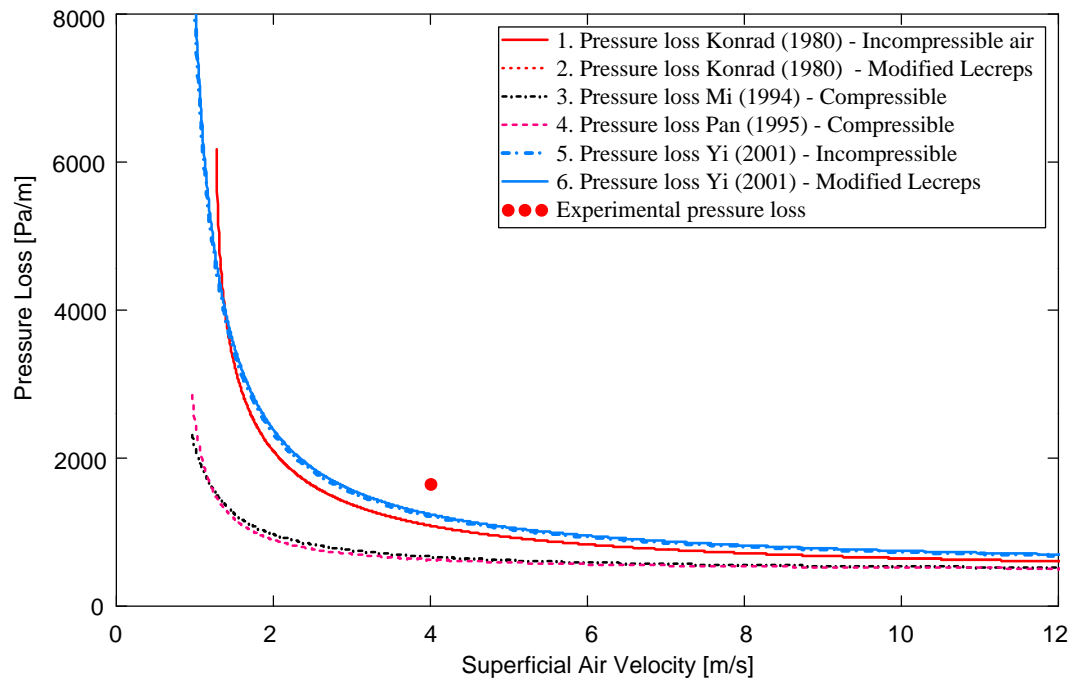


Figure 3.12: Pressure drop prediction with assumption of an active stress case -  $K_w = 0.4$

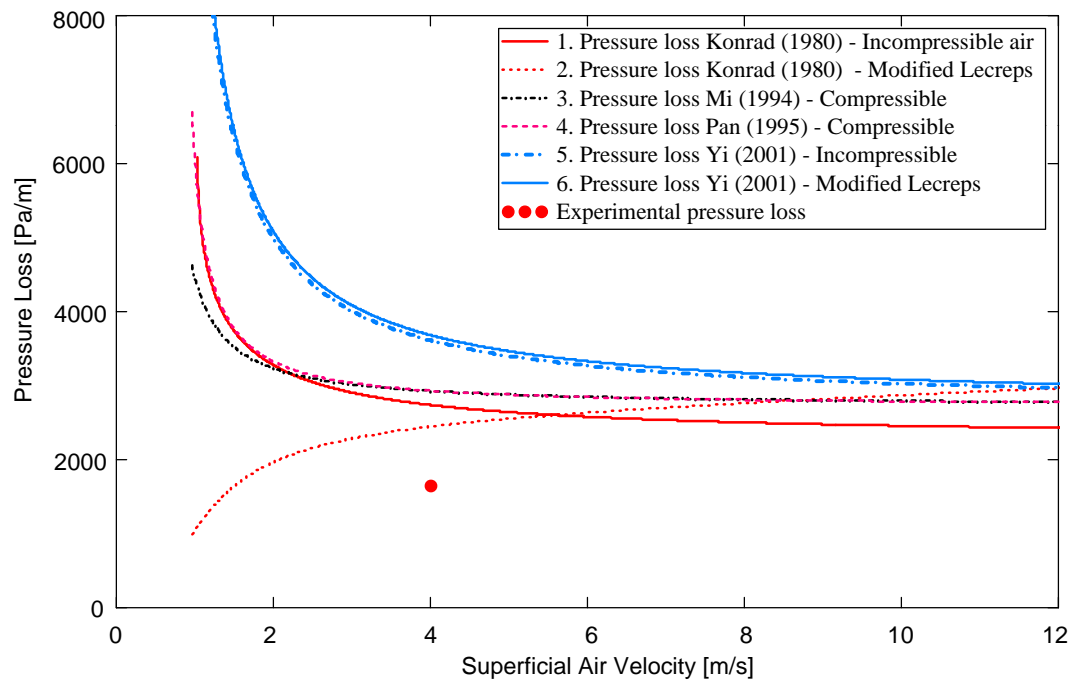
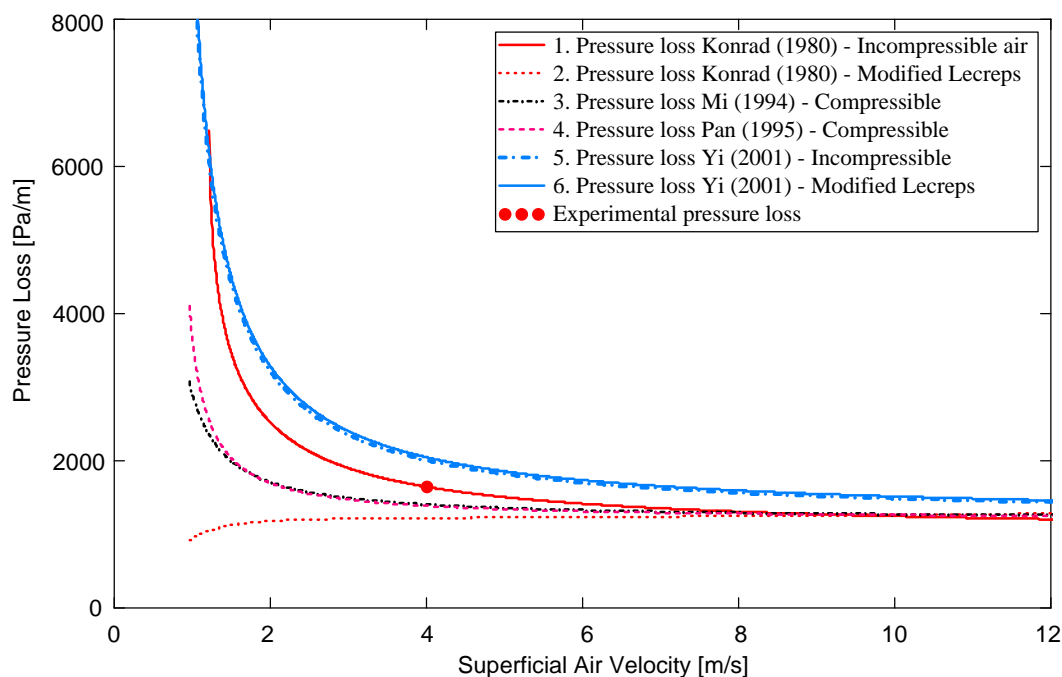
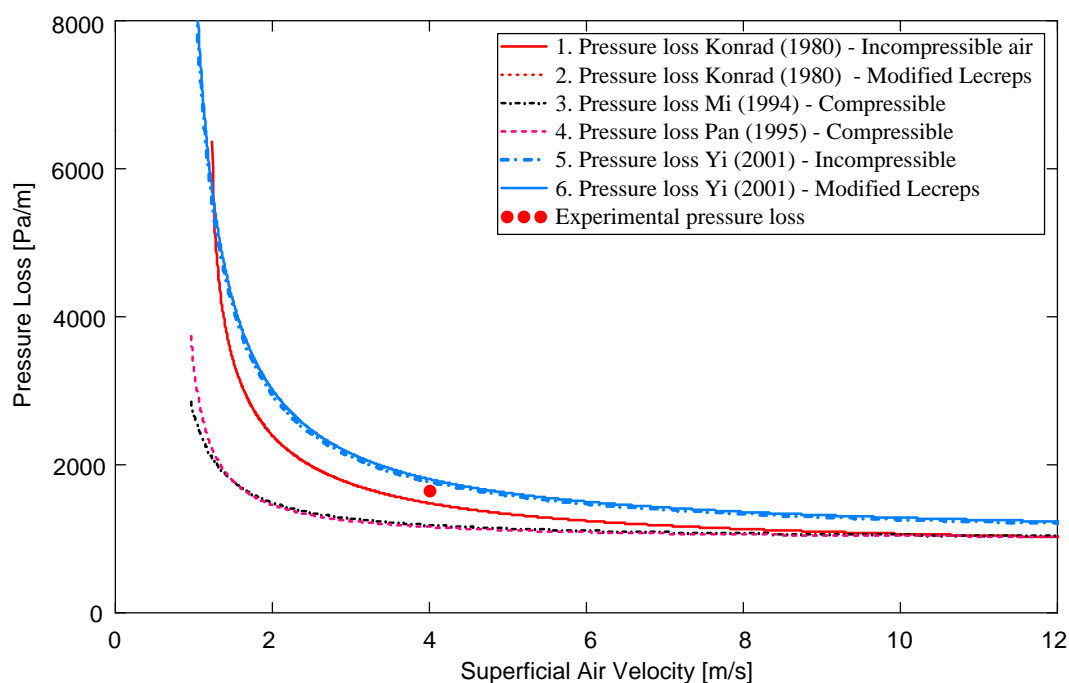


Figure 3.13: Pressure drop prediction with assumption of a passive stress case -  $K_w = 2.3$



Figure 3.14: Pressure drop prediction with  $K_w = 1.0$ Figure 3.15: Pressure drop prediction with the  $K_w$ -value calculated by applying Mi's model -  $K_w = 0.8$ 

In the range of air supply velocity where slug flow occurs, it is acknowledged that an increase in the air velocity leads to the decrease of the pressure gradient. The pressure gradient predicted by applying the models proposed by Konrad, Mi, Pan and Yi shows effectively such a trend. However, the pressure gradient calculated by applying the Konrad model modified to consider the gas expansion shows the opposite trend for  $K_w$ -values bigger than 0.5. The same observation can be made when the calculations

are carried out for a bigger pipe length, for example  $L = 10$  m, independently on the  $K_w$ -value used (Fig. 3.16).

The increase of the pressure loss calculated with Konrad's model with the increase of the air supply velocity is due to the cubic equation used by Konrad to predict the particle velocity. Fig. 3.17 shows the particle velocity calculated by using the cubic equation proposed by Konrad.

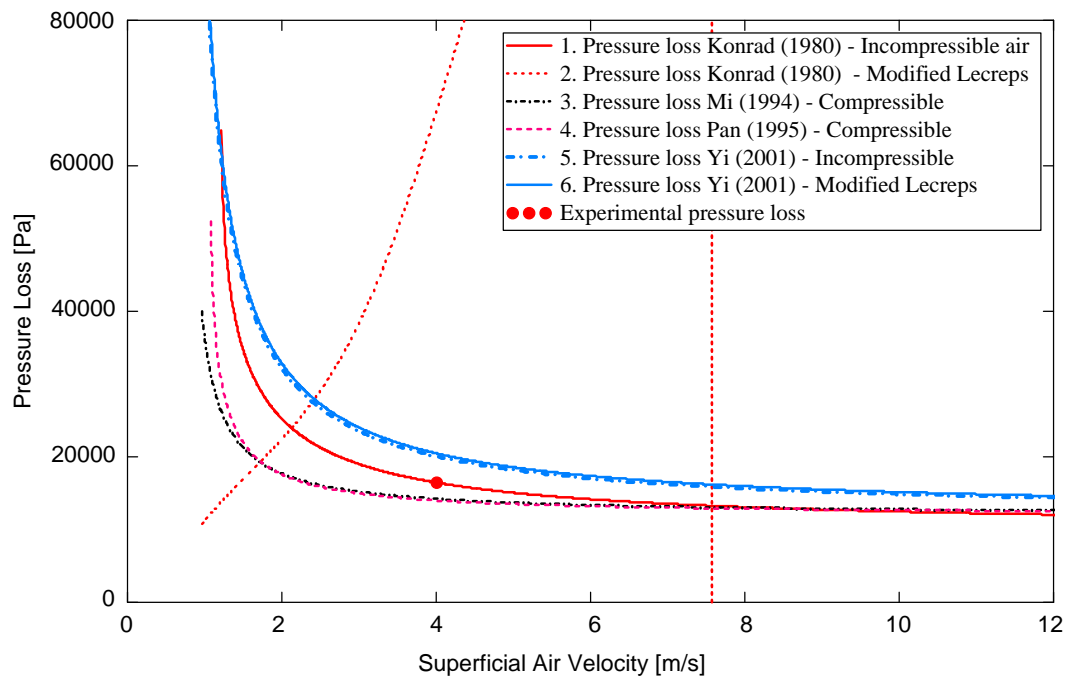


Figure 3.16: Pressure drop prediction with  $K_w = 1.0$  for a pipeline of  $L = 10$  m length

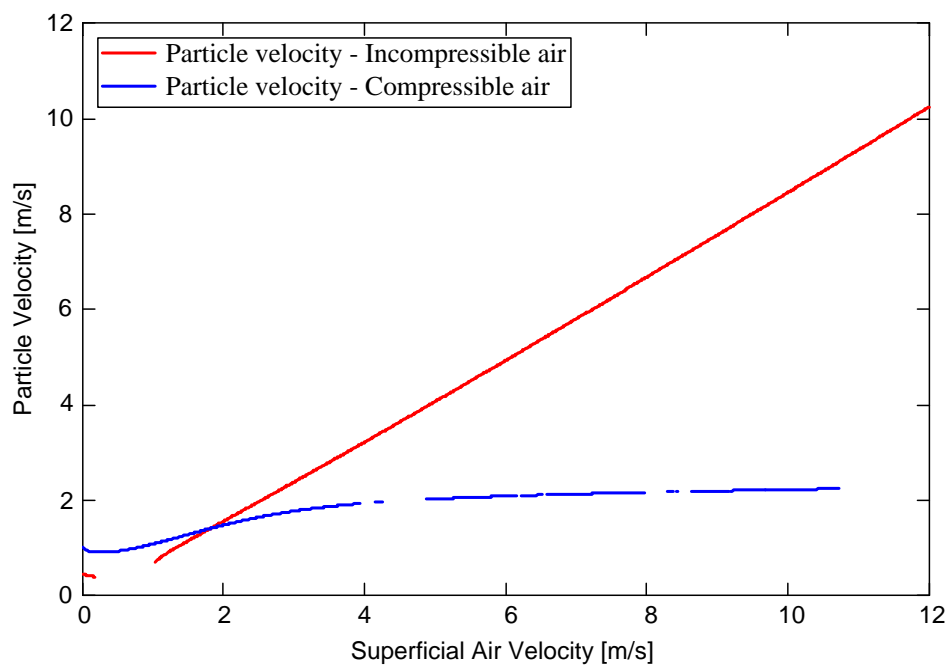


Figure 3.17: Particle velocity calculated by applying the cubic equation proposed by Konrad  
 $L = 10$  m -  $K_w = 1.0$

When the air expansion is not considered, an increase in the air velocity leads to the linear increase of the particle velocity. In this case, the air density is assumed to be a constant, i.e.  $\rho_f = 1.2 \text{ m}^3/\text{kg}$  along the entire pipe section. However, when the air expansion is taken into account, the particle velocity reaches an asymptote and is not higher than  $v_p = 2.2 \text{ m/s}$ . In this case, the particle velocity is a function of the air density.

The air density used for the calculation is the average air density for the pipeline section considered. Since the air density decreases with the decrease of the pressure along the pipeline, the longer is the length of the pipe considered for the calculation, the smaller is the value of the air density used for the calculation. In addition, the particle velocity is also a function of the  $K_w$ -value. As a consequence, not only the length of the pipe considered but also the  $K_w$ -value significantly affect the particle velocity and the pressure loss calculated. Konrad initially developed a model to predict the pressure loss in horizontal slug flow pneumatic conveying without considering the air expansion. Therefore, he recommended to apply the calculation procedure he proposed only for very short pipe sections. In this work, the model of Konrad was modified to consider the changes in the air density. However, the results show that the equations used in the model are not capable of taking into account the changes in the air density. As a further result, the Yi model was found to display similar pressure loss values when either air compressibility or incompressibility is considered.

The models of Konrad, Mi, Pan and Yi require a value for the slug porosity. Slugs are usually assumed to be packed columns with a porosity equal to the bulk porosity. Therefore, the calculations presented above were performed for a slug porosity of 0.38, which is the bulk porosity of the material conveyed. In order to illustrate the influence of the porosity value on the predicted results, the pressure loss was predicted for porosity values up to 0.60. Fig. 3.18 shows that the influence of the slug porosity is particularly significant for very low values of air velocity. However, those values are located under the minimum air velocity where conveying occurs. An increase in the slug porosity leads to the increase of the pressure gradient calculated by applying the models of Mi, Pan and Yi. However, the model of Konrad shows the opposite trend. According to Konrad's model, the transport of denser slugs is characterised by a higher pressure gradient. Such a trend reflects at best the physical mechanisms occurring during slug flow pneumatic conveying: fluidised slugs are easier to transport than dense slugs.

It should be pointed out that the models of Konrad, Mi, Pan and Yi were developed for the transport of slugs, which are dense enough to allow the transmission of stresses by interparticle contacts. Therefore, the porosity values chosen to perform the pressure loss calculation presented in Fig. 3.18 serve only as parameters to illustrate mathematically the influence of this slug characteristic on the prediction results.

The discussion of the existing models shows that experimental investigations on slugs are necessary to validate the different assumptions made by the authors of the models. In particular, investigations should focus on the internal porosity within slugs and the existence of a stress transmission across the pipe cross-section.

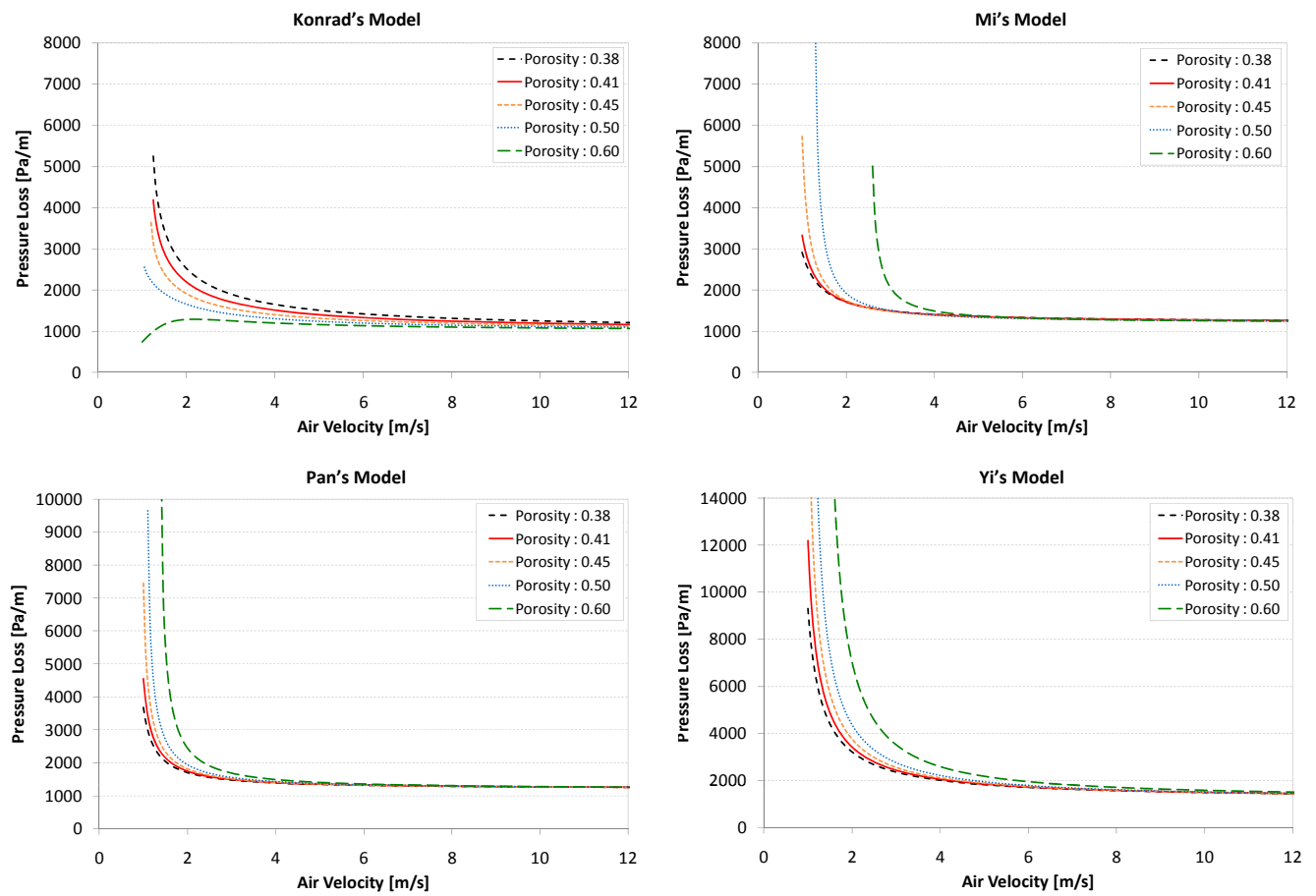


Figure 3.18: Influence of the slug porosity on the calculation results

## 4. Material and methods

### 4.1. Test material

Conveying experiments were carried out with Polypropylene-granules (PP) from the firm Tragor GmbH, Mainz. The granules are white, have a regular shape and a form between lentils and spheres. Table 4.1 lists the main physical properties of the material tested. The wall friction angle  $\phi_w$  was determined using a Jenike shear cell TSG-70/140. The bulk porosity  $\varepsilon_{bulk}$  is 0.38. Based on particle size and material characteristics, the product conveyed displays non-cohesive behaviour.

Table 4.1: Physical characteristics of the test material

Material characteristic	
Test material	Polypropylene
Aerodynamic equivalent diameter (AED)	3 mm
Equivalent spherical diameter (ESD)	4.3 mm
Particle density $\rho_s$	889 kg/m <sup>3</sup>
Bulk density $\rho_b$	553 kg/m <sup>3</sup>
Wall friction angle on stainless steel $\phi_w$	9.7°±0.7°

To improve the optical tracing of slugs during conveying and allow reliable determination of the particle velocity, black particles were added to the white Polypropylene pellets in a ratio of 1/100 to play the role of tracers without changing the characteristics of the product transported. The black particles consist in the same granules than the white Polypropylene pellets investigated but are coated with black colour.

### 4.2. Conveying rig

The test product was conveyed in a 80 mm i.d. industrial-scale pilot plant (Fig. 4.1). The total conveying length from product feeding to the last bend after which the material conveyed enters the last vertical section downward to the storage silo is 35.3 m. Two horizontal sections of 15.0 m and 13.7 m enclose a 6.5 m long vertical pipeline. The conveying rig is fully controllable by a SPS-Step7® of the firm Siemens AG by using the user interface provided by the software SIMATIC MANAGER of the same firm. The product feeding is performed using a dual silos system: two silos are positioned on each other so that at the end of a conveying test, the product can fall from the storage silo (element 6 in Fig. 4.1) in which atmospheric conditions prevail back into the pressure vessel (element 7 in Fig. 4.1). The product transport takes place in-batch. With the material tested, stable slug flow can be maintained over ninety seconds when conveying is performed with the lowest air supply velocity where slug flow occurs. During conveying, overpressure prevails in the pressure vessel, so that the product

can fall into the conveying pipeline solely under effect of the force of gravity. The particles are fed into the pipe when the inlet air velocity is larger than some threshold value and feeding is naturally stopped when the air velocity becomes smaller due to the pressure increase. Using this system, the product mass flow rate can only be controlled by adjusting the air supply velocity. Therefore, a strong relation exists between air and solids mass flow rate.

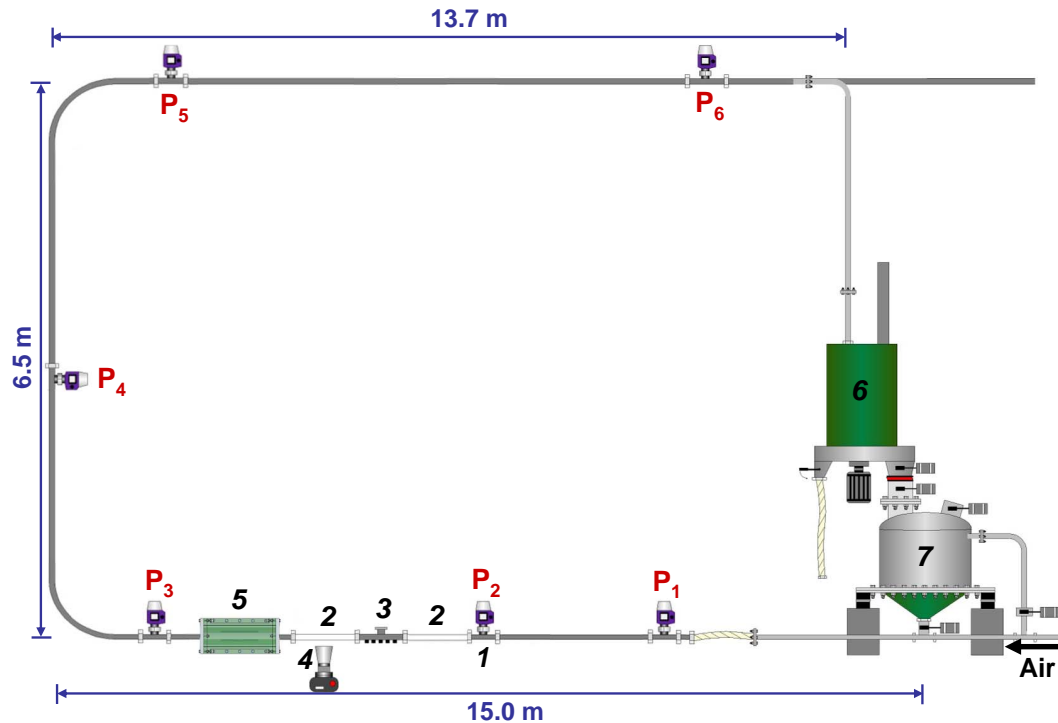


Figure 4.1: Industrial-scale pilot plant: 1. pressure transducer, 2. Plexiglas pipes, 3. probe for force and pressure measurements, 4. CCD camera, 5. slug-catcher, 6. storage silo, 7. pressure tank

The solids mass flow rate can be followed using four load cells on which the pressure vessel is positioned. The load cells deliver a continuous signal about the weight, whereby the trend of the product mass flow rate can be calculated.

Six pressure transducers type Cerabar M Endress+Hauser, Germany (element 1 in Fig. 4.1) allow the measurement of the total wall pressure at different locations over the pipeline and therefore provide information about the pressure loss along the entire conveying pipeline. Fig. 4.1 shows the position of the pressure transducers in the pipeline. Details about the configuration of the pipe sections separated by the pressure transducers are given in Table 4.2.

Further details about the components 2 to 5 described in Fig. 4.1 will be provided in the next sections.

Table 4.2: Length of the different sections of the 80 mm i.d. pipeline

Section	Length <sub>horizontal</sub> [m]	Length <sub>vertical</sub> [m]	Length <sub>bend</sub> <sup>a</sup> [m]
1-2	5.08	-	-
2-3	2.00	-	-
3-4	-	3.24	8.96
4-5	1.15	3.60	8.96
5-6	12.05	-	-
1-6	20.28	6.84	17.93

<sup>a</sup>Fictive length [25]

### 4.3. Control of air supply

The supply of air mass flow rate is controlled using four de Laval nozzles, which ensure a constant air mass flow rate independently from the back pressure changes. The control of the de Laval nozzles is realised by means of a pressure regulator placed ahead, whose opening angle can be varied by the SPS. The air mass flow rate delivered was calibrated for NIST standard conditions of temperature and pressure (20°C; 1 atm). During the experiments, the temperature is assumed as a constant. Therefore, both air mass flow rate and superficial air velocity are known (Eq. 4.1).

$$\dot{V}_f = \frac{\dot{V}_N \cdot P_N \cdot T_0}{T_N \cdot P_f} \quad (4.1)$$

### 4.4. Determination of slug velocity

The slug velocity was determined using optical tracking of black tracer particles mixed with the test material. Two short sections of stainless steel pipeline were replaced by two transparent Plexiglas pipes in front of which a camera was positioned. The motion of the black tracer particles transported by a slug was recorded using a CCD camera Type CV-M10BX firm JAI Corporation, Japan with a 6 mm objective lens. To optimise the image shot, the shutter speed was set to 0.25 ms and the maximum frame frequency of 30 Hz was chosen. A 640 W photo lamp was used to deliver the additional light necessary to optimise the photo contrasts. The computer programme OPTIMAS of the firm Weiss Imaging And Solutions GmbH, Bergkirchen/Gründing, Germany was used to analysis the images.

To determine the particle velocity, the horizontal motion of tracer particles was followed between each couple of successive images. The vertical motion of the particles is assumed to be negligible. Therefore, the particle position on two successive images can be directly compared. Because of the optical distortion resulting from the lens on the one hand and from the pipe curvature on the other hand, the distance between two points had to be calibrated according to their position over the pipeline

height. Fig. 4.2 shows the cylinder marked with a net placed inside the Plexiglas pipeline to realise the calibration. The net was used as reference image and served as a scale for distance determination. 0.5 cm separates two marked points in both the horizontal and vertical direction.

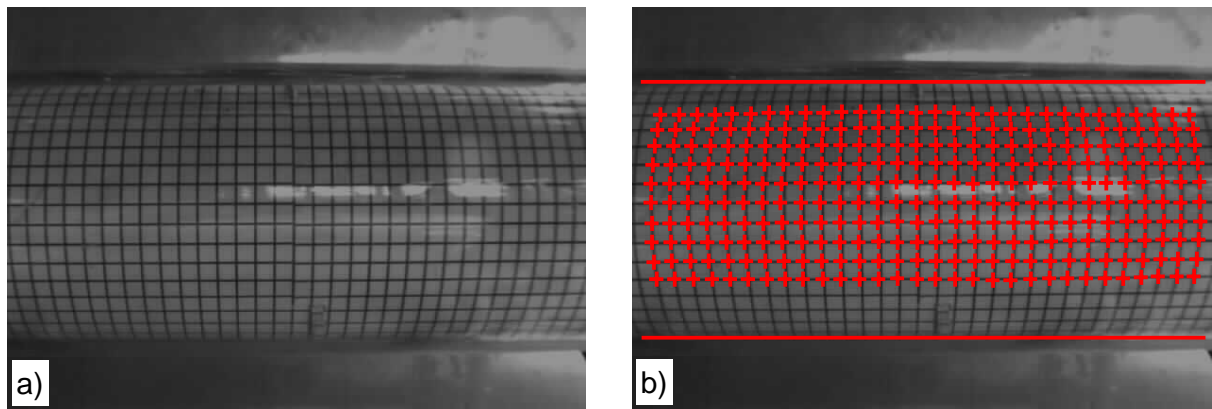


Figure 4.2: a) Reference image of a Plexiglas pipe with net; b) Marked points reflecting the net scale

The velocity of the particles was calculated with respect to the distance covered by a particle and the frame frequency. Fig. 4.3 shows a marked tracer particle and the distance it travelled in 33 ms.

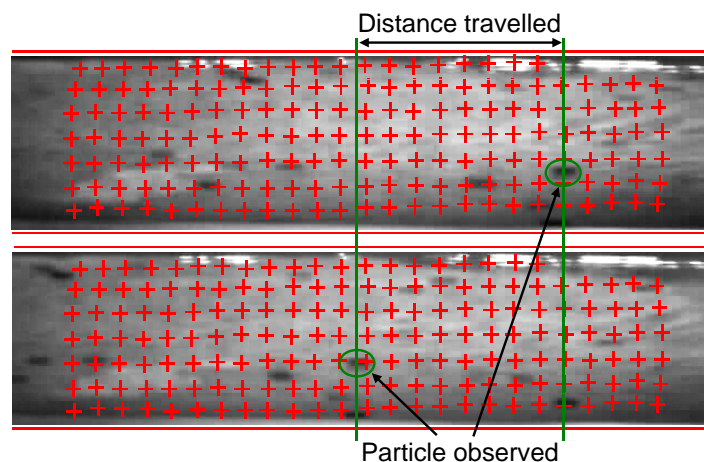


Figure 4.3: Two successive camera images with superposition of the net used to determine the particle velocity within a slug

According to their position along a slug, the particles display different velocities. Slug flow can be compared to a wave-like flow where particles move slower at the front because they have just been picked up and have to be accelerated to the slug velocity but also at the back because particles have lost energy and drop back. By assuming that the slug velocity corresponds to the particle velocity in the centre of a slug, the influence of the air supply velocity on the slug velocity could be investigated.



## 4.5. Measurement probe for the simultaneous detection of pressure, radial and wall shear stress

### 4.5.1. General description and measurement principle of the probe

Niederreiter [60] developed and constructed a measurement device that allows the simultaneous detection of two key physical characteristics for slug flow pneumatic conveying, i.e. the pressure within a slug and the stresses a slug induces at the pipe wall. The measurement probe has the particularity to allow both the radial and wall shear stress to be measured simultaneously and locally around the pipeline circumference. For this purpose, a short pipeline section has been instrumented with both pressure and force sensors (Figure 4.4). Two piezoelectric force sensors type 208C01 PCB Piezotronics Inc., USA perpendicular to each other are connected to a measurement plate of 970 mm<sup>2</sup> surface area, which simulates a piece of the pipeline wall and enables the simultaneous detection of the wall shear stress and normal stress induced by a slug (Fig. 4.5). Moreover, six miniature pressure sensors XTM-190M, Firm Kulite Semiconductor Products INC, New Jersey measure the pressure along a slug each 35 mm apart. Another pressure sensor is located in the measurement chamber where both force sensors are built in. It aims to check that no significant pressure difference takes place between the conveying pipe and the measurement chamber, i.e. that no force resulting from a potential overpressure in the conveying pipe is detected by the measurement plate. The pressure equilibrium is ensured by small holes drilled on each side of the measurement plate. Tests showed that the pressure equilibrium takes place relatively instantaneously and does not affect the measurement of the forces. In addition, a NTC-thermocouple placed directly in the measurement chamber enables a sensitive control of the temperature. This control is necessary since piezoelectric components are very sensitive to temperature. During conveying, these components undergo a temperature increase. However, since the force measurements were realised over a short time, the influence of the temperature on the results was negligible and could be corrected manually.

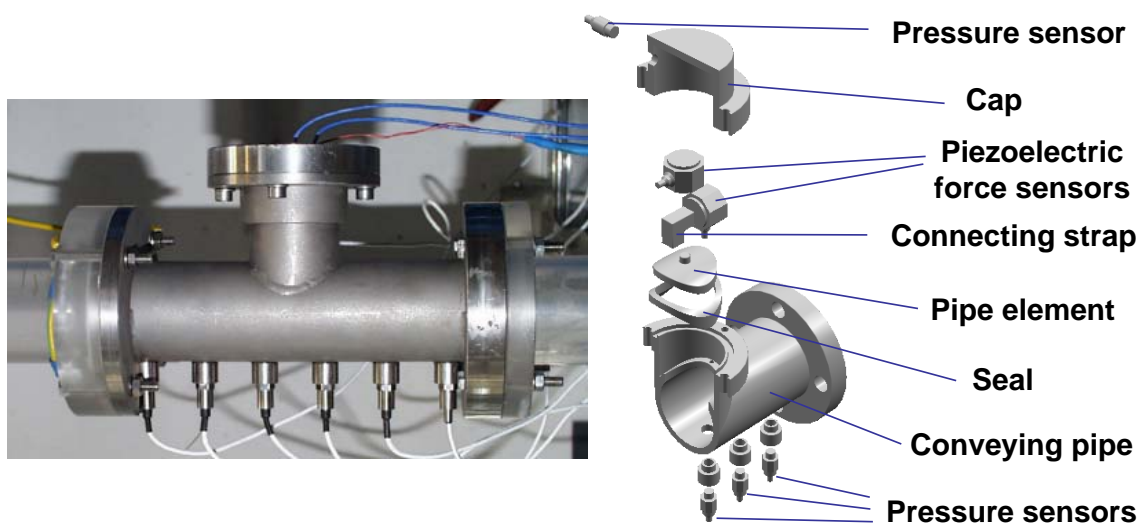


Figure 4.4: Image and construction scheme of the probe for the simultaneous detection of wall shear stress, normal stress and pressure inside a slug [60]

The probe was rotated over the horizontal axis, so that the forces were detected successively at different positions around the pipeline circumference. All measurements were realised without the conveying process being disturbed. The forces were measured at the bottom, side and top of the pipeline, with 90° between each measurement position.

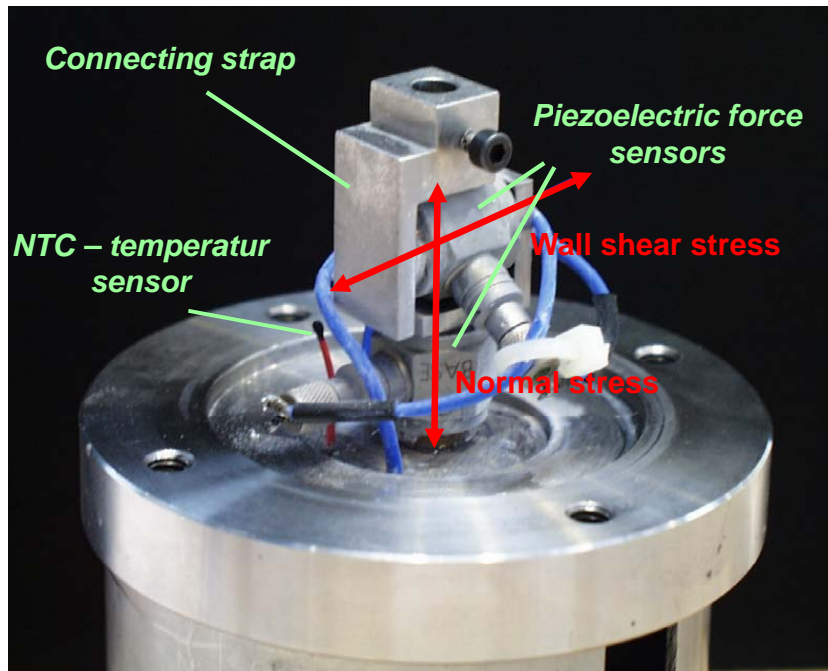


Figure 4.5: Perpendicular arrangement of the force sensors in the measurement chamber [60]

The stresses induced by slugs in the wall area can be calculated from the force measurements using Eq. 4.2 and 4.3. Because of the curvature of the measurement plate whose geometry follows the geometry of the pipe, the plate has both a contact surface and a projection surface. The projection surface is used for the calculation of the radial stress whereas the contact surface is used for the calculation of the axial stress at the wall.

$$\sigma_{radial} = \frac{F_{radial}}{A_{plate\_projection}} \quad (4.2)$$

$$\sigma_{axial} = \frac{F_{axial}}{A_{plate}} \quad (4.3)$$

#### 4.5.2. Investigations on the raw force signals and optimisation of measurement quality

Niederreiter designed a probe and developed a concept not only to detect both radial and wall shear stresses but also to process the data obtained from the force signals so that results are reliable. However, the optimisation of the data process was required to guarantee the accurate detection of the forces during pneumatic conveying. Therefore, investigations were carried out on the raw signals delivered by the force sensors in order to optimise the force detection from an electrotechnical point of view, to relate

the signals to the physical phenomena occurring in the pipeline and to ensure reliability of the results. The investigations focused particularly on the determination and analysis of the frequencies contained in the signals measured.

#### 4.5.2.1. Determination of the natural frequency of the system

The piezoelectric sensors constitute a spring–mass system. On condition that the stress point is well defined and the stress direction remains constant, the system can be approximated by a linear system with a single degree of freedom. Therefore, the frequency response can be described using a differential equation of second order [72].

The natural frequency of the system, which characterises its dynamic properties, is affected by all components, i.e. all masses taking part to the system as defined. The natural frequency of the system was determined by applying a unit impulse function (Dirac delta function) on the measurement plate. By determining the damping factor and the cutoff frequency of the response, it is possible to verify if the sensors can correctly reproduce the signal frequencies provided by a mechanical stress. Fig. 4.6 shows the impulse response of the radial force sensor after application of a local and short stress on the measurement plate by using a 3 g heavy steel bullet.

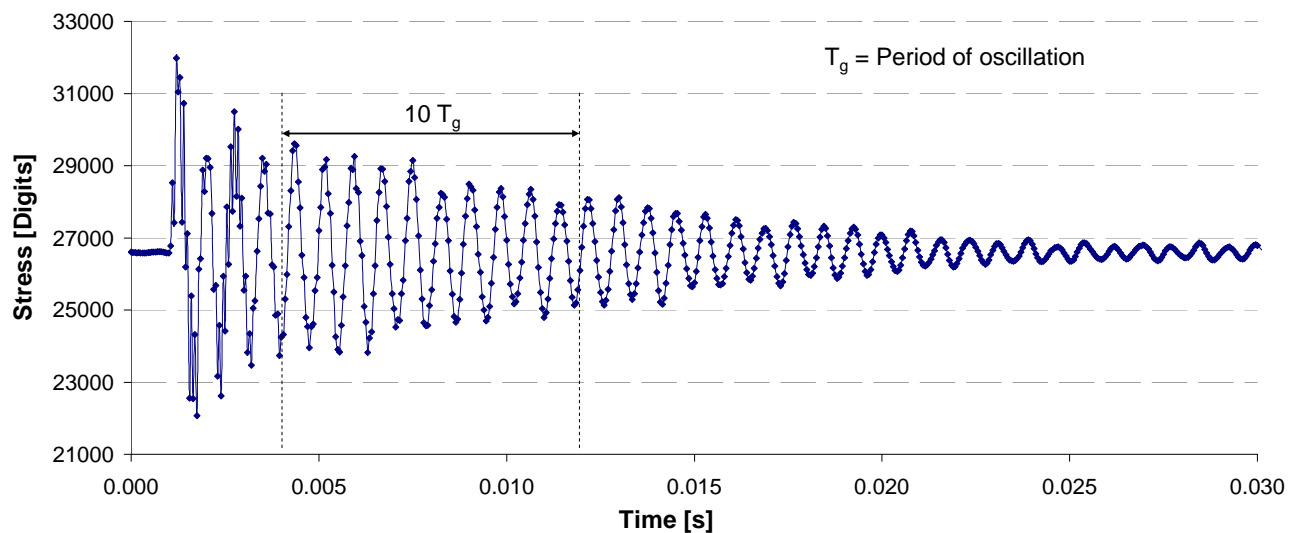


Figure 4.6: Impulse response of the radial force sensor to the impact of a 3 g heavy steel bullet,  $f_{sampling} = 20.000$  Hz

To be able to determine the natural frequency of the system, it is assumed that a system stimulated in all band of frequencies oscillates with the cutoff frequency  $f_g$ . For instance, this is what happens when a system is stimulated by a short and local impact. In this case, the period of oscillation  $T_g$  (Fig. 4.6) and the resulting undamped angular frequency  $\omega_0$  can be determined (Eq. 4.4).

$$\omega_0 = \frac{2 \cdot \pi}{T_g} \quad (4.4)$$

The damping ratio of the system is determined by calculating the amplitude attenuation using the envelope curve of the oscillating signal. An exponential function is obtained, which contains the damping coefficient  $K_s$ .  $K_s$  is used together with the undamped angular frequency  $\omega_0$  to calculate the damping ratio  $\zeta$  (Eq. 4.5).

$$\zeta = \frac{K_s}{\omega_0} \quad (4.5)$$

The damped natural frequency of the system is finally calculated according to Eq. 4.6.

$$f_N = \omega_0 \cdot \sqrt{1 - \zeta^2} \quad (4.6)$$

The dynamic characteristics of the force measurement system are summarised in Table 4.3.

Table 4.3: Dynamic characteristics of the force measurement system

	Angular frequency $\omega_0$ [Hz]	Damping coefficient $K_s$ [Hz]	Damping ratio $\zeta$ [-]	Natural frequency $f_N$ [Hz]
axial	1250	107	0.086	1240
radial	1250	104	0.083	1240

Since the natural frequency of the system depends on all elements composing the entire system, it has to be re-determined after each change made in the construction such as the exchanging of the silicone seal (Fig. 4.4).

#### 4.5.2.2. Nyquist-frequency

The Nyquist–Shannon sampling theorem states that the perfect reconstruction of a signal is possible when the sampling frequency is greater than twice the maximum frequency of the signal being sampled [75] or equivalently, when the Nyquist frequency exceeds the highest frequency of the signal being sampled. The Nyquist-frequency is half the sampling frequency of a discrete signal processing system (Eq. 4.7):

$$f_{Nyquist} = \frac{1}{2} \cdot f_{sampling} \quad (4.7)$$

If lower sampling rates are used, the original information contained in the signal may not be completely recoverable from the sampled signal. Basically, a Nyquist frequency just larger than the signal bandwidth is sufficient to allow the perfect reconstruction of the signal from the samples. Signal frequencies higher than the Nyquist frequency will encounter a "folding" about the Nyquist frequency, back into lower frequencies. This is called aliasing (Fig. 4.7). To avoid aliasing, the Nyquist frequency must be strictly greater than the maximum frequency component within the signal. For example, if a signal has an upper band limit of 10,000 Hz, a sampling frequency greater than 20,000 Hz will avoid aliasing and allow theoretically perfect reconstruction.

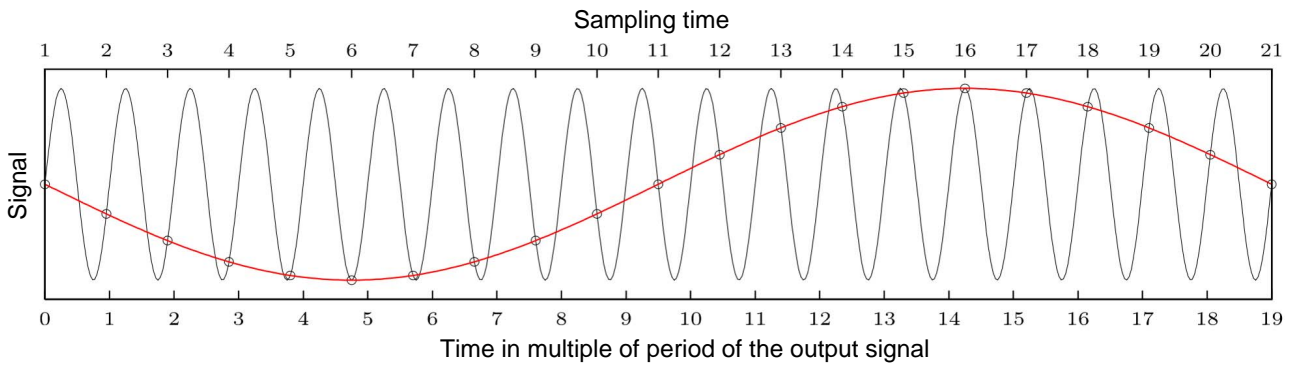


Figure 4.7: Aliasing: The signal reconstructed from samples is different from the original continuous signal

#### 4.5.2.3. Determination of the optimal measurement frequency

The measurement plate detects the forces induced by slugs in the wall area and transmits them to the force sensors. The piezoelectric sensors deliver analogue signals, which are first digitalised using an A/D converter 16 bit / 1000 Hz before being processed using the software LabVIEW (Fig. 4.15). The resolution of the signals is limited by the maximum sampling rate of the A/D converter. The A/D converter allows a maximum sampling rate of 200,000 Hz when a single channel is used. This maximum sampling rate is divided in half for each doubling of the number of measurement channels. The choice of the accurate sampling frequency results from a compromise between accurate signal reproduction and computer data overload. Therefore, the raw signals were investigated to determine the minimal sampling rate allowing the accurate reconstruction of the signals.

The radial forces induced by a single slug during pneumatic conveying were detected in the wall area using sampling rates of 100,000 Hz, 40,000 Hz and 10,000 Hz successively. The raw signals obtained were analysed by applying a special form of Fourier transform, the Fast Fourier transform (FFT). FFT permits to describe which frequencies are contained in the original signal and provides a continuous and periodic spectrum of frequencies. The Fourier transform has perfect frequency resolution, but no time information. Therefore, FFT delivers which frequencies are contained in a defined signal area but does not give any information on the moment they occur. On the one hand, the errors in the frequency spectrum can be minimised if the time interval chosen for the FFT-analysis is big. On the other hand, a better frequency-time correlation is provided if this time interval is small. Based on a compromise between a good time-frequency correlation and a precise frequency spectrum, intervals of  $2^{13}$  values were chosen to perform the FFT-analysis.

Fig. 4.8 a) shows the raw signal detected by the measurement plate during the passage of a slug conveyed with 7.4 m/s air velocity. The passage of this slug in the time window 1.0 to 1.5 seconds induces a distinct stimulation of the signal. The results of the FFT-analysis carried out on the signal segment indicated in Fig. 4.8 a) shows that the signal detected by the measurement plate oscillates in a frequency domain between 0 and 20,000 Hz (Fig. 4.8 b)). In Section 4.5.2.1, it was shown that the natural frequency of the system is about 1200 Hz. The harmonics have frequencies that are multiples of this natural frequency. In 4.8 b) the natural frequency (1240 Hz), the 1<sup>st</sup> harmonic (2480 Hz), the

8<sup>th</sup> harmonic (9920 Hz), the 12<sup>th</sup> harmonic (14,880 Hz) and the 15<sup>th</sup> harmonic (18,600 Hz) can be recognised.

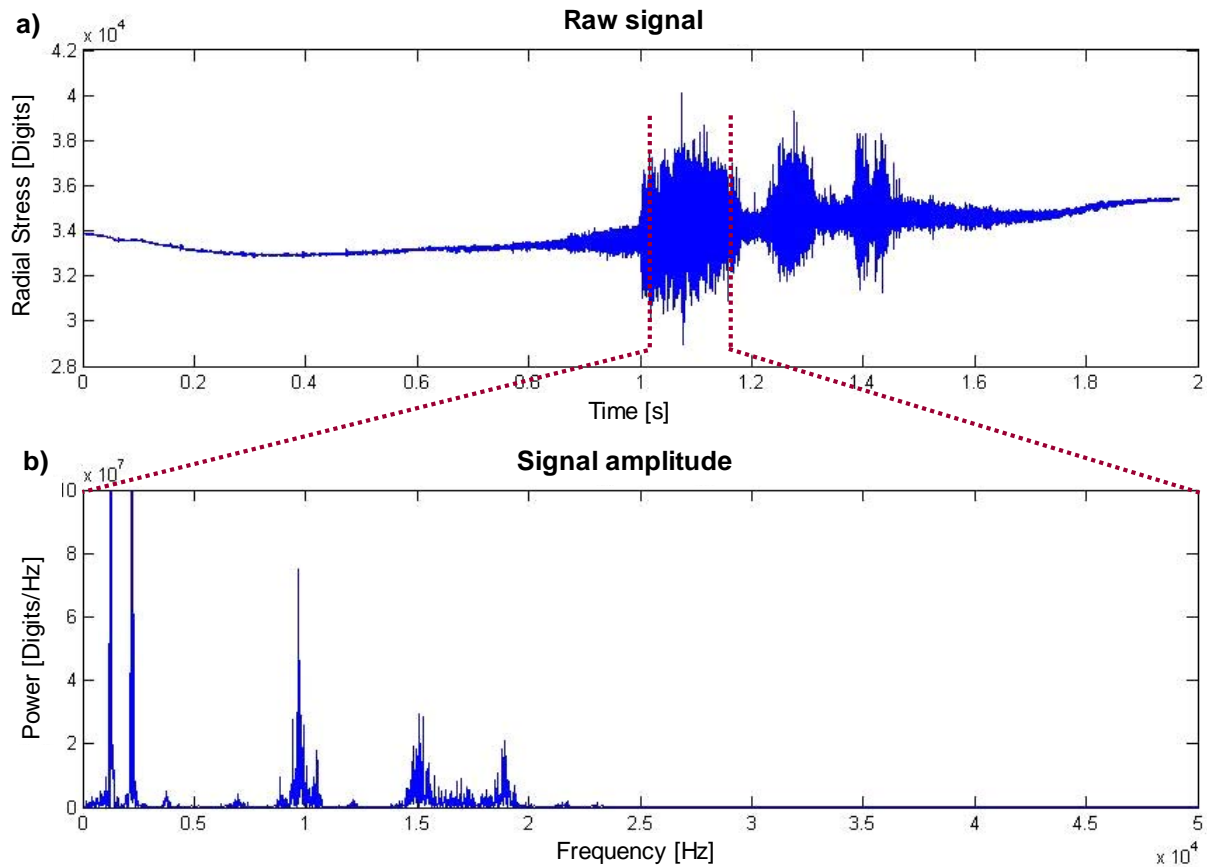


Figure 4.8: Raw signal detected with  $f_{sampling} = 100,000$  Hz during the passage of a slug conveyed with 7.4 m/s air velocity

In addition, FFT-analysis was performed on signals detected during the passage of a slug conveyed with a different air velocity. Fig. 4.9 shows the results of the FFT-analysis performed on a raw signal detected during slug conveying with  $v_f = 8.0$  m/s. The same harmonics as in Fig. 4.8b) can be recognised.

The maximum frequency of the raw signal harmonics amounts to 20,000 Hz. Therefore, according to Nyquist, a sample frequency of at least 40,000 Hz is required to reproduce the signal correctly. Fig. 4.10 shows the FFT analysis performed on a raw signal detected with a sampling rate of 40,000 Hz. To allow the direct comparison with the frequencies spectrum obtained with a sampling rate of 100,000 Hz, the slugs were conveyed in the same conditions than in Fig. 4.8. The comparison of both FFT-analysis shows that the frequencies contained in the raw signals lie in the same frequencies domain, which proves that no signal distortion occurred by reducing the sampling rate to 40,000 Hz. It should be noted that the different scales on the frequency-axis in Fig. 4.8 and Fig. 4.10 are due to the fact that only half the sample frequency is available for a FFT-analysis.

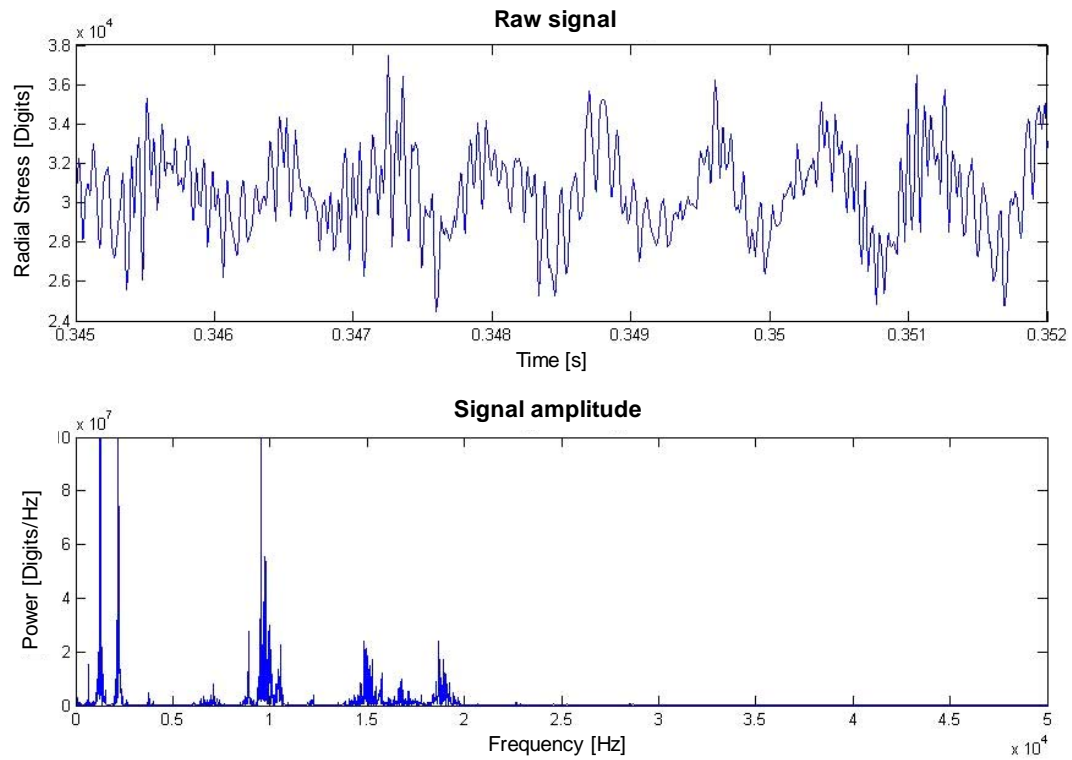


Figure 4.9: Raw signal detected with  $f_{sampling} = 100,000$  Hz during the passage of a slug conveyed with 8.0 m/s air velocity

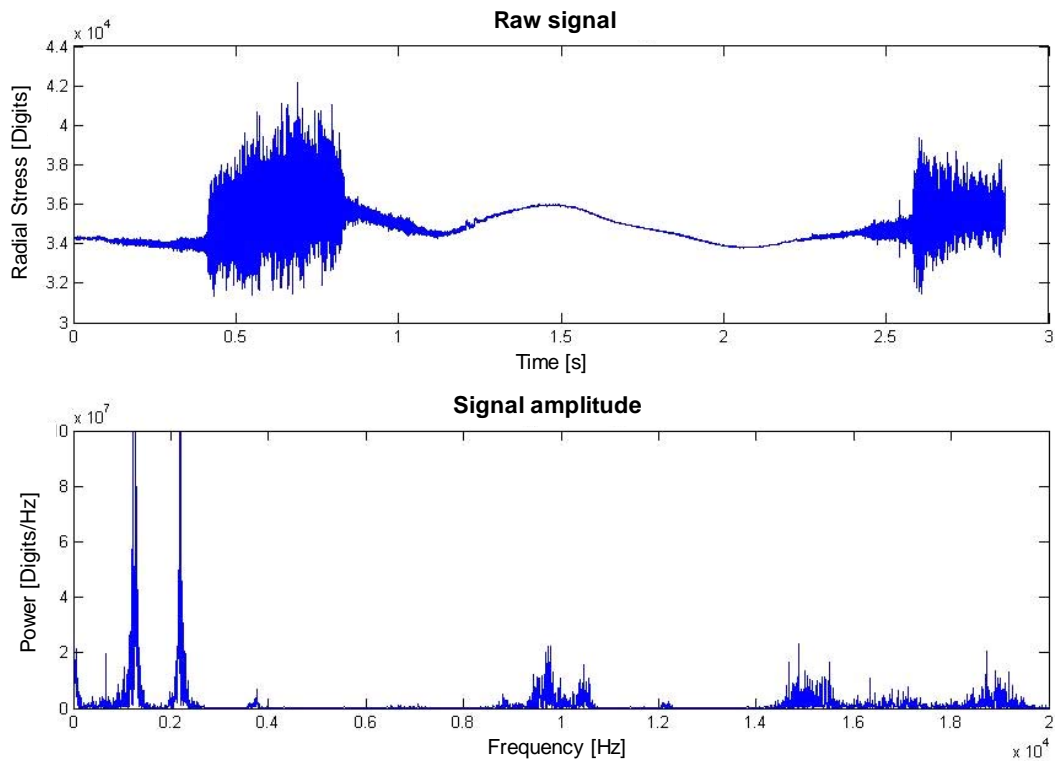


Figure 4.10: Raw signal detected with  $f_{sampling} = 40,000$  Hz during the passage of a slug conveyed with 7.4 m/s air velocity

According to Nyquist, the choice of a sampling rate lower than 40,000 Hz may lead to aliasing, i.e. to incorrect detection of high frequencies, which are recognised as low frequencies and falsely reproduced. However, the detection of the high frequencies is not useful in the present case since they will be filtered out by the application of a Bessel low-pass filter in the next step of the signal process. Nevertheless, it is necessary to verify if additional low frequencies appear in the signal by reducing the sampling frequency. To guarantee a signal with good resolution, the sampling rate has to be at least three times higher than the natural frequency. Fig. 4.11 shows that all frequencies are truly reproduced and that no additional frequency appeared in the signal sampled with 10,000 Hz. Therefore, a frequency of 10,000 Hz is sufficient to sample the signals without overloading the computer.

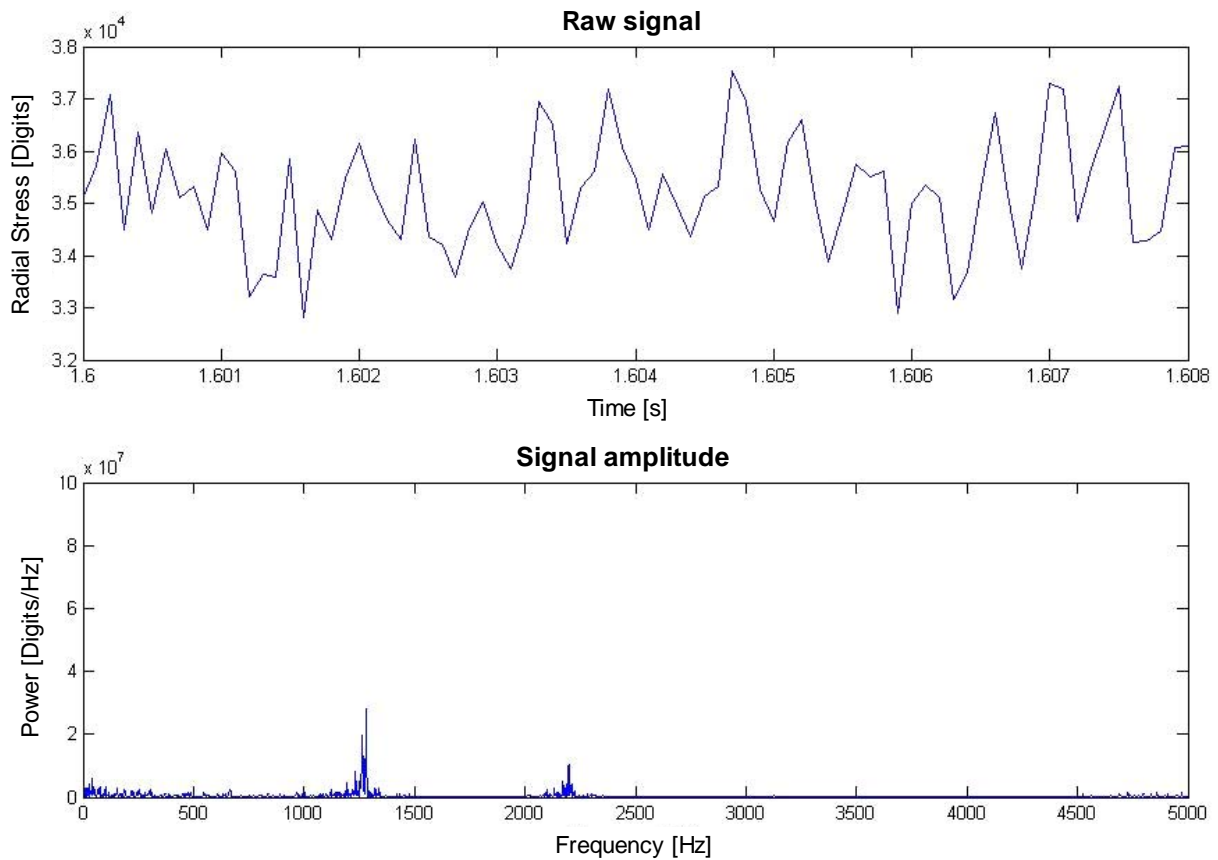


Figure 4.11: Raw signal detected with  $f_{sampling} = 10,000$  Hz during the passage of a slug conveyed with 7.4 m/s air velocity

Fig. 4.8, 4.10 and 4.11 differ in signal power. By sampling with a lower frequency, the oscillations peaks are not perfectly sampled and reproduced. This results in the decrease of the oscillations amplitude. However, the amplitude of the oscillations is not relevant in the present case since the application of a Bessel low-pass filter in the next signal process step will lead to their attenuation. Fig. 4.12 shows a signal before and after application of the Bessel low-pass filter.



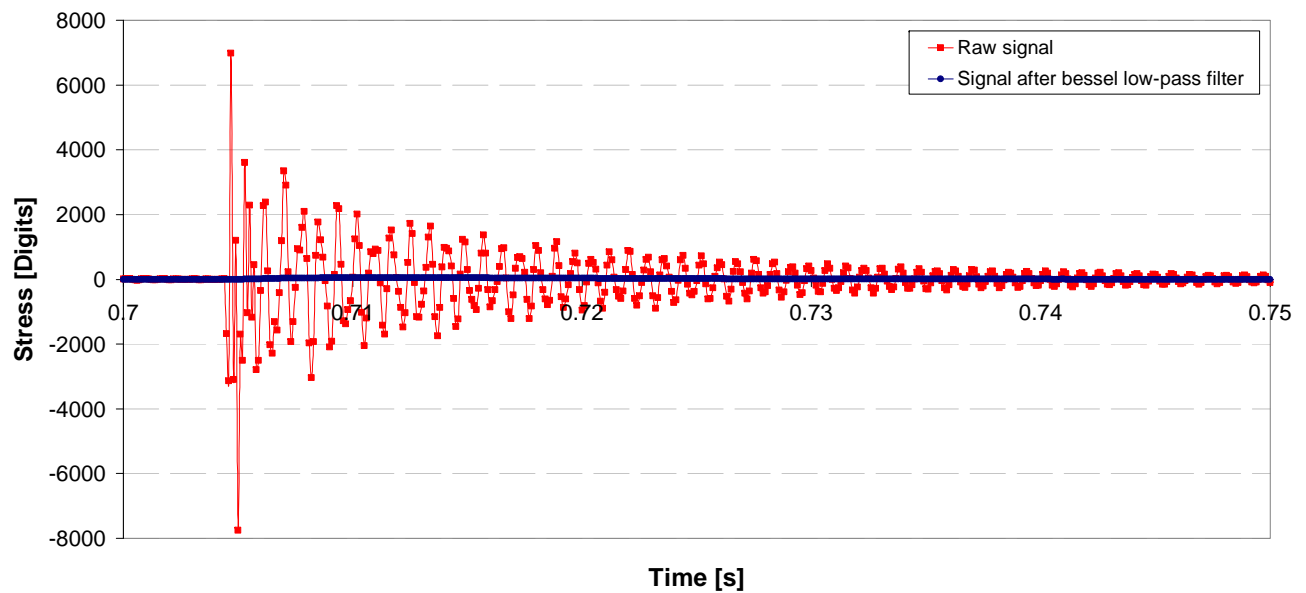


Figure 4.12: Response of the radial force sensor to an impulse before and after application of a bessell low-pass filter;  $f_{sampling} = 10,000$  Hz,  $f_g = 25$  Hz

#### 4.5.2.4. Is the force measurement plate suitable to detect impacts of single particles?

One of the objective of this work is to investigate which forces influence the transport of slugs and how these forces are physically induced. A slug can be considered either as a mass of particles or as an accumulation of single particles. In the last case, each single particle can be assumed as playing a role in the total acting force. Therefore, the hypothesis that similarly to the mechanisms occurring in dilute phase pneumatic conveying, impacts of particles on the pipe wall may have a significant effect on the acting resistance force has been investigated in this work.

The force measurement probe was developed by Niederreiter to investigate the radial and wall shear stress in the contact area between slug and pipeline wall. Due to the significant increase of the speed of computational data process in the last years, the maximum signal sampling rate of 100,000 Hz allowed by the A/D converter when only two channels are used for the measurements could be applied. Consequently, the capability of the measurement plate to detect potential single impacts of particles could be investigated.

In order to estimate the frequency of impulses that may occur during the passage of a slug, it is assumed that each particle in direct contact with the measurement plate is responsible for at least one impulse exchange. Furthermore, it is assumed that only one single layer of granules with a height equal to the equivalent spherical diameter can induce impulses. The minimal number of impulses occurring per time unit can be calculated if slug velocity, contact surface of the measurement plate and number of particles concerned are known.

The number of particles  $N_p$  in contact with the measurement plate can be calculated by using the volume of a single particle given by Eq. 4.8 and the volume over the plate that can be occupied by a layer of particles, which is given by Eq. 4.9.

$$V_p = \frac{4}{3} \cdot r_{eq}^3 \cdot \pi \quad (4.8)$$

$$V_{p_{total}} = A_{plate} \cdot d_{eq} \cdot (1 - \varepsilon_{bulk}) \quad (4.9)$$

$$N_p = \frac{V_{p_{total}}}{V_p} \quad (4.10)$$

On condition that the particle velocity is equal to the slug velocity, the impulse frequency can be calculated by using Eq. 4.11, which can be rearranged into Eq. 4.12. Hence, a linear correlation exists between slug velocity and particle impulses (Fig. 4.13).

$$I = \frac{v_p \cdot N_p}{d_{plate}} \quad (4.11)$$

$$I = \frac{A_{plate} \cdot (1 - \varepsilon_b) \cdot v_{slug}}{\frac{1}{6} \cdot d_{eq}^2 \cdot \pi \cdot d_{plate}} \quad (4.12)$$

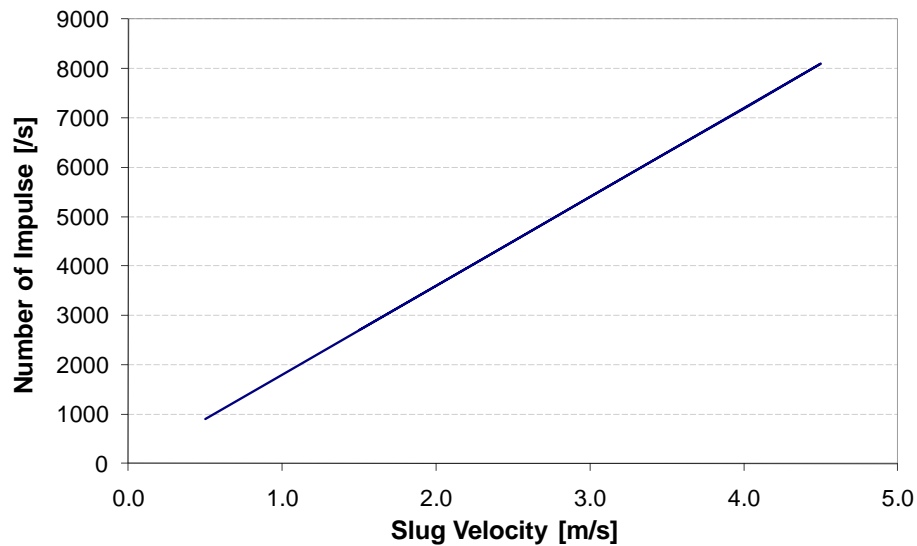


Figure 4.13: Theoretical increase of the estimated frequency of particle impulse on the measurement plate with the increase of the slug velocity

The theoretical impulse frequency illustrated in Fig. 4.13 would occur if particles hit the measurement plate in an equidistant time interval. According to Nyquist, a measurement frequency of 20,000 Hz would be high enough to detect the impulses generated by slugs moving with a velocity up to 5 m/s. However, impulses are generated stochastically and therefore do not follow any time condition. Hence, a sampling frequency of 100,000 Hz was chosen to investigate the signals generated by slugs conveyed with air supplies velocities of 7.4 m/s and 8.0 m/s.

If the measurement plate detects single impulses, the sensors can give two types of response. On the one hand, by detection of equidistant impulses, an increase of the impact frequency could lead the frequency band to move to higher frequencies. On the other hand, a signal noise over a large frequencies domain could appear if impulses occur stochastically. The signals from particles hitting the plate at the same time interfere constructively while signals from lagged hitting particles interfere destructively. Consequently, FFT-analysis would show a multitude of frequencies, which would be illustrated by a signal noise in a large frequencies domain.

If the measurement plate is suitable to detect single particle impulses, the height of the power peaks and their location in the frequencies domain should be a function of the particle velocity. However, the FFT-analysis presented in Fig. 4.8 and Fig. 4.9 show that none of these phenomena occur by increasing the slug velocity although a slight increase in the height of the peaks is discernable. This slight increase is due to the increase of the energy contained in the particles moving with higher velocity.

Impacts of particles on the measurement plate stimulate the measurement plate in a large frequencies domain similarly to a white noise. Therefore, the signals show a frequencies spectrum containing the natural frequency and the corresponding harmonics as shown in the detail of Fig. 4.8 presented in Fig. 4.14. The frequencies detected do not correspond to particle impulses but to oscillations of the measurement plate itself. The measurement plate can detect impulses only as a total force. This phenomenon is comparable to gas pressure, which can only be detected as a total wall pressure even if it results from the impulses of air molecules with the container walls .

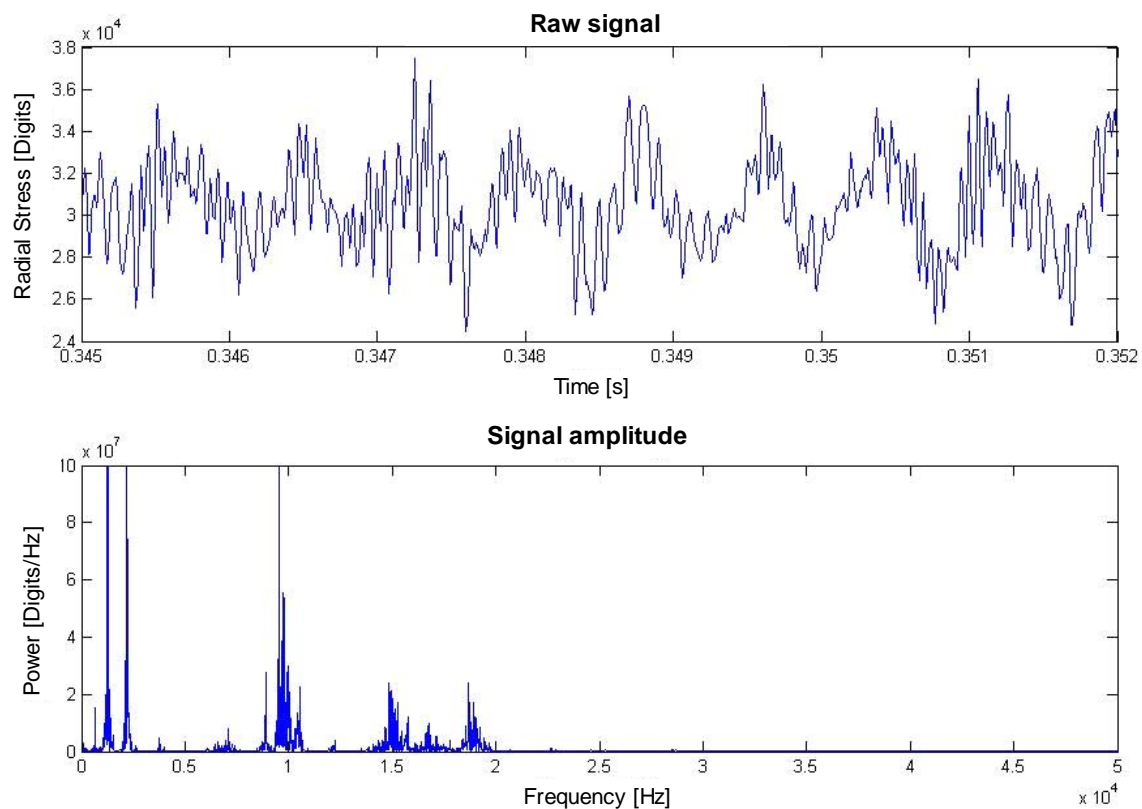


Figure 4.14: Superposition of oscillations - Detail from Fig. 4.8 -  $f_{sampling} = 100,000$  Hz,  $v_f = 7.4$  m/s

### 4.5.3. Signal processing using LabVIEW

The pressure and force sensors deliver analogue signals, which require to be converted in the physical parameters the sensors actually measure. First, the analogue signals in mV/V are amplified and then converted in digital signals using an A/D converter, Firm IOtech, Ohio. In the next step, the digital signals are computerised using the LabVIEW programme. LabVIEW configures the A/D converter with respect to sampling frequency and selection of the measurement channels. Afterwards, the programme is used to correct all factors disturbing the force signals, which result from the probe construction on the one hand and from the sensors themselves on the other hand. Fig. 4.15 shows the different processing steps necessary to obtain accurate measurements. Measurement plate oscillations, electric discharge of the capacitors composing the force sensors, temperature dependence, pressure dependence and interdependence between both sensors due to their perpendicular arrangement have to be calibrated first so that the force signals can be dynamically corrected during the measurements. After calibration of all interaction factors, two signals are delivered for the normal and wall shear stress. The processing of the signals delivered by the piezoresistive pressure sensors is easier since the digital signals in Digits only need to be re-scaled in Pascal using the calibration data.

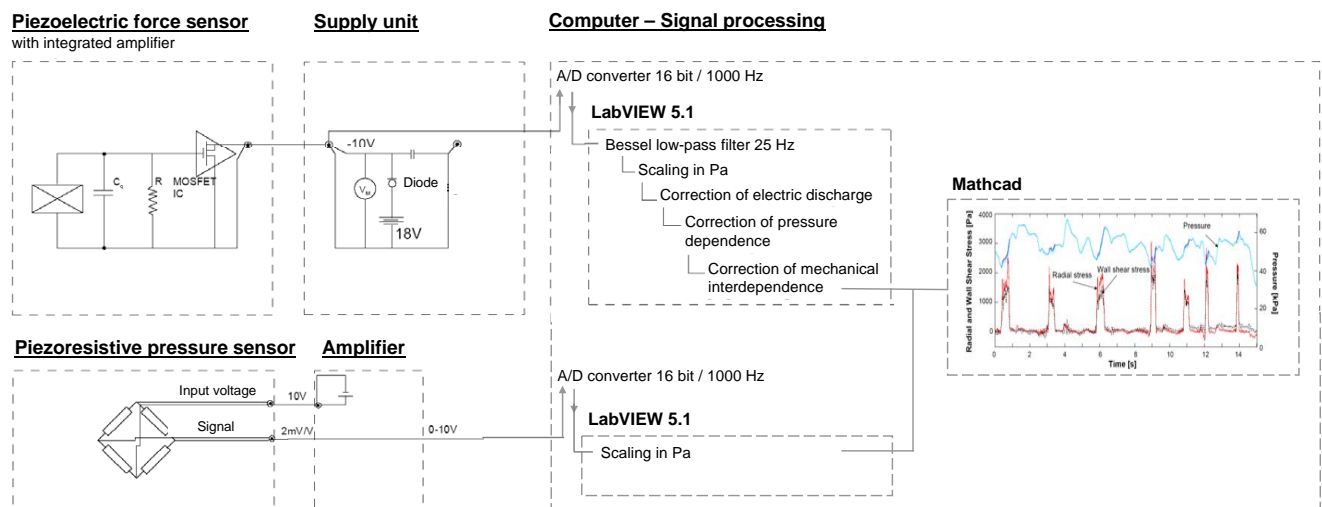


Figure 4.15: Schematic processing of the pressure and force signals

### 4.5.4. Calibration of the force sensors

Due to the nature of piezoelectric sensors on the one hand and to the measuring system itself on the other hand, several corrections have to be carried out on the original data before getting separately two reliable signals for the normal and wall shear stress. All corrections are realised automatically by the software LabVIEW after determination of the correction factors required in a calibration step. The following parameters have to be calibrated and corrected:

- the oscillations of the measurement plate
- the electric discharge of the capacitors composing the force sensors

- the pressure dependence of the sensors
- the interdependence between both force sensors due to their perpendicular arrangement.

Moreover, the correlation between strain and digital signal recorded has to be established.

#### 4.5.4.1. Signal scaling

The piezoelectric force sensors deliver signals whose amplitude is directly proportional to the strain. However, due to the construction form itself, the forces acting on the measurement plate are not fully transmitted to the force sensors (Fig. 4.5). Therefore, a calibration of the sensors is required to convert the signals obtained in Newton and further in Pascal.

The piezoelectric force sensors are calibrated by means of weights, which are used to stress each sensor individually in axial and radial direction (Fig. 4.16). A weight is placed on or is hung to the measurement plate and remains in place until the piezoelements are completely discharged. The measurement begins when the weight is removed. The amplitude of the signal peak obtained corresponds to the weight in Digits. This calibration method can be performed because piezoelements can measure both compressive and tensile forces. This method presents the advantage that the disturbing effect due to a brusque loading by placing the weight on the plate can be avoided.

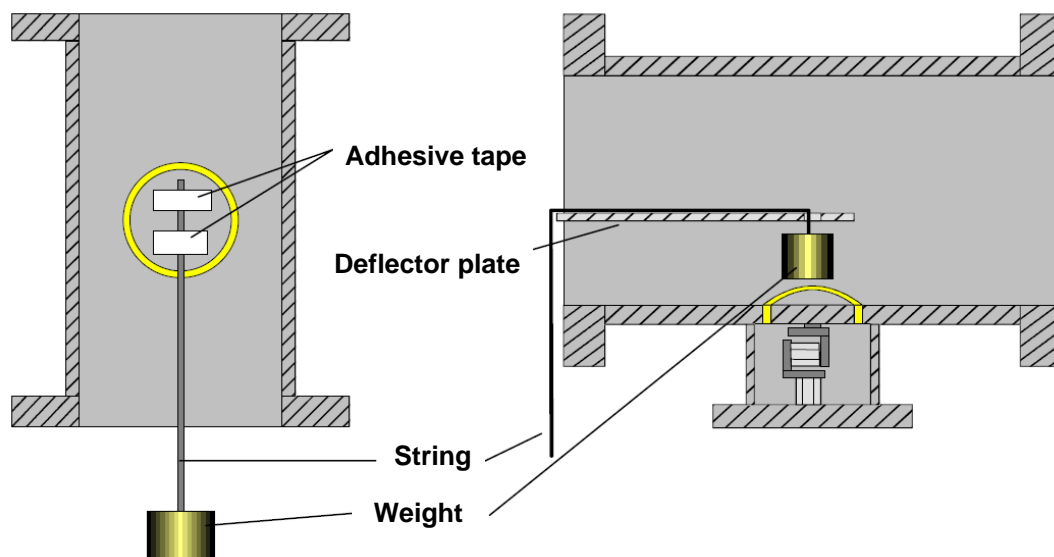


Figure 4.16: Scaling of axial and radial stress sensors using weights [60]

The gain is calculated by taking account of the mass  $m_{cal}$  applied and the loading surface. Eq. 4.13 and Eq. 4.14 permit to convert the signals in digits delivered by the A/D converter in stress in Pascal. By axial strain, the contact surface of the measurement plate  $A_{plate}$  is involved in the calculation whereas the projection surface of the plate  $A_{plate\_projection}$  has to be used by radial strain.

$$Gain(axial) = \frac{m_{cal} \cdot g}{A_{plate}} \cdot Value_{Digits} \quad (4.13)$$

$$Gain(radial) = \frac{m_{cal} \cdot g}{A_{plate\_projection}} \cdot Value_{Digits} \quad (4.14)$$

By applying successively different masses, the linear correlation between height of signal peak and force applied can be verified (Fig. 4.17).

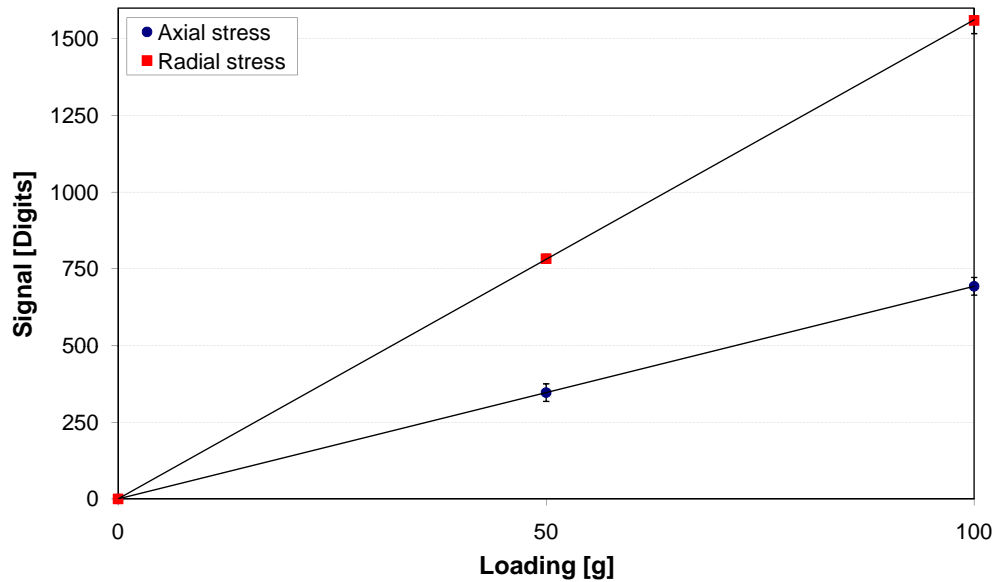


Figure 4.17: Linear correlation between strain and signal detected for both axial and radial force sensors

#### 4.5.4.2. Application of a Bessel low-pass filter

In Section 4.5.2.4, it was shown that the piezoelectric force sensors employed are not able to detect single impacts of particles on the measurement plate. Hence, both the radial and axial force induced by the passage of a slug are recorded as a total force that exhibits a continuous trend. In slug flow, those forces increase and decrease periodically. Therefore, they are detected as low-frequency oscillations corresponding to the frequency of the slug passage. The investigations carried out on raw signals showed that the stimulation of the measurement plate leads to high-frequency oscillations according to the harmonics (see Section 4.5.2.3). In order to eliminate those high frequencies, which can be considered as signal disturbances, a Bessel low-pass filter is applied on the digital signals.

A Bessel low-pass filter with a cutoff frequency of 25 Hz was chosen to damp the high frequencies contained in the signals. Due to the circular geometry of the measurement plate, the increase and decrease of the signals induced by the passage of a slug correspond to a sine function. The circular form of the plate presents advantage in that no abrupt increase and decrease of the signals occur by entry and exit of a slug in the measurement area. An abrupt signal increase or decrease could disturb the signal corrections. The use of a filter type Bessel was chosen because of its suitability to reproduce the rectangular stress function induced by the passage of a slug (Fig. 4.18).

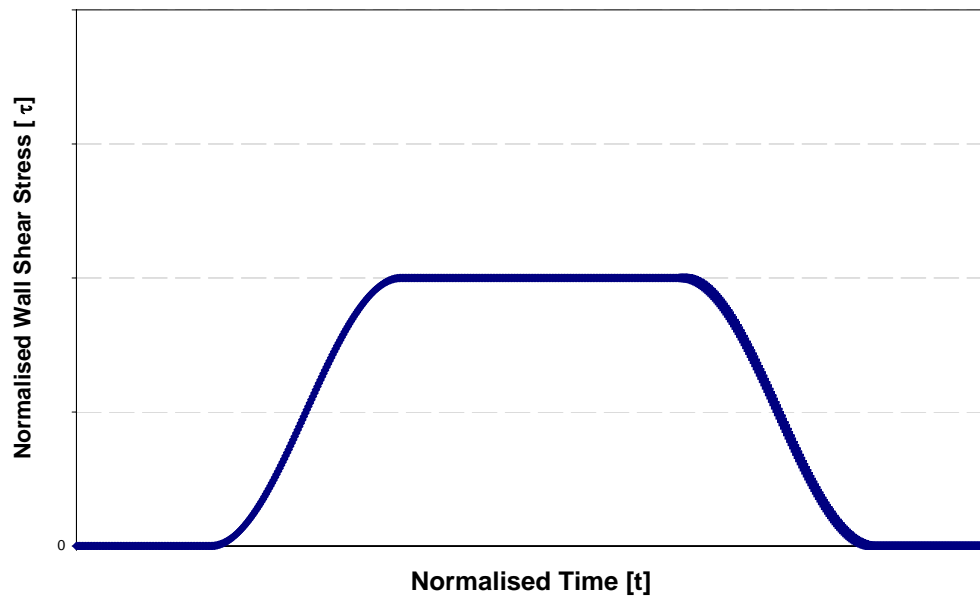


Figure 4.18: Rectangular function illustrating schematically the stress behaviour by passage of a slug on the measurement plate

Fig. 4.19 shows the damping behaviour of a Bessel filter of second order. The cutoff frequency corresponds to the frequency above which the signal amplitude is damped of 3 dB. Above the cutoff frequency, the amplitude damping increases highly. Therefore, frequencies higher than the cutoff frequency are almost totally eliminated from the signal while the low frequency resulting from the passage of a slug pass unchanged. The effectivity of a Bessel low-pass filter depends on the signal sampling rate, i.e. the accurate reconstruction of the signal sampled (see Section 4.5.2.3).

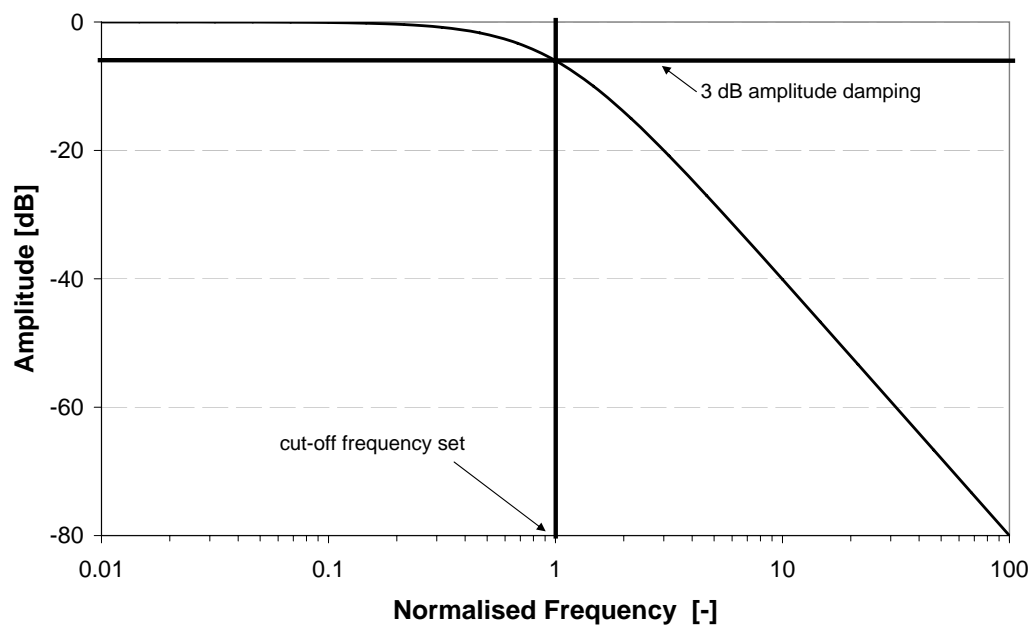


Figure 4.19: Damping behaviour of a Bessel filter of second order

#### 4.5.4.3. Correction of electric discharge of the piezoelements

The piezoelectric force sensors used have a cutoff frequency of 37 kHz, i.e. the amplitude error by signal transmission is lower than 3 dB up to a frequency of 37 kHz. With an amplitude error of 3 dB, only 50% of the real signal amplitude is still transmitted. The structure of the piezoelectric force sensors itself is therefore responsible for errors occurring by measurement of static, almost static and low-frequency signals.

Piezoelectric sensors are constituted of quartz elements, which are able to generate an electric field or electric potential in response to a mechanical stress applied. In equivalent circuit diagram, the quartz element corresponds to the parallel circuit of a capacitor with an ohmic resistance whose discharge follows an exponential function. For this reason, the signal resulting from the application of a constant stress on a piezoelectric sensor does not remain constant over the time but follows the resistance decrease according to an exponential function (Eq. 4.15) as shown in Fig. 4.20.

$$f(t) = a \cdot \exp\left(\frac{t}{b}\right) + e \quad (4.15)$$

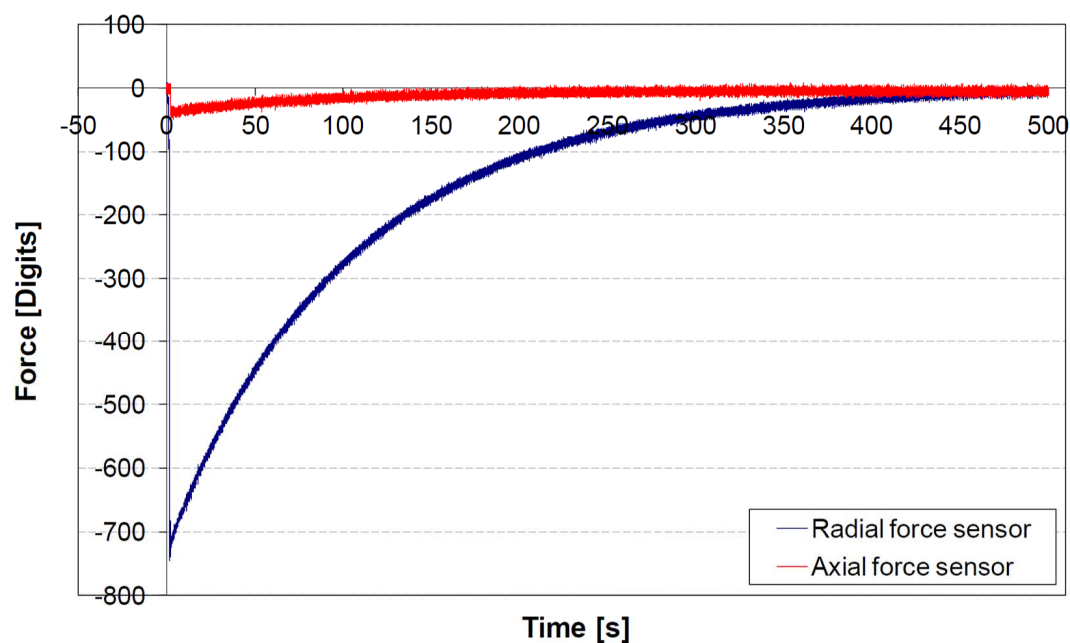


Figure 4.20: Discharge of both radial and axial force sensors by radial loading

By determining experimentally the coefficients in Eq. 4.15, the signal decay can be characterised and corrected. The factor  $b$  is the time constant, which describes the time required to discharge a capacitor to 36.8% of its initial voltage.

During conveying, the dynamic processes occurring in the pipeline lead to high fluctuations of the signals. However, a strain due to the overpressure prevailing in the pipeline steadily acts on the sensors. This permanent strain leads to the continuous discharge of the quartz elements over the time. Consequently, the occurring discharge errors  $\Delta F_i$  add over the time. Each sampled value contains the



errors of all preceding measurement points. In order to eliminate this disturbing effect, the error  $\Delta F_i$  is calculated according to Eq. 4.16 for each discretised value by using the sampling frequency  $f_{sampling}$  and the time constant  $b$  calculated by applying Eq. 4.15.

$$\Delta F_i = F_i \cdot \left( 1 - \exp \left( \frac{1}{b \cdot f_{sampling}} \right) \right) \quad (4.16)$$

The real force  $F_{n,corrected}$  is obtained by adding the sum of the discharge errors of the preceding points to the current value  $F_n$  (Eq. 4.17).

$$F_{n,corrected} = F_n + \sum_1^{n-1} \Delta F_i \quad (4.17)$$

Eq. 4.17 differs from the equation proposed by Niederreiter [60] to correct the same effect. Niederreiter proposed to add to a current value the sum of the discharge errors from the preceding point plus the error of the value considered (Eq. 4.18). However, discharge errors occur after a time period necessary for the quartz crystals to discharge. Therefore, the measurement point  $n$  considered does not display any proper error. The correction proposed by Niederreiter led to a significant negative drift of the signals over the time due to overcorrection.

$$F_{n,corrected,Niederreiter} = F_n + \sum_1^n \Delta F_i \quad (4.18)$$

The higher is the sampling frequency, the more precise is the determination of the error. The calculation of each error is exact up to the eighth decimal. From the ninth decimal place, rounding errors occur, which add over the time. Therefore, a slight drift of the signals over the time remains, which cannot be further corrected.

#### 4.5.4.4. Correction of pressure dependence of the force sensors

During slug flow pneumatic conveying, due to the alternation between slug and gas pockets, high pressure fluctuations occur in the pipeline. The piezo quartz crystals are sensitive to pressure and detect the changes of air pressure  $P_f$  according to the surface of the sensor  $A_{Sensor\_surface}$ :

$$F_{Pressure} = P_f \cdot A_{Sensor\_surface}$$

Therefore, the force sensors detect simultaneously the mechanical stresses and air pressure. During conveying, a miniature pressure sensor permits to detect the air pressure in the area where the forces are measured. By determining the pressure dependence of the sensors, i.e. the correction factor for the pressure effect, the part of the stress due to air pressure can be measured and deducted from the total stress measured. The correction factor can be determined by investigating the force signals obtained by stressing the measurement plate successively with defined air pressures. The slope of the linear

correlation between pressure and stress detected corresponds to the correction factor for the pressure dependence. Fig. 4.21 shows the corrected response of the radial force sensor placed in a closed pipeline section submitted to staged increase of gas pressure. The stress signal is no longer dependent on the gas pressure.

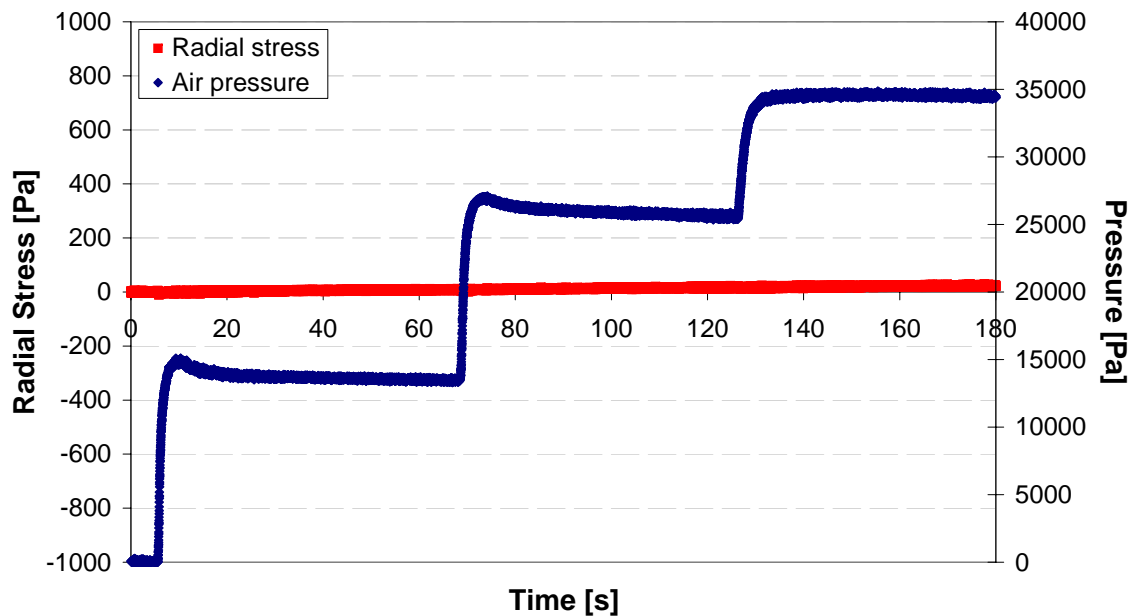


Figure 4.21: Stress signal of the radial sensor by activated pressure correction

However, this correction is accurate only if the same air pressure prevails in both pipeline and measurement chamber where the sensors are built in. Therefore, holes slightly smaller than the granules investigated assure the pressure equilibrium between the conveying section and the measurement chamber (Fig. 4.4). However, because of the small size of the holes, the pressure equilibrium occurs quickly but not instantaneously. As a consequence, an additional stress due to the arising pressure gradient between the front and the backside of the plate may briefly acts on the measurement plate if the pressure increase occurs too fast. However, experimental investigations showed that this not correctable effect is mostly not significant. Nevertheless, an additional pressure sensor positioned in the measurement chamber allows control of the pressure equilibrium.

#### 4.5.4.5. Correction of interdependence between both sensors

Another interference factor concerns the interdependence between the radial and axial sensors due to their perpendicular arrangement. Part of the axial force is transmitted into radial direction and detected by the radial force sensor and inversely. The correction factor for this mechanical interdependence can be determined experimentally by stressing a sensor in one direction and measuring the response of the other sensor theoretically not stressed. Based on the signal amplitude, a correction factor for this interaction can be calculated using Eq. 4.19 and Eq. 4.20.

$$Interaction_{radial \rightarrow axial} = \frac{Axial\_stress [Digits] \cdot Gain_{axial} [Pa/Digits]}{\frac{m_{cal} [kg] \cdot g [m/s^2]}{A_{plate\_projection} [m^2]}} \quad (4.19)$$

$$Interaction_{axial \rightarrow radial} = \frac{Radial\_stress [Digits] \cdot Gain_{radial} [Pa/Digits]}{\frac{m_{cal} [kg] \cdot g [m/s^2]}{A_{plate} [m^2]}} \quad (4.20)$$

Fig. 4.22 shows that after correction, the force sensor not stressed does no longer show any deflection. The sensors are mechanically coupled but the signals are decoupled.

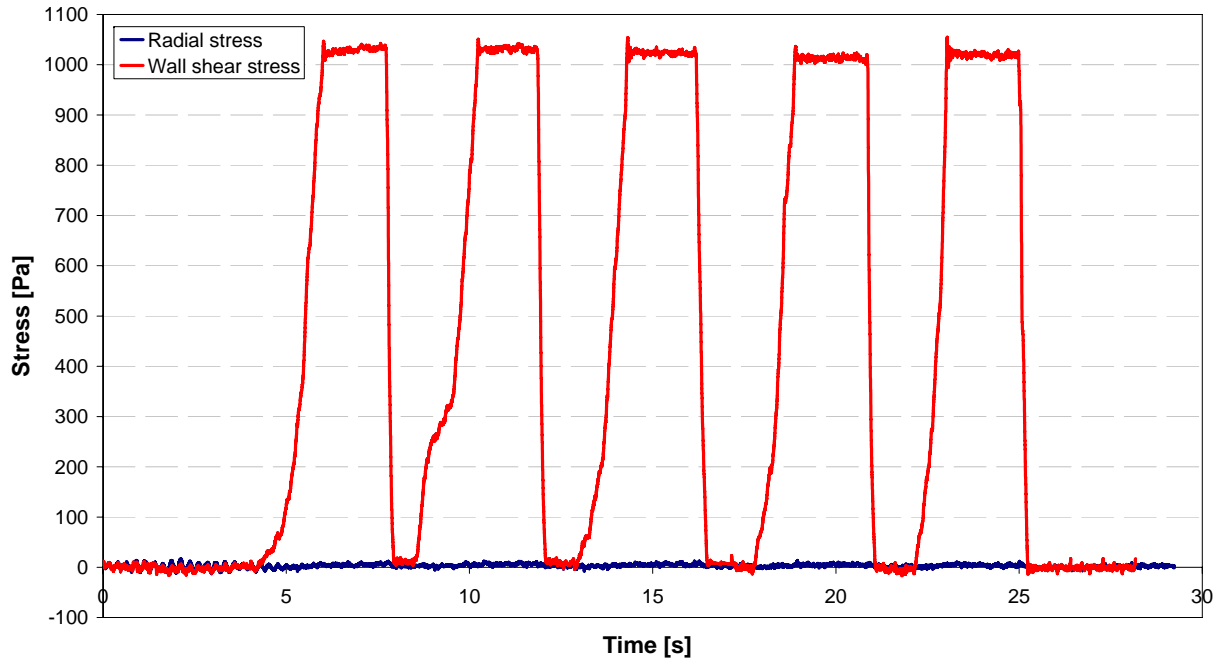


Figure 4.22: Repeated axial stress on the measurement plate by activated correction of the signal interdependence

#### 4.5.4.6. Influence of sampling frequency on the signal correction process

The action of the Bessel low-pass filter and the correction of the electric discharge of the piezo elements are functions of the sampling rate chosen. To guarantee optimal reconstruction of the signals, a compromise between high sampling frequency and lower computer overloading had to be found. The investigations carried out on the raw signals showed that a frequency of 10,000 Hz is appropriate to sample the signals. To illustrate the effect of a too low sampling rate, Fig. 4.23 and Fig. 4.24 show the stresses measured with  $f_{sampling} = 100$  Hz and  $f_{sampling} = 10,000$  Hz during the passage of a slug conveyed with 7.7 m/s air velocity. In Fig. 4.23, it can be seen that due to the too low sampling frequency, the signals were falsely corrected and the trend of the real signals was not reproduced accurately. Aliasing led to arising of low frequencies, which did not exist in the original signal and could not be filtered out by the low-pass filter. The correction of the electric discharge following the Bessel filter amplified those errors further by correcting, i.e. amplifying the virtual points arising from aliasing.

In contrast, Fig. 4.24 shows well reproduced stress signals, which are conformed to the sine signal form expected from the geometry of the measurement plate (Fig. 4.18).

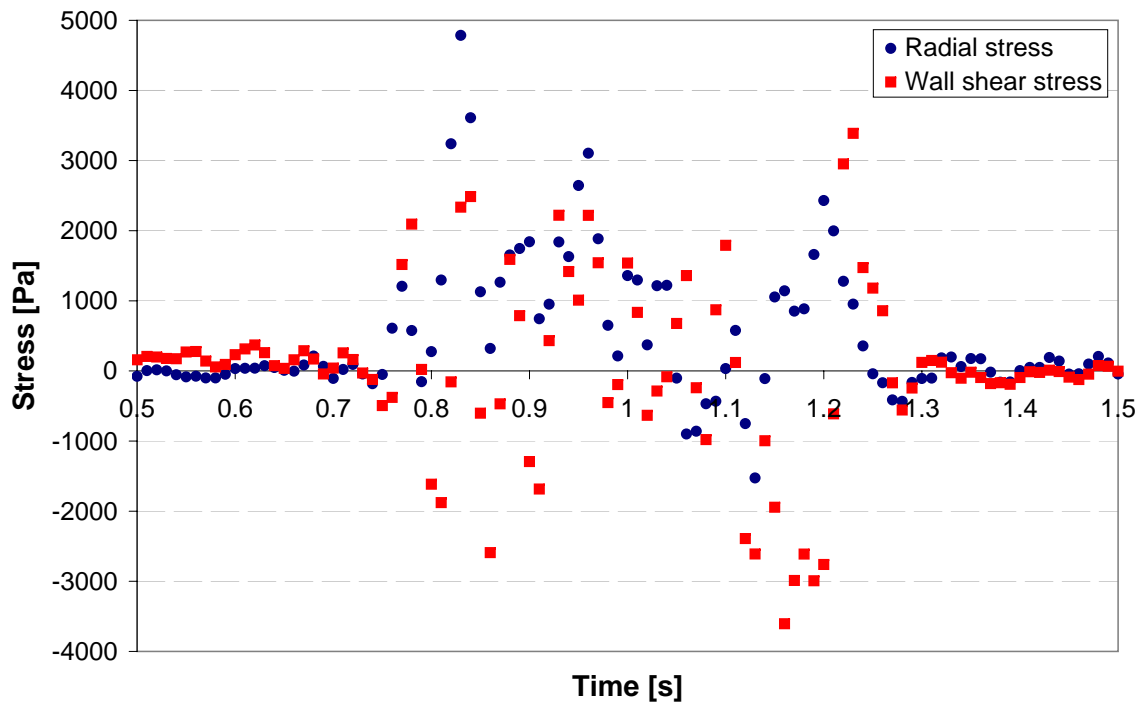


Figure 4.23: Stress induced by a slug conveyed with 7.7 m/s air velocity -  $f_{sampling} = 100$  Hz

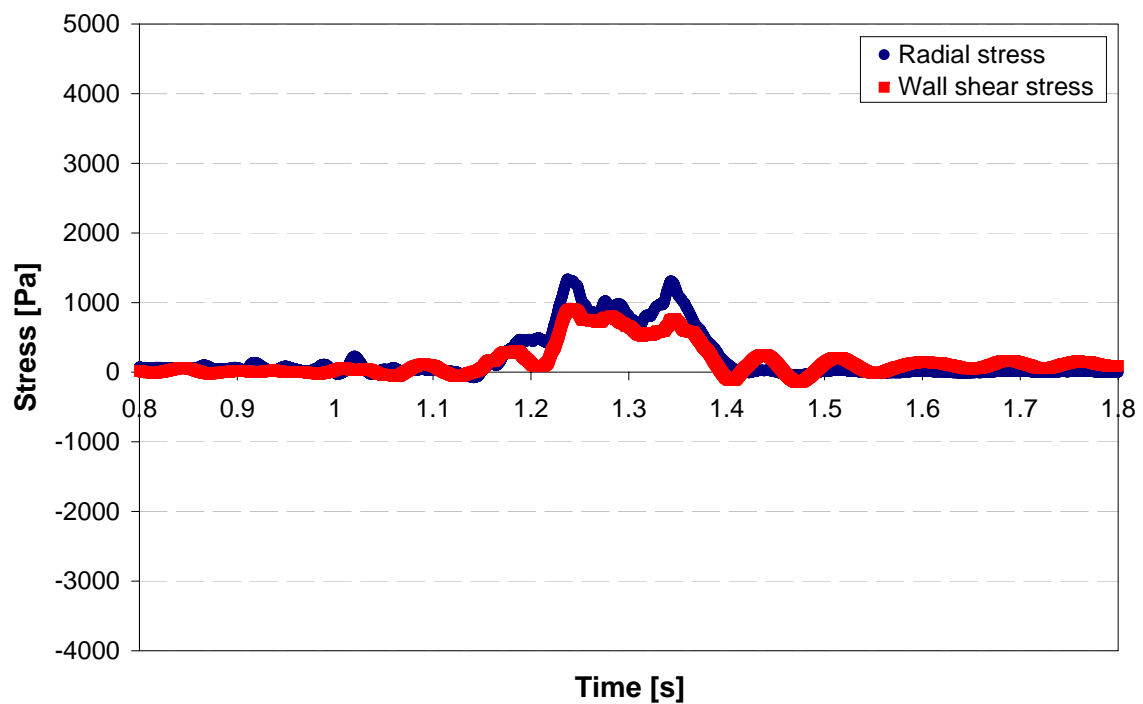


Figure 4.24: Stress induced by a slug conveyed with 7.7 m/s air velocity -  $f_{sampling} = 10,000$  Hz

#### 4.5.5. Determination of the slug porosity

In many theoretical studies about dense-phase pneumatic conveying, slugs are regarded as compact porous solid columns, which are able to transfer axial stresses into radial stresses. In this research, slug porosity was experimentally investigated by using two methods. The first method consists in determining the slug porosity indirectly from local pressure measurements by applying the semi-empirical equation of Ergun in which the pressure loss is expressed as a function of porosity and relative velocity between fluid and particles. The second method consists in a direct porosity determination by using a slug-catcher specially developed for the requirements of this research.

##### 4.5.5.1. Calculation of the slug porosity by applying the Ergun equation

The porosity of a slug is key parameter in most theoretical models to predict the pressure loss along a pipeline. Due to insufficient knowledge of the slug internal state, the porosity of a slug is generally assumed as equal to the bulk porosity and for pressure loss calculation, the slugs are considered as compact porous solid columns. Since the porosity of a slug depends on the slug moving state, porosity investigations have to be carried out in-situ during conveying process without creating any disturbances.

#### Method fundamentals

Measurement of the pressure loss over a given distance constitutes a possibility to extrapolate to the slug porosity. The models developed by Ergun [23], Molerus [54], Carman [14] and many others, which correlate pressure loss and porosity of a packed column can be applied. Niederreiter [60] carried out preliminary tests by applying a method similar to the method of Rumpf [68] to prepare bulk solids columns with porosity values between 0.38 and 0.45 [60]. He showed that for the material tested in this research, the equation of Ergun (Eq. 4.21) gives the best agreements between effective porosity of defined bulk solids columns and calculated porosity:

$$\frac{\Delta P}{L_{slug}} = 150 \cdot \frac{\eta_f \cdot (1 - \varepsilon)^2}{d_p^2 \cdot \varepsilon^3} \cdot v_{rel} + 1.75 \cdot \frac{\rho_b \cdot (1 - \varepsilon)}{d_p \cdot \varepsilon^3} \cdot v_{rel}^2 \quad (4.21)$$

with

$$v_{rel} = v_f - v_p$$

Hence, by applying Eq. 4.21 the porosity within a slug can be determined by means of pressure loss measurements over a given distance where the relative velocity between air and particles is known. The determination procedure is presented in Fig. 4.25. The porosity was determined using the Ergun equation for slugs conveyed with a range of air supply velocities covering the entire area of slug flow.

Ergun developed Eq. 4.21 for fluid flow through homogeneous packed beds with a constant porosity across the cross-section. To establish a correlation between the pressure loss and the porosity of a given packed column, he fixed a packed bed by means of two permeable plates and let gas with defined mass flow rates flow through it. Since the spatial distribution of the particles must conform to the shape of the wall, an annular wall zone exists where the average porosity is greater than in the core of the

bed. The influence of the wall upon flow via channelling becomes more significant as the ratio  $D/d_p$  decreases [24]. Therefore, Ergun chose a ratio pipe diameter to particle diameter big enough to be able to neglect the effect of both pipe and particle geometries.

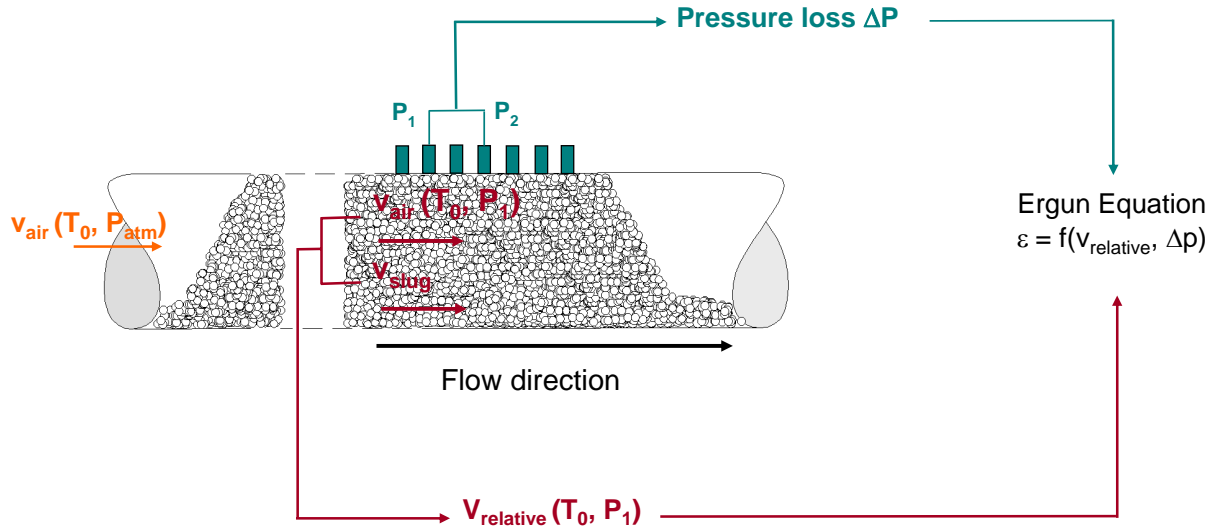


Figure 4.25: Schematic procedure for the porosity determination based on the semi-empirical equation of Ergun

Moreover, in the experimental investigations carried out by Ergun, the high pressure loss resulting from the fixation plates led to a uniform distribution of the gas flowing through the fixed bed. However, since the ratio pipe to particle diameter is given and slugs are not fixed, these conditions are not fulfilled in slug flow conveying. Therefore, significant porosity and gas velocity gradients may take place across the pipe cross-section. The higher porosity in the area close to the wall leads to a higher flow velocity in this zone compared to the uniform flow velocity assumed by Ergun. Consequently, instead of using the mean relative velocity across the pipe cross-section, the best way to proceed to predict accurately the void fraction within a slug consists in determining the velocity profile, i.e. gas velocity in each defined layer across the pipe cross-section and integrating the pressure loss. The gas velocity comes in the equation of Ergun with a second order (Eq. 4.22). Therefore, significant differences may exist between the pressure losses calculated considering either an uniform or non-uniform flow profile across the pipe cross-section, even if the total gas flow rate flowing through the bulk column is the same in both cases.

$$c_1 \cdot \Delta P = c_2 \cdot v_{rel} + c_3 \cdot v_{rel}^2 \quad (4.22)$$

For this reason, the real pressure loss measured for a given porosity may differ from the pressure loss calculated by applying the equation of Ergun. Therefore, to determine the slug porosity from pressure loss measurements, the influence of the flow profile across the pipe cross-section should be considered. For this purpose, Niederreiter [60] proposed a correction factor based on the gas flow rate. By applying the method of Ridgway and Tarbuck [65], he measured the radial porosity distribution and described it mathematically using the method of Rottschäfer [67] (Fig. 4.26). Since he knew the porosity profile,

he was able to determine the flow velocity according to the position over the pipeline radius. Then, using an integrative process (Eq. 4.23), he calculated the real gas flow rate flowing through a slug:

$$\dot{V}_f = \int v_f(r) \cdot A(r) \cdot dr \quad (4.23)$$

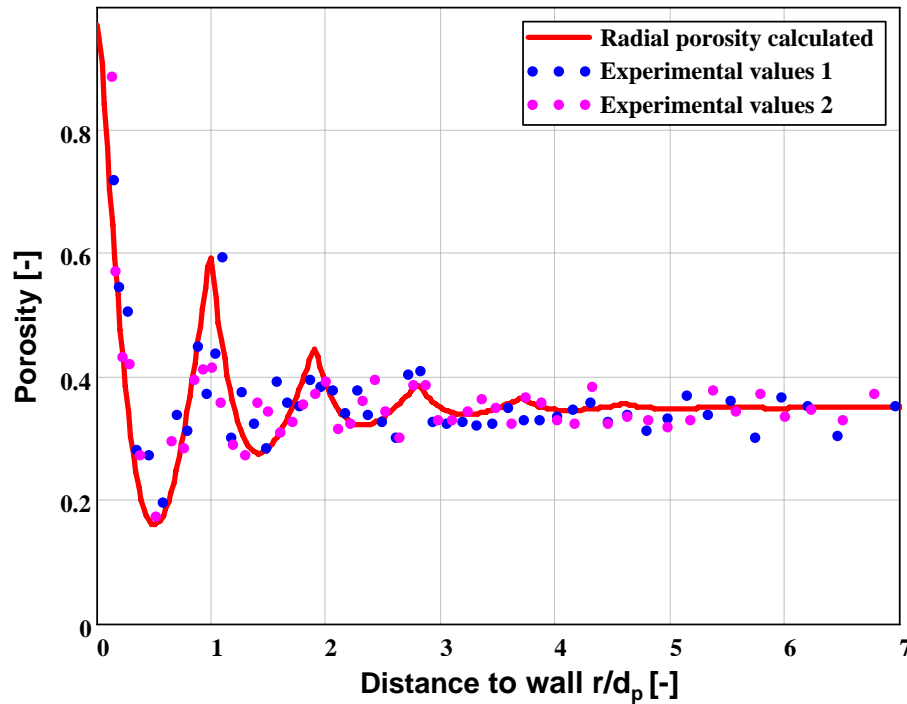


Figure 4.26: Mathematical description of the radial porosity distribution using the method of Rottschäfer [60]

The correction factor proposed by Niederreiter (Eq. 4.24) resulted from the ratio gas flow rate obtained from the porosity distribution (Eq. 4.23) to gas flow rate through ideal packed bed columns according to Ergun (Eq. 4.25):

$$k_{vol} = \frac{\dot{V}_f}{\dot{V}_{f\_Ergun}} \quad (4.24)$$

with

$$\dot{V}_{f\_Ergun} = v_{rel} \cdot A \quad (4.25)$$

This correction factor was developed by Niederreiter to take into account the existence of a flow profile and allow accurate calculation of the slug porosity. However, the volume flow rate of gas that enters in an infinitesimal volume element is in isobaric conditions the same than the volume flow rate leaving this element. Consequently, the volume flow rate of gas conveyed along a pipeline is a function of the pressure along the pipe but not of the flow profile across the pipe cross-section. Therefore, the

volume flow rate of gas cannot be used as a parameter to determine a correction factor. The differences between real and calculated volume flow rate noticed by Niederreiter repose only on imprecision of the measurements and not on the influence of the porosity profile.

Many work focused on the effect of the wall on the pressure loss through a packed bed given by the equation of Ergun. The results recently published by Winterburg [95], Eisfeld [22] and Di Felice [19] agreed with the results of earlier investigations. The results led to the general conclusion that from a practical point of view the Ergun equation, with average values of porosity and superficial velocity, is applicable for a ratio  $D/d_p \geq 10$ . Furthermore, it should be pointed out that all researchers failed to recognise the need of incorporating correction factors in the Ergun equation.

Therefore, the porosity trend over slug length can be determined using the equation of Ergun. However, as a precaution, the values obtained should not be considered as absolute values, i.e. as the real porosity. To keep this fact in mind, the porosity calculated is named "Ergun porosity" in this research. In addition, it should be noted that the slug porosity provided by the Ergun equation corresponds to an average porosity across the entire cross-section for a defined  $x$ -value over the slug length. Therefore, no difference is made between a cross-section completely filled with particles (in the plug part of a slug) and a cross-section not entirely filled (at the front end and rear of a slug).

#### **Effect of a cross-sectional porosity gradient on the calculated porosity**

The model of Ergun describes the pressure loss through a uniform packed bed with constant porosity  $\varepsilon$  across the pipe cross-section. However, in horizontal slug flow pneumatic conveying, a potential density gradient may take place across the pipe cross-section. A higher porosity across the pipe cross-section, i.e. within a slug can lead to a bigger porosity gradient. For the calculation of the Ergun porosity, the pressure loss, superficial gas velocity and particle velocity are the three process variables influencing the results.

Although the existence of a potential porosity gradient across the pipe cross-section does not affect the superficial gas velocity and particle velocity, the pressure gradient is significantly affected by the presence of a porosity gradient. For a given mean porosity across the pipe cross-section, a higher porosity gradient leads to a bigger difference between the pressure loss that occurs in the pipe section considered and the pressure loss that would occur if the suspension was homogeneous. In turn, the difference in the pressure loss leads to a different calculated porosity. As a consequence, the Ergun equation provides a different porosity whether the granules are homogeneously distributed across the cross-section or not.

In order to estimate the effect of an inhomogeneous density distribution on the calculated Ergun porosity, porosity calculations were carried out for different types of particles distribution. Theoretical mean porosities across the pipe cross-section of 0.41 and 0.60 were chosen. Since the porosity of the bulk investigated amounts to 0.38, a porosity of 0.41 corresponds to a slightly fluidised slug whereas a porosity of 0.60 would be measured within a relatively light suspension of particles. For the calculation, the cross-section was divided into two sections. The first section corresponds to a layer of material whose porosity was varied from 0.38 to 0.41 or 0.60, respectively. The second section corresponds to



a suspension with given porosity of 0.6, 0.8 or 1.0. For a given suspension porosity, since the mean porosity across the pipe cross-section is fixed, the variation of the porosity of the particles layer leads to the adjustment of the height that this layer must reach so that the mean porosity set is still fulfilled. This is shown in the graphs on the left hand side in Fig. 4.27. For a given suspension and mean porosity across the pipe cross-section, a higher porosity of the layer is correlated to a bigger fraction of the cross-section occupied by this layer.

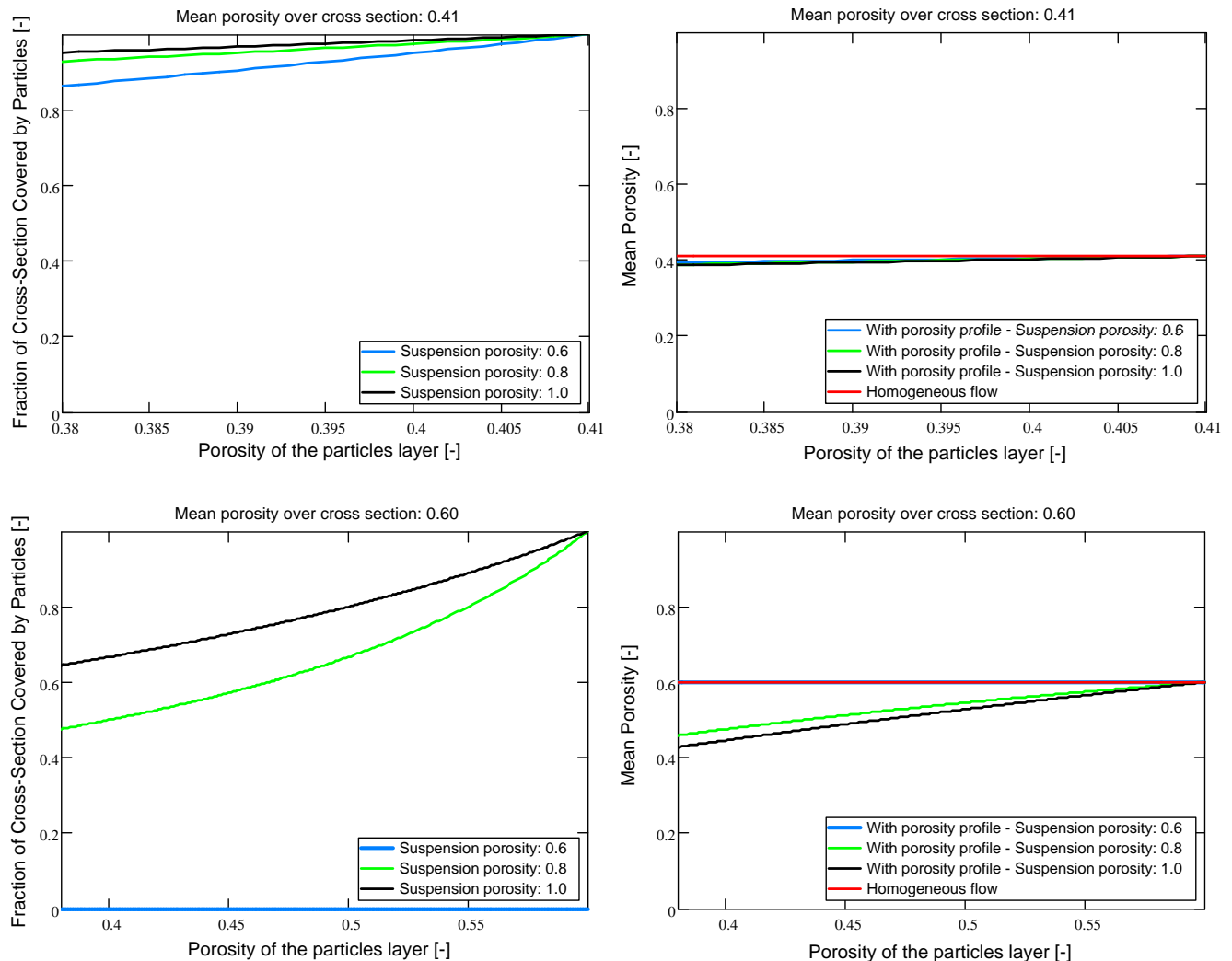


Figure 4.27: On the left hand side: Fraction of the pipe cross-section area covered by a layer of particles according to the porosity of this layer for mean porosities of 0.41 and 0.60 and given suspension porosities of 0.60, 0.80 and 1.00. On the right hand side: Mean porosity across the pipe cross-section calculated by applying the Ergun equation for the same mean porosities and suspension porosities

The graphs on the right hand side in Fig. 4.27 indicate that the existence of a non-uniform porosity distribution across the pipe cross-section leads to calculated porosity values lower than the porosity values obtained for a homogeneous particles distribution. A bigger difference in the density can take place between the two sections if a higher mean porosity is set. In turn, this may result in a bigger difference between the porosity calculated for either homogeneous or inhomogeneous distributions. However, the

results show that for a slightly fluidised slug, i.e. a mean porosity of 0.41, the Ergun porosity calculated for both a uniform and non-uniform particles distribution is similar. Therefore, the Ergun equation is suitable to calculate the porosity within a slug that display the bulk porosity or a porosity slightly higher. This is in accordance with the results of Hill who carried out theoretical simulations of flow through random arrays of spheres and reported that the porosity function of Ergun is well taken into account as long as the porosity is around 0.4. A porosity around 0.4 is commonly displayed by packed beds when made up of spheres [30].

It should be pointed out that the calculation according to Ergun involves the superficial gas velocity and not the interstitial gas velocity. Hence, the porosity calculation is not affected by the gas velocity profile across the pipe cross-section resulting from the porosity gradient.

### **Experimental determination of the physical parameters for the Ergun equation**

The pressure loss measurements took place at the end of the first horizontal pipeline section, about 15 meters after product feeding (Fig. 4.1). Since pneumatic conveying is a dynamic process, the physical parameters required to calculate the porosity by applying the Ergun equation had to be determined for this given area. The pressure loss and particle velocity were measured whereas the gas velocity was calculated for the pressure conditions prevailing in that area using the values of gas supply velocity set at the pipeline inlet.

The pressure loss was measured using miniature piezoresistive pressure sensors over a short distance so that the air expansion resulting from the pressure decrease could be neglected. Nevertheless, the pressure loss must be high enough so that measurement errors have no significant effect on the results. For this purpose, Niederreiter built in the measurement probe he developed miniature piezoresistive pressure sensors positioned 37.5 mm each apart (see Section 4.5.1). The pressure is sampled with a frequency of 10,000 Hz.

The velocity of the particles in the measurement area is determined by following the optical method described in Section 4.4. The velocity of the particles is a function of their position along a slug. At the front end, particles are picked up by the slug. Consequently, they undergo acceleration from static state to the slug velocity. At the rear, the particle velocity decreases until particles drop and become part of the stationary layer again. The CCD-camera has a maximum shot frequency of 30 Hz, that is a sampling frequency 333 times lower than the pressure sampling frequency. Limited by this maximum shot frequency, the particle velocity was determined each 33 ms. Therefore, the velocity profile over the length of a slug could be investigated and taken into account for the porosity calculation.

The third variable parameter whose value in the measurement area is required is the superficial velocity of the gas. The superficial gas velocity was calculated by applying the gas conservation law. At each location along the pipeline, the air velocity can be calculated by using values of volume flow rate in normal conditions as long as the pressure is known. Hence, by applying the gas conservation law at location 1, the air velocity can be calculated by using Eq. 4.26 as long as isothermal conditions can be assumed.

$$v_{f1} = \frac{p_{atm} \cdot \dot{V}_{atm} \cdot 4}{P_1 \cdot D^2 \cdot \pi} \quad (4.26)$$

In order to consider the changes in the air density, i.e. air velocity that result from the pressure fluctuations, the air velocity  $v_{f_i}$  was calculated according to the pressure prevailing in the measurement area with a frequency of 10,000 Hz as well. The number of values available for the particle velocity is 333 times lower than for the air velocity. Therefore, for the calculation of the relative velocity between air and particles  $v_{rel_i}$ , each value of the particle velocity  $v_{p_i(333)}$  was assumed to remain unchanged during 33 ms. Eq. 4.27 illustrates how the air density changes were taken into account by means of the high sampling frequency used.

$$\frac{\Delta P_i}{l} = 150 \cdot \frac{\eta_{f_i} \cdot (1 - \varepsilon_i)^2}{d_p^2 \cdot \varepsilon_i^3} \cdot v_{rel_i} + 1.75 \cdot \frac{\rho_b \cdot (1 - \varepsilon_i)}{d_p \cdot \varepsilon_i^3} \cdot v_{rel_i}^2 \quad (4.27)$$

with

$$v_{rel_i} = v_{f_i} - v_{p_i(333)}$$

During his investigations on vertical slug flow pneumatic conveying, Niederreiter used a similar method to determine the porosity within vertical slugs. However, instead of determining the particle velocity over the entire length of a slug, he used for the calculation of the relative velocity a single value of slug velocity that he assumed to be equal to the particle velocity in the center of a slug.

#### 4.5.5.2. Determination of slug porosity using a slug-catcher

The porosity can be determined indirectly from pressure measurements by using the equation of Ergun. However, this determination is accurate only if the particles distribution across the pipe cross-section is uniform or almost uniform. However, in horizontal slug flow, because the force of gravity acts perpendicularly to the conveying direction, a porosity gradient may take place over the height of the pipeline, which in turn results in a radial flow velocity profile. Therefore, the porosity calculation delivers values that do not exactly correspond to the actual porosity values. For a given air mass flow rate flowing through a volume element, the pressure loss occurring if a velocity, i.e. porosity profile exists across the pipe cross-section would be higher than if a uniform porosity distribution exists. Therefore, the porosity values obtained by considering this lower pressure loss are higher than the actual porosity.

A slug-catcher was developed in order to check the suitability of the Ergun equation to calculate the slug porosity on the one hand and investigate the existence of a potential porosity gradient over the slug height on the other hand. With the aid of a spring-loaded system, the slug-catcher is able to catch a moving slug in a fraction of a second and separate it simultaneously into three horizontal layers.

The slug-catcher had to fulfil diverse requirements on which its development was focused:

- the device must be able to catch a moving slug instantaneously
- the trigger mechanism should be simple and no effort should be required for its release

- the slug-catcher must not disturb the conveying process as long as the trigger mechanism is not released
- the use of a transparent material for the construction should allow the user to see into the catching process
- the forces due to preload and release of the trigger mechanism and separating system must act only on the materials able to withstand those high strains
- no air must be released from the device, i.e. the slug-catcher must remain sealed when overpressure prevails
- the mounting and de-mounting of the device must be easy to allow rapid measurements
- the device must permit to catch simultaneously different horizontal layers of a slug and their separate analysis

The designed device consists of two main components made of aluminium and Plexiglas, a separation and closing mechanism and two aluminium covering plates with threaded connections to integrate the slug-catcher into the pipeline system (Fig. 4.28). The Plexiglas component, which contains the conveying pipe section, is used to control the catching process as well. The tension mechanism located in the aluminium block consists of separating metal sheets, two compression springs (350 N preload force each) and a screw mechanism with whom the springs are preloaded.

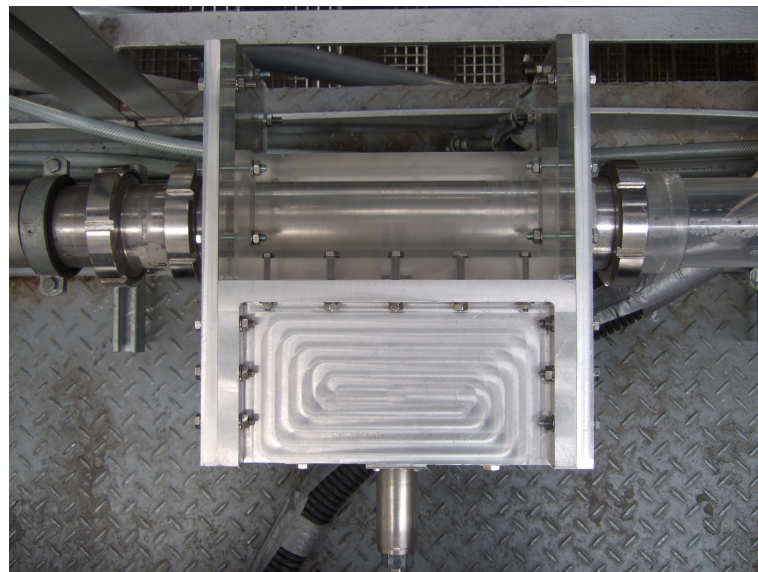


Figure 4.28: Top view of the slug-catcher mounted in the pipeline

Fig. 4.29 shows the exploded assembly drawing of the catching device. All gaps required for the insertion of the separating sheets in the pipeline during the catching process were made as small as possible to avoid any potential disturbances of the conveying process. Plexiglas was chosen as material for the conveying section to permit the control of the catching process. Because of high fragility of this material, the catcher was designed so that all forces occurring by springs pre-loading, springs release and by braking of the separating sheets only act on the metal parts. Diverse seals were built in the

slug-catcher so that the device is pressure-proof in the normal operating conditions. During conveying, the springs are in a preloaded-state and the pipeline is cleared. With the aid of an external preload mechanism using a screw, the springs can be preloaded either before or after the mounting of the slug-catcher in the pipeline. The preloaded springs can be released and the separating sheets sent into the pipeline by an easy 90° rotation of the tension axle realised by means of a spanner. This simple trigger mechanism and the high preloading state of the springs permit to catch the part of the slug wanted in a fraction of a second. The closing time of the device when the pipe is empty amounts to about 5 ms.

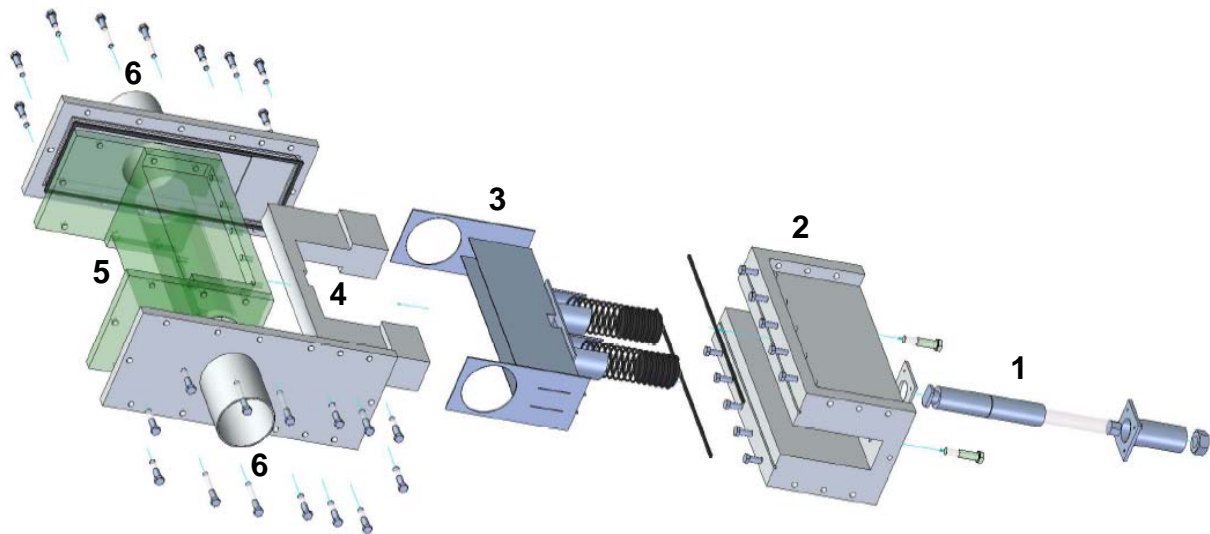


Figure 4.29: Exploded assembly drawing of the slug-catcher. 1. Shaft axle, 2. Aluminum component, 3. Separating metal sheets, 4. Stop position for the separating sheets, 5. Plexiglas component for process control, 6. Connection with the conveying pipeline

The operating principle of the slug-catcher is illustrated in Fig. 4.30. The picture on the left hand side shows the device during conveying. The conveying section is free and the conveying takes place without any disturbance. On the second picture, the closing mechanism has been triggered and the separating sheets are moving into the pipeline. The third picture shows the slug-catcher in its closing state when a part of a slug has been separated from the rest and the three horizontal chambers are filled with material. To facilitate the observation of the separating mechanism in Fig. 4.30, the front plate has been masked. The complete drawings of the device required for the construction can be found in Annex A1.

The following procedure summarises the different steps to determine the porosity of a slug by using the designed slug-catcher:

- Mounting of the slug-catcher in the conveying pipeline
- Pre-loading of the mechanism to clear the conveying pipe
- Trigger of the mechanism when a slug is passing through the catching device
- Device removal from the pipeline system and separate emptying of the three chambers
- Measurement of the mass of granules caught in each chamber

- Porosity determination for each chamber by interrelating mass of product caught, bulk solids density and chamber capacity.

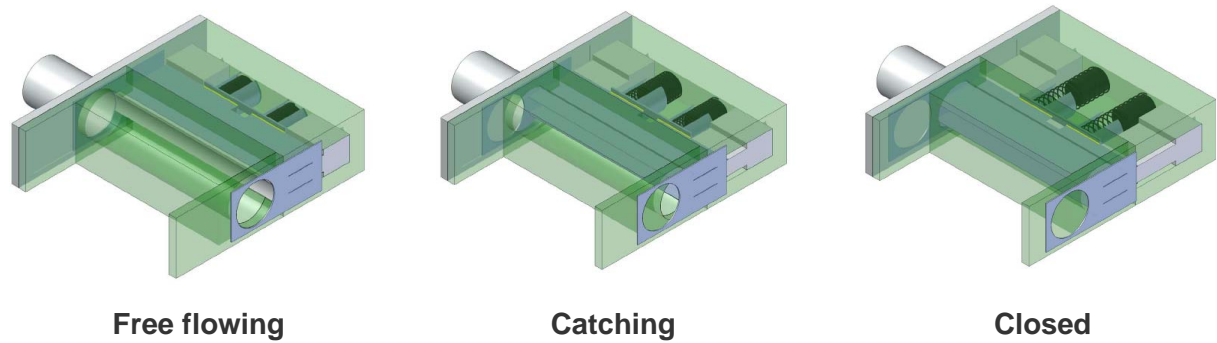


Figure 4.30: The three states of the operating slug-catcher

Basically, a slug can be divided into three regions: the front end, the core and the rear (Fig. 4.31). The porosity determination has to be carried out on the core of a slug where granules theoretically fill the entire pipe cross-section. To ensure that the correct part of a slug was caught, the catching process was additionally filmed.

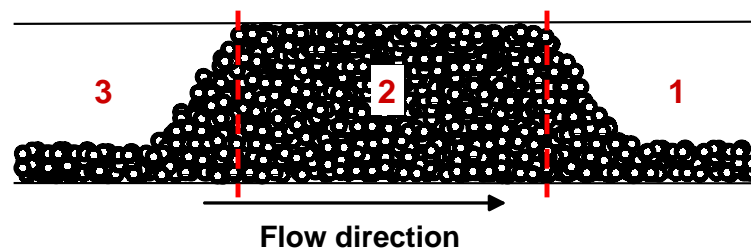


Figure 4.31: Schematic illustration of the three regions composing a slug. 1. Front end, 2. Core, 3. Rear

The device was mounted in the pipeline system after the probe to measure pressure and forces (Fig. 4.4) so that a direct comparison between both porosity determination methods is possible. Slugs conveyed with the minimal and the maximum air velocity at which slug flow occurs as well as slugs conveyed with intermediary velocities were caught and analysed.

## 5. Results and Discussion

### 5.1. General description of slug flow pneumatic conveying

#### 5.1.1. Pressure loss along the conveying pipeline

Besides the choice of the accurate gas mass flow rate to realise the transport of the material in optimal conditions, the designer of a dense-phase pneumatic conveying system has to know the total pressure loss required to ensure the transport up to the system outlet. Low-velocity conveying systems are operated with a very small amount of gas but require a much higher overpressure at the pipeline inlet than dilute-phase conveying systems. Fig. 5.1 shows the relative pressure measured at seven locations along the pipeline. The recording began at the time where the product feeding started. The material that first fall into the pipeline is transported further and reaches successively the points  $P_1$  to  $P_7$  located along the pipeline. As soon as the material reaches a given point, the pressure at this point starts increasing. The increase of the pressure is particularly high until the first slug reaches the pipe outlet. Past this moment, the pressure keeps increasing but in a slowly way until the flow has reached stable conditions. In the conveying trial presented in Fig. 5.1, the pressure at the pipeline inlet and each other locations along the pipeline fluctuates around a constant past 60 seconds.

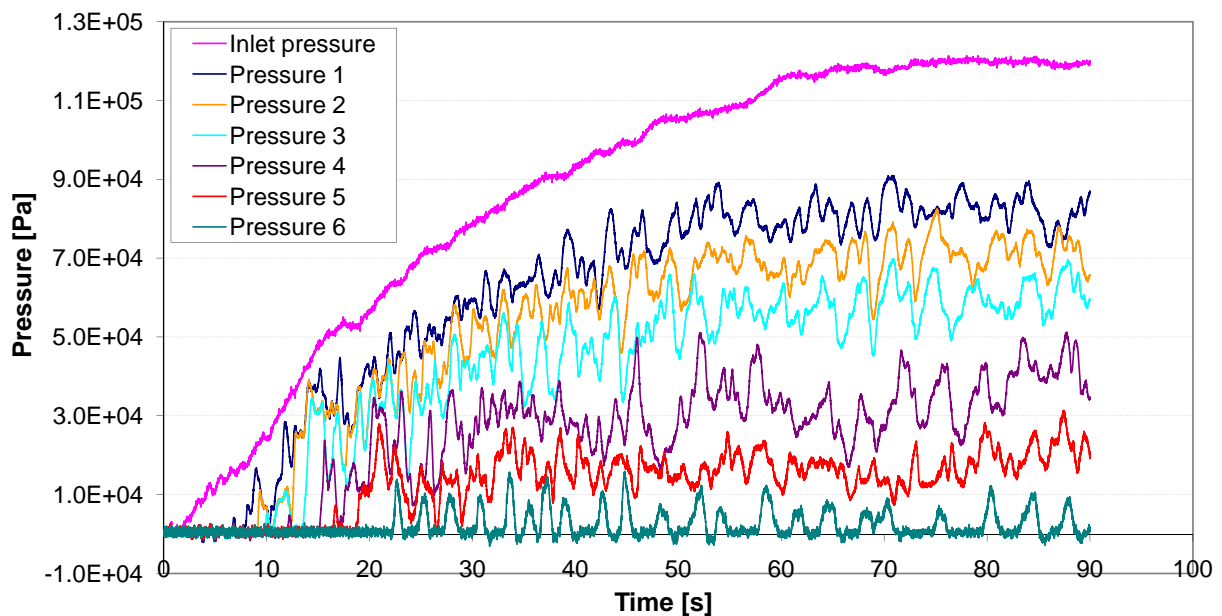


Figure 5.1: Pressure measured at seven locations along the pipeline -  $v_f = 7.4$  m/s

The pressure fluctuations observed at every location except at the inlet of the pipeline illustrate the passage of the slugs. A very similar trend can be observed for the signals Pressure 2 and Pressure 3, especially in the stable conveying area between 60 and 90 seconds. In fact, since the two measurement points are located only two meters apart, the slugs presented a similar structure and behaviour when they successively reached those two points. However, slugs cannot be considered as bulk solids columns moving along the pipeline but as waves. A moving slug picks up material of the stationary particles

layer in front of it and deposits a similar quantity of material at the rear. Consequently, the product composing a slug is continuously exchanged. Therefore, the method of cross-correlation of pressure signals along the pipeline widely used to investigate conveying characteristics such as slug velocity is mostly incorrect.

For a given product, the pressure loss along the pipeline is a function of the key parameters gas and solids mass flow rate. Those two parameters can be combined to form the solids loading. The pressure loss measured between the points  $P_1$  and  $P_6$  (marked in Fig. 5.2) has been compared to the pressure loss predicted by applying the model for horizontal low-velocity slug flow of Yi (see Section 3.5). The results of the prediction are plotted in Fig. 5.2 against the experimental results obtained for five different air supply velocities from 6.8 m/s to 8.5 m/s. Each point corresponds to a conveying trial with a specific solids mass flow rate. Since the product fell into the pipeline solely under effect of the force of gravity, the solids mass flow rate adjusted from itself. The dashed lines in Fig. 5.2 represents the boundaries  $\pm 25\%$  of divergence between experimental and predicted results in which the agreement is usually deemed good in the field of dense-phase flow.

The model of Yi [100] was initially developed to predict the pressure drop in horizontal pipelines. To apply this method to vertical sections, a pressure drop to lift the solid mass had to be added. In the bends, a fictive length of pipeline was calculated with respect to pipeline diameter and bend radius according to Flatt [25].

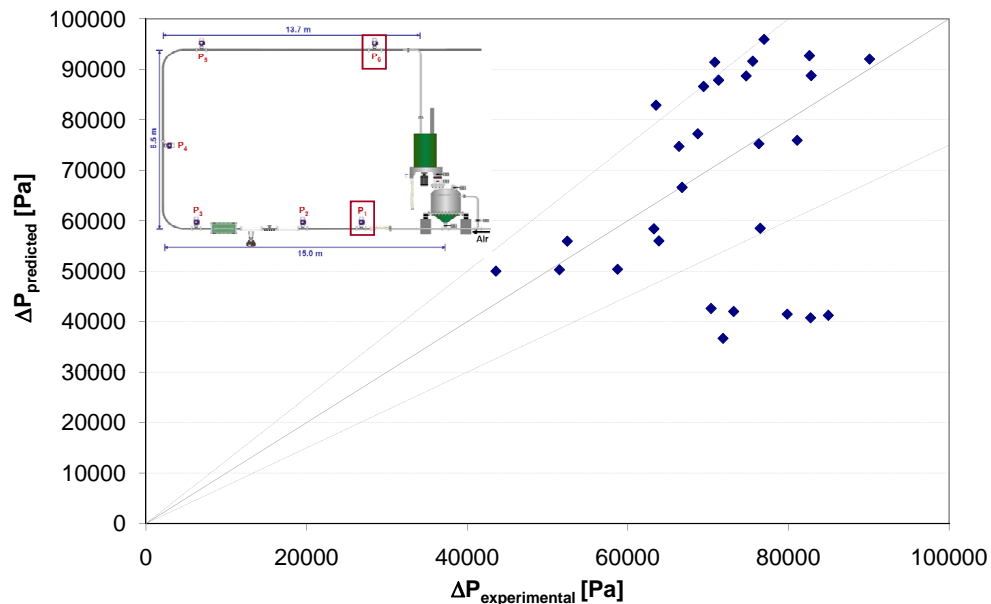


Figure 5.2: Agreement between the experimental pressure loss measured between the points  $P_1$  and  $P_6$  and the pressure loss predicted by applying Yi's method [100]

Fig. 5.2 shows the predicted results for the entire pipeline while Fig. 5.3 shows the results for the horizontal sections only. The results indicate that in 70 % of the cases, the pressure loss predicted for both the entire pipeline and the horizontal sections only is located in the field  $\pm 25\%$  of the experimental pressure loss. Six results differ from the others in that they display a predicted pressure loss about two times lower than the experimental pressure loss. Each of those trials was characterised by a significant



lower solids mass flow rate caused by the occurrence of disturbances in the conveying process. Therefore, the lower mass flow rate, which was used for the calculation led to a lower predicted pressure loss, although it actually resulted from disturbances in the conveying process leading to a higher pressure loss.

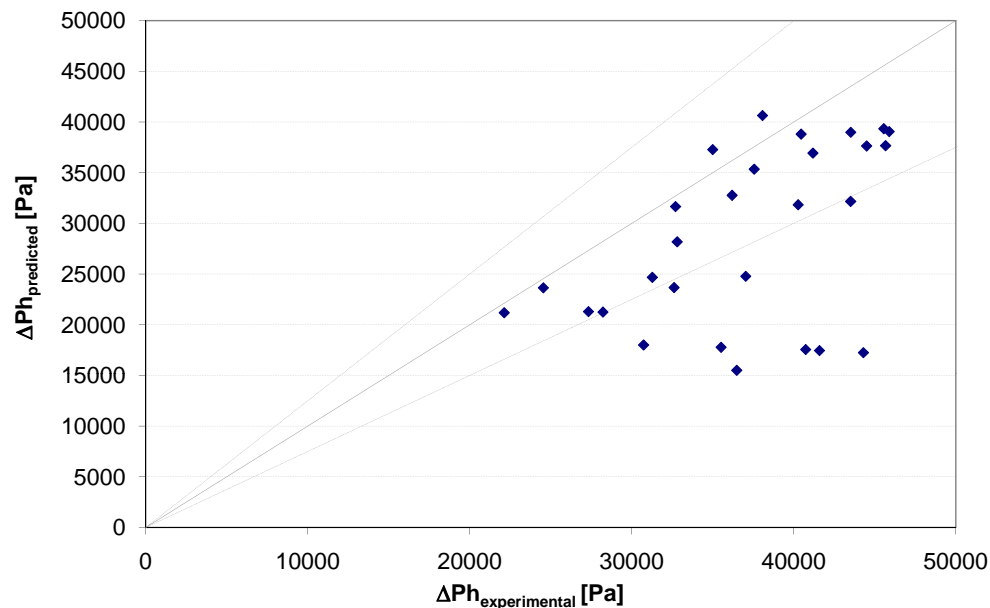


Figure 5.3: Agreement between the experimental pressure loss and the pressure loss predicted by applying Yi's method [100] for the horizontal sections located between the points  $P_1$  and  $P_6$

### 5.1.2. Effect of the air velocity increase on slug flow characteristics

In slug flow, only relatively small amounts of gas are used to transport large volumes of material along short as well as long distances. The determination of the optimal gas supply velocity is one of the key parameters to achieve the accurate design of a pneumatic conveying system. In the conveying area of slug-flow, it was found that an increase in air supply velocity was accompanied by a linear increase of both solids mass flow rate and slug velocity up to a turning point where a further increase in air velocity would have decreased the system performance (Fig. 5.4). Those results agree with the results of Mi [51] who observed that slug and air supply velocity are linearly correlated. Past the turning point, a further increase in the gas velocity would move the flow to strand flow or suspension flow. This, in turn, would lead to a decrease of the solids mass flow rate, i.e. system performance. However, those results do not give any information about the length of the single slugs or total length of the slugs, i.e. total mass of product moving along the pipeline at a given time. Considering the increase of the slug velocity with the gas supply velocity, the parallel increase of the solids mass flow rate may be due to different changes in the flow characteristics. In fact, the increase of the solids mass flow rate may be due to slugs whose length decreases but whose number increases, slugs whose length increases or slugs whose length remains unchanged but velocity increases.

To investigate the reasons for the increase in the solids mass flow rate, the slug frequency was investigated. Fig. 5.5 shows that an increase in the gas supply velocity does not affect significantly the mean slug frequency. However, it can be observed that for higher gas velocities, the number of slugs passing through a pipe section per time unit is more difficult to predict, although the higher fluctuations in the slug number do not affect the solids mass flow rate. A higher air supply velocity may lead to a higher slug frequency or not.

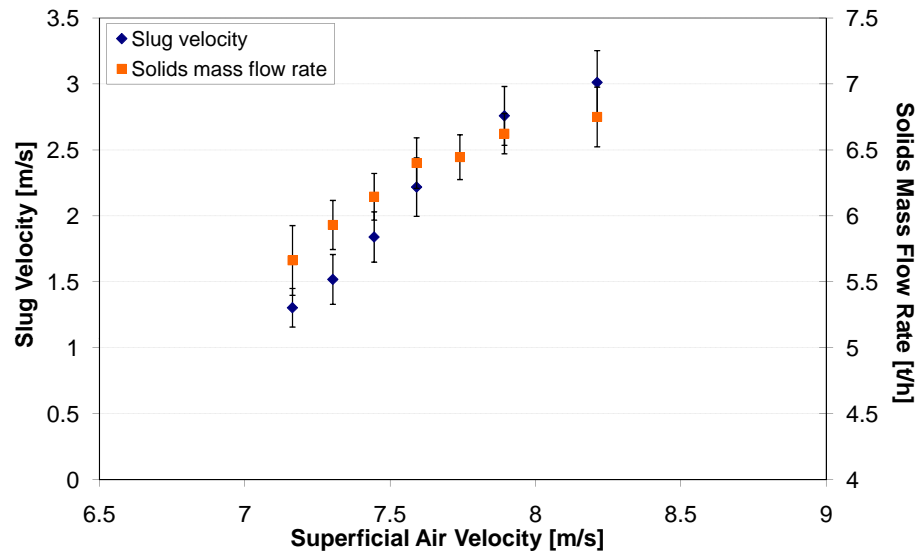


Figure 5.4: Solids mass flow rate and slug velocity experimentally measured

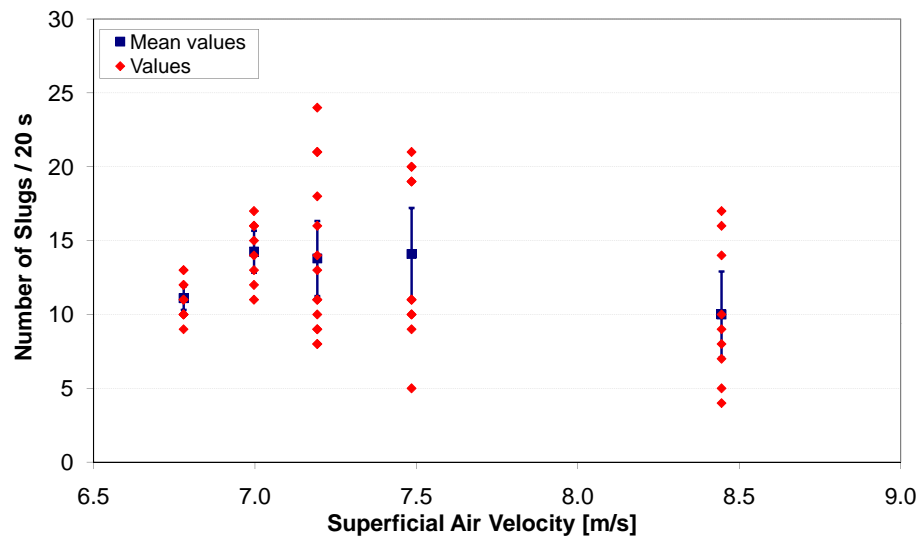


Figure 5.5: Effect of the air velocity on the slug frequency

During slug flow, the material is nearly transported in the slugs only. Therefore, the product can be assumed as being transported only through the fraction of the pipe area  $(1 - \alpha)$  not covered by the stationary layer of particles. In this case, the increase of the solids mass flow rate may not only be due to the increase of the slug velocity, but also to the decrease of the height of the stationary layer,

i.e. increase of the pipe volume available for the active transport. The fraction  $\alpha$  of the pipe area covered by the stationary layer was experimentally investigated. Fig. 5.6 shows that an increase in the air velocity leads to a significant decrease of  $\alpha$ . In addition, Fig. 5.6 shows values for  $\alpha$  calculated by using the expression Konrad [38] developed by applying a gas/liquid analogy (see Section 3.2.3):

$$\alpha = \frac{1}{1 + \frac{\bar{v}_p}{0.542 \cdot \sqrt{g \cdot D}}} \quad (5.1)$$

with

$$\bar{v}_p = v_{slug} - 0.542 \cdot \sqrt{g \cdot D} \quad (5.2)$$

Furthermore, the slug velocity experimentally determined was used in combination with Eq. 5.2 to calculate the theoretical mean particle velocity  $\bar{v}_p$ , which in turn is required to determine the fraction  $\alpha$  by applying Eq. 5.1. Fig. 5.1 shows that experimental and semi-empirical values of  $\alpha$  follow the same trend and are in the same order of magnitude. A better agreement is observed for higher air velocities. These results are in agreement with the results of Mi who stated that the equation of Konrad is suitable to predict  $\alpha$ .

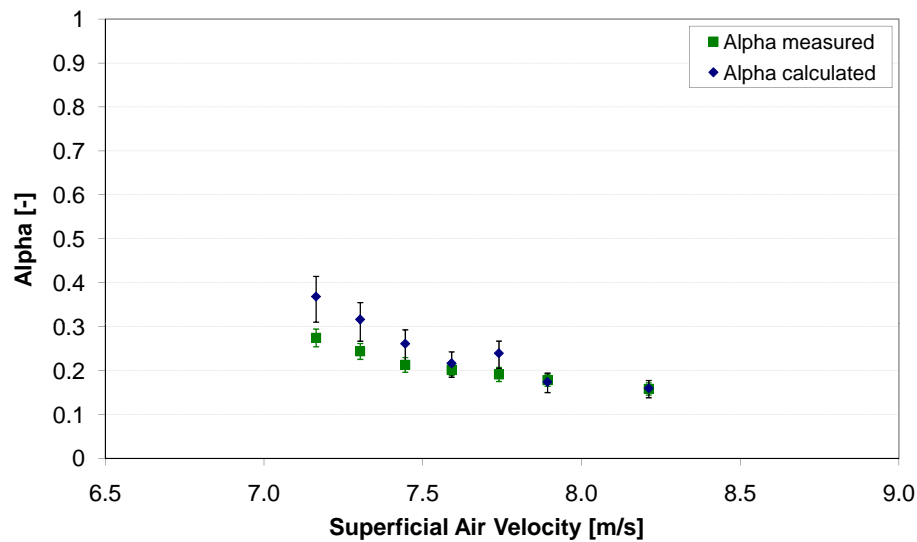


Figure 5.6: Influence of the air supply velocity on the fraction  $\alpha$  of the pipe area covered by the stationary layer

The experimental values for the slug velocity, solids mass flow rate and fraction of the pipe area covered by the stationary layer were used further to calculate the total length of slugs  $L_{slug}$  moving in the pipeline by applying Eq. 5.3. Eq. 5.3 is based on a mass balance over the entire pipeline.

$$L_{slug} = \frac{\dot{m}_s \cdot L_T}{A \cdot (1 - \alpha) \cdot \rho_b \cdot v_{slug}} \quad (5.3)$$

Fig. 5.7 indicates that an increase in the air velocity leads to the decrease of the total length of slugs present in the pipeline. This leads to the conclusion that both the increase of slug velocity and fraction

of the pipe area not covered by the stationary layer together have more effect on the total length of slugs than the increase of the solids mass flow rate. It was found that an increase in the air velocity leads to the decrease of the total slug length and increase of the slug velocity. However, the number of slugs passing through a given pipe-section per time unit remains unchanged. This means that the length of each single slug of particles decreases whereas the length of each gas slugs increases. Furthermore, due to the increase of the fraction  $(1 - \alpha)$ , a bigger volume of particles can be transported in each slug. This results in a significant increase of the total solids mass flow rate. It should be pointed out that diverse authors like Daoud [15] and Hitt [31] reported that an increase in the mass flow rate and/or the conveying length leads to an increase of the length of single slugs of plastic pellets (see Section 2.4.3). However, they did not explore the direct correlation between those parameters and the conveying gas velocity.

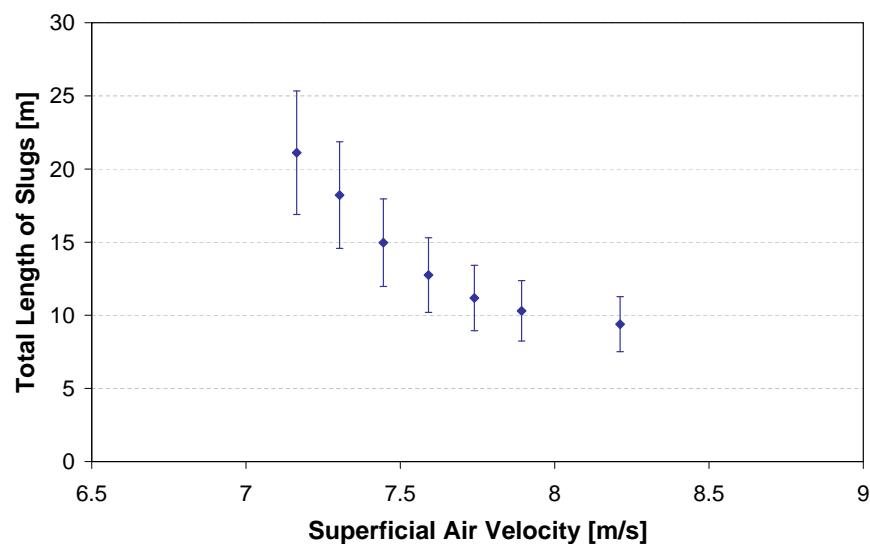


Figure 5.7: Influence of the air velocity on the total slug length

### 5.1.3. Correlation between cross-section fraction $\alpha$ covered by settled particles and slug velocity

In agreement with the literature, both the slug velocity and the height of the stationary layer between two slugs were found to be a function of the air supply velocity (Fig. 5.4 and 5.6). The analysis of several slugs taken from the same conveying trial, i.e. conveyed in the same conditions of air supply velocity and solids mass flow rate showed that slugs display two types of shape both at the front face and rear. If the stationary layer in front of a slug is relatively thin, the slug displays a long and turbulent front, which does not fill immediately the entire cross-section (Front type 1 in Fig. 5.8). Otherwise, the front face consists rather of a suspension of particles in the upper part of the cross-section that fly or slide above a thick stationary layer (Front type 2 in Fig. 5.8).

In Fig. 5.8, some particles have been marked to allow their motion to be followed. When the stationary layer in front of a slug is rather thin, the slug displays high turbulences at the front face and all particles filling the cross-section are simultaneously lifted and rapidly brought into movement.

This results in the existence of a velocity gradient over the pipe height: the particles of the lower layers move slower than the particles of the layers above them. When the stationary layer in front of a slug is rather thick, the particles are first only transported in the upper part of the pipe cross-section, i.e. suspension. As soon as the density in particles in the cross-section reaches a certain value, the particles of the stationary layer are slowly accelerated and transported with a velocity close to the velocity of the particles already composing the slug. The particles remain on the same height and only a small velocity gradient exists over the slug height. The significant acuity difference of the images illustrating the first and the second front types in Fig. 5.8 indicates that a significant difference in the particle velocity exists, although both slugs are coming from the stable operating area of the same conveying trial.

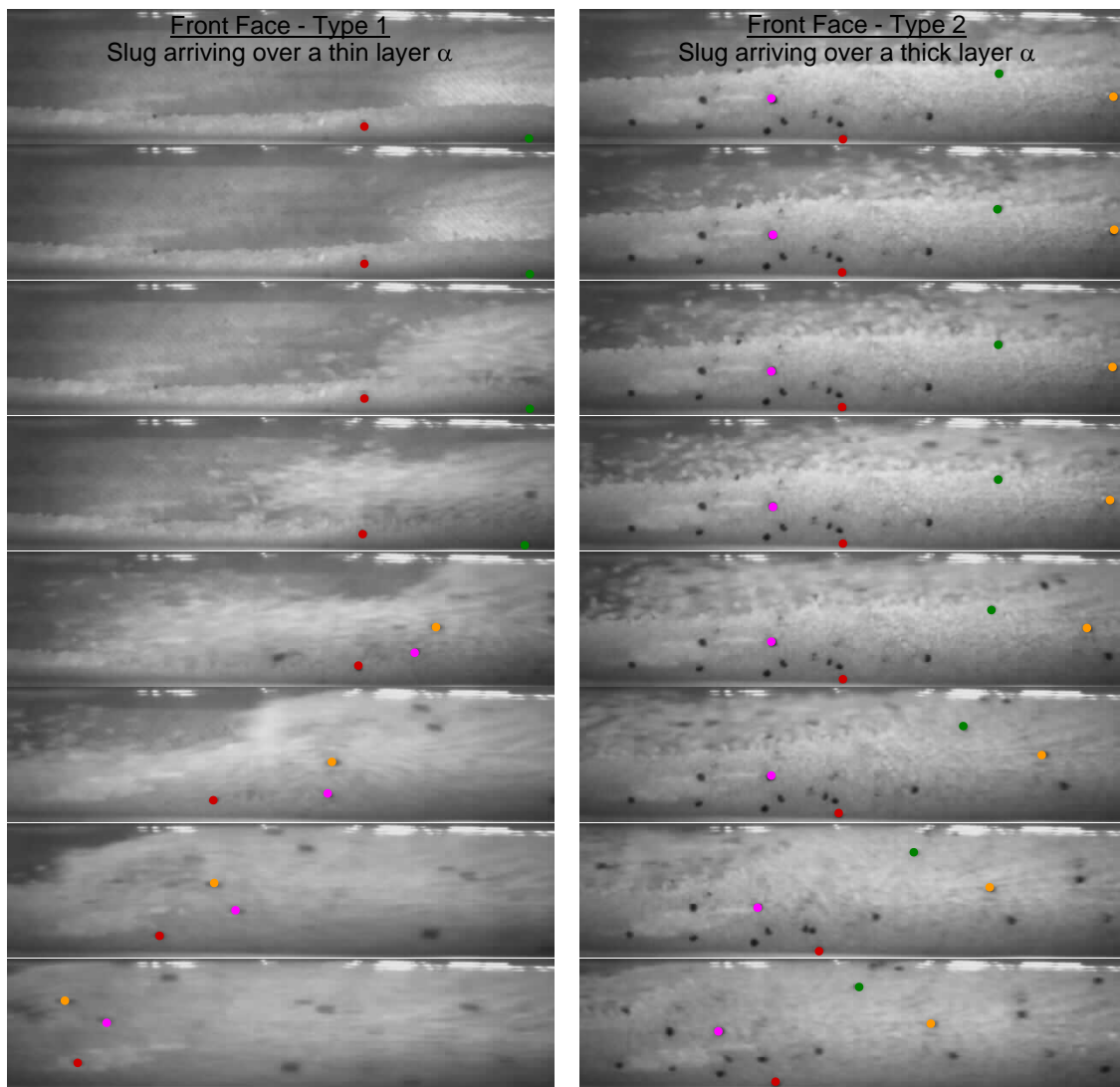


Figure 5.8: The two main types of front face displayed by slugs -  $v_f = 6.8$  m/s.

Similar to the front face, two types of slug rear were observed. A slug displays either a flat or a steep tail. Many authors reported that the slope of the slug rear is steeper than the slope of the slug front (see Section 2.4.4). The height of the layer of particles remaining at the rear of a slug depends on the shape of the rear, as shown in Fig. 5.9. The two types of rear presented 5.9 belong to the slugs that

displayed the front types presented in Fig 5.8. As previously mentioned, the acuity difference of the images illustrates the difference in the particle velocity. Fig. 5.10 shows the velocity of the particles along the two slugs presented. A higher particle velocity was measured at the back of Slug 1 than at the front whereas the particles of Slug 2 moved faster at the front end than at the rear. Therefore, a strong correlation exists between slug aspect, i.e. behaviour and profile of particle velocity over a slug.

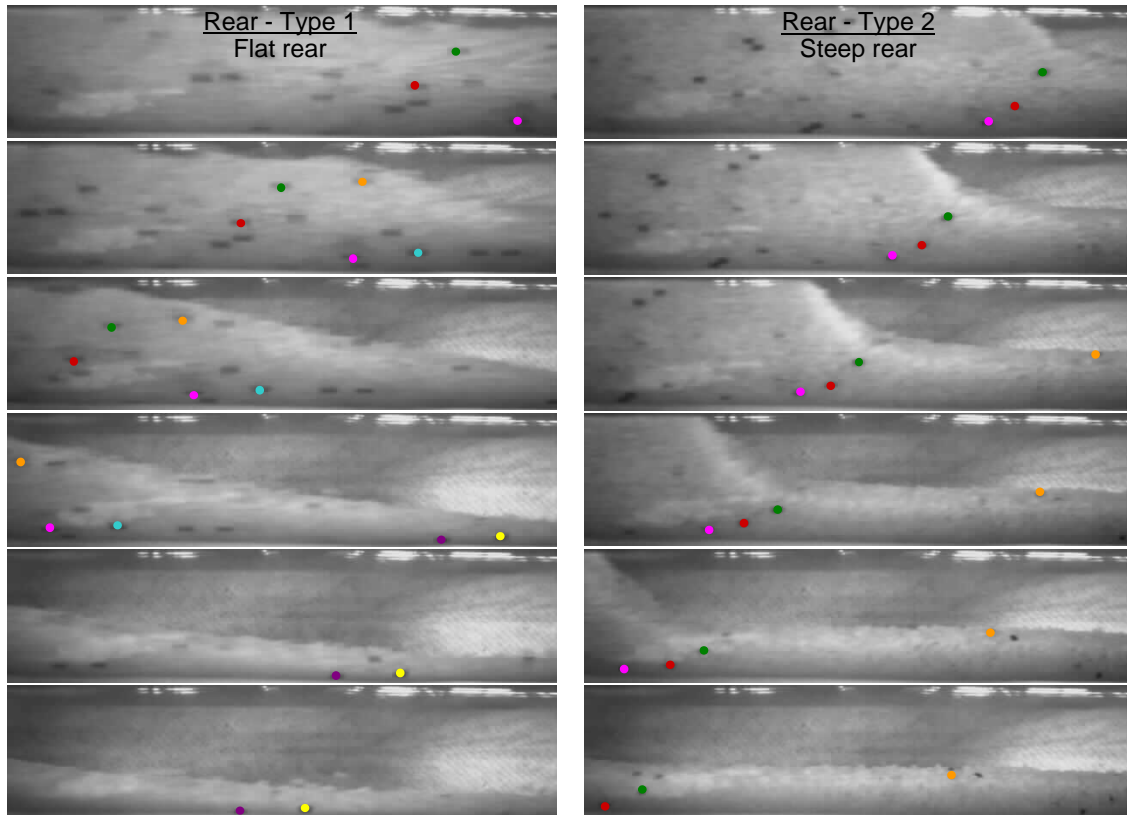


Figure 5.9: The two main types of rear displayed by slugs -  $v_f = 6.8$  m/s. The images belong to the slugs whose fronts are presented in Fig. 5.8

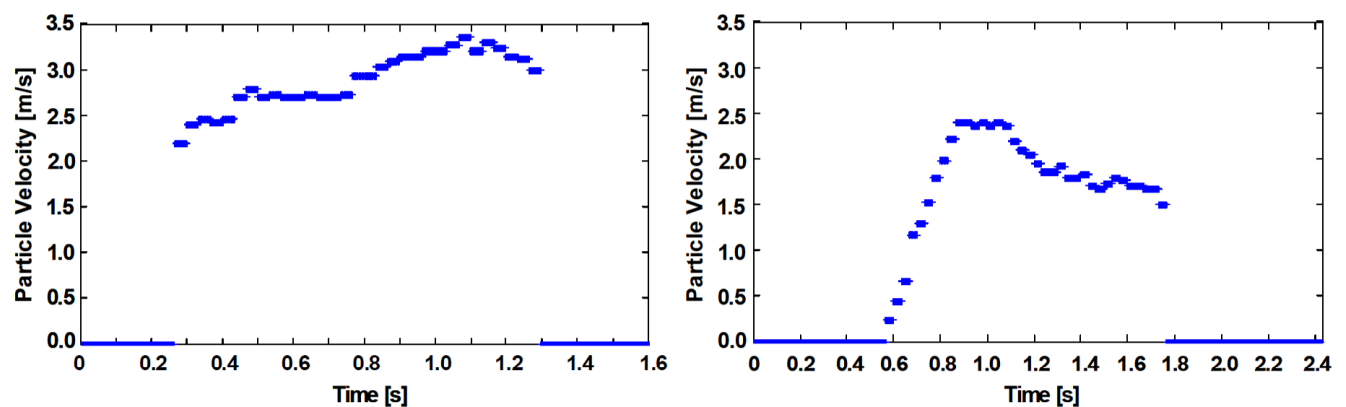


Figure 5.10: Particle velocity along the two slugs illustrating type 1 and 2 of slug front and rear

Furthermore, experimental investigations were carried out to identify a potential correlation between the height of the stationary layer, i.e. the fraction  $\alpha$  of the cross-section area covered by stationary

particles and the velocity of the slug arriving ( $v_{slug} = f(\alpha_{slug-1})$ ) and between the velocity of a slug and the height of the layer the slug leaves behind ( $\alpha = f(v_{slug-1})$ ). The results presented in Fig. 5.11 indicate that slugs tend to move faster if the stationary layer in front of them is thinner. This is due to the lower resistance force caused by a thinner stationary layer whose particles have to be picked up and accelerated at the velocity of the slug. As a further result, the height of the particles layer a slug leaves behind, i.e. the fraction of the cross-section area covered by the stationary layer tends to be smaller if the slug moves faster (Fig. 5.12). However, if tendencies could be recognised in both cases, no systematic behaviour was found.

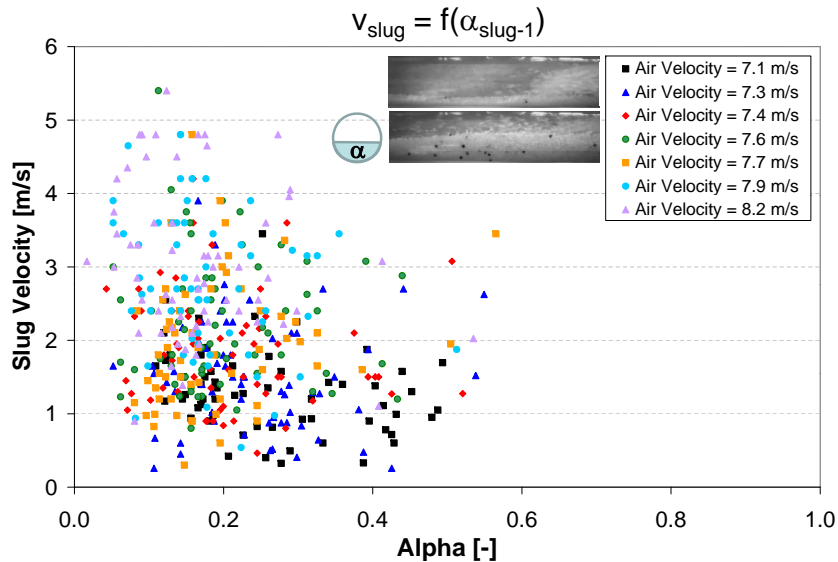


Figure 5.11: Correlation between the fraction of the pipe area covered by the stationary layer and the velocity of the slug arriving

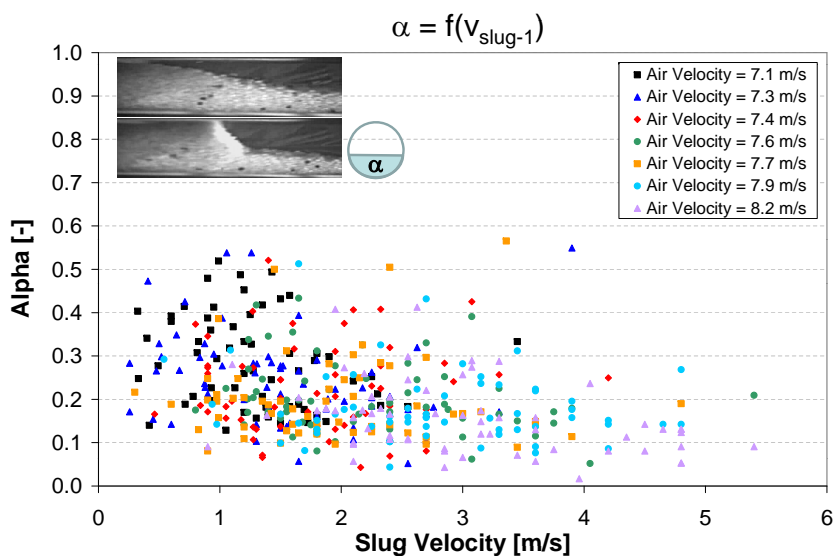


Figure 5.12: Correlation between the velocity of a slug and the fraction of the pipe area covered by the particles left behind

#### 5.1.4. General description of pressure, radial and wall shear stress induced by slugs

Besides the solids mass flow rate, slug velocity, height of the stationary layer and slug frequency, the pressure profile and the radial and wall shear stresses induced by moving slugs were measured. Slugs conveyed with different superficial air velocities from 6.8 m/s to 8.5 m/s were analysed. This range of velocities covers the entire area of slug flow. However, conveying with the minimum velocity of 6.8 m/s can lead to pipeline blockage if slight disturbances occur in the conveying process. On the other hand, conveying with the maximum velocity where slug flow occurs is accompanied by first instabilities and a tendency for the flow to move to another flow-mode.

Each single slug induces significant radial and wall shear stresses around the entire pipeline circumference that disappear immediately after the slug passage. Fig. 5.13a) shows a 15-seconds-recording of pressure as well as radial and wall shear stresses measured at the side of the pipe in slug flow conveying operated with  $v_f = 7.2$  m/s. The segment of the signals corresponding to Slug 1 is additionally detailed in Fig. 5.13b).

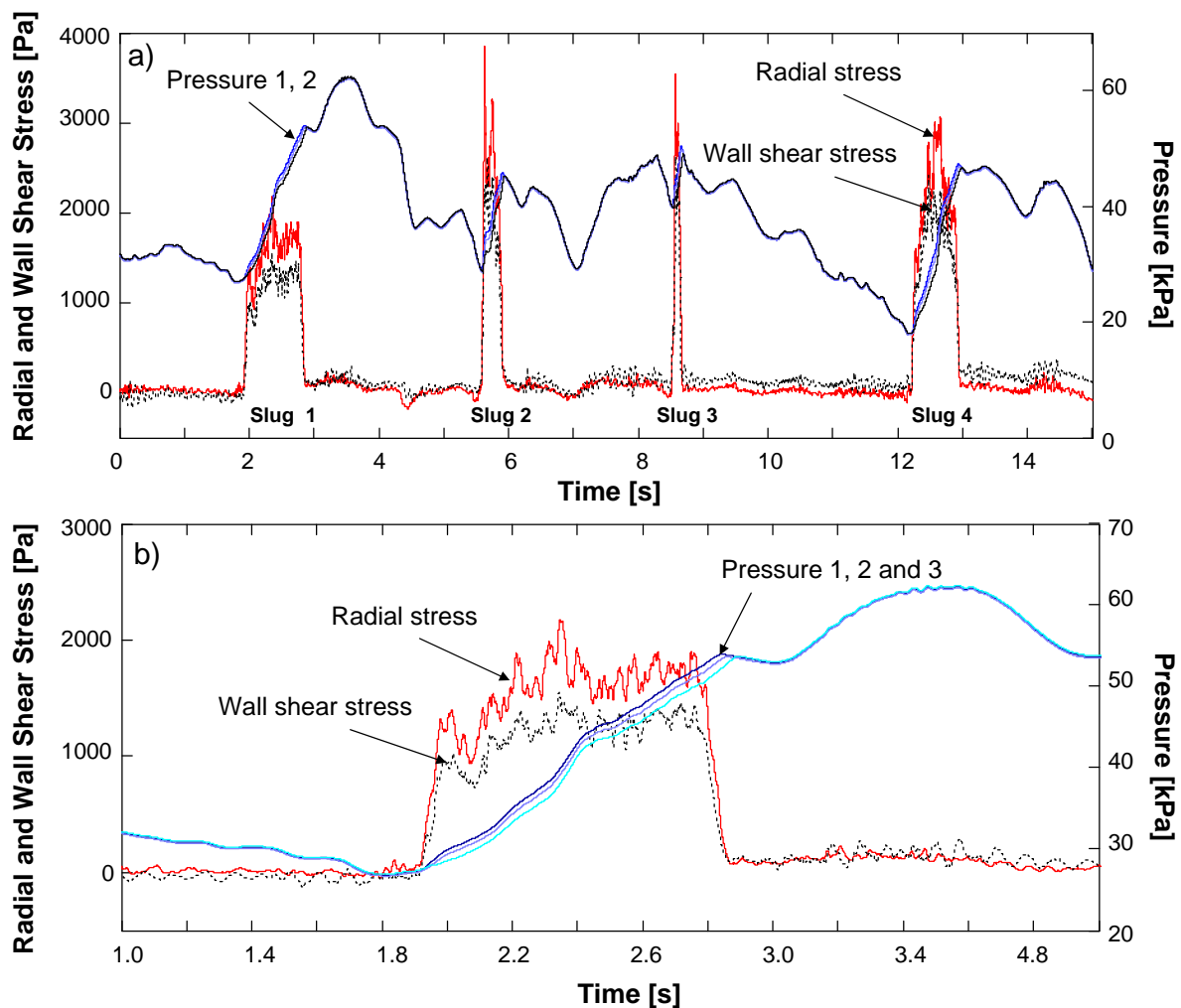


Figure 5.13: Pressure and stress signals measured at the side of the pipe -  $v_f = 7.2$  m/s. a) 15-seconds-recording; b) Segment of the signals corresponding to Slug 1



An increase in the air supply velocity leads to the increase of the slug velocity and may result in an increase of the number of slugs passing through the probe per time period. Four slugs conveyed with 7.2 m/s air velocity passed through the probe in a time period of 15 seconds. In Fig. 5.14, seven slugs conveyed with an air velocity of 8.5 m/s were detected in the same period. However, the results of the investigations carried out on the slug frequency showed that the mean slug frequency does not significantly increase with the increase of the air supply velocity. Besides radial and wall shear stresses, each slug induces a pressure increase as well. Between two slugs, a layer of motionless particles that have been just deposited by a slug and are going to be picked up by the next one lies at the bottom of the pipeline. Therefore, slug flow can be described as a wave motion. When a slug is passing through the measurement probe, a significant difference is detected between the pressures measured using two miniature pressure sensors 75 mm apart. This is illustrated by the deviation of the pressure curves that originally lied on each other (Fig. 5.13). The pressure along a slug reaches a maximum value at the rear where the conveying air is supplied. The pressure decreases in the direction of the flow, i.e. slug front. Because the front face of a slug reaches the sensors before the rear, this pressure decrease is not illustrated on the curves by a decrease of the signals but an increase.

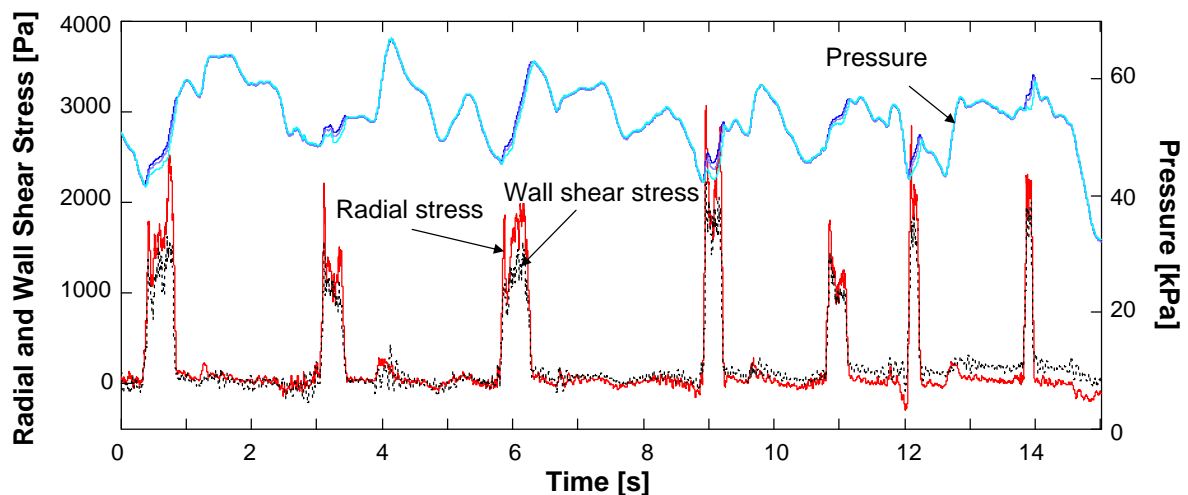


Figure 5.14: Pressure and stress signals detected at the side of the pipe -  $v_f = 8.5$  m/s

## 5.2. Porosity within single slugs

The stresses measured during slug flow are usually assumed to be directly correlated to the internal porosity of the slugs. Slugs are generally assumed to be and behave like packed beds percolated by the transported gas. Therefore, the stresses at the wall are assumed to result principally from the axial compression of the slugs. Because slugs are supposed to display the bulk porosity, the compact arrangement of the bulk material and the many interparticle contacts existing are assumed to allow the transmission of the stresses across the slug cross-section.

Based on the local determination of the particle velocity along a slug and local pressure loss measurements in a slug slice of 35 mm thickness, the porosity trend over the slug length could be calculated

by applying the Ergun equation. However, it should be pointed out that the values calculated should not be considered as absolute values, i.e. as the actual porosity but as the Ergun porosity (see Section 4.5.5.1). In addition, the slug porosity was directly determined with the aid of a slug-catcher. Both determination methods were applied on the same slugs so that the results obtained can be directly compared.

It should be mentioned one more time that the slug porosity provided by the Ergun equation corresponds to an average porosity across the entire cross-section for a given  $x$ -value over the slug length. Therefore, the porosity at the slug front and rear is an average value for the entire cross-section, although the material only covers part of this cross-section.

### 5.2.1. Porosity according to Ergun

Similar to the stress determination, the Ergun porosity was investigated for the entire area of slug flow, i.e. for slugs conveyed with velocities from 6.8 m/s to 8.5 m/s. To be able to detect a general trend, several successive slugs of the same conveying trial were each time analysed. The effect of the air supply velocity on the internal porosity was investigated by comparing the porosity trend over both short and long slugs conveyed with various supply air velocities.

#### 5.2.1.1. Porosity trend over moving slugs

Fig. 5.15 shows the particle velocity and porosity trend over four slugs conveyed with the minimum air velocity where slug flow occurred.

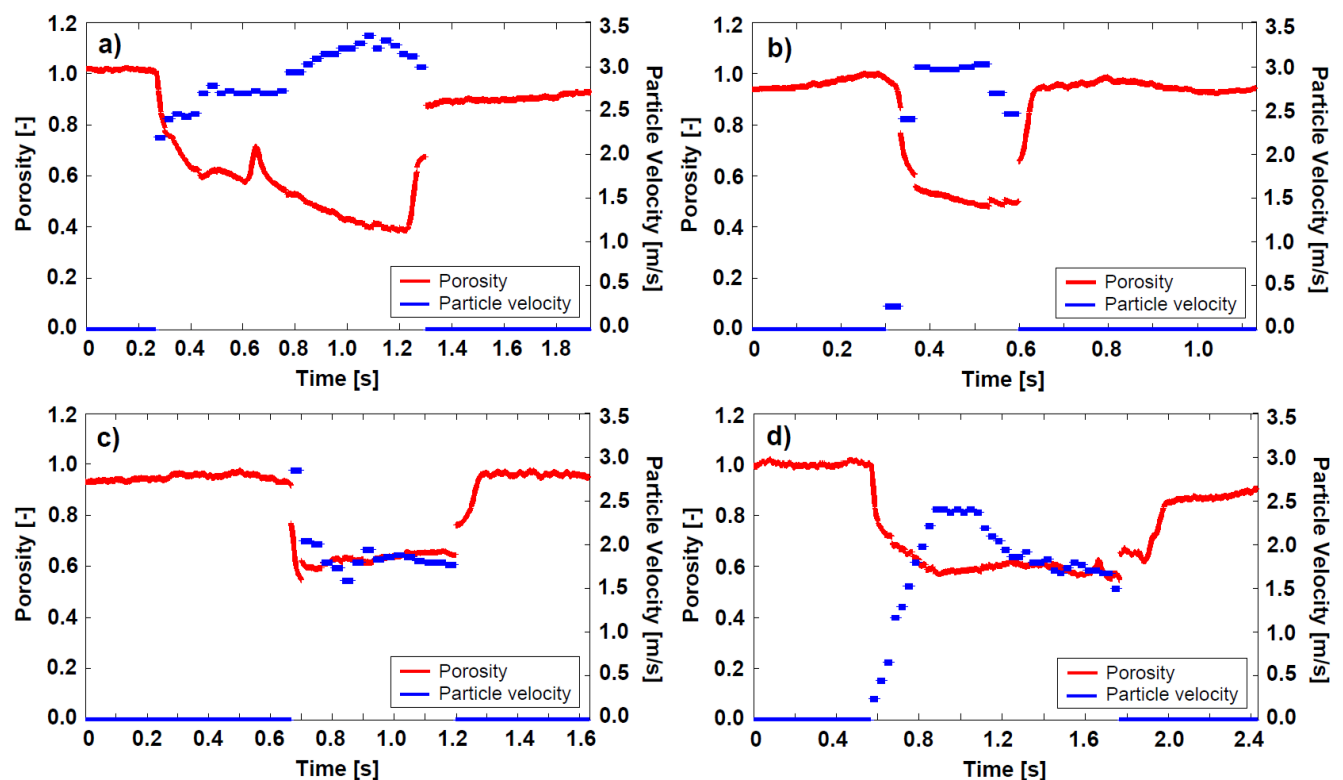


Figure 5.15: Four slugs of the same conveying process -  $v_f = 6.8$  m/s

The results indicate that the porosity displays different trends over the slug length. Sometimes, slugs display porosity that decreases over the slug length, i.e. the slugs are denser at the rear (Fig. 5.15a)). Other slugs display lower density at the rear compared to the front end (Fig. 5.15c)) whereas some slugs display relatively constant porosity over their entire length (Fig. 5.15b) and d)). No general rule could be found regarding the porosity trend exhibited by the slugs. However, although different types of porosity trend were observed, most of the slugs were found to display porosity that decreased over the slug length as illustrated in Fig. 5.15a). Moreover, the particle velocity was mostly found to increase over the slug length.

Slugs display porosity values between 0.4 and 0.6 in their core part where the whole cross-section appears full, i.e. the Ergun porosity is always higher than the porosity of the bulk solids itself ( $\varepsilon_{bulk} = 0.38$ ). These results agree with the results of Kuang who reported from numerical simulations carried out on plastic granules that the average solid concentration of a slug over the pipe cross-section fluctuates around a constant that is lower than the bulk density [40].

### 5.2.1.2. Effect of the air supply velocity on slug porosity

Fig. 5.16 and Fig. 5.17 show for different conveying velocities the porosity trend over two slugs chosen from the same conveying trial. The two slugs presented for each velocity correspond to a short and a longer slug as far as both types were available in the same conveying trial.

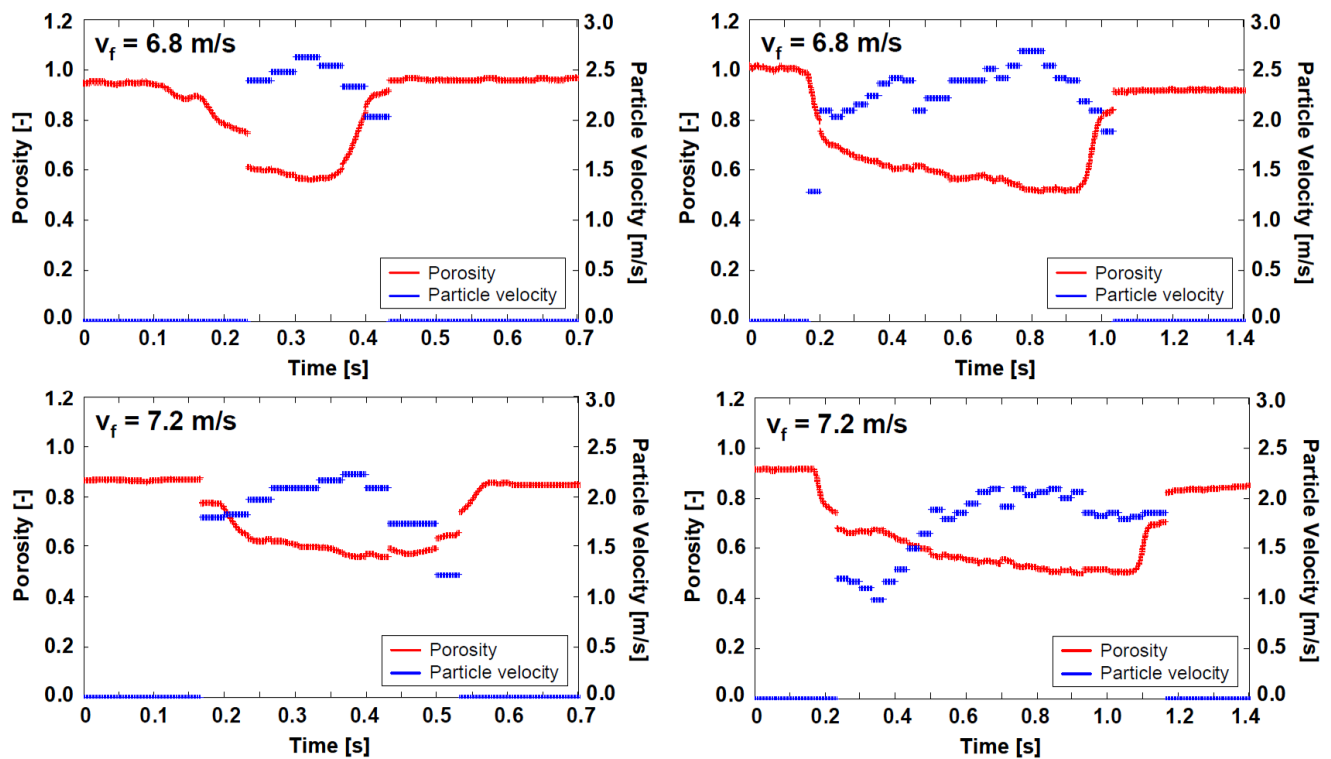


Figure 5.16: Effect of the conveying velocity on the slug porosity for  $v_f = 6.8$  m/s and  $v_f = 7.2$  m/s

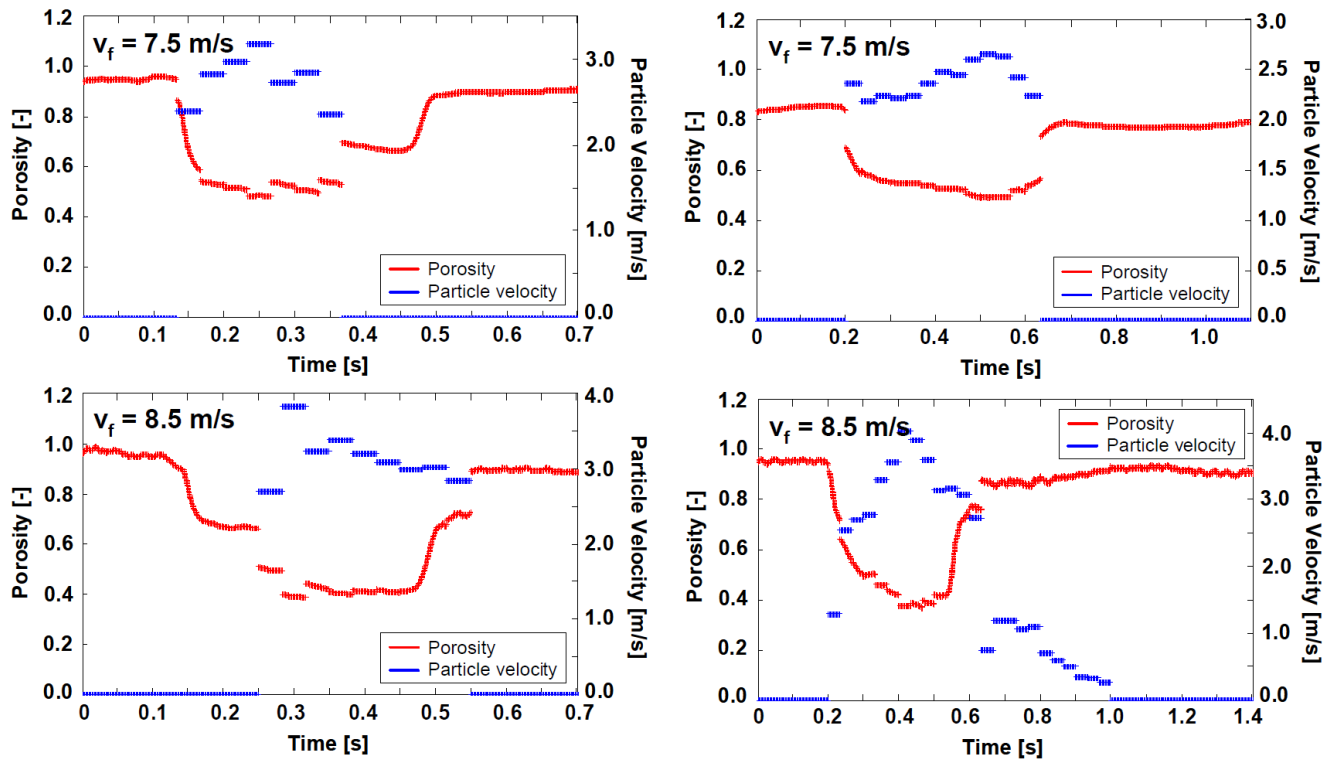


Figure 5.17: Effect of the conveying velocity on the slug porosity for  $v_f = 7.5$  m/s and  $v_f = 8.5$  m/s

The results indicate that the Ergun porosity is not affected by the conveying gas velocity. Slugs display porosity values higher than the bulk porosity itself, mostly between 0.4 and 0.6. The porosity appears independent of the conveying velocity. Moreover, short and long slugs display similar values and trends. As mentioned earlier, most of the slugs display porosity that decreases over the slug length. This observation is valid for all conveying velocities.

### 5.2.2. Direct determination using a slug-catcher

The porosity calculation according to Ergun is based on pressure measurements. Therefore, it does not allow the detection of a potential porosity gradient over the height of a slug. In the literature, different approaches can be found that assume the existence of a density gradient over the slug height. Moreover, a density gradient over the slug height is frequently observed in the pneumatic conveying of powders, especially in pipelines with big diameters. Therefore, the slug porosity was also investigated by using a direct determination method, which allows the porosity of different horizontal layers of a slug to be determined. For the entire range of air velocity where slug flow occurred, the core of horizontal slugs was caught using a slug-catcher. With the aid of two horizontal sheets, which were additionally pushed into the conveying section by releasing the catching mechanism, each caught slug was divided into three horizontal layers simultaneously to the catching process. Therefore, the existence of a density gradient over the slug height could be investigated. The high rapidity with whom the whole catching process takes place permits to obtain an accurate picture of the internal state of the slug in movement.

The slug-catcher was always activated after at least 30 seconds of stable slug flow but the choice itself of the slugs caught was randomly made.

The volume of the catching chamber separated by the two vertical sheets during the catching-process corresponds to  $1.66 \cdot 10^{-3} \text{ m}^3$ , which is reduced of  $4.7 \cdot 10^{-5} \text{ m}^3$  by the additional horizontal separating sheets. Therefore, the insertion of those separating sheets corresponds to a volume reduction of the sample chamber of 3%. With respect to the bulk density of the material conveyed, there is space for 917 g of granules in the opened chamber of the slug-catcher. However, 900 g of granules are enough to completely fill the sample chamber when the slug-catcher is closed, i.e. when the additional sheets have been inserted in the catching-section.

Fig. 5.18a) shows the total weight of particles caught for different conveying velocities. The three horizontal chambers were found to be similarly filled with granules. Therefore, no significant porosity gradient exists over the height of a slug. As a consequence, the results for the three layers are presented together in the form of total mass of granules caught and mean slug porosity.

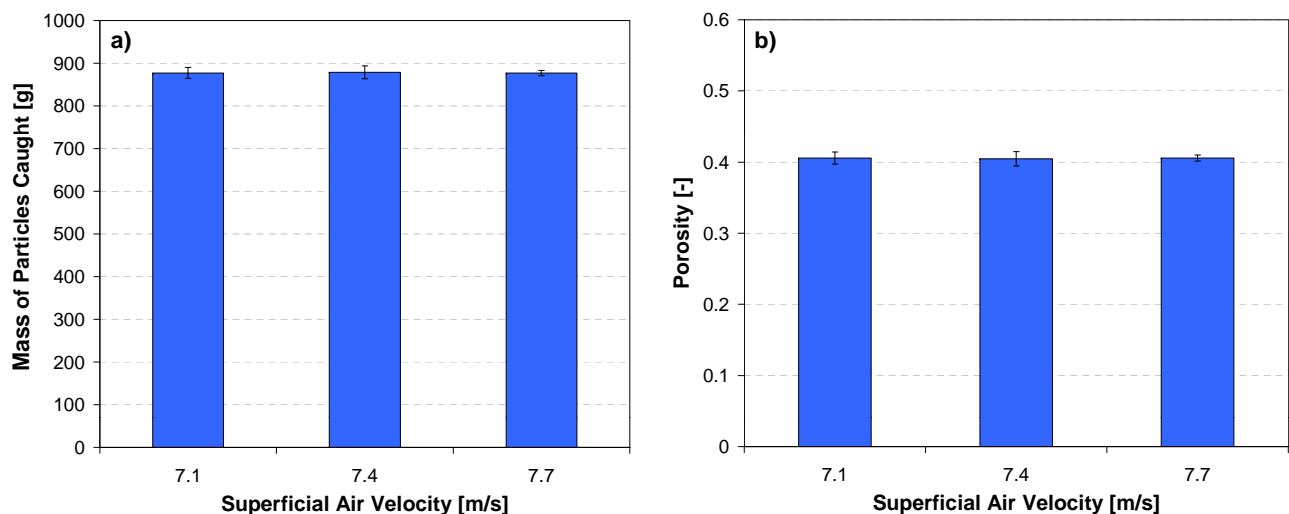


Figure 5.18: Influence of the air supply velocity on the slug porosity. a) Total mass of granules caught in the sample chamber, b) Porosity displayed by the slugs at the time when the catching mechanism was triggered

The total mass of particles caught was found to be similar for the three conveying velocities tested. After the insertion of the sheets in the sample chamber, 2 to 3% of the volume remained free of particles. With respect to the volume occupied by the sheets, it can be concluded that a total volume of 5 to 6% was free of particles when the moving slug was caught. By extrapolating the value of the additional free volume of gas (in comparison to the free volume contained in the loose poured bulk), the porosity a slug displayed at the time it was caught could be calculated.

Fig. 5.18b) shows that the caught slugs displayed mean porosity values between 0.40 and 0.42, that is a porosity slightly higher than the bulk porosity of 0.38. Hence, slugs can be considered as slightly fluidised entities. These results agree with the results of the porosity determination method based on the Ergun equation. Niederreiter [60] obtained similar results by investigating the porosity of vertical

moving slugs composed of the same material. He noticed that slugs moving in a vertical pipe section display porosity values of about 0.40 and concluded that the porosity of vertical moving slugs is slightly higher than the bulk porosity.

All slugs investigated displayed a similar porosity. Therefore, the conveying velocity does not affect the slug porosity. Slugs correspond to slightly fluidised structures, which are transported by the percolating air. This fluidised state appears necessary for the slugs to be conveyed. The volume of air contained in the slugs is significant, which indicates that not enough contacts exist between particles to allow a potential transmission of the stresses across the slug cross-section.

The results obtained indicate that the equation of Ergun is suitable to follow the density changes over the length of a slug. For all conveying velocities where slug flow occurred, the slugs investigated by applying the Ergun equation and/or by using the slug-catcher were found to be slightly fluidised. Therefore, the theoretical concept of stress transmission from axial into radial direction by means of interparticle contacts could not be validated. However, the existence of both axial and radial stresses have been frequently reported in the literature. The next Section is dedicated to the stresses induced by moving slugs during horizontal slug flow pneumatic conveying. In particular, the focus is on the identification of the physical mechanisms generating the stresses and their mathematical description.

### **5.3. Radial and wall shear stress during the transport of slugs**

#### **5.3.1. Stresses according to the circumferential pipe location**

##### **5.3.1.1. Stresses induced by slugs at the pipe bottom**

Both the distance between two slugs and the width of the stress peaks observed during a defined conveying experiment are inhomogeneous. Smaller spaces can be observed between narrower stress peaks. With the assumption that during conveying, all slugs move with a similar velocity, the width of the stress peaks is directly proportional to the slug length and mass of product transported. The particles transported in short slugs moving close to each other can join to form a longer slug. This results from the disintegration of the slugs, which is signalled by the apparition of air cavities at the top of the slugs. The force measurement probe is able to detect those cavities, which is illustrated by the occurrence of fluctuations in the force signals. This phenomenon can be observed in Fig. 5.19 and on the corresponding image in Fig. 5.20. The cavities in the structure at the top of the slug lead to the decrease of the force signals corresponding to Slug 12 in Fig. 5.19. With the aid of the force measurements and the corresponding images of the slug, the disintegration process could be followed. Some small cavities free of particles appear at the top of the slugs. Between those cavities, the pipe cross-section is shortly totally filled with particles. The size of the cavities increases until the slug becomes a wave. First, the top of the wave does no longer touch the upper part of the pipe wall. Then, the wave flattens until a high stationary layer of particles is formed. Besides the formation of the gas pockets at the top of the slugs, the disintegration is helped by the deposition of a bigger amount of

granules at the slug rear. When the slug structure becomes unstable, the particles slow down and the quantity of granules deposited at the rear is higher than the quantity of granules picked up at the front. As a result, the slug length decreases. At the same time, the next slug will pick up the additional mass of granules deposited. Therefore, the length of the following slug and the distance between this long slug and the previous slug both increase.

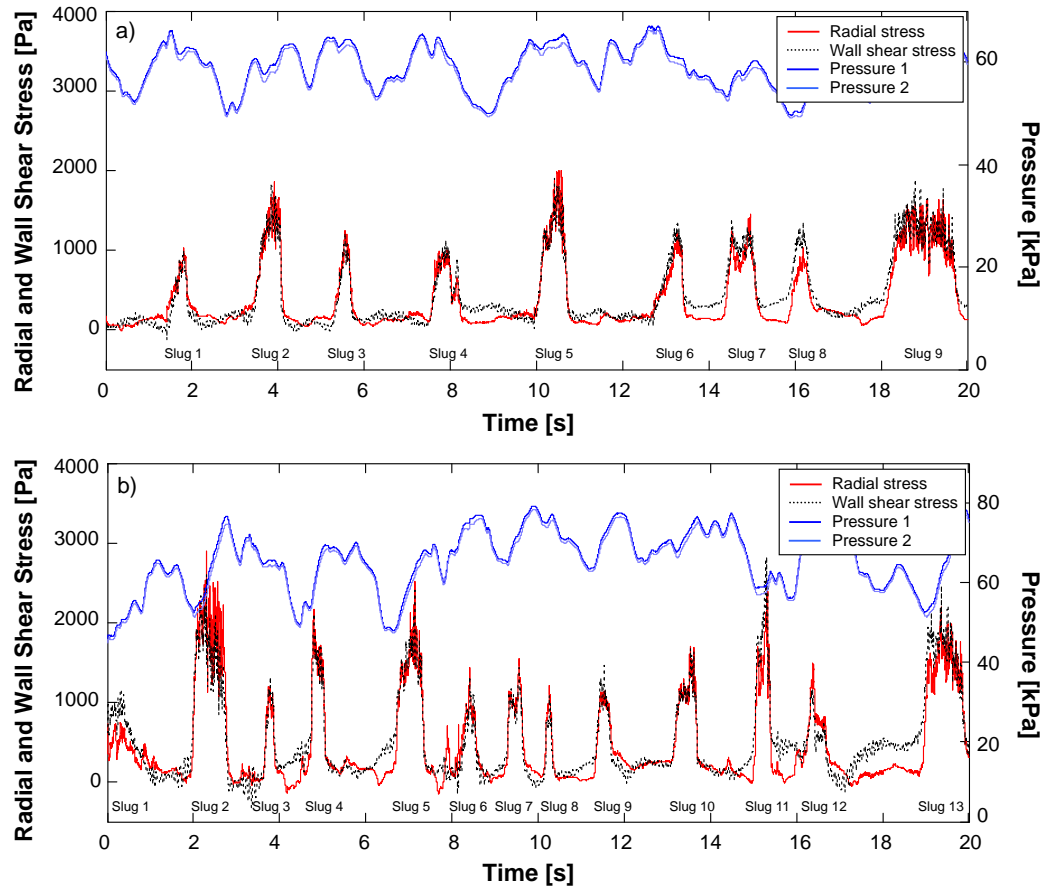


Figure 5.19: 20-seconds-recording of pressure and force signals detected at the pipeline bottom.  
a)  $v_f = 7.0$  m/s; b)  $v_f = 7.5$  m/s



Figure 5.20: Air cavity at the top of a slug -  $v_f = 7.5$  m/s

The amplitude of the stresses induced by slugs does not depend on the slug length. However, only slugs whose front face and rear are perfectly defined are able to induce significant stresses. Even if they fill shortly the entire pipe cross-section, waves do not induce high values of stress. This phenomenon is illustrated in Fig. 5.19 and 5.21. In Fig. 5.19, the signals induced by a separate wave of particles whose

height reaches the pipeline top can be observed after Slug 4 (Fig. 5.21). A layer of particles moved over the stationary layer without affecting it. Therefore, only slight fluctuations in the radial stress values were observed whereas the wall shear stress remained unaffected. This slight increase in the radial stress values results most probably from the additional mass of particles acting on the measurement plate located at the bottom of the pipeline. In fact, when the measurement plate is located at the pipeline bottom, the stress due to the weight of the particles is fully detected. This stress was evaluated to 290 Pa when the pipe cross-section is totally filled with particles.



Figure 5.21: Wave of particles -  $v_f = 7.5$  m/s

### 5.3.1.2. Stresses induced by slugs at the side of the pipe

High values of radial and wall shear stress were also measured when the measurement plate was positioned at the side of the pipe (Fig. 5.22).

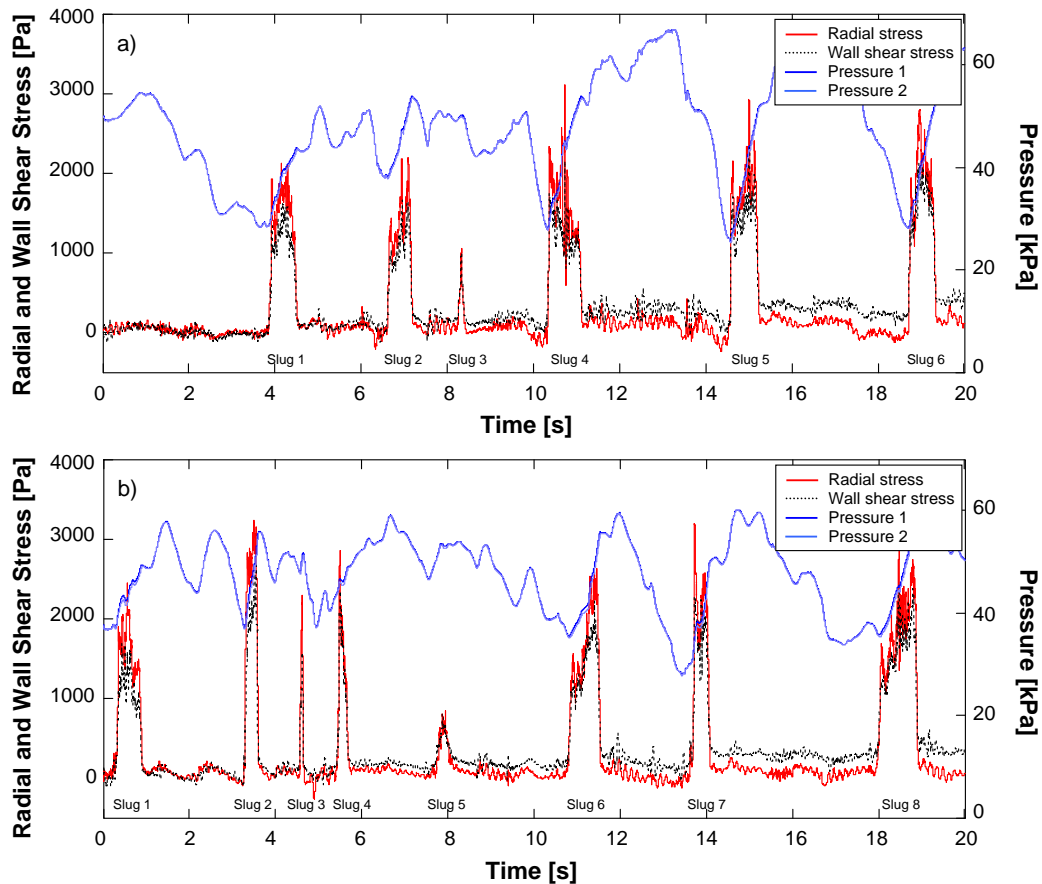


Figure 5.22: Signals of pressure and stresses measured at the side of the pipe  
a)  $v_f = 7.0$  m/s, b)  $v_f = 7.5$  m/s



Fig. 5.22 shows that the signals fluctuations occurring between the stress peaks generated by the passage of the slugs are lower when the measurement plate is positioned at the pipeline side than at the bottom. This results from the fact that the stationary layer between two slugs is mostly not high enough to reach the measurement plate. However, after Slug 5 in Fig. 5.22a), the remaining layer of particles covers more than  $2/3$  of the pipe cross-section (Fig. 5.23). Some particles are flying over this layer. However, they do not induce enough shear force to bring the layer into movement. The presence of those flying particles lead to the significant increase of the pressure. However, they do not generate any significant stress values.

The amplitude of the radial stress values induced by slugs is higher than the amplitude of the wall shear stress. For  $v_f = 7.0$  m/s, the similar width of each stress peak, large distance between the peaks and height of the stress values measured during 20 seconds indicate that the flow regime was particularly stable. However, the third slug in Fig. 5.22a) induced significant lower stress values over a very short time. This slug is close to disintegration.

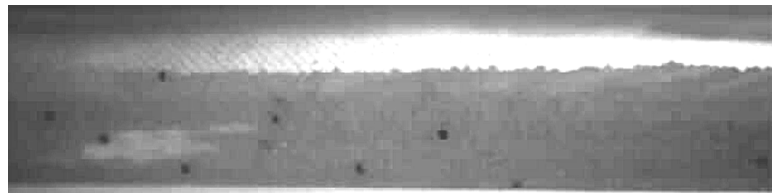


Figure 5.23: Layer of particles covering  $2/3$  of the pipe cross-section

On the opposite, Fig. 5.22b) shows that slugs with very different lengths separated with irregular spaces were obtained with an air supply velocity of 7.5 m/s. Short slugs moved close to each other (Slug 2 to 4) whereas higher spaces separated long slugs from the previous ones (Slug 6 and 8). After the 4<sup>th</sup> slug, small stress peaks identified as Slug 5 were detected. The small amplitude of the stress values induced by this slug were caused by the presence of air cavities at the top of the pipe. Slug 5 disintegrated slowly. Between the 7<sup>th</sup> and the 8<sup>th</sup> slug, a wave of particles passed through the measurement probe (Fig. 5.24). This wave, whose particles did not fill completely the pipe cross-section can be identified on the curves by the pressure increase. However, this wave did not induce any significant stresses at the side of the pipe.

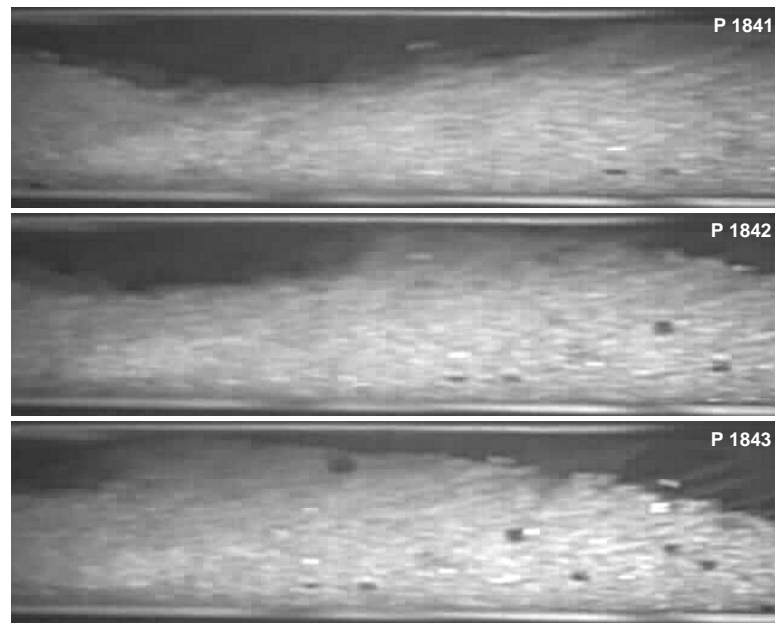


Figure 5.24: Wave of particles -  $v_f = 7.5$  m/s

### 5.3.1.3. Stresses induced by slugs at the top of the pipe

Significant stress values were detected at the top of the pipeline as well (Fig. 5.25). However, the height of the stress values detected is significantly smaller at this location than at the two other measurement positions. The 9<sup>th</sup> slug in Fig. 5.25a) led to a significant pressure loss. However, the stress values remained low. The stresses measured for a higher conveying velocity (Fig. 5.25b)) show a narrower width of peak in comparison to the stresses measured at the bottom and side of the pipe. This results from the fact that stresses are detected only if the granules reach the top of the pipe, i.e. no stresses are detected at the front face and rear of a slug where the cross-section is not entirely filled with product. Short high stress peaks were frequently detected at the pipeline top (Slug 4, 8 and 10 in Fig. 5.25b)). They may be caused by the presence of a higher gas velocity at the top of the slug, i.e. by particular boundary conditions of the gas that generate high turbulences in the particle movement.

The image analysis of the slugs whose stress signals are presented in Fig. 5.25a) showed that many instable slugs were formed and transported during the conveying process. Those slugs partly did not fill the entire pipe cross-section and the granules did not come into contact with the measurement plate positioned at the top of the pipe. Therefore, no stresses were measured when a slug displayed some air cavities at its top. Furthermore, the presence of air cavities led to significant fluctuations in the trend of the stress curves.

It should be pointed out that the slight increase in the stress values occurring over the time, especially in the wall shear stress values in Fig. 5.25a) does not result from an actual increase of the stress values induced by the slugs but from the high temperature sensitivity of the piezoelectric sensors used to detect the stresses. However, although the curves show a deviation, the amplitude of the peaks, i.e. the difference between the stress before the slug enters the measurement area and during the slug passage remains unaffected.

As a further result, the radial stress values detected at the top of the pipeline are higher than the wall shear stress values.

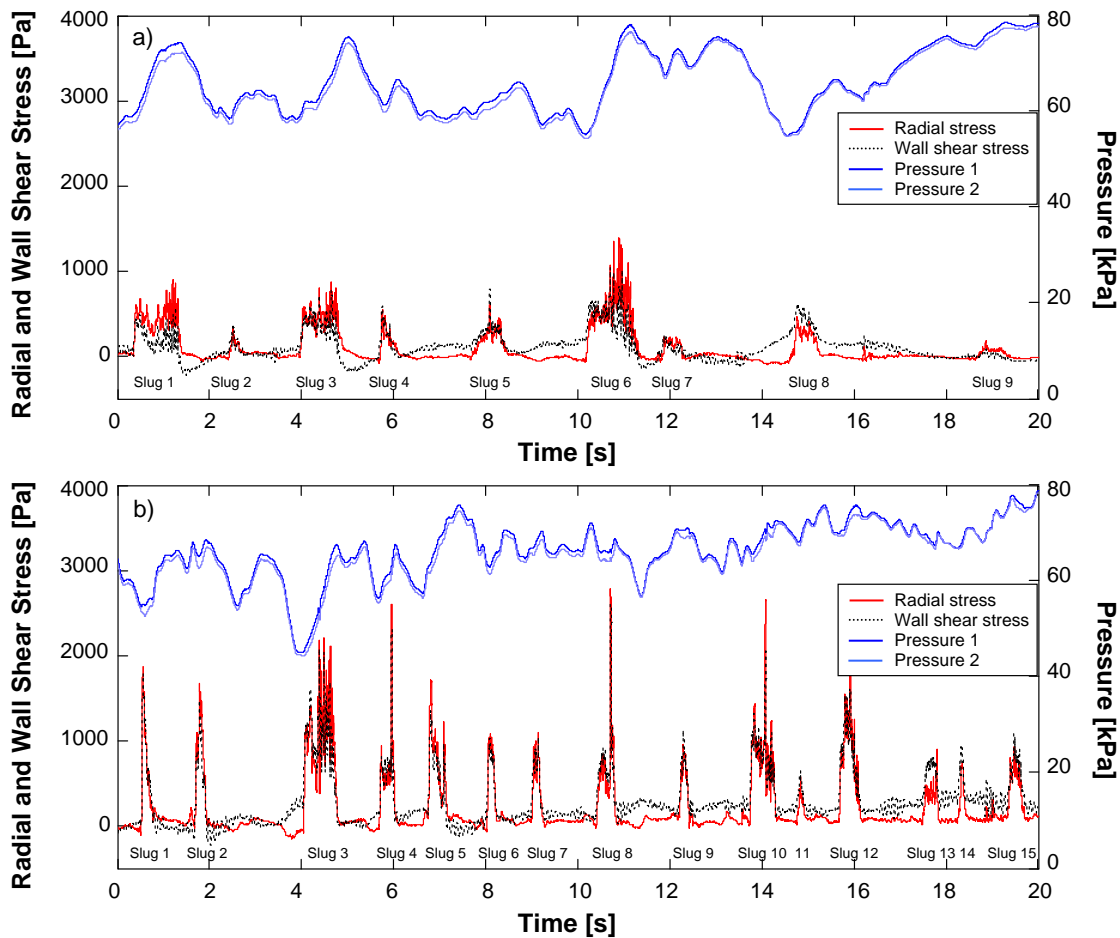


Figure 5.25: Signals of pressure and stresses detected at the pipeline top. a)  $v_f = 7.0$  m/s, b)  $v_f = 7.5$  m/s

### 5.3.2. Effect of the air supply velocity on the stresses induced by slugs

Fig. 5.26 shows 20-seconds-recordings of pressure, radial and wall shear stress detected for different air supply velocities. The time and the stress scales are the same on each graph so that the stress signals can be directly compared. For velocities from 6.8 m/s to 7.5 m/s where stable slug flow occurred, the curves show a similar aspect. For each of those velocities, between six and eight slugs passed through the probe within 20 seconds. Furthermore, each slug induced stress values between 1000 and 3000 Pa. Except for the minimum air supply velocity where slugs were conveyed, i.e. 6.8 m/s, the distance between the peaks is relatively uniform. This uniformity indicates the presence of stable slugs.

Slugs conveyed with a velocity close to the upper boundary of slug flow induced significantly higher stress values between 3000 and 4000 Pa. The fourth slug conveyed with  $v_f = 8.5$  m/s induced stress values higher than 7000 Pa. However, this slug did not display any particular behaviour. These results suggest that short slugs are able to induce higher stress values than longer slugs. It should be pointed out that for  $v_f = 8.5$  m/s, the smaller number of slugs that passed through the probe within 20-seconds

results from the fact that the process was carried out close to the upper boundary of slug flow where first instabilities took place.

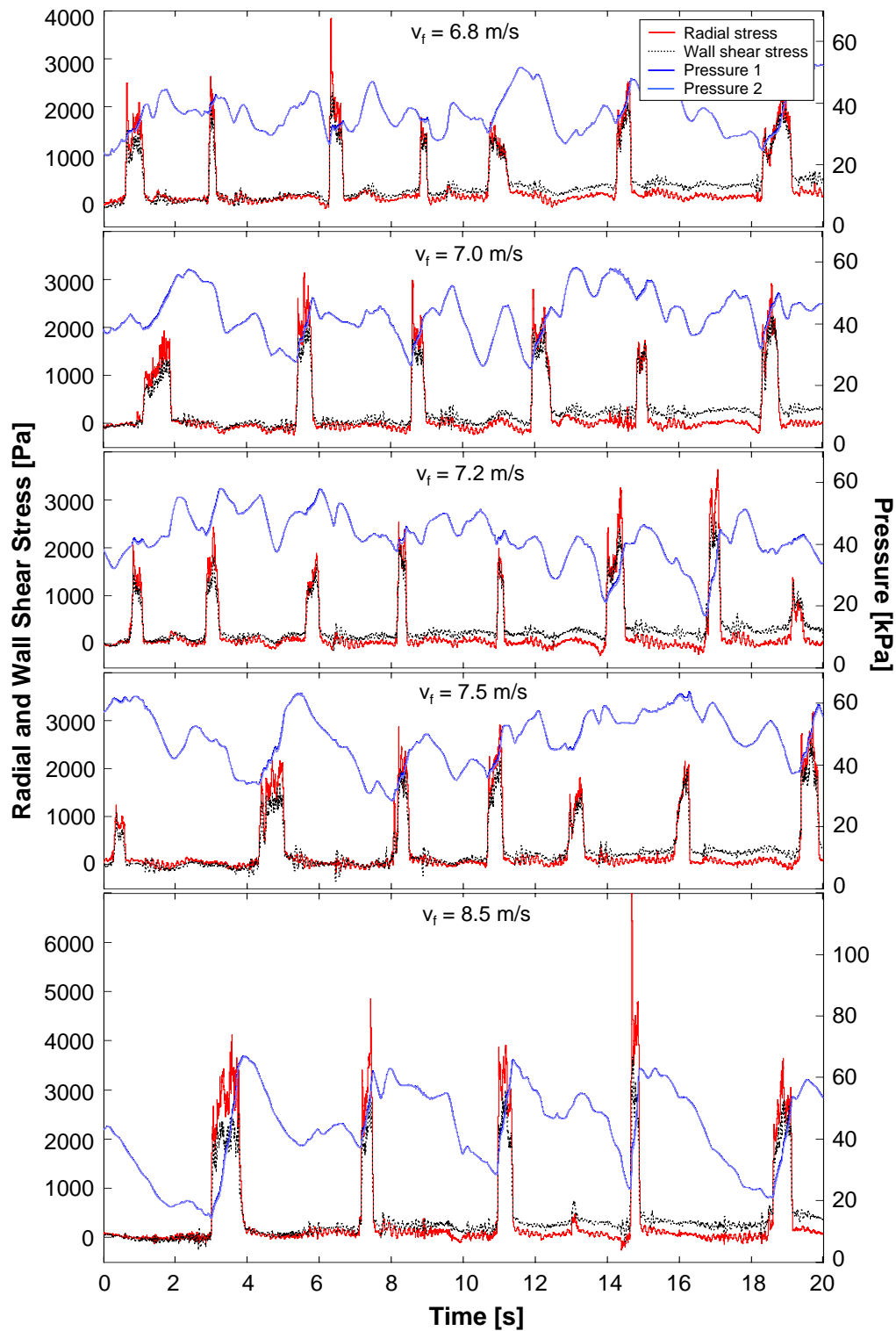


Figure 5.26: 20-seconds-recording of pressure, radial and wall shear stress for air supply velocities covering the entire area of slug flow - Measurement position: pipeline side

### 5.3.3. Discussion of the stresses induced by slugs during pneumatic conveying

#### 5.3.3.1. Summary of the stresses measured during horizontal slug flow pneumatic conveying

The height of the forces induced by single slugs was statistically investigated according to the circumferential pipe location. Fig. 5.27 shows the summary of the radial and wall shear stress values induced by slugs during pneumatic conveying. The mean values are presented with confidence intervals of 95 %.

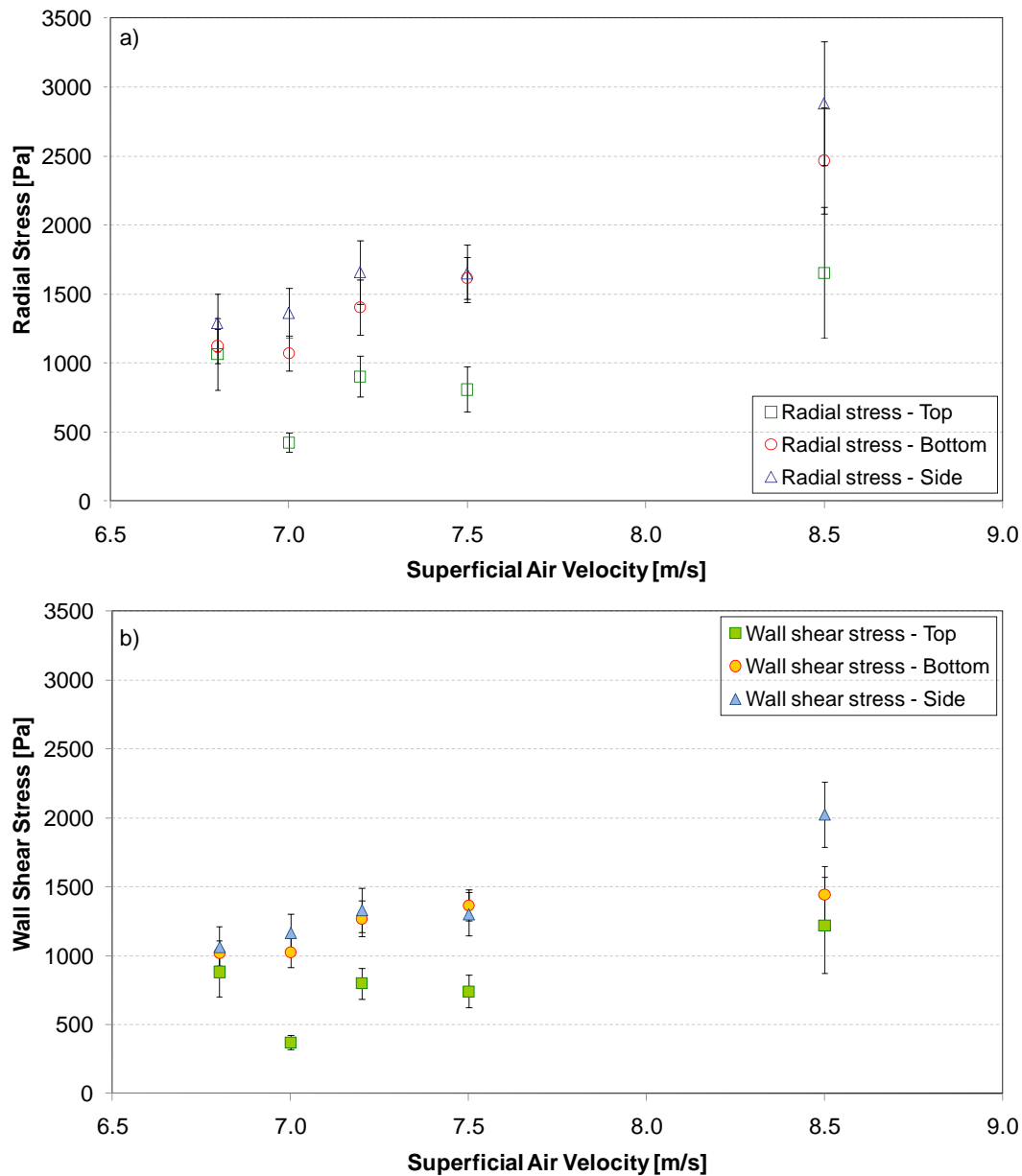


Figure 5.27: Stresses induced by horizontal moving slugs pneumatically conveyed. a) Radial stress, b) Wall shear stress

Both the radial and wall shear stress distributions were found to be non-uniform across the pipe cross-section. The highest stresses were detected at the side of the pipe whereas the lowest stresses were measured at the pipeline top. For both the radial and wall shear stress, the stress values measured

at the pipeline bottom are in between the values at the top and side. However, the stresses measured at the side and top are significantly different only at  $v_f = 7.0$  m/s for the radial stress and  $v_f = 8.5$  m/s for the wall shear stress. The significant confidence intervals on the values at  $v_f = 8.5$  m/s are due to the occurrence of first flow instabilities in this operating area, which is close to the boundary with the unstable zone.

It should be pointed out that a non-uniform radial stress distribution has already been suggested by Klinzing, who observed that most of the slug collapses occur in the top section of a slug and suggested that this indicates a non-uniform radial stress distribution in the slug. However, he proposed that the greatest stresses should act at the bottom half due to the weight of the slug [2].

At the top of the pipe, the conveying velocity does not significantly affect the stresses induced by slugs except for  $v_f = 8.5$  m/s where the flow is submitted to first instabilities. At the pipe side and bottom, an increase in the air supply velocity leads to the increase of the stresses at the pipeline wall. The weight of granules deposited on the measurement plate is detected as normal stress as well. When the measurement plate is located at the pipeline bottom, the stress due to the particles weight reaches a maximum value, which has been evaluated to 290 Pa. The radial stress values measured during pneumatic conveying are mostly comprised between 1000 Pa and 2500 Pa. Therefore, the slug weight represents only small part of the total radial stress detected, which results principally from other physical phenomena.

Since the action of the force of gravity limits the contacts between particles and the pipeline top, lower stresses occur in this area. For the opposite reason, the highest stresses are expected at the pipeline bottom. Moreover, between two slugs, a layer of motionless particles remains at the bottom of the pipeline. Those particles lead to an additional resistance force at the pipe bottom. When the slug front arrives, according to their position in the pipe cross-section, the particles of the stationary layer have to be lifted up and accelerated. The adhesion forces between particles and between particles and wall are overcome and a transition to sliding friction takes place. The stationary layer has no contact with the pipe top and only partly contact with the wall at the mid-height of the pipe. Therefore, no adhesion force has to be overcome at the top and only a small amount at the side. Consequently, the additional resistance force caused by the layer of motionless particles should be mainly detected at the pipeline bottom.

However, the highest stresses were not detected at the pipe bottom but at the side. Therefore, an additional force, which is higher than the forces due to the granules weight and the stationary layer together acts at the pipe bottom. One reason for the occurrence of higher stresses at the pipe side than at the bottom was found by analysing images of the process. In the area close to the wall, particles were found to move faster at the mid-height of the pipe than at the bottom. Fig. 5.28 shows that a velocity gradient exists between particles moving close to the wall but at different height over the cross-section. The marked particle at the pipe bottom moves slower than the particles at the mid-height of the pipe. Therefore, this particle will be overtaken over the course of the images. Due to the resistance forces cited earlier, which particularly act at the bottom, the slug particles move slower in this area.

Consequently, the existing forces, which are a function of the particle velocity are lower at the bottom than at the mid-height of the pipe.

As a further result, no velocity gradient could be found between particles moving at the top and at the mid-height of the pipe. At the top, the granules weight does not induce any friction force. Moreover, in this area, the conveying gas undergoes wall effect and fewer granules come into contact with the wall. In addition, because of the presence of gas cavities at the top of the slugs, the slug particles partly do not come into contact with the top of the pipe, i.e. measurement plate. The forces induced by a slug at the pipe top are frequently inhomogeneous over the slug length (Fig. 5.29). Hence, although particles at the top move with a similar velocity than at the pipe mid-height, the mean forces measured at the top over the entire slug length are significantly lower than at the bottom and mid-height.

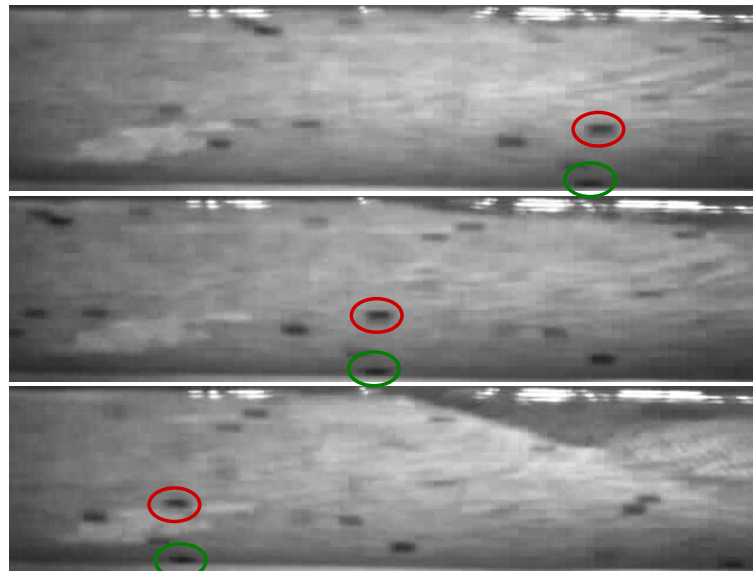


Figure 5.28: Velocity gradient according to the position over the pipeline height.  $f = 30$  images/s

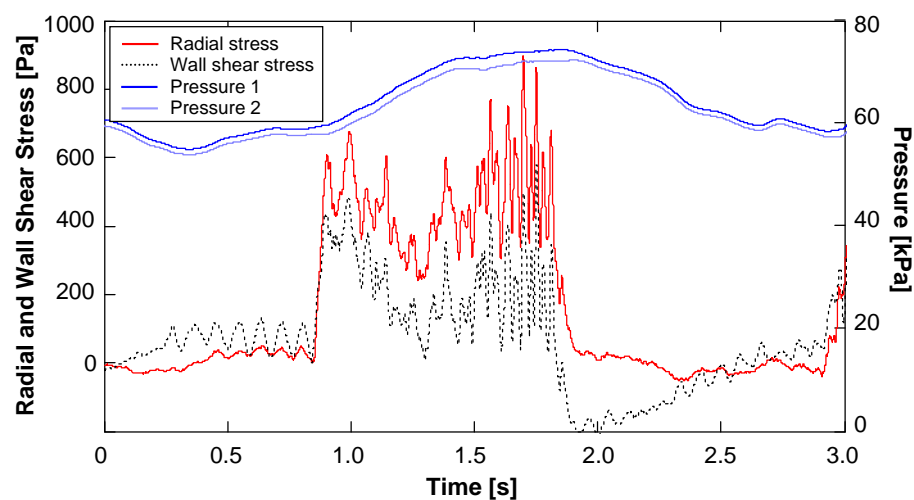


Figure 5.29: Example of irregular stress signals measured at the top of a slug -  $v_f = 7.0$  m/s

Fig. 5.27 shows that radial and wall shear stresses follow the same trend. Where Coulomb's failure criterion applies, the shear stress is related to the normal stress by  $\tau_w = \sigma_{r/w} \cdot \tan \phi_w + c_w$ . Fig. 5.30 allows a direct comparison between both stresses by illustrating the ratio wall shear stress to radial stress at the wall. For air velocities up to 7.5 m/s, the ratio remains constant with values between 0.8 and 1.0, which are a function of the circumferential location. The ratio values at the pipe side are mostly significantly lower than at the bottom and top. Moreover, the ratio at the bottom and side, where the slugs were found to induce the highest stresses, shows a tendency to decrease, i.e. the radial stress increases more significantly than the wall shear stress with the increase of the air supply velocity.

This tendency is confirmed by the stress ratio obtained for an air supply velocity of 8.5 m/s, which displays significantly lower values for those two positions around the pipe circumference. Generally, an increase in the air supply velocity leads to a bigger difference between the radial and the wall shear stress values. Around the entire pipe circumference and at all conveying velocities, slugs induce higher radial than wall shear stresses.

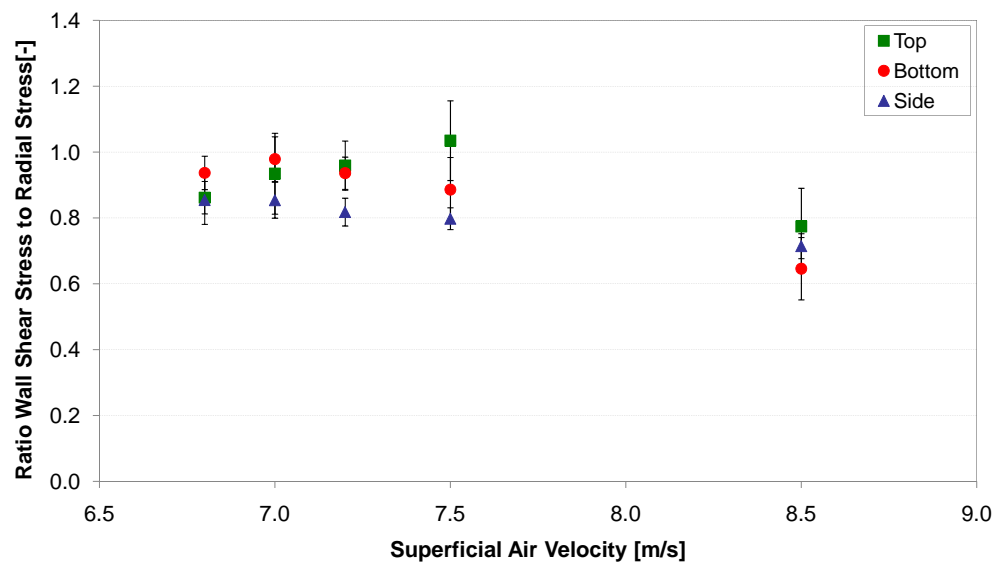


Figure 5.30: Behaviour of the ratio wall shear stress to radial stress

If the stresses result from the bulk solids mechanics and Coulomb's failure criterion applies at the boundary between particles and wall, a mean ratio wall shear stress to radial stress of 0.9 corresponds to a wall friction angle of  $42^\circ$ . However, the wall friction angle measured by using a Jenike shear cell was  $9.7^\circ$ . Therefore, another type of relationship prevails between the wall shear stress and the radial stress as induced by the moving slugs.

### 5.3.3.2. Stresses induced at the pipe wall by pushing of a model-slug through the pipeline

Since many theoretical studies are based on balance of forces and stress transmission occurring when a slug is compressed, additional experiments were carried out to investigate the effect of both the slug weight and slug compressive state on the stresses. A model-slug composed of the same bulk material than the one transported in the conveying experiments was placed in the pipe between two circular



plates. The plates, which retain the granules, were pushed simultaneously forward so that the model-slug was transported along the pipeline through the measurement probe. For the same amount of granules, the distance between the two plates was successively reduced. Therefore, different levels of compression were provided. The experimental set-up and the results are presented in Fig. 5.31.

The compression level is represented on the  $x$ -axis by the difference between the theoretical porosity of the model slug set and the loose poured bulk porosity. This leads to a negative value when the slug is compressed. The resulting forces were measured at the top, bottom and side of the pipeline. A decrease in the distance between the plates leads to an increase in the slug compressive state, which in turn results in the significant increase of the stresses measured at the pipeline wall.

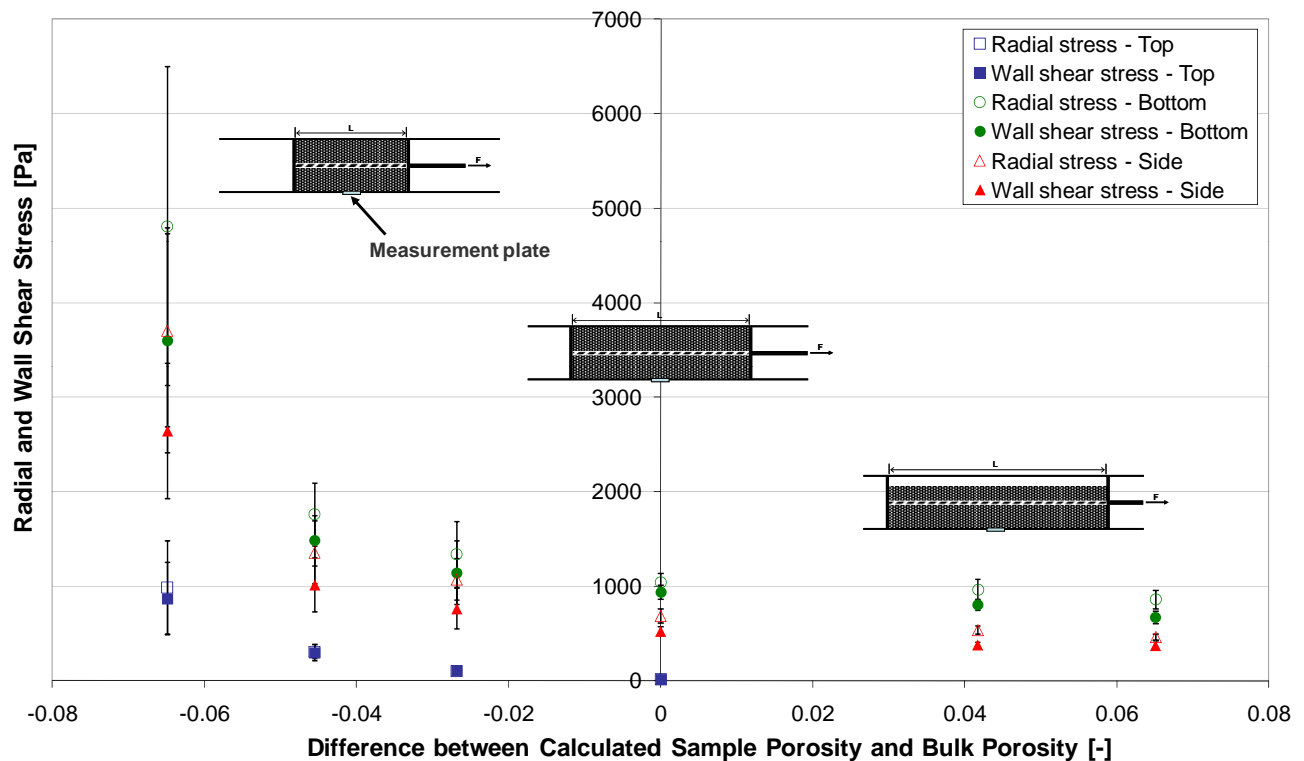


Figure 5.31: Stresses induced at the pipe wall by pushing of a model-slug through the pipeline

As expected, the highest stresses were measured at the pipeline bottom whereas the lowest stresses were measured at the top. For positive  $x$ -values, i.e. set porosities higher than the bulk porosity, no stresses were detected at the pipeline top. This results from the non-uniform distribution of the particles, which reach the pipeline top only when the set porosity is equal to or higher than the bulk porosity. However, stresses were detected at the bottom and side of the pipe. For positive  $x$ -values, these stresses are not caused by the compressive state of the slug but are due to the weight of the granules and the resulting frictions forces. An increase in the distance between the plates leads to the decrease of the height of the particles slug, which in turn results in the decrease of the weight acting on the measurement plate.

The compression of the granules results in the significant increase of both the radial and wall shear stresses measured at the pipeline wall around the pipe circumference. The highest increase in the stress

values occurs at the pipeline bottom where the influence of the particles weight is more significant. For a porosity reduction of 0.065, a radial stress of about 5000 Pa was detected at the pipe bottom. In this case, an axial force of about 200 N had to be applied to overcome the high resistance forces and move the 30 cm long model-slug along the pipe section.

### 5.3.3.3. Comparison between stresses induced by compressed moving slugs and slugs pneumatically conveyed

The model-slug investigated was about three times shorter than most of the slugs that formed during pneumatic conveying process. A longer slug corresponds to a higher pressure loss. Therefore, the axial force required at the back of a slug to allow the transport is a function of the slug length. Consequently, a slug of the size of the model-slug would be easier to convey pneumatically than slugs of the regular size. Fig. 5.31 indicates that the force required to push a non-fluidised slug increases considerably with the increase of the compression state.

The comparison between those results and the stresses measured during pneumatic conveying shows that the stresses induced by horizontal conveyed slugs are similar to the stresses measured in non-fluidised packed columns exhibiting high compression. Therefore, high stress values would be obtained at the wall if moving slugs were compressed. However, investigations on the internal porosity of moving slugs showed that slugs are slightly fluidised over their entire length (see Section 5.2). Moreover, the experiments carried out on the transport of a non-fluidised model-slug showed that an axial force over 120 N is required to transport a compressed slug of 30 cm length, which is characterised by radial stress values of about 2500 Pa. Therefore, an overpressure over 0.2 bar would be necessary to transport a single short slug in a pipe system with 80 mm internal diameter.

This leads to the conclusion that the high level of axial force required to push a packed bed over the length of a pneumatic conveying system cannot be provided by the conveying gas. Therefore, compressed slugs cannot be pneumatically conveyed and the high stress states detected within moving slugs do not result from the compressive state of the slugs.

High stress values were detected around the pipe circumference when blockage of the pipeline occurred in the measurement area. Fig. 5.32 shows an example of pressure and stress signals recorded when a slug remained blocked in the probe. In this case, the blockage cleared itself without further intervention. Based on the above, an increase in the slug compressive state may have caused the blockage. Section 5.5 is dedicated to the physical mechanisms involved in the slug transport and blockage of the pipeline. Therefore, this topic will not be developed any further here.

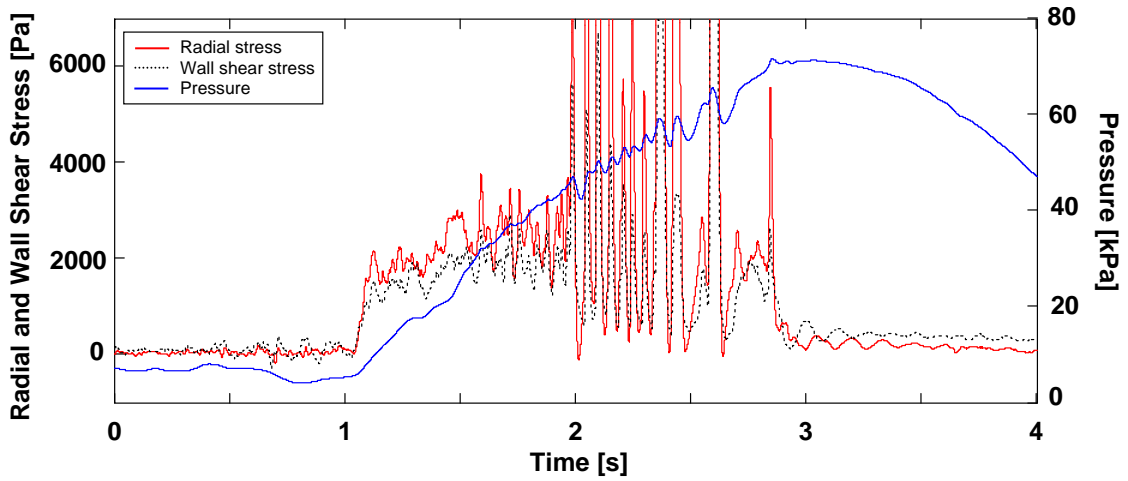


Figure 5.32: Pressure, radial and wall shear stress measured within a slug blocked in the pipeline -  $v_f = 8.5$  m/s

## 5.4. Application of the kinetic theory to explain the stresses induced by slugs

### 5.4.1. Mathematical model

Based on the experimental results described in this study, the forces induced by fluidised slugs at the pipeline wall cannot be explained solely by bulk solids mechanics. Therefore, a new approach based on the kinetic theory of gases is proposed to explain the high values of radial and wall shear stress occurring by slug flow. Kinetic theory, also named collision theory, posits that gas molecules are in constant, random motion. The rapidly moving particles collide constantly with the walls of the enclosing container [1]. This theory can be adapted to the plastic particles/pipeline wall system considered in the study. Each particle within a fluidised slug is in suspension, moving stochastically and therefore ceaselessly collides with other particles. During each collision, a momentum transfer takes place. In close proximity to the wall, particles transfer their entire momentum to the wall, resulting in a wall shear stress. In this area, the flow can be considered in a state of Newtonian flow, which can be imagined as occurring by a series of layers moving past one another. Each layer has the width of a particle diameter. The apparent viscosity of the particles composing a slug arises from the transport of linear momentum from a layer to the layer next to it. The layers far from the wall move at the same velocity whereas the layer next to the pipeline wall can be considered as stationary. Since frictional forces due to the pipe wall retard the motion of the gas, the flow in the two or three successive layers next to the wall is laminar. The velocity of these layers varies linearly with distance  $z$  from the pipeline wall. Newton postulated that the shear stress  $\tau$  between layers is proportional to the velocity gradient in the direction perpendicular to the layers. Therefore, the shear stress can be expressed as:

$$\tau = \eta_{slug} \cdot \frac{dv}{dz} \quad (5.4)$$

It is assumed that the flux of the momentum component normal to the wall is big. The particles in the layer next to the wall are supposed to transfer their entire momenta to the pipeline wall. The amount of momentum  $p_m$  transferred depends on mass and velocity of the particles in the frame of reference:

$$p_m = m_{particle} \cdot v_p \quad (5.5)$$

However, in air, elastic collisions take place and particles transfer their double momenta  $2 \cdot p_m$ . To simplify, it is supposed that one third of the particles is moving in each direction  $x$ ,  $y$  and  $z$  and in each of those directions, half of the particles are moving towards positive axis, half towards negative axis. Therefore,  $1/6$  of the slug particles are moving in the direction normal to the wall. Hence, the viscosity can be expressed as following:

$$\eta_{slug} = 2 \cdot p_m \cdot \lambda \cdot \frac{1}{6} \cdot N \quad (5.6)$$

$$\eta_{slug} = \frac{1}{3} \cdot v_{normal} \cdot m_{particle} \cdot \lambda \cdot N \quad (5.7)$$

where  $v_{normal}$  is the particle velocity normal to the wall,  $\lambda$  is the mean free path also called collision distance and  $N$  is the number of particles per unit volume. The number density  $N$  can be determined from the porosity values over a slug calculated by means of the equation of Ergun as follows:

$$N = \frac{(1 - \varepsilon) \cdot \rho_s}{m_{particle}} \quad (5.8)$$

The particle velocity perpendicular to the wall is calculated by using the normal stress experimentally measured at the pipeline wall:

$$v_{normal} = \sqrt{\frac{3 \cdot \sigma_r}{m_{particle} \cdot N}} \quad (5.9)$$

Based on this approach, not only the wall shear stress but also the viscosity is a function of the velocity gradient. Consequently, the amplitude of the wall shear stress depends on three factors namely the number density, i.e. porosity of the slug, the velocity of the particles, which is a function of the air supply velocity and the mean collision distance, which is unknown and has to be assumed.

#### 5.4.2. Investigations on the velocity gradient

In horizontal pneumatic conveying, due to the force of gravity that acts perpendicularly to the conveying direction, the mechanisms involved in the slug transport are quite different from those present in vertical conveying. The force of gravity affects also the distribution of the particles across the pipe cross-section. However, the results of investigations carried out on the potential existence of a porosity gradient over

the height of a slug showed that the particles composing a slug are uniformly distributed over the pipe cross-section (see Section 5.2). Therefore, to investigate the velocity gradient at the pipe wall, the effect of the force of gravity can be neglected .

The velocity gradient  $\frac{dv}{dz}$  cannot be experimentally determined. However, the effect of the conveying gas velocity on the calculated velocity gradient can be investigated by applying Eq. 5.4. The wall shear stress  $\tau_w$  was directly measured while the viscosity  $\eta_{slug}$  was calculated by using Eq. 5.7. The normal velocity  $v_{normal}$  required in Eq. 5.7 was calculated by using radial stress measurements and applying Eq. 5.9. The velocity gradient is assumed to be independent on the circumferential position. However, to verify this assumption, the velocity gradient at  $v_f = 6.8$  m/s was determined for the three locations around the pipe circumference where the stresses were measured, i.e. top, bottom and side of the pipeline.

The values required for the calculation of the velocity gradient are determined by using the physical properties of the material, experimental measurements and assumptions. It is assumed that in close proximity to the wall, the flow is in a state of Newtonian flow and the width of each layer of the flow is equal to one geometric diameter of particle. Therefore, the mean free path is assumed as a constant and equal to the diameter of one particle. The determination of the slug porosity required to calculate  $\eta_{slug}$  results from the application of the Ergun equation.

The calculated velocity gradients are presented in Fig. 5.33. The results indicate that the velocity gradient calculated from radial and wall shear stress measurements is not affected by the gas supply velocity. However, in the area of stable slug flow, the velocity gradient tends to increase with the conveying velocity. The higher confidence interval on the mean velocity gradient at  $v_f = 8.5$  m/s is due to the flow instabilities that characterised the conveying process in those operating conditions.

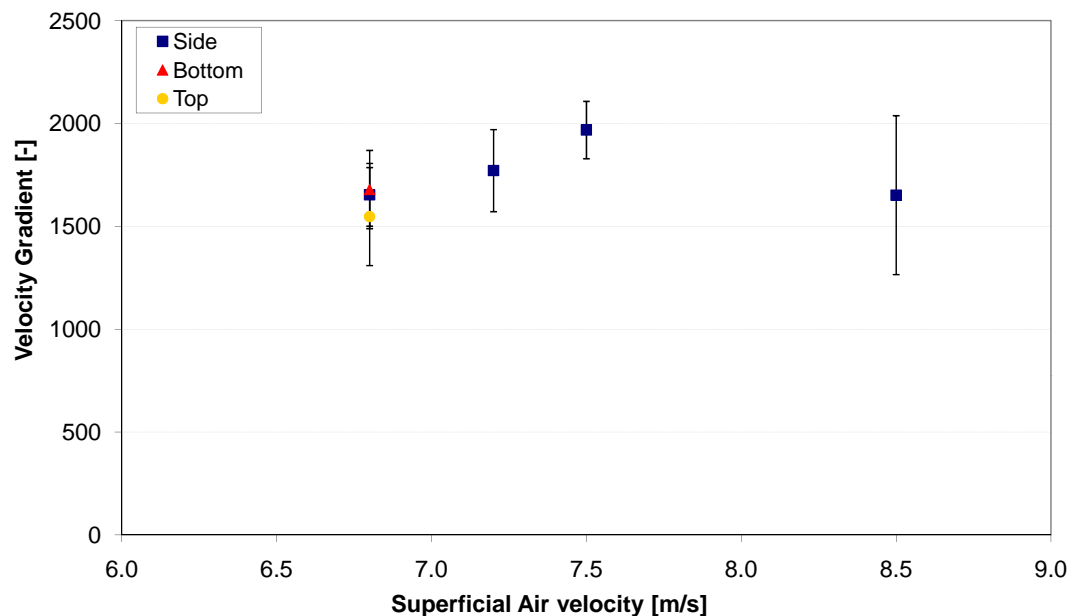


Figure 5.33: Velocity gradient at the wall calculated from radial and wall shear stress measurements

### 5.4.3. Application of the impulse theory to describe the stresses induced by slugs

The wall shear stress along a slug can be calculated by applying Eq. 5.4. For the calculation, it is assumed that by contact with the pipeline wall, the particles transfer their double momenta and stop. Hence, the velocity gradient  $\frac{dv}{dz}$  in close proximity to the wall is calculated by using Eq. 5.10 with respect to the evolution of the particle velocity over the slug length. The width of one layer of the flow is assumed as a constant and equal to one geometric diameter of particle:

$$\frac{dv}{dz} = \frac{v_{p333}}{d_p} \quad (5.10)$$

When the kinetic theory is applied at a molecular scale, the mean free path  $\lambda$  is usually estimated from the measurement rate of penetration of one gas by the other, i.e. how quickly a gas diffuses into another. The mean free path is usually derived in units of the diameter of the molecules. If two spherical particles both have diameter  $d_p$ , they will collide if their centres get within  $d_p$  of each other. Hence, the mean free path  $\lambda$  is assumed equal to one geometric diameter of particle. In this case,  $\tau$  appears not to be directly a function of the particle diameter (Eq. 5.11). However, the particle diameter is still involved in the porosity calculation, which in turn is involved in the calculation of the number density  $N$ .

$$\tau_{cal} = \frac{1}{3} \cdot v_{normal} \cdot m_{particle} \cdot N \cdot v_{p333} \quad (5.11)$$

By inserting Eq. 5.8 and Eq. 5.9 in Eq. 5.11, the following expression is obtained:

$$\tau_{cal} = v_{p333} \cdot \sqrt{\frac{1}{3} \cdot \sigma_r \cdot (1 - \varepsilon) \cdot \rho_s} \quad (5.12)$$

Both the wall shear stress calculated by applying the kinetic theory and the wall shear stress measured at different locations around the pipe circumference have been compared. Fig. 5.34 shows the results for an air supply velocity of  $v_f = 6.8$  m/s. To allow a better comparison between the results, the scale on the  $y$ -axis was kept the same for the different slugs presented. It should be pointed out that the particle velocity used for the calculation of the velocity gradient was measured at the side of the pipe. Therefore, the velocity gradient in close proximity to the wall is assumed constant around the entire pipe circumference. This assumption is supported by Fig. 5.33, which showed that the velocity gradient at the top, mid-height and bottom of the pipe is similar.

Fig. 5.34 shows that depending on the position on the pipe circumference, the kinetic theory is able to predict either the full amount or part of the wall shear stress. The stress at the side of the pipe, where the determination of the particle velocity took place, could be calculated by applying the kinetic theory with great accuracy (Fig. 5.34 c and d)). At the top of the pipe, the calculations gave either values in very good agreement with the stress measured (Fig. 5.34 a and b)) or values slightly higher or lower. At the bottom of the pipe, the kinetic theory underpredicted the stress occurring during slug flow pneumatic conveying (Fig. 5.34 e and f)).

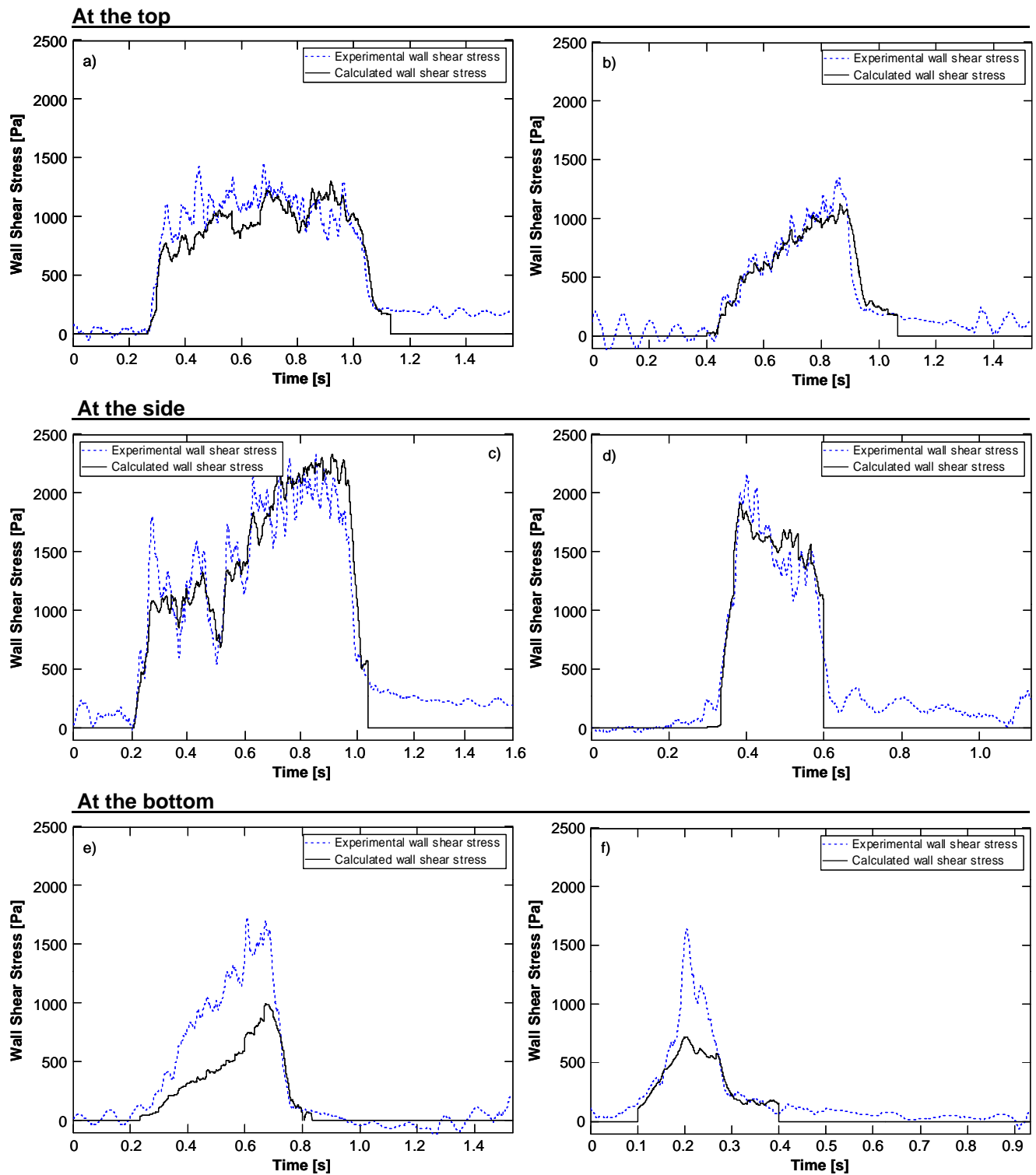


Figure 5.34: Experimental wall shear stress and wall shear stress calculated by applying the kinetic theory for slugs conveyed with  $v_f = 6.8$  m/s. a and b) Wall shear stress at the top of the pipe, c and d) Wall shear stress at the pipe side, e and f) Wall shear stress at the pipe bottom

These results support the theory that according to the position on the pipe circumference, different physical mechanisms are involved in the contact area between the particles and the pipe wall, i.e. in the formation of the stresses. At the top of the pipe, the contacts or collisions between the particles and

the wall are counteracted by the force of gravity that acts in the opposite direction. Hence, the stresses at the top wall may be lower than the stresses predicted by the kinetic theory. However, the presence of a narrow channel at the top of the pipe where the gas velocity is higher may also lead to collisions between particles and wall where higher momenta are transferred, which result in higher stresses. At the bottom of the pipe, the kinetic theory was able to describe only one part of the stress occurring during slug flow pneumatic conveying. The remaining stress may be caused by the friction of the slug sliding on the pipe wall.

Application of the kinetic theory did not only allow to predict the mean wall shear stress along a slug but also accurately described the wall shear stress along the slugs. The wall shear stress was calculated for slugs conveyed with different air supply velocities covering the entire area of slug flow. Fig. 5.35 illustrates the wall shear stress within a rather long (on the left hand side) and rather short slug (on the right hand side) for three different conveying velocities. For all conveying velocities where slug flow took place, the kinetic theory could be successfully applied to accurately describe the wall shear stress at the side of the pipe. Great accuracy was found for the whole range of values in which the wall shear stress lied, for example under 1000 Pa as in b) or over 2000 Pa as in f). In addition, Fig. 5.36 shows that even the lowest values of wall shear stress induced by moving slugs could be accurately calculated by applying the kinetic theory.

Calculations and experimental measurements show very good agreement, which demonstrates that the high stresses induced by a slug on the pipe wall are a result of the stochastic agitation of the suspended particles composing the slug. Consequently, the presence of higher stresses at the pipe mid-height than at the bottom can be explained by a different amount of momentum transferred according to the location on the pipe circumference. Particles were found to move faster at the mid-height of a slug than at the bottom. Therefore, those particles transfer a bigger momentum to the wall, which results in the presence of higher stresses.

The velocity gradient was found to be independent on the air supply velocity. Therefore, the increase of the wall shear stress induced by a slug with the air velocity increase is due to the increase of the viscosity (Eq. 5.4). Furthermore, the mean free path was taken as a constant and the porosity within a slug was found to be independent on the air velocity, i.e.  $N$  is constant. Therefore, according to Eq. 5.7, an increase of the viscosity is due to the increase of the velocity perpendicular to the wall  $v_{normal}$ . In turn, an increase of  $v_{normal}$  results from an increase of the interstitial relative velocity between particles and conveying gas, i.e. corresponding turbulent conditions. According to Eq. 5.9, an increase in the normal velocity, which results from the increase in the air supply velocity, leads to the increase of the radial stress.

Fig. 5.37 shows that both the radial and wall shear stresses induced by a slug at the pipe side (Fig. 5.37 a and b)) and bottom (Fig. 5.37 c and d)) follow the trend of the particle velocity. It should be pointed out that the particle velocity was measured at the pipe side. However, a very good correlation was also observed between the particle velocity measured at the mid-height of the pipe and the stresses at the pipe bottom. Therefore, it can be concluded that a strong functional correlation exists between particle velocity, slug viscosity and wall shear stress. The lower stresses detected at the pipeline bottom



(see Section 5.3.1.1) are effectively affected by the presence of particles moving slower in this area than at the mid-height of the pipe.

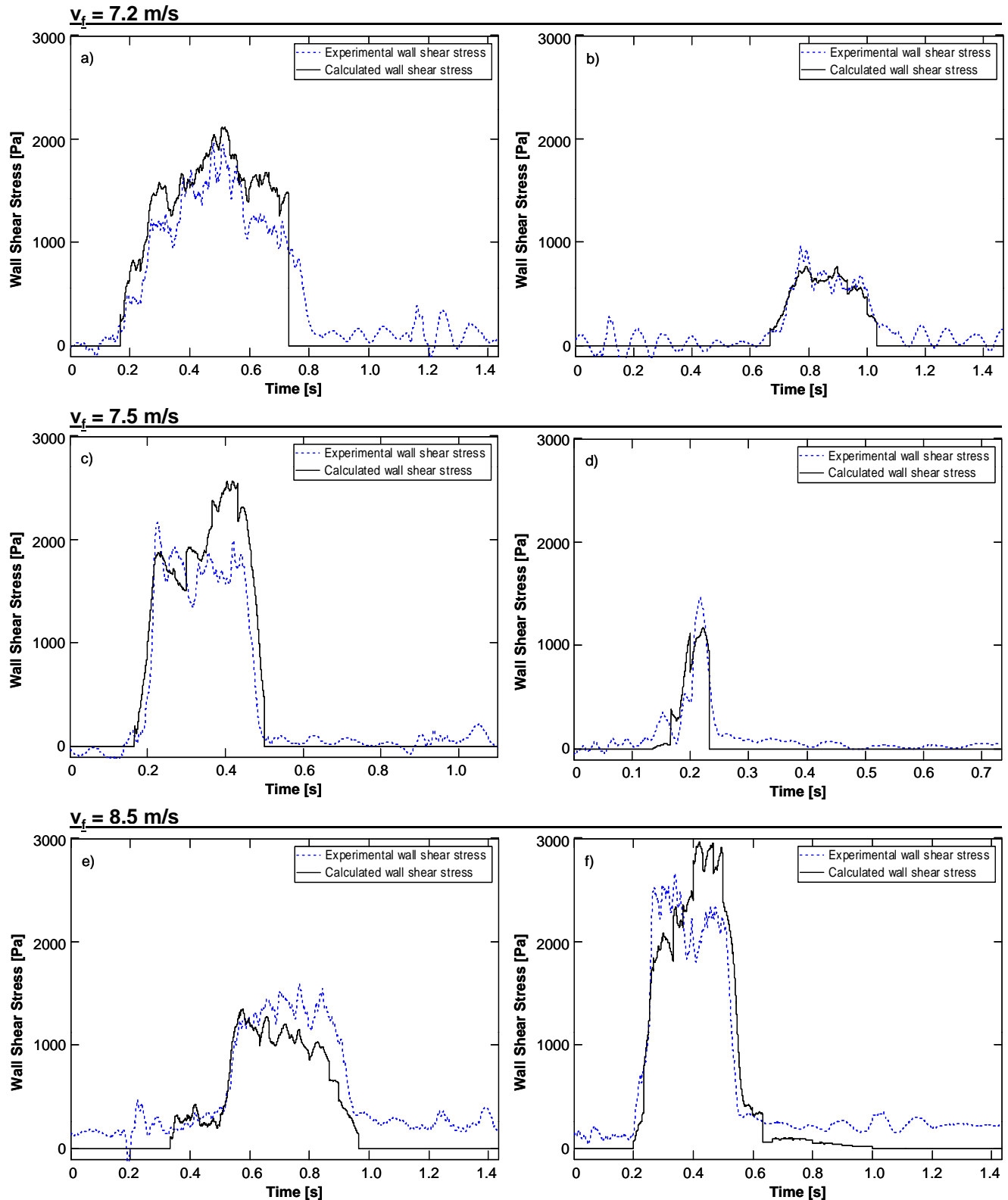


Figure 5.35: Experimental wall shear stress and wall shear stress calculated by applying kinetic theory for slugs conveyed with velocities covering the whole slug flow area.  
a and b)  $v_f = 7.2$  m/s, c and d)  $v_f = 7.5$  m/s, e and f)  $v_f = 8.5$  m/s

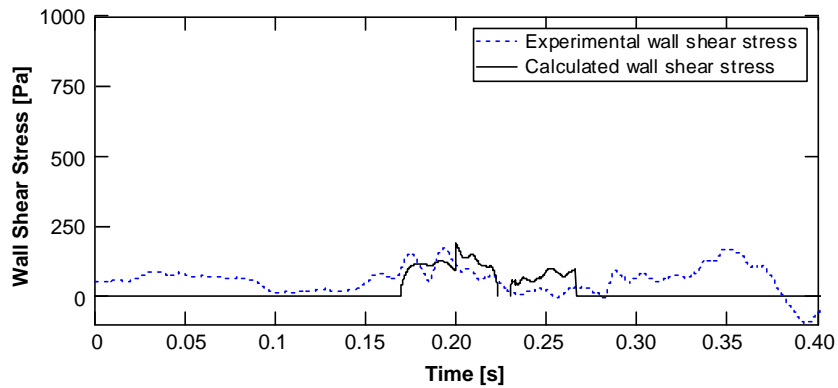


Figure 5.36: Low values of wall shear stress at the pipe side correctly predicted by applying the kinetic theory

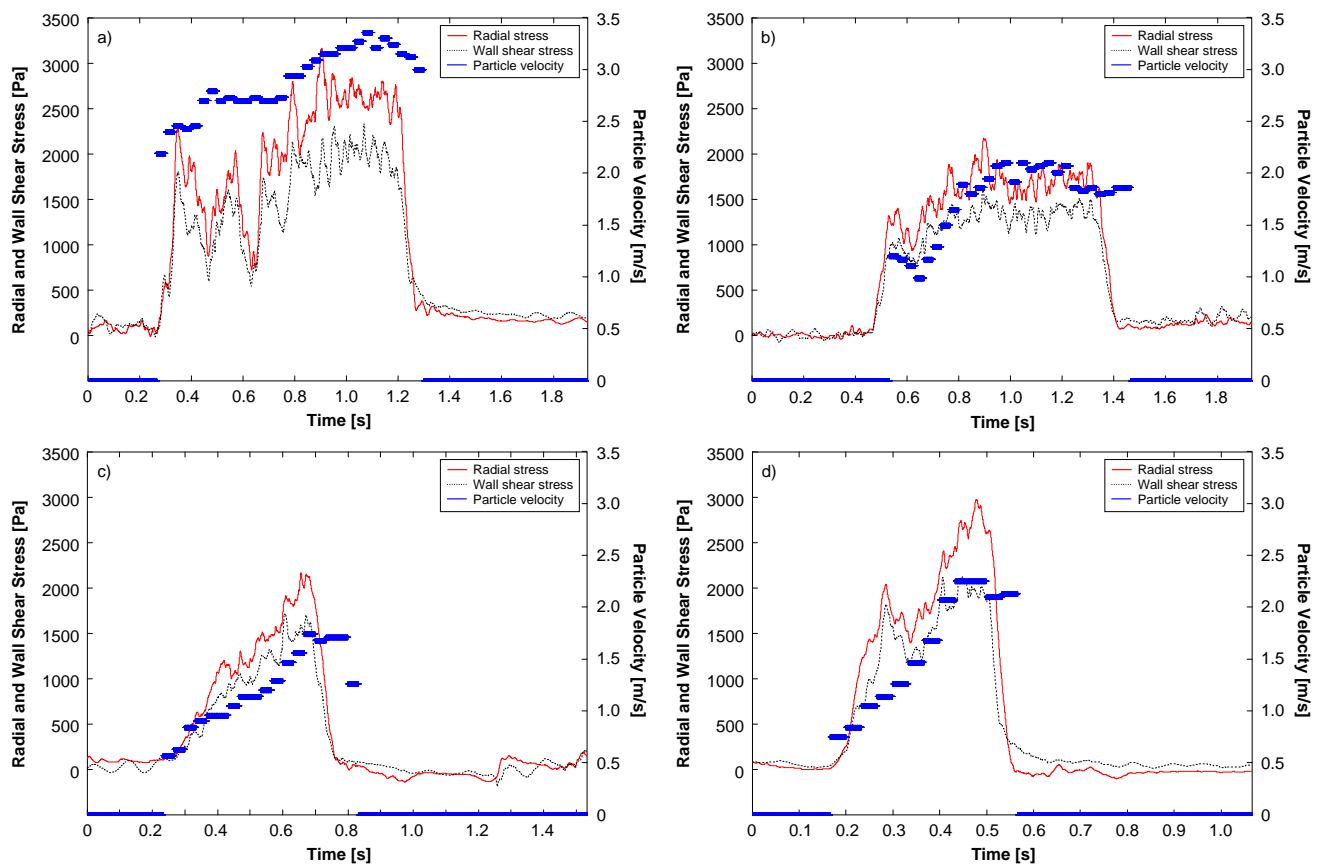


Figure 5.37: Correlation between particle velocity, radial and wall shear stress measured over slugs. a)  $v_f = 6.8$  m/s - side, b)  $v_f = 7.2$  m/s - side, c and d)  $v_f = 6.8$  m/s - bottom

Fig. 5.38 shows the stresses and the particle velocity measured within a slug that remained temporarily blocked at the exit of the measurement probe. Both the stresses and the particle velocity were correlated until blockage occurred. Past this time, the velocity of the slug particles decreased while the stresses at the wall increased significantly. It should be pointed out that the particle velocity was measured at a location placed 50 cm ahead of the stress measurement plate. Therefore, at this location, particles

located at the slug rear still moved whereas they remained blocked shortly after, i.e. when they reached the stress measurement probe.

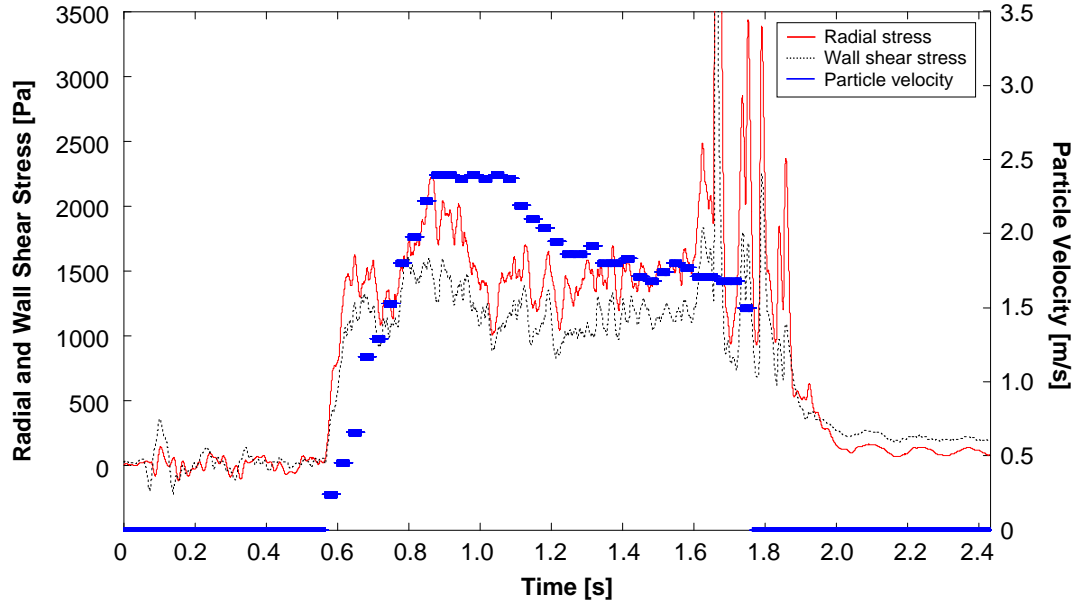


Figure 5.38: Particle velocity, radial and wall shear stresses measured within a slug whose rear remained blocked in the stress measurement probe -  $v_f = 6.8$  m/s

#### 5.4.4. Application of the kinetic theory to predict the pressure loss

By applying the kinetic theory, the wall shear stress induced by horizontal moving slugs could be accurately calculated. This demonstrates that the main part of the resistance force that required to be overcome to transport slugs along the pipeline is due to the momentum exchange of the turbulent particles hitting the pipeline wall. Therefore, the pressure loss occurring during the transport of slugs can be determined by applying the kinetic theory.

##### 5.4.4.1. Correlation between wall shear stress and pressure loss along a single slug

Slugs were found to be slightly fluidised. Therefore, no axial stress exists inside of a slug and the force balance on a slug element commonly used can be simplified (Eq. 3.1). The driving force due to the pressure can be written as follows:

$$F_{driving} = P \cdot A - (P - \Delta P) \cdot A \quad (5.13)$$

$$F_{driving} = \Delta P \cdot A \quad (5.14)$$

The retarding force is assumed to be due to the shear stress by the walls. Therefore, the retarding force is equal to the shear stress multiplied by the area over which it acts (Eq. 5.15).

$$F_{retarding} = \tau_w \cdot A_m \quad (5.15)$$

where  $A_m$  is the lateral surface of the pipe section where the wall shear stress is applied.

Hence, a simple relation exists between the pressure loss over a given length of slug and the wall shear stress detected at the pipe wall. This relation illustrates that the pressure loss existing between two points over the pipeline results directly from the force required to overcome the wall shear stress.

$$\tau_w \cdot A_m = \Delta P \cdot A \quad (5.16)$$

At a defined location along the pipeline, the total wall pressure is equal across the entire pipe cross-section. Therefore, a single value of pressure loss is obtained between two given measurement points. However, the wall shear stress was successively measured at the bottom, side and top of the pipeline. Moreover, the results showed that the wall shear stress is non-uniform around the pipe circumference (see Section 5.3.3.1). Therefore, to correlate the wall shear stress measured at different locations around the pipe circumference with the pressure loss measured over a slug, the wall shear stress must be integrated over the pipe circumference. To simplify, the stresses measured at the top and bottom are assumed to be constant around one quarter of the pipe circumference each whereas the stress measured at the pipe mid-height is assumed constant around two quarters of the pipe circumference (Fig. 5.39). Fig. 5.39 shows the resulting experimental wall shear stress after integration over the entire pipe circumference.

By using the pressure loss experimentally measured by means of two miniature pressure sensors positioned  $l = 35$  mm apart and the experimental wall shear stress integrated over the pipe circumference, the part of the pipe lateral surface between the two measurement points on which the wall shear stress acts can be calculated:

$$A_m = \frac{\Delta P_{exp} \cdot A}{\int_0^{2\pi} \tau_{exp}} \quad (5.17)$$

The wall shear stress was found to act on average on 37 % of the lateral surface of the pipe section occupied by a plug:

$$A_m = 0.37 \cdot A_{m\_total} \quad (5.18)$$

where  $A_{m\_total}$  is the entire lateral surface of the pipe section full of particles. However, it should be pointed out that this relation is not in accordance with the results of the experimental stress measurements. The local measurements of wall shear stress showed that significant stresses were detected at the top, side and bottom of the pipe. Consequently, it would be natural to assume the wall shear stress as acting on the entire lateral surface of the pipe section filled with a slug and not only on 37 % of it.

However, it should be pointed out that this coefficient does not represent the absolute surface on which the stress acts but illustrates the inhomogeneous stress distribution around the pipe circumference as well.

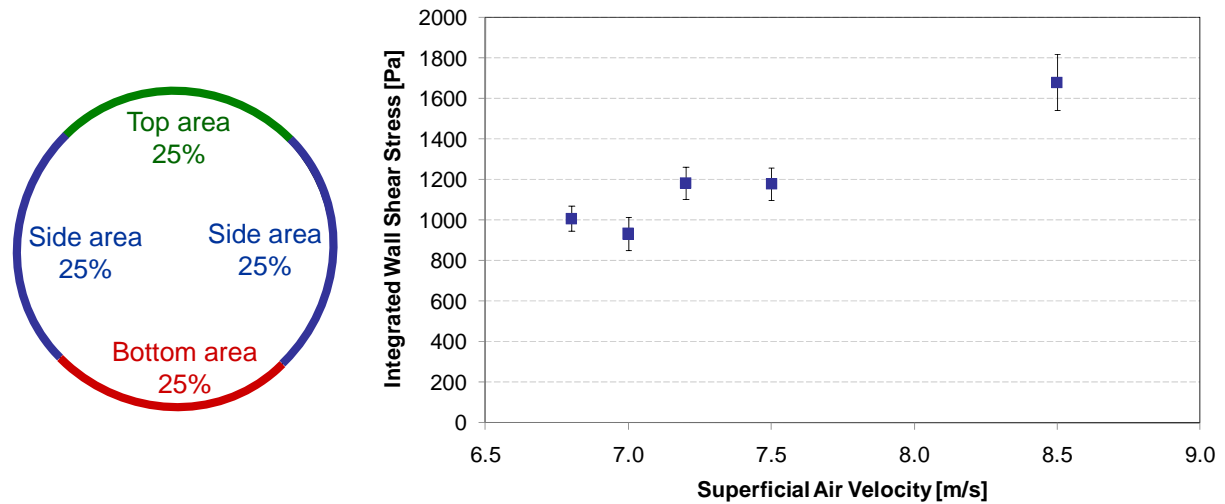


Figure 5.39: Integration of the experimental wall shear stress over the entire pipe circumference. On the left hand side: Schematical integration of the experimental values. On the right hand side: Wall shear stress after integration over the pipe circumference

In order to check the suitability of this method to predict the pressure loss over a moving slug, the pressure loss over a slug element of length  $l$  was calculated by applying Eq. 5.19:

$$\frac{\Delta P}{l} = \frac{0.37 \cdot \tau_{cal} \cdot \pi \cdot D}{A} \quad (5.19)$$

where  $\tau_{cal}$  is the wall shear stress calculated by applying the kinetic theory according to Eq. 5.12. The pressure loss was calculated by using the experimental radial stress values measured at the top, side or bottom of the pipe respectively and compared with the experimental pressure loss measured continuously over 35 mm. Fig. 5.40 shows the pressure loss along the six slugs conveyed with  $v_f = 6.8$  m/s whose wall shear stress profile was illustrated in Fig. 5.34.

The pressure loss calculated is in a more or less good agreement with the experimental pressure loss. As a logical consequence of the non-uniform stress distribution, the calculations involving the radial stress measured at the pipe side overpredict the pressure loss whereas the pressure loss is underpredicted when calculations involve the radial stress detected at the pipe bottom, which was found to be significantly lower than at other locations around the pipe circumference. The best agreement with the experimental pressure loss is obtained for calculations carried out with the radial stress values measured at the pipeline top. In fact, it has been shown in Fig. 5.34 that calculations of the wall shear stress deliver values that agree with the wall shear stress measured at the pipe side at best. Therefore, best agreements would be obtained if the correlation between pressure loss and wall shear stress given in Eq. 5.18 would have been determined by using only the stress values measured at the pipe side. However, the use of such a correlation would not be physically justified.

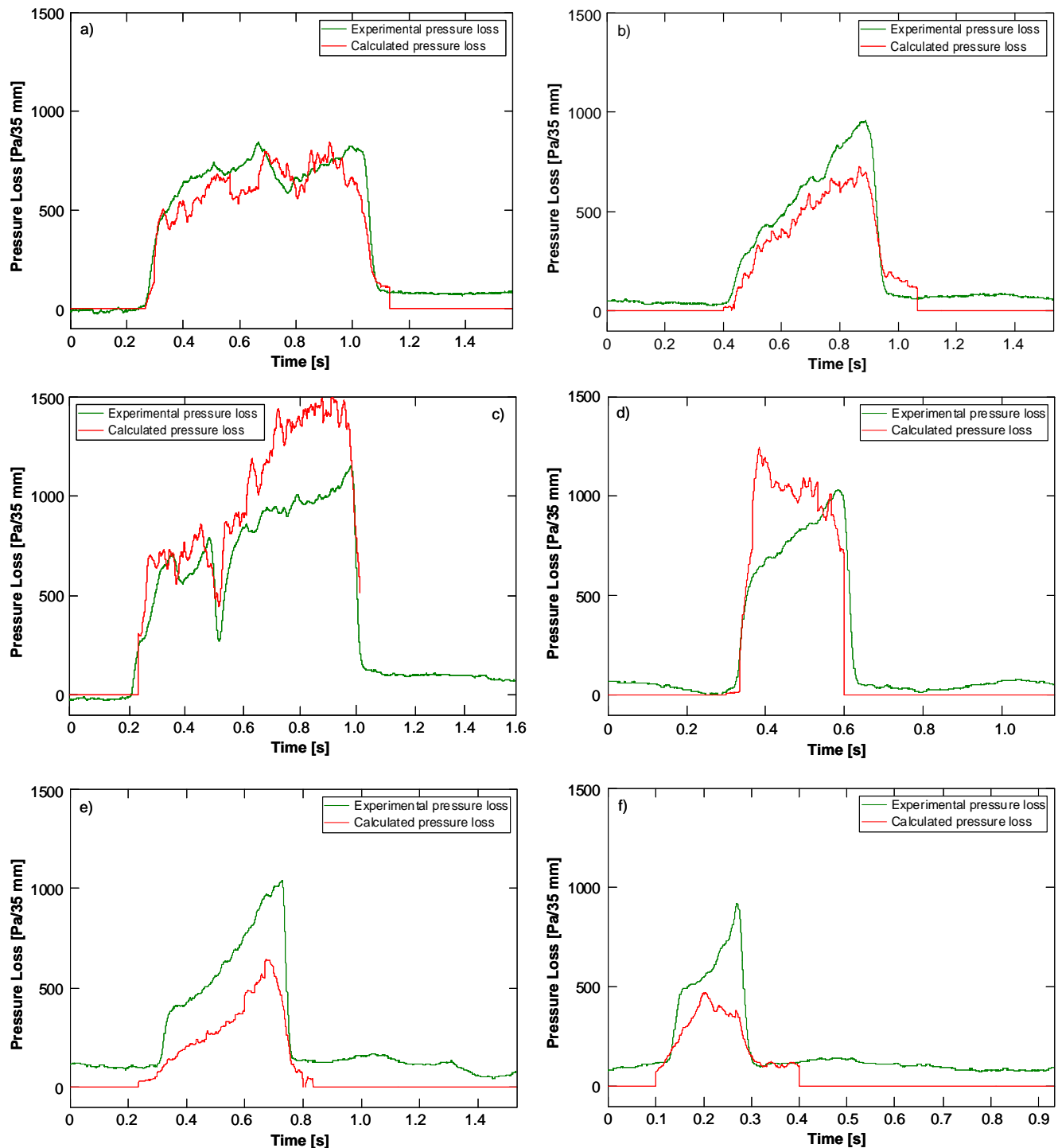


Figure 5.40: Pressure loss over single slugs calculated by applying the kinetic theory. a and b) By using radial stress values measured at the top, c and d) By using radial stress values measured at the side, e and f) By using radial stress values measured at the pipe bottom

The calculation of the pressure loss along a slug as illustrated in Fig. 5.40 requires the accurate determination of the particle velocity, porosity and radial stress profiles over a slug. However, for design purposes, the total pressure loss over the length of the pipe is needed rather than the pressure loss over a single slug. Therefore, the use of average values that describe the process entirely appears more convenient. This will be discussed in the next section.

#### 5.4.4.2. Prediction of the pressure loss over the conveying pipeline

In slug flow pneumatic conveying, the material conveyed fills the entire cross-section of the pipe. Slugs are separated by gas pockets through which the pressure loss can be assumed as negligible. Hence, the pressure loss along the entire pipe corresponds to the sum of the pressure losses through the slugs. As shown previously, the application of the kinetic theory permits to accurately calculate the wall shear stress  $\tau_{cal}$  acting on the pipe wall where the cross-section is full of material. Moreover, the fraction of the lateral pipe surface on which the wall shear stress acts has been determined (Eq. 5.18). Therefore, if the total length of slugs is known, the pressure loss can be calculated as follows:

$$\Delta P_{cal} = \frac{0.37 \cdot \tau_{cal} \cdot \pi \cdot D \cdot L_{slug}}{A} \quad (5.20)$$

where the total length of slugs  $L_{slug}$  can be calculated by performing a mass balance over the entire pipeline. The mass balance involves the fraction  $\alpha$  of the pipe area covered by the stationary layer, the solids mass flow rate  $\dot{m}_s$ , the total length of the pipeline  $L_T$  and the slug velocity  $v_{slug}$  (Eq. 5.21):

$$L_{slug} = \frac{\dot{m}_s \cdot L_T}{A \cdot (1 - \alpha) \cdot \rho_b \cdot v_{slug}} \quad (5.21)$$

The correlation existing between the total length of slugs and the air supply velocity was previously presented in Fig. 5.3. Eq. 5.20 indicates that for a given pipe diameter, the pressure loss is only a function of the wall shear stress and total length of slugs.

By observing Eq. 5.22, it becomes obvious that the velocity of the particles  $v_p$  is a key parameter in the determination of the wall shear stress. However, it has been shown that the particle velocity is not only dependent on the air supply velocity (Fig. 5.4) but also varies over the slug length (Fig. 5.10). Furthermore, the velocity profile over a slug is a function of the height of the stationary layer in front of it (Fig. 5.11).

$$\tau_{cal} = v_p \cdot \sqrt{\frac{1}{3} \cdot \sigma_r \cdot (1 - \varepsilon) \cdot \rho_s} \quad (5.22)$$

Since the particle velocity is a function of many key parameters, its prediction is difficult. Therefore, one solution is to assume the mean particle velocity to be equal to the slug velocity. Because the slug velocity is a parameter in the equation for the total length of slugs (Eq. 5.21) necessary to calculate the total pressure loss by applying Eq. 5.20, this assumption permits to eliminate the slug velocity from the final expression (Eq. 5.23). This presents great advantage in that the equation for the total pressure loss is now independent on both the particle and slug velocity:

$$\Delta P_{cal} = \frac{0.37 \cdot 4 \cdot \dot{m}_s \cdot L_T \cdot \sqrt{\frac{1}{3} \cdot \sigma_r \cdot (1 - \varepsilon) \cdot \rho_s}}{D \cdot A \cdot (1 - \alpha) \cdot \rho_b} \quad (5.23)$$

It follows that besides the material characteristics and pipe dimensions, only radial stress  $\sigma_r$ , slug porosity  $\varepsilon$ , solids mass flow rate  $\dot{m}_s$  and fraction  $\alpha$  of the pipe area covered by the stationary layer affect the total pressure loss. Fig. 5.41 shows the influence of those parameters on the pressure loss

calculated by applying Eq. 5.23. The following basic values were chosen for the calculation:  $\alpha = 0.2$ ,  $\varepsilon = 0.6$ ,  $\sigma_r = 1400$  Pa and  $\dot{m}_s = 6000$  kg/h. Each single parameter was varied in a range of values where it may lie (for example 0 to 1 for the porosity) or in which it was found to lie during the slug flow pneumatic conveying experiments. To allow an easier comparison between the curves, the same scale was used in ordinate. The results indicate that the influence of each of the parameters is in the same order of magnitude. However, an increase in the fraction of the pipe area covered by the stationary layer above 60% leads to an exponential increase of the pressure loss. Once the layer of settled particles reaches a certain height, blockage of the pipeline usually occurs.

Basically, according to Eq. 5.20, Eq. 5.21 and Eq. 5.22, the prediction of the pressure loss for a whole pipe system requires knowledge of the correlations between wall shear stress  $\tau_w$ , slug velocity  $v_{slug}$ , radial stress  $\sigma_r$  and slug porosity  $\varepsilon$ . Investigations carried out in this work showed that a strong correlation exists between wall shear stress and particle velocity but no correlation between particle and slug velocity was established. Furthermore, investigations into the so-called friction factor describing the ratio of the wall shear stress to the radial stress for cohesionless materials showed that this ratio is relatively constant in the area of stable slug flow. Finally, no significant correlation between the porosity and the radial and wall shear stresses could be found.

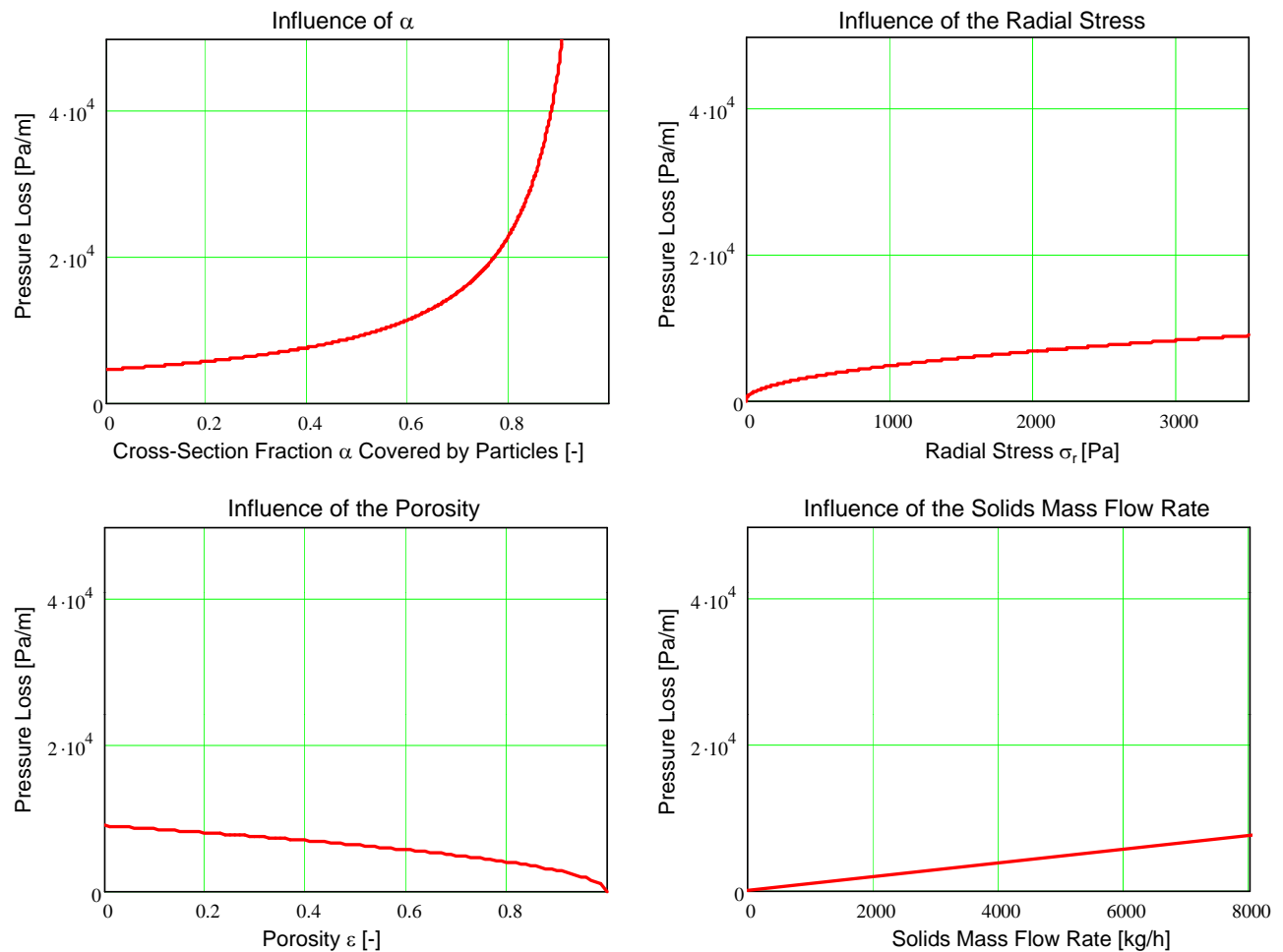


Figure 5.41: Influence of the fraction of the pipe area covered by settled particles, radial stress, porosity and solids mass flow rate on the pressure loss calculated by applying the kinetic theory



Eq. 5.23 presents advantage in that the calculation of the pressure loss is independent of the slug velocity. Because the slug porosity was found to be independent of the conveying velocity, i.e. it is constant for a given material, the pressure loss for a given solids mass flow rate only depends on the radial stress and the height of the layer of settled particles.

Based on average values of experimental radial stress, fraction of the pipe area covered by the settled particles and solids mass flow rate (see Section 5.1), the pressure loss for the different horizontal sections of the conveying system has been calculated. The data used for the calculation are summarised in Fig. 5.42. It should be pointed out that for all pipe sections, the calculations are based on values of radial stress and  $\alpha$  measured in the pipe section 2-3 (Fig. 4.1).

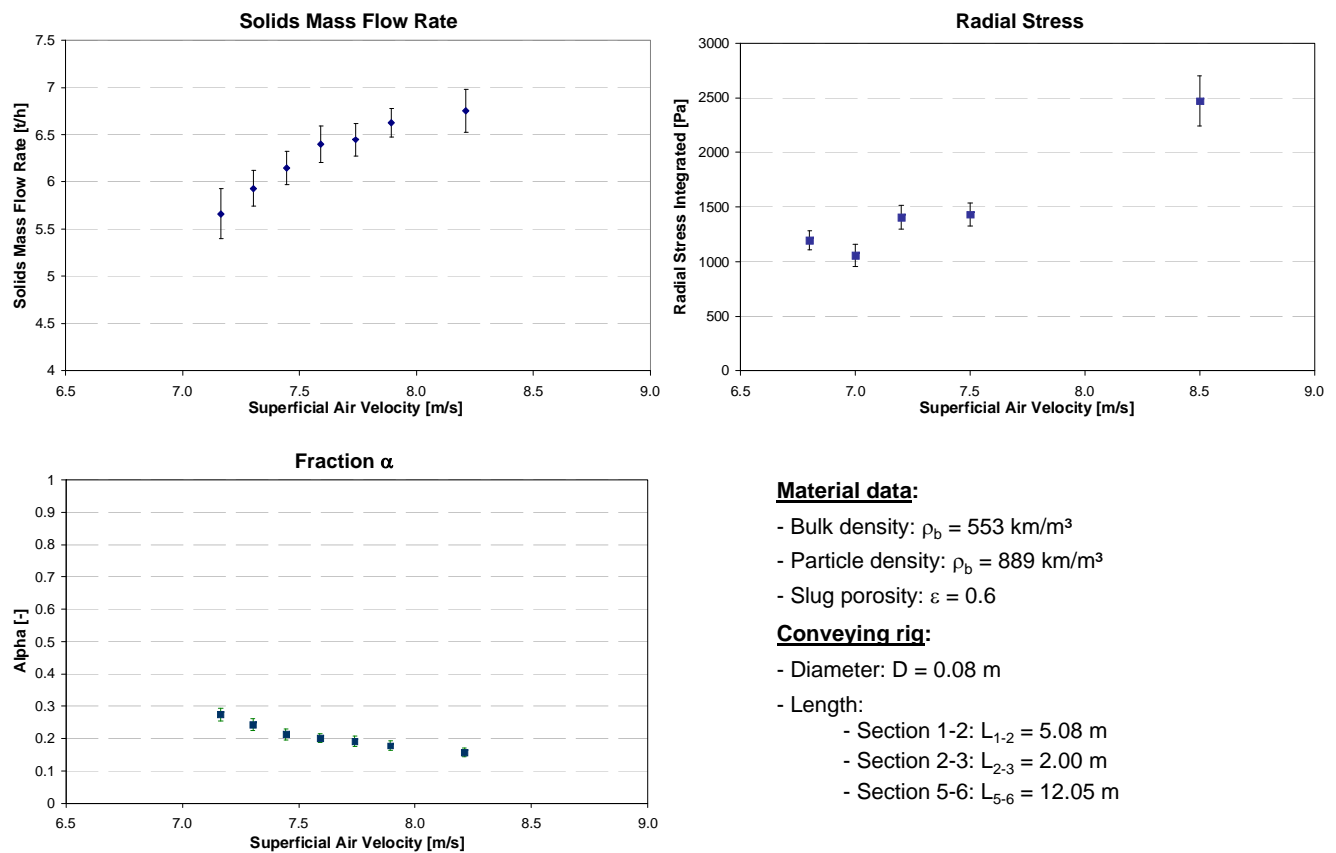


Figure 5.42: Summary of the material characteristics, pipeline layout and flow dependent parameters required for the pressure loss calculation in the horizontal sections of the conveying system

Fig. 5.43 permits to compare experimental and calculated pressure loss for each horizontal section of the conveying system. For section 2-3, in the center of which the radial stress was measured, the pressure loss calculated by applying the impulse theory shows very good agreement with the pressure loss measured for  $v_f = 6.8 \text{ m/s}$ ,  $v_f = 7.2 \text{ m/s}$  and  $v_f = 7.5 \text{ m/s}$ . For  $v_f = 7.0 \text{ m/s}$ , the calculation underpredicted the pressure loss. This underprediction is due to the unexpected low values of experimental radial stress at the pipeline top that were required for the calculation. However, no reason could be found to explain those low stress values.

Furthermore, the calculation overpredicted the pressure loss for  $v_f = 8.5$  m/s. This results from the fluctuations in the flow mode occurring in these operating conditions. The transport took place close to the upper boundary of slug flow. Therefore, the occurrence of flow instabilities led to the partial transport of the particles in form of strand flow. However, for the calculation it was assumed that the particles were only transported within the slugs. Consequently, the total length of slugs has been overpredicted, which in turn has led to the overprediction of the pressure loss. Moreover, strand flow is characterised by a lower pressure loss than slug flow.

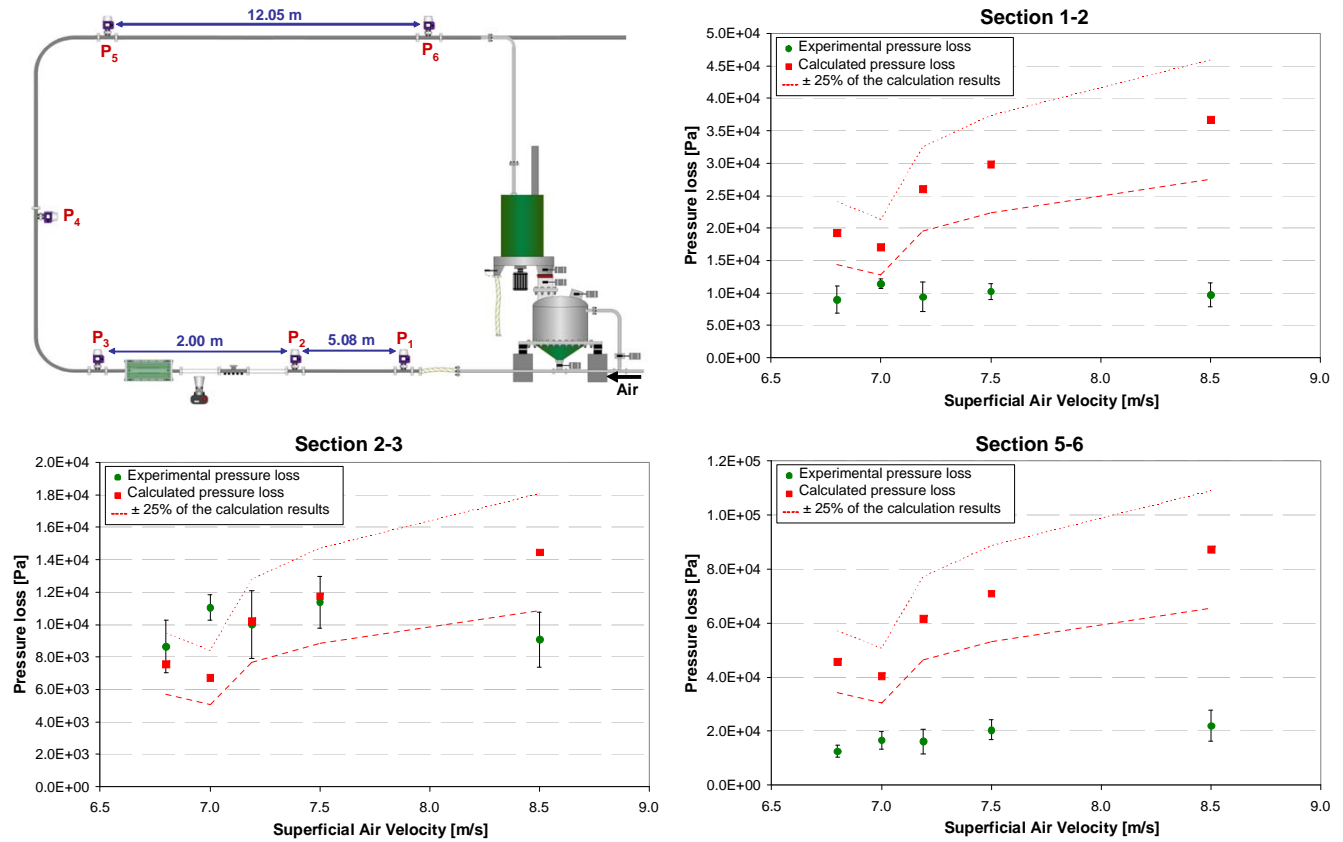


Figure 5.43: Comparison between experimental and calculated pressure loss for the three horizontal sections of the conveying system

The kinetic theory was successfully applied to predict the pressure loss along the two-meters long pipeline section where slug characteristics were measured. However, the extrapolation of the slug characteristics measured in a defined area to other pipe sections led to overprediction of the pressure loss in additional horizontal pipe sections. The results indicate that the impulse model is not suitable to predict the pressure in section 1-2 where the flow is still forming after material feeding into the pipeline. In fact, the application of the impulse model overpredicts the pressure loss. Furthermore, the expansion of the air along the pipeline is responsible for the overprediction of the pressure loss in section 5-6. Due to the significant pressure gradient observed in slug flow pneumatic conveying, the velocity of the conveying air increases significantly along the length of the pipe. Consequently, the transport cannot be assumed as taking place in the same conditions over the entire pipeline length. This results in significant changes of slug and transport characteristics such as particle velocity, radial stress and height of the

layer of settled particles along the pipeline. These changes have to be considered to achieve accurate pressure loss prediction over the entire pipeline.

Fig. 5.44 shows for each air supply velocity tested the evolution of the superficial air velocity with the decrease of air pressure along the pipe. For the representation, atmospheric conditions have been assumed at point  $P_6$ . Due to air expansion, the velocity increases significantly along the pipeline. Flow instabilities were observed in section 2-3 for the highest velocity tested, i.e.  $v_f = 8.5$  m/s. Since the air velocity at point  $P_5$  for the lowest velocity tested is even higher than the velocity in section 2-3 for the highest velocity tested ( $v_f = 8.5$  m/s), it can be concluded that stable slug flow no longer took place in section 5-6. Therefore, the impulse model for slug flow is no longer applicable.

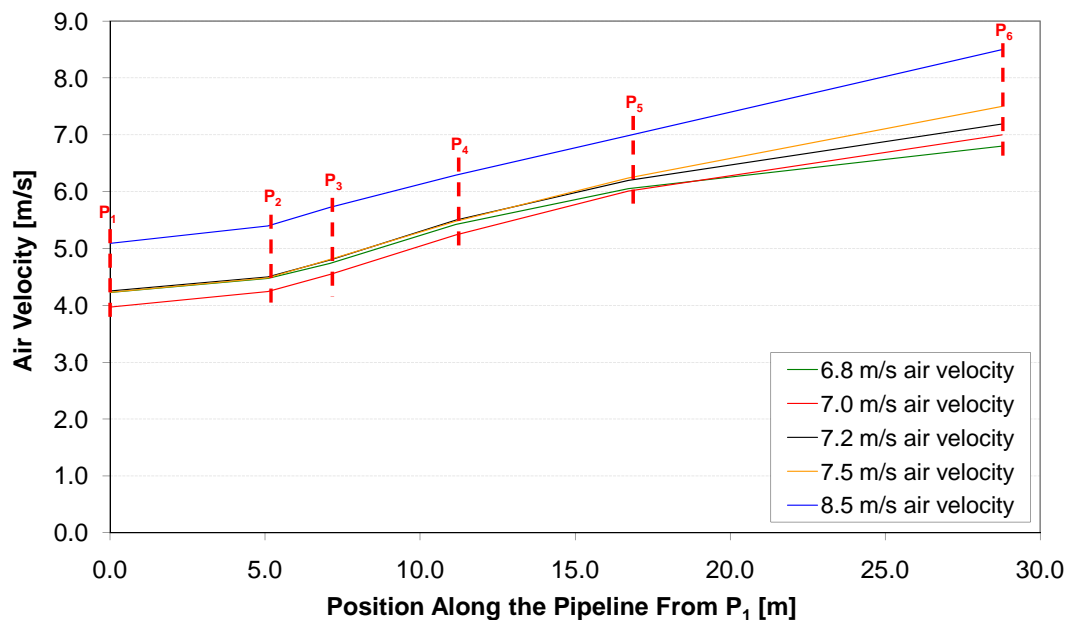


Figure 5.44: Influence of the changes in the air density on the superficial air velocity

## 5.5. Correlation between pressure, stresses, porosity and particle velocity

### 5.5.1. Investigation on single slugs in stable state

One of the objectives of this work is the investigation of the physical mechanisms involved in the formation, transport and disintegration of slugs pneumatically conveyed. Therefore, single slugs have been experimentally investigated with respect to internal stress states, porosity, pressure loss, particle velocity and physical aspect. By combining all those characteristics, knowledge can be gained on the physical mechanisms involved in horizontal slug flow pneumatic conveying.

It should be pointed out that the behaviour characterising the five single slugs detailed in this chapter does not only represent single cases but was observed on many slugs. These slugs have been chosen because they illustrate particularly clearly some of the physical mechanisms that were frequently observed.

### 5.5.1.1. Slug 1: $v_f = 6.8$ m/s - Measurement position of the forces: pipe side

Fig. 5.45 shows the pressure, stresses, pressure loss and particle velocity measured on a single slug conveyed with  $v_f = 6.8$  m/s as well as the porosity calculated by applying the Ergun equation.

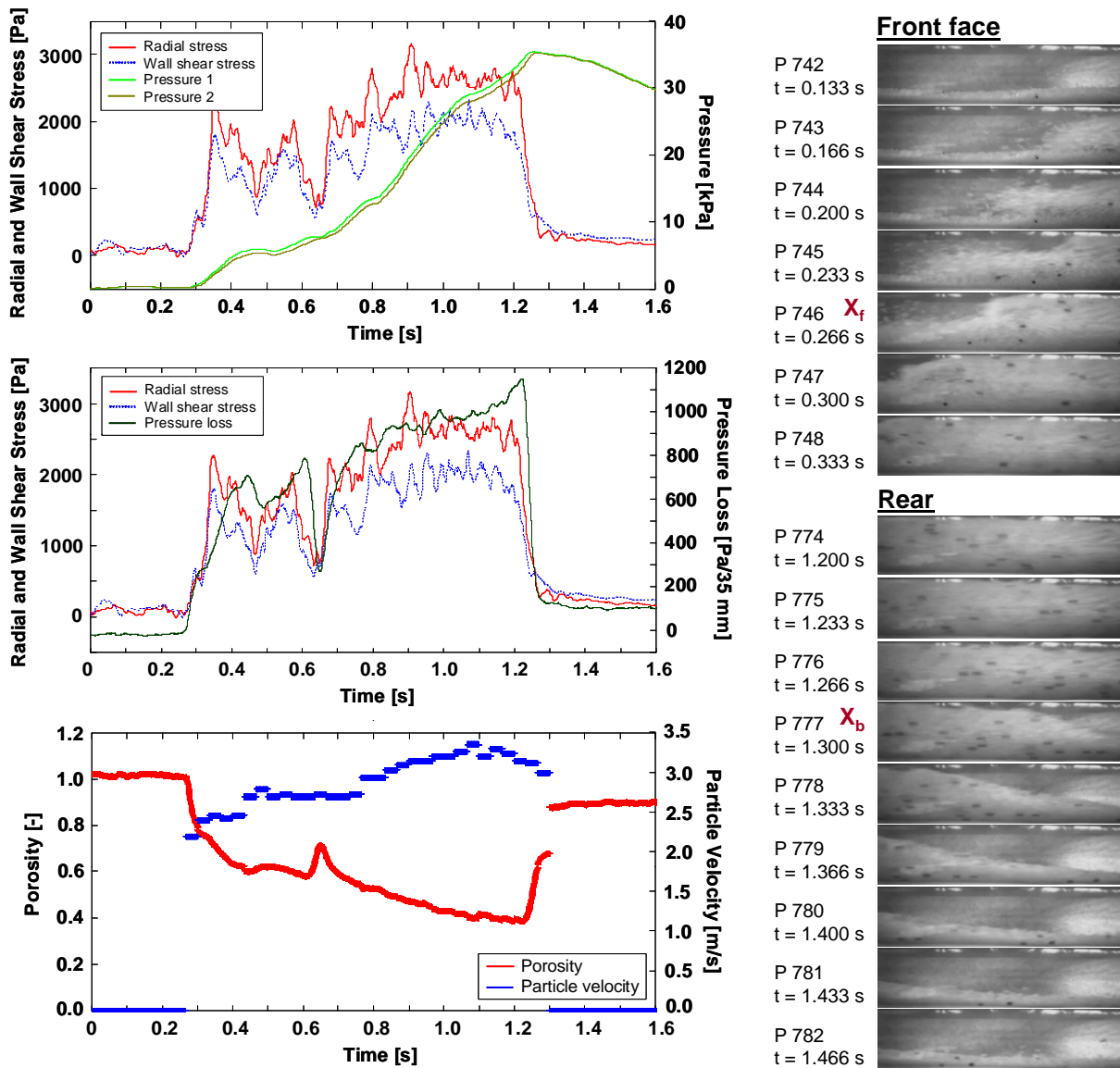


Figure 5.45: Slug 1: Single slug conveyed with  $v_f = 6.8$  m/s - Stress measurement position: pipeline side

From the stress signals and pressure loss analysis, it can be concluded that the slug needed 1.01 s to pass the measurement plate. This time is in good agreement with the time needed for the slug to pass completely in front of the camera since 31 photos were taken between the points  $X_f$  and  $X_b$ , i.e. the rear of the slug passed in front of the camera 1.03 s later than the front face. This proves that the length and velocity of the slug remained constant over the short distance between the camera and the stress measurement plate. Both the radial and wall shear stress tend to increase over the slug length. However, the stresses show local minima, particularly at  $t = 0.64$  s, where the pressure loss shows a significant and rapid decrease as well. At this location over the slug length, the particles moved with

the same velocity than the particles in front of and behind them but the slug locally displayed a higher porosity. The analysis of the slug images revealed the presence of many air cavities at the top of the slug. Fig. 5.46 shows the air cavity that generated the local porosity increase at  $t = 0.64$  s. The particle velocity shows an increasing trend over the slug length whereas the porosity shows the converse trend, i.e. the rear of the slug is denser than the front. Most of the slugs investigated in this research displayed similar characteristics: The stresses induced by the slugs are often higher at the rear where particles move faster and where the slug is denser.

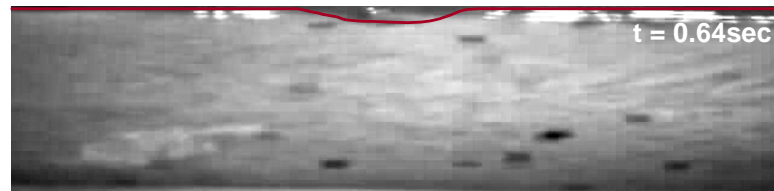


Figure 5.46: Air cavity at the top of Slug 1 at  $t = 0.64$  s

#### 5.5.1.2. Slug 2: $v_f = 6.8$ m/s - Measurement position of the forces: pipe top

Fig. 5.47 illustrates the behaviour of another slug conveyed with  $v_f = 6.8$  m/s. In this case, the stresses were measured at the top of the pipeline. The curves illustrating the pressure loss and the stresses follow the exact same trend. As soon as the pipe cross-section is entirely filled with particles, the pressure loss increases significantly and significant stresses are detected at the top of the pipeline. Besides the sharp signal increase induced by the arrival of the front face above the measurement plate, a sharp decrease of the signal is also detected as soon as the slug rear leaves the measurement area.

In front of the slug front face itself, an inhomogeneous group of particles flew over the stationary layer (Photos marked in red in Fig. 5.47). Those suspended particles have been picked up by the slug front where particularly turbulent flow conditions prevailed and transported faster than the rest of the slug in the form of isolated particles less prone to friction forces. The turbulent flow conditions prevailing at the slug front face facilitated the lifting of particles from the stationary layer. In fact, Tomita [83] noticed an increase in gas velocity preceding the slug arrival and suggested that it would explain the jump of particles frequently observed in front of a slug. In addition, the shear force that flying particles generated at the surface of the stationary layer could have initiated the particles lifting. This shear force results from the momentum exchange of particles hitting the surface of the stationary layer. Finally, the backflow of gas that Kuang [40] sometimes observed inside the settled layer before and after a slug conveyed with very low velocity may play a significant role in the initiation of the particle lifting (see Section 2.4.2).

Despite their high velocity, i.e. energy, those flying particles did not generate any stress that could be detected at the top of the pipe where the measurement plate was positioned. Moreover, those particles did not induce any significant pressure loss, which suggests that this mass of particles consists of only few particles moving in a stream with high velocity. The oscillations of the wall shear stress signal in front of the slug are caused by the measurement plate, which oscillates with its natural frequency. Moreover, the slight vibrations of the pipeline that preceded the slug arrival amplified those oscillations.

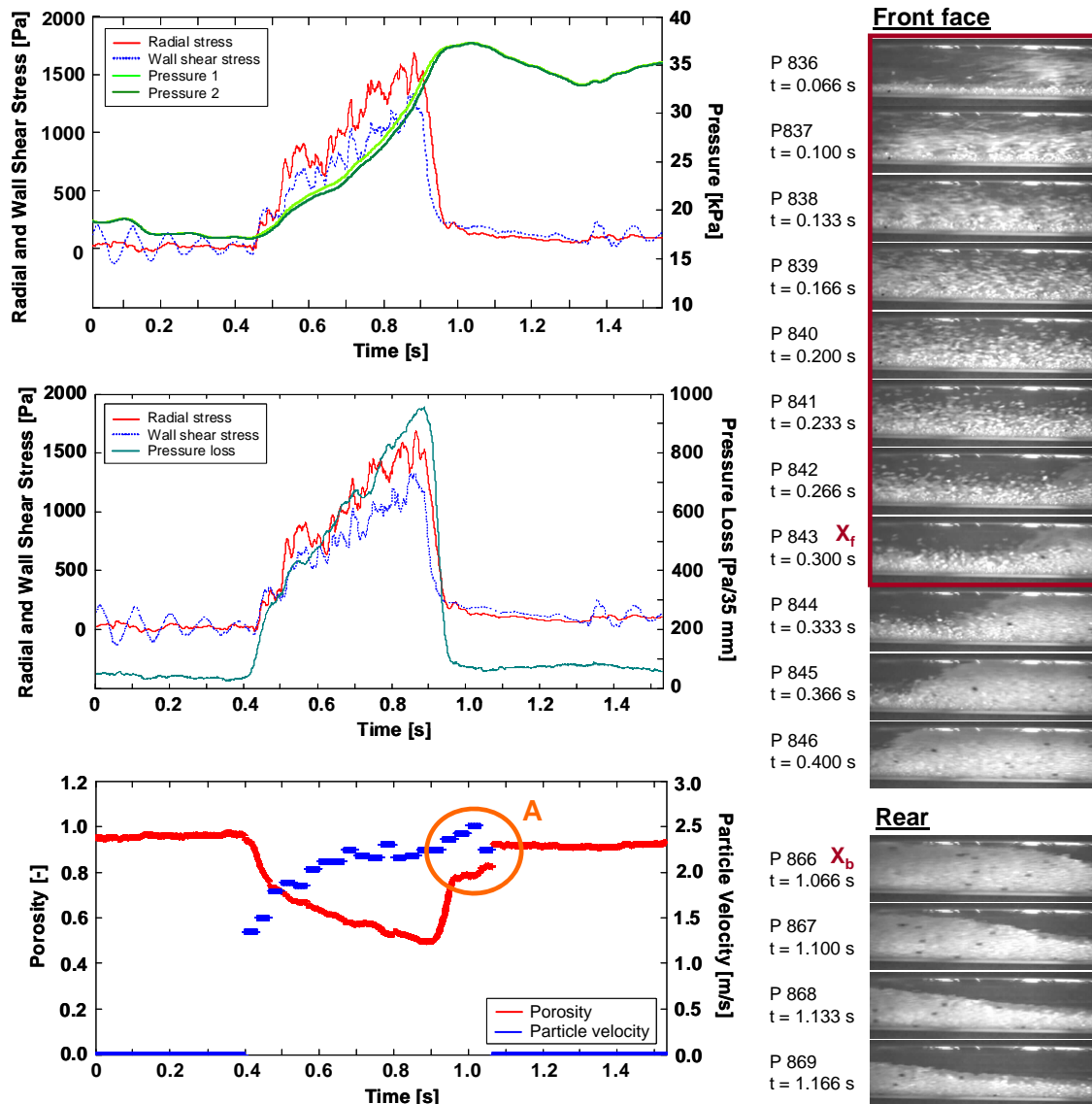


Figure 5.47: Slug 2: Single slug conveyed with  $v_f = 6.8$  m/s - Stress measurement position: pipeline top

The pressure over the slug decreases relatively constantly from the rear in the direction of the flow. In fact, the curve illustrating the pressure loss shows a linear increase over the slug length. At the same time, the closer the particles are to the front face, the slower they move. The particles are picked up from the stationary layer by the front face and have to be accelerated to the slug velocity. In this case, the particle velocity appears to increase along the entire slug length. Therefore, the fastest particles are located at the slug rear. By extrapolating the experimental pressure loss and particle velocity in the Ergun equation, the slug porosity could be calculated. The third graph in Fig. 5.47 shows that the porosity decreases towards the rear, i.e. the slug is denser at the rear. However, area A indicates a sudden increase of the slug porosity at the rear while the particle velocity keeps increasing significantly. This phenomenon results from different measurement locations for the key parameters required to calculate the Ergun porosity. The particle velocity is measured 50 cm above the point where the measurement of the pressure loss takes place. Therefore, the possible changes occurring in the slug



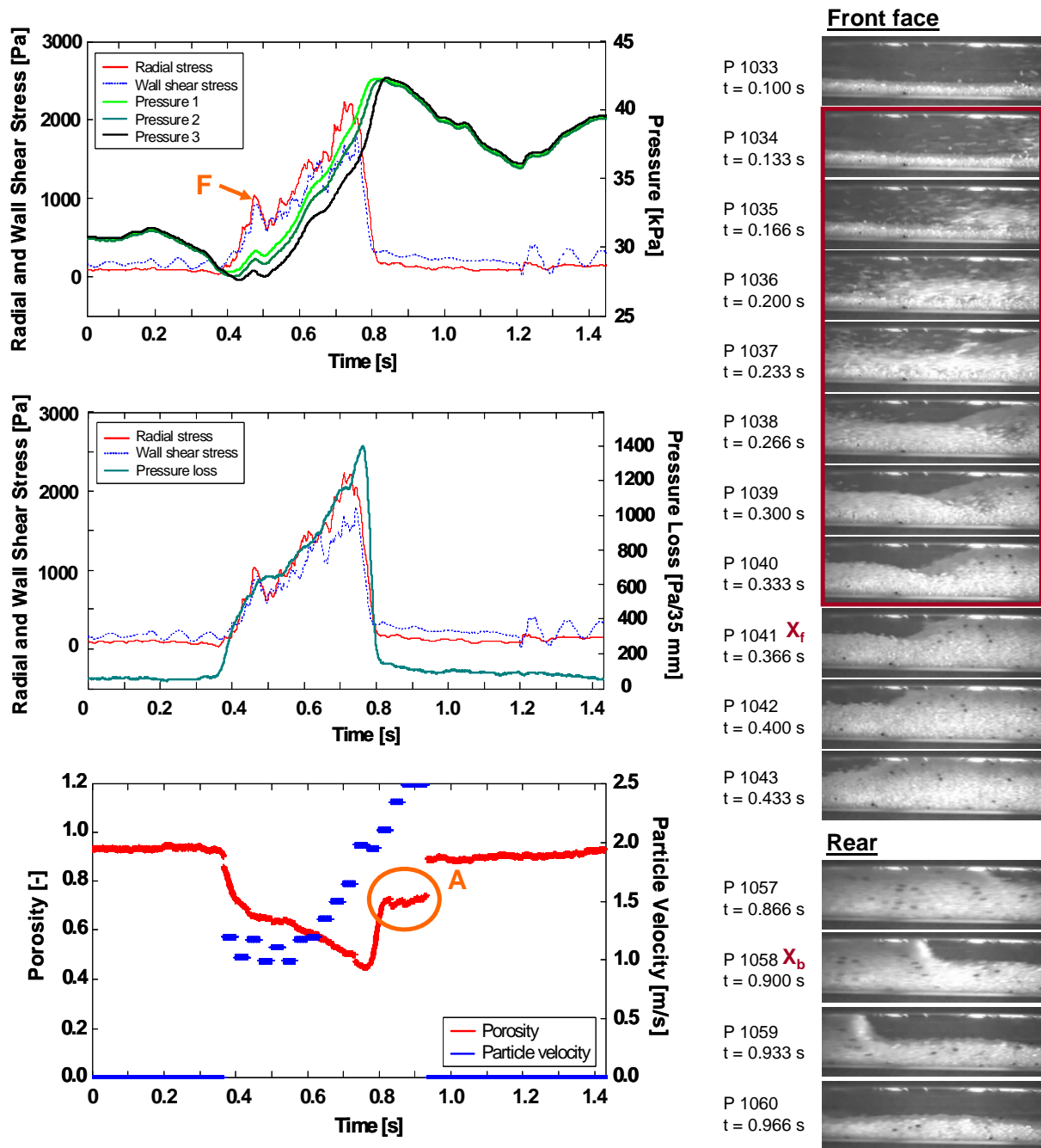


Figure 5.49: Slug 3: Single slug conveyed with  $v_f = 6.8$  m/s - Stress measurement position: pipeline top

The images of the pipe taken before the arrival of the slug front face (red marked in Fig. 5.49) reveal the presence of a turbulent layer of particles moving immediately in front of the slug. Due to the turbulent flow ahead of the slug, particles could be more easily picked up and transported further. As a result of the friction forces existing between those moving particles and between those particles and the pipe wall, the particles slowed down and finally settled. Although this turbulent moving layer occupied more than half of the pipe area, it did not reach the top of the pipe. Consequently, since the stress measurement plate was positioned at the pipe top, no stresses due to this moving layer were detected. The settling of the particles led to the reduction of the pipe area free of particles and the



resulting increase of the resistance forces against the slug movement. This, in turn, resulted in the low velocity of the slug front where particles were found to move with a constant velocity of about 1.1 m/s up to the mid-part of the slug. From the mid-part of the slug towards the rear, the particle velocity increased significantly and a similar trend could be observed as in the slugs previously analysed. The particles at the rear displayed a velocity of 2.5 m/s, i.e. moved two and a half times faster than the particles located at the front end or in the mid-part of the slug.

Similar to the slug previously analysed, the slug length decreased over the short way from the camera to the measurement probe. In fact, the slug needed 0.60 s to pass completely in front of the camera while it needed only 0.43 s to pass completely above the measurement plate. The same phenomenon happened as for Slug 2. The closer the particles are to the rear, the faster they move. Therefore, the particles located at the back tend to move closer to the particles in front of them so that the porosity decreases towards the rear of the slug, which is illustrated on the graph by the negative porosity gradient. Consequently, a similar erroneous porosity as for Slug 2 was calculated in area A.

In spite of the slow movement of the front end of the slug, the blurring observed on the images of this slug part (P 1040 and P 1041) reveal that the particles were prone to high turbulences. The particles collided with the particles of the particularly high settled layer and a high momentum exchange took place. While the particles located at the slug front were passing through the reduced pipe cross-section, they induced the stress peak denoted by F. Afterward, the process within the slug became stable and the stresses displayed a usual constant increase over the slug length. Stress and pressure loss curves have been generally found to follow the same trend. However, such stress peaks were never accompanied by any fluctuation of the pressure loss. This indicates that a high air velocity and particularly turbulent flow conditions occurred in this area. Further investigations on such phenomena showed that similar stress peaks were always observed when the layer in front of the slug filled at least half of the pipe area and high turbulences took place at the front. Such peaks were detected at the pipe side and top but never at the bottom where a layer of settled particles always lies. This demonstrates that those stresses result from the turbulent movement of the particles and not from the existence of a radial force transmitted across the pipe cross-section.

#### 5.5.1.4. Slug 4: $v_f = 8.5$ m/s - Measurement position of the forces: pipe side

Fig. 5.50 shows the pressure, pressure loss, particle velocity, stresses measured at the pipe side and porosity calculated within a slug conveyed with  $v_f = 8.5$  m/s. Although the conveying still took place in the slug flow mode, the first flow instabilities characterising the process suggested that the operations were performed close to the lower boundary of the transition zone. The signals presented in Fig. 5.50 correspond to the passage of two slugs, which however can be considered as one single slug. The front face of the main slug denoted on the images by  $X_{f2}$  can be recognised through the rapid increase of both the stresses and the pressure loss at  $t = 0.50$  s.

Contrary to Slug 1 to 3 investigated earlier, this slug displayed stress values that remained globally on the same level over the entire slug length. However, the stress signals showed significant oscillations, especially the radial stress, which oscillated around a value of 1500 Pa. Moreover, contrary to the

previous slugs where the particles located at the back moved faster than the particles in front of them, Slug 4 displayed a negative particle velocity gradient. The particles located at the front end moved fast with a velocity of 3 m/s whereas the particles located at the back moved over two times slower. Furthermore, instead of an increase in density over the slug length, as observed for the majority of slugs, this slug displayed porosity that remained constant over the slug length and increased slightly at the slug rear.

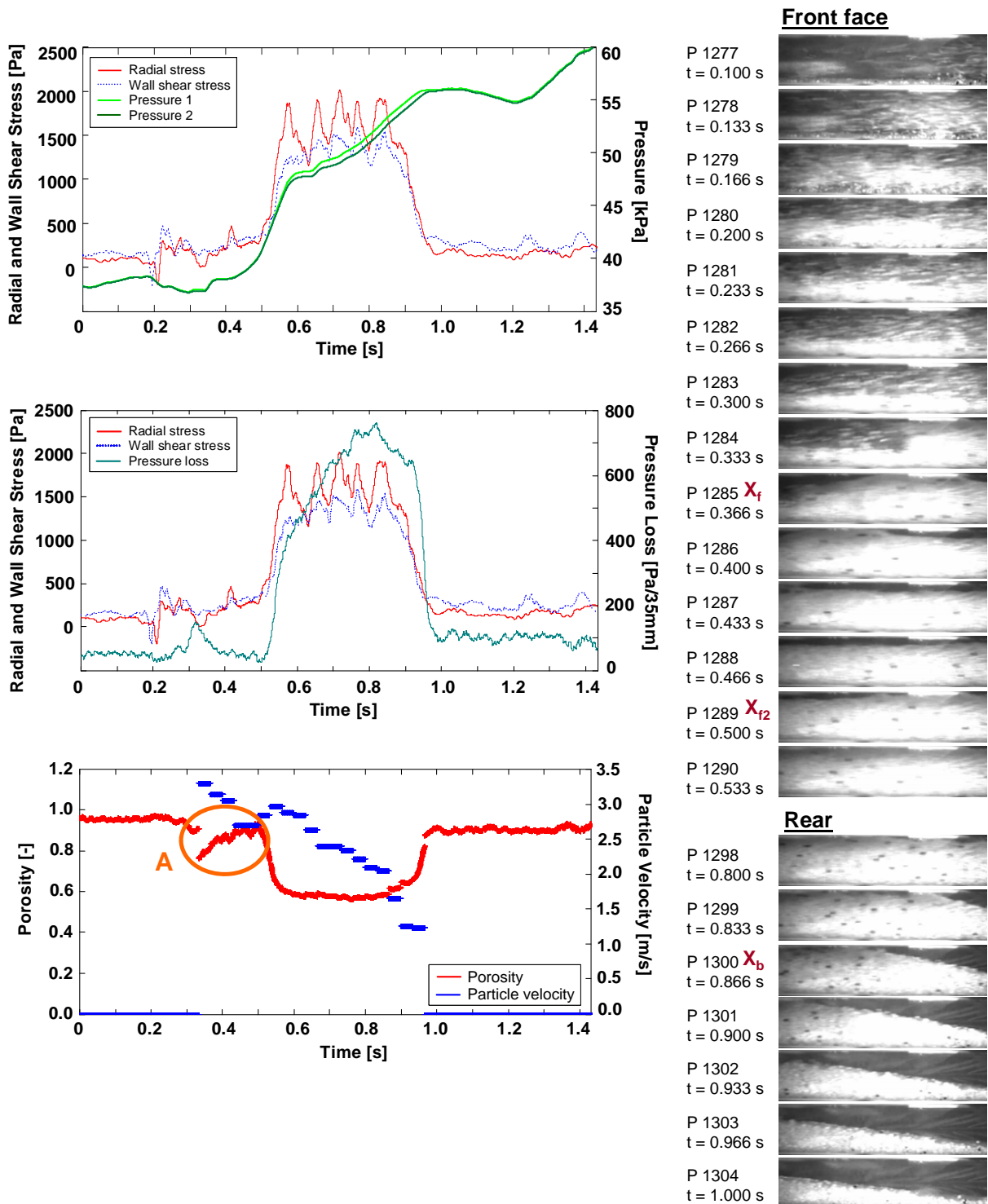


Figure 5.50: Slug 4:  $v_f = 8.5$  m/s - Measurement position of the forces: pipe side

The analysis of both the pressure and stress signals and the images taken 50 cms ahead revealed the existence of a pre-slug, which immediately preceded the main slug and filled the entire cross-section very shortly (P 1285 and P 1286). Since no stationary layer separated this pre-slug from the main slug, both moving structures can be considered as parts of the one and same slug. By entering the pipe cross-section where the stress measurement plate is located, the first slug front denoted by  $X_f$  generated an increase of the stresses. This front is made of particles moving faster than the particles composing the second front  $X_{f2}$ . Although the images show that the particles fill the complete pipe cross-section, the high porosity of about 0.75 calculated for the first front (Area A) suggests that this pre-slug consists of particles highly fluidised, which flow rapidly through the cross-section.

The comparison between the time needed for the whole slug to pass in front of the camera and later on the measurement plate revealed that the structure of the slug changed over this short distance. The slug needed 0.50 s to pass in front of the camera but 0.77 s to pass the measurement plate. However, the time separating the entering of the front faces  $X_f$  and  $X_{f2}$  in front of the camera and later onto the measurement plate remained unchanged. This suggests that the slug velocity remained constant but the slug length increased, either by extending itself or by picking up more material than it deposited. This theory is supported by the negative velocity gradient over the slug length and the presence of a pre-slug.

The closer the particles are to the front face, the faster they move. Therefore, the slug tends to extend. Whereas the Ergun-porosity at the front  $X_{f2}$  displays a value of about 0.6, which is a porosity similar to the porosity observed at the front of many slugs investigated, the rear displays a higher porosity. A stable moving slug is characterised by a higher density at the rear. In this case, the slug is no longer in a stable state. Each particle tends to gain some space on the particles following it. The particles of the back tend to reach the front of the slug so that the porosity gradient slowly disappears and the slug extends from the rear in the direction of the front. If particles at the front face move significantly faster, those particles may part from the rest of the slug and form a short slug on their own. This slug may grow further.

By analysing the distance between the rear of this slug and the rear of the preceding and following slugs, it was found that this distance remained unchanged on the way from the camera to the stress measurement section. However, the distance between the front ends of the slugs changed. The front end of the analysed slug came closer to the front end of the previous slug. Fig. 5.51 illustrates schematically this phenomenon, which supports the theory that there is the possibility for slugs to extend from the rear in the direction of the flow. However, this is characteristic of a slug in an unstable state, a slug that extends but can also lose material by separation of the front part due to a higher velocity of the particles in this area. Such slugs are characterised by a diffuse front end and a flat tail and also have a tendency to leave a higher layer of settled particles behind it.

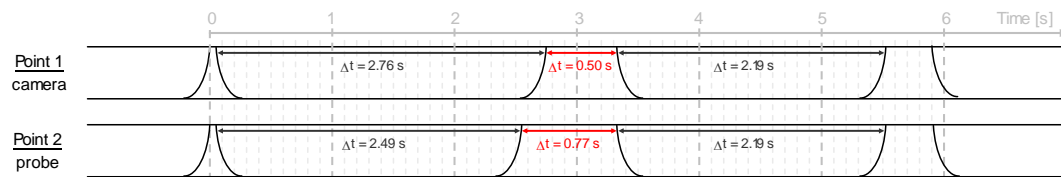


Figure 5.51: Scheme illustrating the expansion of Slug 4 from the rear in the direction of the flow

### 5.5.2. Investigation on a single slug that remained temporary blocked in the pipeline

The transport of Polypropylene pellets in the form of slugs occurs problem-free as long as operations take place far enough from the lower and upper boundaries of slug flow. In close proximity to the lower boundary, the flow steady slows down until slugs remain motionless. A subsequent re-increase of the air supply velocity generally leads to the reformation of the flow. In close proximity to the upper boundary of slug flow, the flow undergoes instabilities caused by the high pressure fluctuations due to the alternation between slug flow and strand flow. These instabilities easily lead to pipeline blockage. However, during the experimental investigations, the occurring pipe blockages cleared themselves without further intervention. Therefore, the flow was only temporary interrupted. It should be pointed out that the occasional blockage of the pipeline occurred only when operations were performed with the highest air supply velocity tested. Although tests were performed with the minimum air supply velocity, i.e. in close proximity to the lower boundary of transport as well, pipe blockage never occurred in these operating conditions. The occasional blockage of a slug within the measurement probe permitted to investigate the mechanisms involved in both the slug blockage and release.

Fig. 5.52 shows the results obtained by investigating a single slug conveyed with  $v_f = 8.5$  m/s that remained temporary blocked in the pressure and stress measurement probe. The stress measurement plate was located at the side of the pipeline. According to the stress signals, the slug was present during 1.84 s over the measurement plate. This time agrees with the time needed for the slug to pass the camera since the part of the slug between  $X_f$  and  $X_b$  is present on 55 images, which correspond to a time of 1.83 s. This leads to the conclusion that the slug kept moving with the same velocity on its way between the camera and the measurement probe.

Shortly before the arrival of the slug front face, the images show a suspension of particles moving over the stationary layer, which filled almost half of the pipe cross-section. The passage of the slug front face followed immediately the passage of those suspended particles. The arrival of the front face was accompanied by the usual increase of pressure, pressure loss and stresses. Without showing any changes in its velocity, the slug front face picked up the particles of the stationary layer (P 829 and P 830). However, a velocity gradient can be observed over the slug height. The velocity of the particles located at the pipe top was significantly higher than the particle velocity at the bottom. The lower part of the slug appeared to be driven by the shear force generated by the upper layer, which moved faster because of the absence of a stationary layer in front of it to slow down its movement.

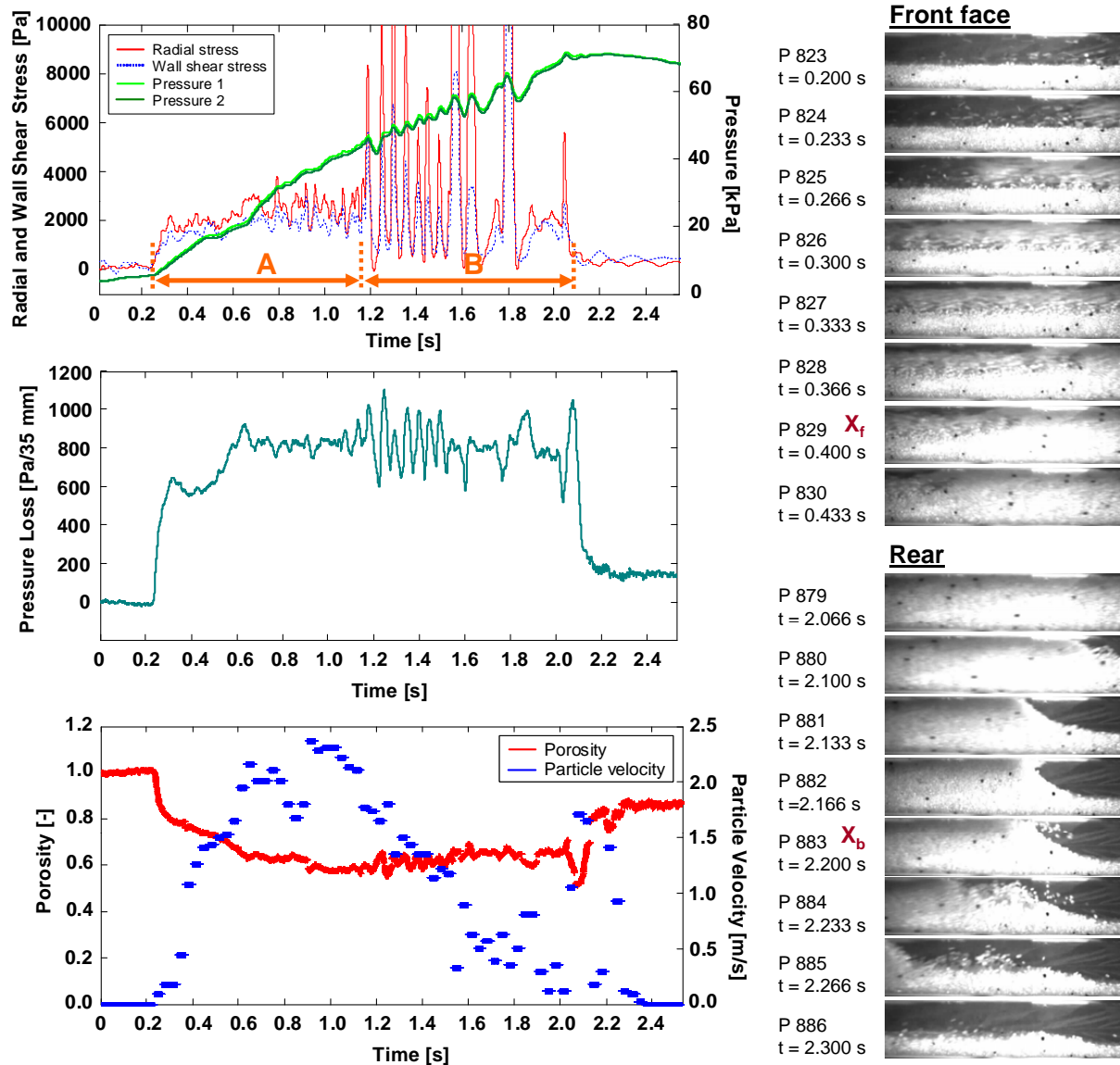


Figure 5.52: Slug 5:  $v_f = 8.5$  m/s - Measurement position of the forces: pipeline side

The front part of the slug denoted by  $A$  displays a similar behaviour as stable slugs: The stresses and the particle velocity increase over the slug length whereas the porosity decreases slowly. In area  $A$ , the slug differs from stable slugs only with respect to the trend of the pressure loss. Instead of the pressure loss increase usually observed over stable slugs, the pressure loss measured over this slug first increased at the front end and then remained constant with slight fluctuations around 800 Pa/35 mm. Such values were commonly measured at the back of slugs conveyed over the entire area of stable slug flow.

At  $t = 1.16$  s, the particle velocity decreased abruptly from 2.15 m/s to 1.75 m/s. From this point, the particle velocity kept decreasing constantly. In addition, the curves for both the radial and wall shear stress show high fluctuations with values between 0 and over 10,000 Pa for the radial stress and slightly lower values for the wall shear stress. These oscillations are present on the curves illustrating the pressure and pressure loss as well. Therefore, they do not result from the construction of the

measurement plate whose oscillations with natural frequency could have been amplified. These high stresses result from the blockage of the slug in the pipeline.

From  $t = 1.17$  s, the slug no longer moved constantly forward but displayed a pulsative movement. The blockage is due to the compressive state of the slug, which no longer permits air percolation. Until air percolation through the slug improves, the slug transport is stopped and the pressure upstream increases. Once the pressure is high enough to overcome the friction forces at the pipe wall, the entire slug moves forward by a small distance. During this movement, particles rearrange themselves but the rapid decrease of pressure behind the slug leads to a new blockage. The sudden motion of the slug is accompanied each time by a significant decrease of the stresses at the pipeline wall. The stresses increase again as soon as a new blockage occurs. This process repeats itself until the particle rearrangement is optimal, i.e. the porosity reaches a critical value to allow the transport to continue. The oscillations on the porosity signal in area B are similar to the oscillations on the stress and pressure curves. This is indicative of the particles rearrangement. In addition, in area B, the porosity tends to increase over the slug length. Despite this trend to increase, the minimum porosity values are reached in form of a local negative peak at the back of the slug. Fig. 5.53 shows four consecutive images of the slug rear where the density was found to reach its maximum and the particles are almost motionless (P882). The higher acuity of image P882 in comparison to P881 and P883 is indicative of the pulsative movement of the slug.

The slug rear is locally compacted. This local compressive state leads to the release of particles in the direction opposite to the flow (P882 and P883 in Fig. 5.53).

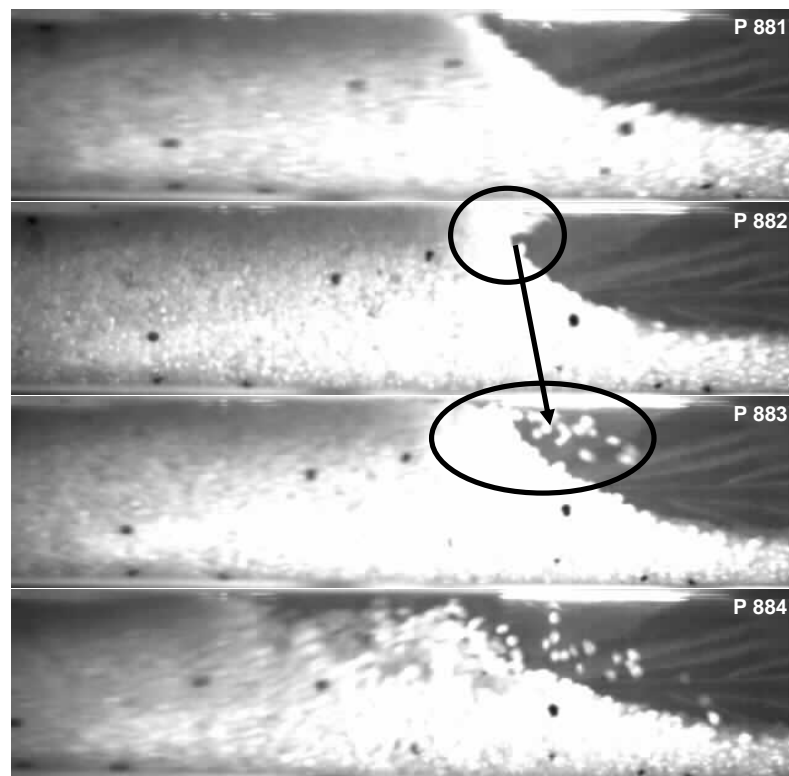


Figure 5.53: Release of particles at the back of a slug blocked in the pipeline

The release of particles allows better percolation of the air through the slug. After the release of those particles, the slug, which was almost motionless, moved abruptly forward with a sudden increase of the particle velocity from 0.1 to 1.7 m/s.

It should be pointed out that although the particle velocity was measured 50 cm ahead of the location where both the stresses and the pressure were detected, a very good agreement could be found between all physical parameters. Moreover, although the slug exhibited discontinuous motion, the length and the mean velocity of the slug remained unchanged on its way between the camera and the stress measurement probe. The blockage occurred first at the front face of the slug and spread towards the rear. Therefore, given particles displaying motion in front of the camera were later partly motionless in the stress measurement probe. As a consequence, the slug cannot be assumed as moving with a constant velocity between the camera and the stress measurement probe and the relationship between particle velocity and pressure as well as between particle velocity and stresses may be incorrect, particularly at the slug rear. Nevertheless, a good agreement was found.

## **5.6. The Bernoulli principle: part of the slug transport mechanism?**

Experimental investigations carried out in this study showed that a certain degree of fluidisation is required for slug transport. All slugs moving in stable state were found to display a similar porosity, which is independent of the air velocity. Investigations on the porosity trend over the slug length revealed that stable slugs are characterised by a rear denser than the front end. Moving slugs caught instantaneously with the aid of the slug-catcher were found to display a porosity between 0.40 and 0.42, i.e. the slug porosity was slightly higher than the bulk porosity of 0.38. No significant porosity gradient was detected over the slug height by analysing the three horizontal slug layers separately caught. However, since the three chambers of the closed slug-catcher were relatively full of particles, the detection of a slight porosity gradient is limited by the measurement exactitude of the catching system.

The presence of air cavities were frequently observed at the top of moving slugs. Those air cavities could also be identified on the curves illustrating the porosity over the slug length. Furthermore, a free channel is commonly observed at the top of the pipe during slug flow pneumatic conveying in systems with bigger pipe diameters.

### **5.6.1. Presentation of Bernoulli's principle and application on slug flow pneumatic conveying**

The transport of slugs requires the existence of a certain degree of internal fluidisation so that air permeation is provided through the slugs. The presence of this significant degree of internal fluidisation in horizontal slugs and the existence of a free channel at the top of the pipeline suggests the presence of an air velocity gradient over the pipe height. According to Bernoulli, the presence of a velocity gradient would generate a lifting force proportional to the difference in dynamic pressure.

The total pressure  $P_{total}$  at a defined position  $x$  over the pipeline is the sum of the static pressure  $P_{stat}$  and dynamic pressure  $P_{dyn}$ . The static pressure is induced by the collision of gas molecules with the wall whereas the dynamic pressure is principally a function of the gas velocity.

$$P_{total} = P_{stat} + P_{dyn} \quad (5.24)$$

with

$$P_{dyn} = \frac{1}{2} \cdot \rho_f \cdot v_f^2 \quad (5.25)$$

The pipeline area can be divided into two parts. The lower part, called strand, is assumed to be covered by a layer of particles with variable height. The upper part, called suspension, is nearly free of particles. Because the air molecules can be assumed to move with an infinitely high velocity, the same total pressure prevails in the upper and lower part of the pipe.

$$P_{total} = P_{su\_stat} + P_{su\_dyn}$$

$$P_{total} = P_{st\_stat} + P_{st\_dyn}$$

The gas flows faster in the upper part free of particles than in the lower part, which results in a higher dynamic pressure at the top than at the bottom. Since the total pressure is equal across the entire pipe cross-section, the local increase of the dynamic pressure leads to a decrease of the static pressure at this given point. This results in a static pressure, which is higher in the strand than in the suspension part.

$$v_{f\_su} > v_{f\_st}$$

$$P_{su\_dyn} > P_{st\_dyn}$$

$$P_{st\_stat} > P_{su\_stat}$$

The difference in static pressure generates a force  $F_{lift}$  able to lift a certain mass of particles. If the pipe cross-section is assumed as consisting of a suspension and a strand only, the lifting force is directly proportional to the static pressure difference between those two parts. Furthermore, the static pressure difference is a function of the fraction  $\alpha$  of the pipe area covered by particles and the fraction  $a_f$  of the total gas mass flow rate flowing through the strand. The remaining fraction  $(1 - a_f)$  of the total gas mass flow rate flows in the suspension over the strand.

$$\Delta P_{stat}(\alpha, a_f) = P_{st\_stat} - P_{su\_stat}$$

$$\Delta P_{stat}(\alpha, a_f) = P_{su\_dyn}(\alpha, a_f) - P_{st\_dyn}(\alpha, a_f)$$



The lifting force is calculated with respect to the surface area of the particles layer  $A_{layer}$ :

$$F_{lift} = \Delta P_{stat}(\alpha, a_f) \cdot A_{layer}(\alpha, a_f) \quad (5.26)$$

As a result of the lifting force  $F_{lift}$ , the particles are lifted and go into suspension over the pipe cross-section. This suspension is easier transported by the conveying gas compared to a compact mass of particles. As soon as this suspension is uniformly distributed over the pipe cross-section, the channel at the top of the pipe where the air velocity was higher ceases to exist. The flow rearranges and the velocity gradient over the pipe height disappears. The lifting force resulting from Bernoulli's principle ceases to exist as well and the particles begin to settle again. The channel at the top of the pipe eventually reappears and the same process is repeated. This cycle occurs continuously and facilitates the transport of slugs along the pipeline. The role played by the Bernoulli principle in the slug transport is schematically presented in Fig. 5.54.

### 5.6.2. Calculation of the lifting force resulting from the Bernoulli principle

#### 5.6.2.1. Specifications and assumptions for the parameters necessary to calculate the lifting force

Calculations were performed to estimate the percentage of particles present in the pipeline that can be lifted by application of the Bernoulli principle. For a given gas mass flow rate  $\dot{m}_f$ , three parameters influencing the calculation vary according to the amount of particles lying at the bottom of the pipe at a given location over the pipeline:

- the fraction  $\alpha$  of the pipe area covered by particles
- the surface  $A_{layer}$  of the boundary between the strand and the suspension
- the part  $a_f$  of the total gas mass flow rate  $\dot{m}_f$  that flows through the layer of particles, i.e. through the strand and the remaining part  $(1 - a_f)$  that flows in the suspension.

The total air mass flow rate  $\dot{m}_f$  is known. A certain part of  $\dot{m}_f$  flows through the strand whereas the remaining part flows in the suspension above. The following equations apply:

$$\begin{aligned} \dot{m}_f &= v_f \cdot A \cdot \rho_f \\ \dot{m}_{st} &= v_{st} \cdot A_{st} \cdot \rho_f \\ \dot{m}_{su} &= \dot{m}_f - \dot{m}_{st} \end{aligned}$$

However, the part of the total mass of air flowing either in the suspension or through the layer is unknown. Hence, calculations have been performed for different fractions  $a_f$  varying from 0 % to 100 %, i.e. for a fraction of the air mass flow rate flowing in the suspension varying from 100 % to 0 %.

$$\dot{m}_{st} = a_f \cdot \dot{m}_f$$

The fraction  $\alpha$  of the pipe area is covered with particles. Therefore:

$$A_{st}(\alpha) = \alpha \cdot A$$

$$A_{su}(\alpha) = (1 - \alpha) \cdot A$$

For a given total gas mass flow rate, the velocity of the air flowing in the suspension and through the strand are functions of the air mass flow rate in the respective area and the part  $\alpha$  of the pipe area covered with particles:

$$v_{st}(\alpha, a_f) = \frac{\dot{m}_{st}(a_f)}{A_{st}(\alpha) \cdot \rho_f} \quad (5.27)$$

$$v_{su}(\alpha, a_f) = \frac{\dot{m}_f - \dot{m}_{st}(a_f)}{A_{su}(\alpha) \cdot \rho_f} \quad (5.28)$$

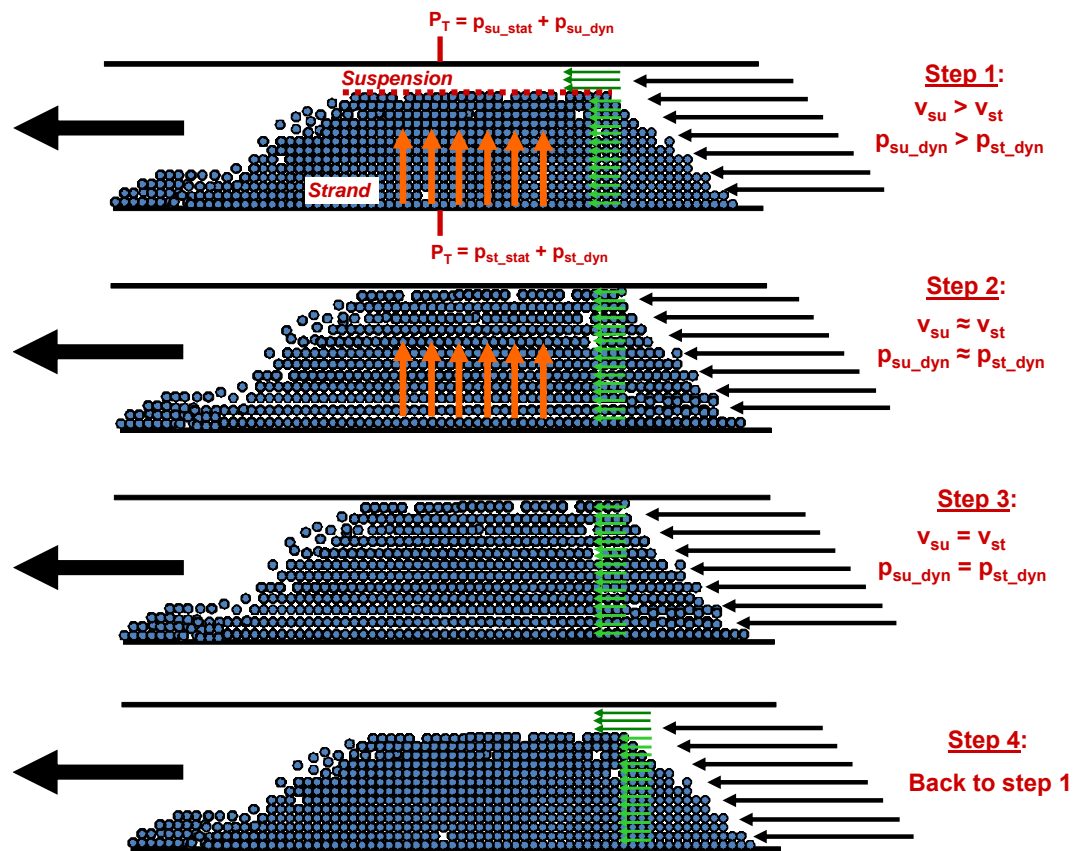


Figure 5.54: Scheme illustrating the Bernoulli principle applied on slug flow pneumatic conveying

The lifting force resulting from the difference in static pressure between the top and the bottom of the pipe is a function of the surface area of the particles layer  $A_{layer}$  with respect to the slug length  $l_{slug}$ :

$$A_{layer}(\alpha) = l_w(\alpha) \cdot l_{slug} \quad (5.29)$$

where the width  $l_w$  of the layer can be geometrically approximated by the following equation:

$$l_w(\alpha) = [4 \cdot \alpha \cdot (1 - \alpha)]^{1/3} \cdot D \quad (5.30)$$

### 5.6.2.2. Calculation of the percentage of lifted particles

The force  $F_{lift}$  resulting from the static pressure difference between the suspension area and the area covered by particles is able to lift a certain mass of particles. If the friction forces are neglected, the mass of particles lifted can be calculated as following:

$$m_{particles}(\alpha, a_f) = \frac{F_{lift}(\alpha, a_f)}{g} \quad (5.31)$$

The mass of particles contained in a pipe section of length  $l$  is a function of the height of the particles layer, i.e. of  $\alpha$ :

$$m_{particles\_max}(\alpha) = A_{st}(\alpha) \cdot l \cdot \rho_b \quad (5.32)$$

Hence, the part of the particles present in a given pipe section that can be lifted is:

$$Fraction(\alpha, a_f) = \frac{m_{particles}(\alpha, a_f)}{m_{particles\_max}(\alpha)} \quad (5.33)$$

To illustrate the application of the Bernoulli principle on slug flow, the percentage of the particles that can be lifted has been calculated for both the minimum and maximum air supply velocity where slug flow occurred, i.e.  $v_f = 6.8$  m/s and  $v_f = 8.5$  m/s. The results are presented in Fig. 5.55 and 5.56.

Fig. 5.55 shows for example that all particles in a layer covering 94 % of the pipe cross-section would be lifted if 25 % or more of the total mass of air flows in the upper part of the pipe, i.e. through the 6 % of the cross-section area free of particles. An increase of the part of the air mass flowing through the free channel at the top of the particles mass leads to the increase of the lifting force. This, in turn, results in a higher amount of particles lifted for a given fraction  $\alpha$  of the pipe area covered with particles. Basically, for given masses of gas flowing through the suspension and through the strand, the increase of the layer of settled particles results in the reduction of the channel area located at the pipeline top. Therefore, the air velocity in the channel, i.e. free cross-section area increases, which

leads to the increase of the amount of particles that can be lifted. However, the height of the settled layer has to reach a minimum value for the Bernoulli principle to be able to lift particles.

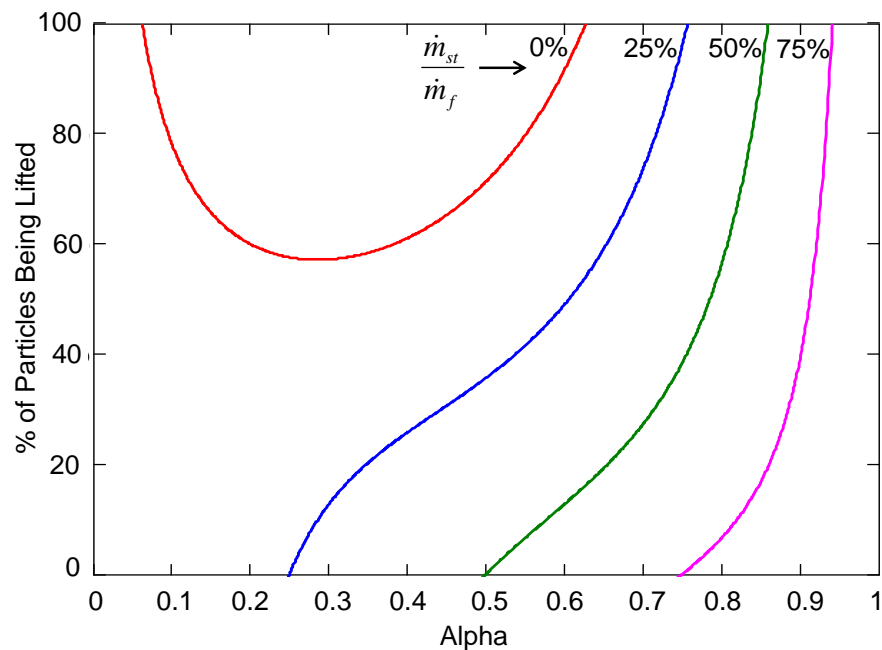


Figure 5.55: Fraction of the particles that can be lifted for  $v_f = 6.8$  m/s

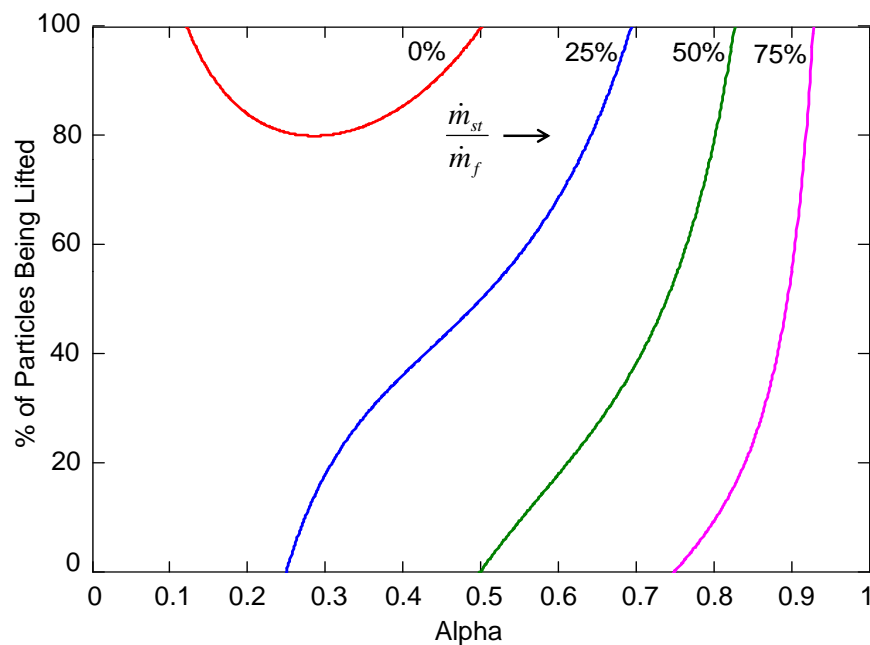


Figure 5.56: Fraction of the particles that can be lifted for  $v_f = 8.5$  m/s

In Fig 5.55, the curve corresponding to 100 % of the air mass flowing through the suspension shows a minimum point. If more than 28 % of the pipe area is covered with particles, an increase in the height of the layer of settled particles results in the increase of the amount of particles lifted. However, for  $\alpha$ -values lower than 0.28, the lower is the quantity of particles settled at the pipe bottom, the higher

is the percentage of those particles, which can be lifted by application of the Bernoulli principle. For a superficial air velocity  $v_f = 6.8$  m/s and the entire air flowing in the suspension, 100 % of the settled particles can be lifted if  $\alpha > 0.65$  or  $\alpha < 0.05$ .

Fig. 5.56 indicates that the capacity of the flow to lift particles increases with the increase of the air velocity. Basically, as the air velocity increases, the minimum cross-section area free of particles required to lift a given amount of particles increases. To compare with the results illustrated in Fig. 5.55 for  $v_f = 6.8$  m/s, all particles in a layer covering 93 % of the pipe cross-section would be lifted if at least 25 % of the total air mass flows in the upper area, i.e. through the 7 % of free cross-section area.

Based on the above, it can be concluded that the Bernoulli principle may play a key role in the slug transport. These results acknowledge with the theory of Klinzing who suggested that as the free cross-section area increases, the air velocity over the layer decreases and so does the capacity of the stream to pick up more particles [12].

## 6. Conclusion

In dense-phase pneumatic conveying and particularly in slug flow conveying, only relatively small amounts of gas are used to transport large volumes of material. The transport takes place with high pressure but low velocity, which permits to significantly reduce both pipe wear and product attrition. In slug flow pneumatic conveying, particles are conveyed in the form of slugs, which fill the entire cross-section of the conveying pipe. Between two slugs, a layer of motionless particles lies on the bottom of the pipeline. These particles will be picked up by the next slug, transported through the slug over a small distance and finally dropped at the back of the slug. Slug flow pneumatic conveying is gaining importance in industry, particularly in the transportation of friable particulate materials. However, the complexity of the physical laws governing this mode of transport makes it difficult to understand and to predict. In the last thirty years, many models were developed to describe mathematically slug transport behaviour and derive models for the key design parameters, i.e. pressure loss and optimal gas supply velocity. Nevertheless, the calculation models give very different results and a great part of empiricism remains in systems design procedures. Because scale-up rules are not available and the results usually cannot be extrapolated for another material, the design is generally realised for a specific material conveyed in a predetermined system. Priority is given to minimisation of risk of pipe blockage and process failure.

Whereas for dilute phase, calculation models are mainly based on the determination of a friction and/or impact coefficient between particles and pipe wall, theoretical models developed for slug flow mainly use an approach based on bulk solids mechanics. This is the case for the models of Konrad, Mi, Pan and Yi that were reviewed in this work. Slugs are usually assumed as packed beds that are able to transmit axial into radial stresses by interparticle contacts. The axial stress is assumed resulting from the momentum exchange taking place at the front of the moving slug where particles of the stationary layer are picked up and accelerated to the velocity of the slug. Part of this frontal stress, which depends principally on slug velocity and height of the settled layer in front of the slug is assumed to be transmitted through the slug of packed particles to the pipe wall where it generates a shear stress. The calculations presented in this work showed that for those models reviewed that are built on force balances for a moving slug, the greatest part of the pressure loss occurring in slug flow results from the friction force due to this stress transmission. In the models, the amount of stress transmitted is influenced by the stress transmission coefficient whose value affects the prediction results significantly.

However, the stress transmission coefficient has rarely been measured successfully by experiments. In some cases accurate stress measurement devices were available, but in the experiments the authors failed to reproduce the actual transport conditions that occur during slug flow pneumatic conveying or in other studies the measurements took place directly in the conveying pipe but the results were not reliable due to inadequate measuring devices. As a consequence, the Mohr circle has been generally used to determine the range in which the stress state must lie, i.e. active or passive failure. In calculations, it has to be assumed that either an active or passive stress case exists, i.e. pulling or pushing failure occurs.

In order to apply Mohr's circle theory, a key condition is that slugs display a density equal to the bulk density. In order to check if this condition prevailed in the slugs of plastic pellets investigated, a special system was developed to catch horizontal moving slugs during the conveying process. With the aid of a spring-loaded system, the slug-catcher is able to catch a moving slug in a fraction of a second and separate it simultaneously into three horizontal layers. Therefore, not only the internal porosity but also the presence of a porosity gradient over the slug height could be investigated. The porosity within a slug was found to be independent of the conveying velocity, with values between 0.40 and 0.42, i.e. the slug porosity was slightly higher than the bulk porosity of 0.38. As a consequence, the slugs investigated can be considered as slightly fluidised entities. As a further result, no significant porosity gradient was detected over the slug height.

In a different approach, the slug porosity was also determined indirectly from local pressure measurements by applying the semi-empirical equation of Ergun. This method permits to investigate the porosity trend over the slug length. The model of Ergun describes the pressure loss through homogeneous bulk solids columns with a constant porosity over its cross-section. Although the use of the slug-catcher did not reveal any density gradient over the slug height, the effect of an inhomogeneous density distribution on the calculated Ergun porosity was investigated. The results showed that for a mean porosity of 0.41 the presence of either a uniform or non-uniform particle distribution over the pipe height did not affect significantly the result of the porosity calculation. Therefore, the equation of Ergun is suitable to investigate the porosity trend over slugs as conveyed in this study.

Slugs in a stable state were found to display porosity that decreased over the slug length, i.e. most of the slugs were denser at the rear. However, other slugs were found to display lower density at the rear compared to the front end whereas some slugs displayed relatively constant porosity over their entire length. No general rule could be found regarding the porosity trend exhibited by the slugs. The Ergun porosity was not affected by the conveying gas velocity and slugs displayed porosity values higher than the bulk porosity itself, mostly between 0.4 and 0.6. It was also found that short and long slugs displayed similar values and trends.

The free volume of air contained in the slugs was found to be significant, which indicates that not enough contacts exist between individual particles within the slug to permit the transmission of stresses across the slug cross-section. However, each single slug was found to induce high levels of radial and wall shear stresses. The stresses were measured using the measurement probe initially developed by Niederreiter to investigate stress states of vertical moving slugs. Besides pressure sensors, the probe included two force sensors perpendicular to each other to permit a simultaneous and in-situ measurement of radial and wall shear stresses during the conveying process. The measurement principle of the probe was optimised to allow accurate detection of the stresses at a sampling frequency of 10,000 Hz. The probe was then used to measure radial and wall shear stresses induced by slugs moving horizontally at different positions around the circumference of the pipe, i.e. top, bottom and side of the pipe. Each single slug induces significant radial and wall shear stresses around the entire pipeline circumference that disappear immediately after the slug passes. Although radial and wall shear stresses follow a similar trend, slugs always induced a higher radial stress than wall shear stress. In most theoretical approaches,

Coulomb's failure criterion is assumed to apply at the boundary between the particles and the wall. However, investigations on the ratio between the wall shear stress and the radial stress showed that this ratio does not correspond to the wall friction coefficient. Hence, the assumption that the Coulomb failure criterion applies could not be validated, i.e. another type of relationship prevails between the wall shear stress and the radial stress as induced by the moving slugs.

Both the radial and wall shear stress distribution were found to be non-uniform across the pipe cross-section. The highest stresses were detected at the side of the pipe whereas the lowest stresses were measured at the pipeline top. For both the radial and wall shear stress, the stress values measured at the pipeline bottom are in between the values at the top and side. This contradicts the common assumption that during slug flow pneumatic conveying, the highest stresses are located at the bottom of the pipe due to an additional force caused by the weight of the slug particles. However, for non-fluidised slugs, investigations on the forces required to push such packed columns showed effectively that higher stresses are located at the pipe bottom. Moreover, stresses induced by the non-fluidised bulk solids columns were found to increase considerably with an increase in slug compression over the entire pipe cross-section. In this case, the stresses can be explained solely by bulk solids mechanics. A comparison between stresses induced by non-fluidised slugs and by pneumatically conveyed slugs showed that the stresses induced by horizontal conveyed slugs are similar to the stresses measured in non-fluidised packed columns exhibiting high compression. However, the high level of axial force required to push a packed bed over the length of a pneumatic conveying system cannot be provided by the conveying gas. Therefore, compressed slugs cannot be pneumatically conveyed. A certain degree of internal fluidisation appears to be a fundamental requirement for slugs to be transported pneumatically.

Since bulk solids mechanics could not explain the stresses induced by pneumatically conveyed slugs, subsequent investigations focused on the characteristics of the slugs and the identification of the physical mechanisms involved in slug transport. It was found that the conveying velocity did not significantly affect the stresses at the top of the pipeline, whereas higher stresses were measured at the side and the bottom of the pipeline with an increase in air supply velocity. Due to the force of gravity that acts perpendicularly to the conveying direction, the mechanisms involved in horizontal slug flow conveying are quite different from those present in vertical conveying. In particular, the slug characteristics cannot be assumed as constant across the pipe cross-section. A strong correlation was found between the stresses and the particle velocity, not only over the length of the slugs but also across the pipe circumference. The faster a particle moves in a defined area, the higher the measured stresses. This correlation was particularly significant at the bottom and at the side of the pipe where both the radial and wall shear stress were found to follow the trend of the particle velocity.

Based on the above, the kinetic theory of gas was adopted to explain high values of radial and wall shear stress occurring during slug flow. Each particle within a fluidised slug is in suspension, moving stochastically and therefore ceaselessly collides with other particles. During each collision, a momentum transfer takes place. In close proximity to the wall, particles transfer their entire momentum to the wall, resulting in a wall shear stress. Newton postulated that the shear stress between layers of a fluid is proportional to the viscosity of the medium and the velocity gradient in the direction perpendicular



to the layers. The velocity gradient close to the pipe wall was found to be similar at each location on the pipe circumference and showed only a slight tendency to increase with the conveying velocity. The viscosity of a slug depends on the mass of a particle, mean free path, particle number density and velocity. For a given material, particle mass and mean free path are a constant. Moreover, the research presented in this work showed that the porosity within a slug does not depend on the air velocity, i.e. the number density of particles is independent of conveying velocity. Therefore, the particle velocity was identified as the main factor influencing the stresses at pipe wall. It was found that an increase in the air supply velocity led to a higher particle velocity, which in turn resulted in a higher momentum transfer to the wall and a higher wall shear stress. Particles at the bottom of the pipe induced lower stresses than particles at the side of the pipe because they moved slower in this area.

Depending on the position on the pipe circumference, the kinetic theory was able to predict either the full amount or part of the wall shear stress. These results support the theory that according to the position on the pipe circumference, different physical mechanisms are involved in the contact area between the particles and the pipe wall, i.e. in the formation of the stresses. The application of the kinetic theory permitted to calculate the wall shear stress at the side of the pipe with great accuracy. At the top of the pipe, the contacts or collisions between particles and the wall are counteracted by the force of gravity that acts in the opposite direction. Hence, the stresses at the top wall may be lower than the stresses predicted by the kinetic theory. However, the presence of a narrow channel at the top of the pipe where the gas velocity is higher may also lead to collisions between particles and wall where higher momenta are transferred, which result in higher stresses. At the bottom of the pipe, the kinetic theory was able to describe only one part of the stress measured during slug flow pneumatic conveying. The remaining stress may be caused by the friction of the slug sliding on the pipe wall.

Application of the kinetic theory did not only allow to predict the mean wall shear stress along a slug but also accurately described the wall shear stress along the slugs. For all conveying velocities where slug flow took place, the kinetic theory could be successfully applied to accurately describe the wall shear stress at the side of the pipe. The results presented in this research demonstrate that the high stresses induced by a slug on the pipe wall are a result of the stochastic agitation of the suspended particles composing the slug.

Since slugs are slightly fluidised, no axial stress exists inside a slug and the retarding force is principally due to the shear stress on the walls resulting from the momentum exchange of particles hitting the pipe wall. Therefore, if the wall shear stress can be calculated accurately, the pressure loss necessary to overcome the friction forces and permit the transport of slugs can be determined. The pressure loss over single slugs could be predicted satisfactorily by applying the kinetic theory. The calculation of the pressure loss along a slug required accurate determination of particle velocity, porosity and the radial stress profile along a slug. It was found that the radial stress is not distributed uniformly across the pipe circumference. Therefore, to predict the pressure profile of a single slug, the radial stress must be integrated along the pipe circumference. However, the stress measurement probe delivered radial stress values for only one location on the pipe circumference per slug. As a consequence, the accuracy of the prediction of the pressure loss profile for a given slug was limited. However, for design purposes, the

total pressure loss over the length of the pipe is needed rather than the pressure loss over a single slug. Therefore, the use of average values that describe the process entirely appears more convenient.

For a given pipe diameter, the main part of the pressure loss depends principally on the wall shear stress and on the surface on which it acts, i.e. the total length of slugs. The prediction of the pressure loss for a whole pipe system requires the knowledge of the correlations between wall shear stress, slug velocity, radial stress and slug porosity. Investigations carried out in this work showed that a strong correlation exists between the wall shear stress and particle velocity but no correlation between the particle and slug velocities was established. Furthermore, investigations into the so-called friction factor describing the ratio of the wall shear stress to the radial stress for cohesionless materials showed that this ratio is relatively constant in the area of stable slug flow. Finally, no significant correlation between the porosity and the radial and wall shear stresses could be found.

The most important factor influencing the wall shear stress is the velocity of the particles composing the slugs. However, it was shown that the particle velocity is not only a function of the air supply velocity but also varies along the length of a slug. Furthermore, the velocity profile across a slug is a function of the height of the stationary layer in front of it. Since the particle velocity is a function of many key parameters, its prediction is difficult. Therefore, one solution is to assume the mean particle velocity to be equal to the slug velocity. Because the slug velocity is a parameter in the equation for the total length of slugs which is necessary to calculate the total pressure loss, this assumption permits to eliminate the slug velocity from the final expression. This presents great advantage in that the equation for the total pressure loss is now independent of the particle and slug velocities. Besides the material characteristics and pipe dimensions, only radial stress, slug porosity, solids mass flow rate and fraction of the pipe cross-section covered by the stationary layer affect the total pressure loss. The research presented in this work showed that the influence of each of these parameters on the pressure loss is similar. However, an increase in the fraction of the pipe cross-section covered by the stationary layer above 60% leads to an exponential increase of the pressure loss. This illustrates a fact frequently observed in pneumatic conveying: once the layer of settled particles reaches a certain height, blockage of the pipeline occurs.

Because the slug porosity was found to be independent of the conveying velocity, i.e. it is constant for a given material, the pressure loss at a given solids mass flow rate only depends on the radial stress and the height of the layer of settled particles. The fraction of the pipe cross-section covered by particles decreases when the air velocity increases. It was shown by experiments that this fraction can be accurately predicted by the equation Konrad developed based on a gas-liquid analogy. However, Konrad's equation requires the prediction or measurement of the slug velocity. For a given particle number density, the radial stress can be calculated if the particle velocity perpendicular to the wall is known. Therefore, the knowledge of particle velocity, i.e. slug velocity, is a key requirement to calculate the pressure loss without knowledge of other parameters than the material characteristics and pipe layout.

The kinetic theory was successfully applied to predict the pressure loss along the two-meters long pipeline section where slug characteristics were measured. By applying the kinetic theory to calculate

the wall shear stress and using a mass balance of the entire pipe system to predict the total length of slugs, the pressure loss could be calculated very accurately as long as stable slug flow occurred. However, the extrapolation of the slug characteristics measured in a defined area to other pipe sections located downstream led to overprediction of the pressure loss in additional horizontal pipe sections. In fact, the transport cannot be assumed as taking place in the same conditions over the entire pipeline length. Due to the significant pressure gradient that is observed in slug flow pneumatic conveying, the velocity of the conveying air increases significantly along the length of the pipe. This results in significant changes of slug and transport characteristics such as particle velocity, radial stress and height of the layer of settled particles along the pipeline. These changes have to be considered to achieve accurate pressure loss prediction over the entire pipeline. Hence, correlations between the most important slug characteristics must be established.

In slug flow conveying area, an increase in air velocity leads to an increase in slug velocity and a decrease in slug length whereas the slug frequency remains unaffected. When the air velocity increases, a bigger volume of particles can be transported in each slug due to a decrease in the height of the stationary layer. Hence, even if the total length of slugs in the entire pipeline decreases, an increase in air supply velocity leads to the increase of the solids mass flow rate. In fact, in the conveying system used for the experimental investigations, it was observed that an increase in air supply velocity was accompanied by a linear increase of both solids mass flow rate and slug velocity up to a turning point where a further increase in air velocity would have decreased the system performance. Moreover, a correlation was found between the height of the stationary layer between two slugs and the slug velocity. Slugs tend to move faster if the stationary layer in front of them is of less height. Furthermore, the height of the particle layer left behind, i.e. the fraction of the cross-section covered by the stationary layer tends to be smaller if the slugs move faster. In addition, a strong correlation was found between the height of the stationary layer between two slugs, the shape of the front and rear of a slug, the particle velocity profile and the porosity profile over the slug length. In turn, these characteristics significantly influence the stresses at the pipe wall and hence the pressure loss.

Most of the slugs investigated in this research displayed similar characteristics: The stresses induced by the slugs are often higher at the rear where particles move faster and where the slug is denser. This type of behaviour is indicative of stable moving slugs, which are characterised by their capacity of moving in form of a slightly fluidised particles mass with a well-defined front and rear. Due to a positive velocity gradient over the slug length, the closer the particles are to the back of the slug, the faster they move. Hence, during transport, the particles located at the back tend to move closer to the particles in front of them so that the porosity decreases towards the rear of the slug and the slug becomes shorter until there is no porosity gradient over the slug length. The mass of particles transported within the slug remains unchanged.

Some slugs were characterised by a negative particle velocity gradient over the length of the slug. Further, instead of an increase in density over the slug length, as observed for the majority of slugs, some slugs displayed porosity that remained constant or even slightly increased from the front to the back face of the slugs. The closer the particles are to the front face, the faster they move, leading to

the slug tendency to extend. Each particle tends to gain some space on the particles following it. If particles at the front face move significantly faster, those particles may part from the rest of the slug and form a short slug on their own. This slug may grow further. Hence, there is the possibility for slugs to extend from the rear in the direction of the flow. However, this is characteristic of a slug in an unstable state, a slug that extends but can also lose material by separation of the front part due to a higher velocity of the particles in this area. Such slugs are characterised by a diffuse front end and a flat tail and also have a tendency to leave a higher layer of settled particles behind it.

The height of the layer of stationary particles between two slugs is the most important influence leading to pipe blockage. Calculations have shown that for the granular material investigated in this work, the pressure loss along the pipe increases exponentially when the fraction of the pipe cross-section covered by stationary particles increases past 60 %. In the case of a cohesionless granular material, pipe blockages mostly clear themselves without further intervention such as increasing the air supply velocity. This is due to the capacity of individual particles composing a slug to rearrange themselves to permit better percolation of the air as is required for transport. Blockages occur when a slug exhibiting a denser front end than rear is not able to pick up and accelerate all particles of the high stationary layer in front of it. The slug density increases to bulk density and the degree of internal fluidisation is insufficient to keep conveying and resistance forces in balance. Axial stresses arise, which are partly transmitted to the pipe wall through interparticles contacts. Until air percolation through the slug improves, the slug transport is stopped and the pressure upstream increases. Once the pressure is high enough to overcome the friction forces at the pipe wall, the entire slug moves forward by a small distance. During this movement, particles rearrange themselves but the rapid decrease of pressure behind the slug leads to a new blockage. This process repeats itself until the particle rearrangement is optimal, i.e. the porosity reaches a critical value to allow the transport to continue. Experimental investigations carried out in this study showed that a certain degree of fluidisation is required for slug transport.

The presence of a significant degree of internal fluidisation in horizontal slugs suggests the presence of an air velocity gradient over the pipe height. In this study, the use of a slug-catcher to investigate internal slug porosity did not reveal any significant density gradient over the slug height. However, a free channel is commonly observed at the top of the pipe during slug flow pneumatic conveying in systems with bigger pipe diameters. According to Bernoulli, the presence of a velocity gradient would generate a lifting force proportional to the difference in dynamic pressure. The theoretical calculations presented in this work showed that Bernoulli's principle may play a significant role in slug transport. As a result of the lifting force, the particles are lifted and go into suspension over the pipe cross-section. This suspension is easier transported by the conveying gas compared to a compact mass of particles. As soon as this suspension is uniformly distributed over the pipe cross-section, the channel at the top of the pipe where the air velocity was higher ceases to exist. The flow rearranges and the velocity gradient over the pipe height disappears. The lifting force resulting from Bernoulli's principle ceases to exist as well and the particles begin to settle again. The channel at the top of the pipe eventually reappears and the same process is repeated. This cycle occurs continuously and facilitates the transport of slugs along the pipeline. The smaller the free pipe cross-section, the higher the air velocity over the layer and the greater the ability of the stream to pick up particles.

The main objective of this research work was to investigate the physical mechanisms involved in slug transport. It was shown that the momentum exchange of particles impacting the pipe wall and the resulting macroscopic viscosity of the slugs are the key parameters responsible for the significant pressure loss observed during slug flow. Based on these findings, a new calculation procedure based on the kinetic theory of gas was proposed to predict the pressure loss during slug flow pneumatic conveying. Experimental investigations showed that an accurate prediction requires the determination of important transport characteristics like solids mass flow rate, slug velocity, slug porosity and height of the stationary layer between two slugs. Since these parameters depend on the air velocity, which increases along the length of the pipe as the pressure decreases, the air velocity needs to be considered in the calculation models. The main physical mechanisms involved in horizontal slug flow pneumatic conveying of granular materials were identified and quantified. Through experimental and theoretical investigations, some of the basic concepts used in existing prediction procedures were validated or critically evaluated. This work contributes substantially to the physical understanding of horizontal slug flow pneumatic conveying.

## 7. Outlook

The wall shear stress induced at the pipe wall by moving slugs in stable state was described very accurately by applying the kinetic theory of gas. This indicates that the main resistance force to the slug motion, i.e. the main part of the pressure loss, which characterises slug flow pneumatic conveying is due to the momentum exchange of the particles hitting the pipe wall. Based on this theory, a model to predict the pressure loss (Eq. 5.23) was developed and successfully applied to calculate the pressure loss in the conveying pipe as long as stable slug flow takes place. The expression correlates the pressure loss with the radial stress, mean porosity of a slug in fluidised state and fraction of the pipe area covered by the layer of particles lying at the pipe bottom between two slugs. In comparison to other correlations existing in the field of slug flow pneumatic conveying, this model presents the advantage that particle and slug velocities are no further required for the calculation.

For the material tested in this research, the slug porosity was found to be independent on the air supply velocity. However, further work should show if the porosity a slug displays during horizontal pneumatic conveying is only a function of the material characteristics. As a further result, it was found that an increase in the air velocity leads to the increase of the radial stress and the decrease of the pipe area covered by the layer of settled particles. This is due to the particle velocity, which increases as the air velocity increases. In fact, the radial stress is a function of the particle velocity normal to the wall. Moreover, it was found that the correlation Konrad developed based on a gas-liquid analogy can be applied to predict the part of the pipe area covered by the layer of stationary particles if the particle velocity is known. Therefore, further investigations are required to establish an accurate correlation between particle and air velocity.

The results of the experimental investigations presented in this work showed that the stress distribution at the pipe wall is not uniform around the pipe circumference. Although slugs are slightly fluidised structures, it was found that the application of the impulse theory underpredicts the stresses induced by slugs at the bottom of the pipe. This indicates that additional forces act at the pipe bottom. Therefore, further investigations should focus on the co-existence of particle impulses and a wall friction force due to the weight of the slug sliding along the pipe.

Most of the existing models to predict the pressure loss in slug flow pneumatic conveying use both the theory based on bulk solids mechanics and fluid flow through packed beds. However, the results presented in this work showed that high levels of stresses exist, even though a slug is not compressed. The material investigated consisted of Polypropylene pellets with an equivalent diameter of 3 mm. This material has been chosen not only because it represents a typical product conveyed pneumatically but also because of its physical properties and ability to be pneumatically conveyed. Moreover, many investigations found in the literature involved a similar material, so that the results obtained during this research work and former works could be compared. However, additional investigations involving other materials are required. The probe used to measure the radial and wall shear stresses can be employed without further changes to investigate all kind of materials as long as the particle size is bigger than 1 mm diameter, i.e. bigger than the holes drilled in the probe to allow a rapid pressure equilibrium

between the front and the back face of the measurement plate. This pressure equilibrium is required to ensure accurate measurements. To investigate powders, another system should be used to permit a rapid pressure equilibrium such as air permeable membranes.

Even though many attempts have been made to develop a reliable predictive approach for pressure loss, very few authors considered in their models the changes in the conveying gas density along the pipeline. Hence, they recommended to predict the pressure loss only for a short pipeline section and proposed a stepwise calculation procedure. All key parameters for an accurate prediction of the pressure loss were found to be slightly correlated to the particle velocity, which in turn is a function of the air velocity. The air velocity increases along the pipeline as the pressure decreases. Because of the significant pressure gradient that characterises slug flow pneumatic conveying, the increase in the air velocity and the effects on the key parameters cannot be neglected. Therefore, the establishment of an accurate model to predict the pressure loss requires the gas expansion to be taken into account.

To simplify the development of predictive models, steady state conditions are usually assumed to describe slug flow pneumatic conveying. However, due to the nature of discontinuous flow, slug flow is characterised by high pressure fluctuations. Therefore, further investigations should focus on the tracing of the system pressure for industrial scale systems in order to identify potential conveying problems such as blockages and unstable zones [82].

## References

- [1] P. Atkins: Atkins' Physical Chemistry. 8<sup>th</sup> ed. Oxford: Oxford University Press. (2006)
- [2] Z.B. Aziz and G.E. Klinzing: Plug flow transport of cohesive coal: Horizontal and inclined flows. Powder Technology 55, pp. 97-105 (1988)
- [3] Z.B. Aziz and G.E. Klinzing: Optimizing the performance of a plug flow system. Powder Technology 62, pp. 77-84 (1990)
- [4] W. Barth: Strömungstechnische Probleme der Verfahrenstechnik. Chemie Ingenieur Technik 16 (1), pp. 29-34 (1954)
- [5] W. Batel: Kennzeichnung der Zwischenräume in Schüttgütern im Hinblick auf verfahrenstechnische Prozesse. Chemie Ingenieur Technik 31 (6), pp. 388-393 (1959)
- [6] F.E. Blake: Transactions of the American Institute of Chemical Engineers 14, p. 415 (1922)
- [7] H. Blasius: Grenzschichten in Flüssigkeiten mit kleiner Reibung. Z. Math. Phys. 56, pp. 1-37 (1908)
- [8] M. Bohnet: VDI-Forschungsheft 507 (1965)
- [9] M. Bohnet: Fortschritte bei der Auslegung pneumatischer Förderanlagen. Chemie Ingenieur Technik Nr.7, pp. 524-539 (1983)
- [10] T. Brooke Benjamin: Gravity currents and related phenomena. Journal of Fluid Mechanics 31 (2), pp. 209-248, Section 3 (1968)
- [11] S.P. Burke and W.B. Plummer: Gas flow through packed columns, Ind. Eng. Chem. 20, pp. 1196-1200 (1928)
- [12] F.J. Cabrejos and G. Klinzing: Incipient motion of solid particles in horizontal pneumatic conveying 72, pp. 51-61 (1992)
- [13] C.W. Cairns, A. Levy and D.J. Mason: Detection of wave-like gas-solids flow in a horizontal pipe using pressure difference technique. Sensors Series: Sensors and their Applications VIII, Institute of Physics Publications and A.T. Augousti, N.M. White (Eds.), England, pp. 95-100 (1997)
- [14] P.C. Carman: Fluid flow through granular beds. Transactions of the Institution of Chemical Engineers 15, pp. 150-166 (1937)
- [15] K. Daoud, A. Ould Dris, P. Guigon and J.F. Large: Experimental study of horizontal plug flow of cohesionless bulk solids. Kona 11, pp. 119-124 (1993)



- [16] H. Darcy: Les Fontaines Publiques de la Ville de Dijon ("The Public Fountains of the Town of Dijon"), Dalmont, Paris (1856)
- [17] J.F. Davidson and D. Harrison: Fluidized Particles, Cambridge University Press, New York (1963)
- [18] J.T. Davies: Calculation of critical velocities to maintain solids in suspension in horizontal pipes. *Chemical Engineering Science* 42/7, pp. 1667-1670 (1987)
- [19] R. Di Felice and L.G. Gibilaro: Wall effects for the pressure drop in fixed beds. *Chemical Engineering Science* 59, pp. 3037-3040 (2004)
- [20] G. Dixon: How do different powders behave? In: Proceedings of the conference "Pneumatic Conveying", London, January 16-18 (1979)
- [21] S.V. Dhodapkar, S.I. Plasynski and G.E. Klinzing: Plug flow movement of solids. *Powder Technology* 81, pp. 2-7 (1994)
- [22] B. Einfeld and K. Schnitzlein: The influence of confining walls on the pressure drop in packed beds. *Chemical Engineering Science* 56, pp. 4321-4329 (2001)
- [23] S. Ergun: Fluid flow through packed columns. *Chemical Engineering Progress* 48, pp. 89-94 (1952)
- [24] R. Fand and R. Thinakaran: The influence of the wall on flow through pipes packed with spheres. *Journal of Fluids Engineering* 112, pp. 84-88 (1990)
- [25] W. Flatt: Grundbuch für die pneumatische Förderung. Gebrüder Bühler AG, Uzwil, Switzerland (1975)
- [26] W. Flatt and W. Allenspach: Erhöhung der Foerderleistung und Verbessern des Wirkungsgrades pneumatischer Foerderanlagen. *Chemie Ingenieur Technik* 41(21), pp. 1173-1176 (1969)
- [27] P. Forchheimer: *Hydraulik*. Third Edition, Teubner, Leipzig, Berlin (1930)
- [28] J. Gasterstädt: Die experimentelle Untersuchung des pneumatischen Foerdervorganges. VDI-Forschungsheft 265, Berlin (1924)
- [29] [35] D. Geldart: Types of gas fluidization. *Powder Technology* 7, pp. 285-292 (1973)
- [30] R.J. Hill, D.L. Koch and A.J.C. Ladd: Moderate-Reynolds-number flows in ordered and random arrays of spheres. *Journal of Fluid Mechanics* 448, pp. 243-278 (2001)
- [31] R.J. Hitt: An investigation into the low velocity pneumatic conveying of bulk solids, PhD Thesis, Thames Polytechnic, London, UK (1985)

- [32] H.A. Janssen: Versuche über Getreidedruck in Silozellen. Zeitschrift des Vereines deutscher Ingenieure 39, pp. 1045-1049 (1895)
- [33] M.G. Jones and D. Mills: Product classification for pneumatic conveying. Powder Handling and Processing 2(2), pp. 117-122 (1990)
- [34] T. Kano: Reduction of power consumption in pneumatic conveying of granular materials through a pipeline. Kona, 2, pp. 24-35 (1984)
- [35] T. Kano, F. Takeuchi, H. Sugiyama and E. Yamazaki: A study of the optimum conditions for plug-type pneumatic conveying of granular materials. International Chemical Engineering 24 (4), pp. 702-709 (1984)
- [36] G.E. Klinzing, N.D. Rohatgi, A. Zaltash and C.A. Myler: Pneumatic transport - A review (Generalized phase diagram approach to pneumatic transport). Powder Technology, 51, pp. 135-149 (1987)
- [37] K. Konrad: Boundary element prediction of the free surface shape between two particle plugs in a horizontal pneumatic transport pipeline. The Canadian Journal of Chemical Engineering Vol. 66 (1988).
- [38] K. Konrad, D. Harrison, J.F. Davidson and R.M. Nedderman: Prediction of the pressure drop for horizontal dense phase pneumatic conveying of particles. In Pneumotransport 5, Proceedings of International Conference on Pneumatic Transport of Solids in Pipes. BHRA Fluid Engineering, U.K. pp. 225-244 (1980)
- [39] T. Krull: Slug flow pneumatic conveying: Stress field analysis and pressure drop prediction. PhD thesis, The University of Newcastle, Australia (2005)
- [40] S.B. Kuang, K.W. Chu, A.B. Yu, Z.S. Zou and Y.Q. Feng: Computational investigation of horizontal slug flow in pneumatic conveying. Ind. Eng. Chem. Res. 47, pp. 470-480 (2008)
- [41] D. Legel and J. Schwedes: Investigation of pneumatic conveying of plugs of cohesionless bulk solids in horizontal pipes. Bulk Solids Handling 4 (2), pp. 53-59 (1984)
- [42] A. Levy: Two-fluid approach for plug flow simulations in horizontal pneumatic conveying. Powder Technology 112, pp. 263-272 (2000)
- [43] A. Lippert: Chemie Ingenieur Technik 38, p. 350 (1966)
- [44] N.J. Mainwaring and A.R. Reed: Permeability and air retention characteristics of bulk solid materials in relation to modes of dense-phase conveying. Bulk Solids Handling, 7, pp. 415-425 (1987)
- [45] D.J. Mason: A study of the modes of gas-solids flow in pipelines. PhD thesis, Thames Polytechnic, UK (1991)

- [46] D.J. Mason, E.A. Knight, C.W. Cairns and J.R. Pugh: An investigation of wave-like gas-solids flow in pipelines using a variety of measurement techniques. In Proceedings of the ASME Heat Transfer Fluids Eng. Div., pp. 525-529 (1995)
- [47] D.J. Mason and J. Li: A novel experimental technique for the investigation of gas-flow in pipes. *Powder Technology* 112, pp. 203-212 (2000)
- [48] S. Matsumoto, M. Kikuta and S. Maeda: Effect of particle size on the minimum transport velocity for horizontal pneumatic conveying of solids. *Journal of Chemical Engineering of Japan* 10 (4), pp. 273-279 (1977)
- [49] S. Meyers, R. Marcus and F. Rizk: The state diagram for fine-particle gas/solids suspensions, *Bulk Solids Handling* 5 (4), pp. 779-782 (1985)
- [50] B. Mi and P.W. Wypych: Particle slug velocities in horizontal slug-flow pneumatic conveying. *Powder Handling and Processing* 5 (3), pp. 227-233 (1993)
- [51] B. Mi and P.W. Wypych: Pressure drop prediction in low-velocity pneumatic conveying. *Powder Technology* 81, pp. 125-137 (1994)
- [52] B. Mi and P.W. Wypych: Investigations into wall pressure during slug-flow pneumatic conveying. *Powder technology* 84, pp. 91-98 (1995)
- [53] D. Mills: *Pneumatic conveying design guide*. Elsevier Butterworth-Heinemann, Second Edition (2004)
- [54] O. Molerus: *Fluid-Feststoff-Strömung - Strömungsverhalten feststoffbeladener Fluide und kohäsiver Schüttgüter*. Springer Verlag Berlin, pp. 134-156 (1982)
- [55] O. Molerus: Overview: Pneumatic transport of solids. *Powder technology* 88, pp. 309-321 (1996)
- [56] O. Molerus and A. Burschka: Pneumatic transport of coarse-grained materials. *Chemical Engineering and Processing* 34, pp. 173-184 (1985)
- [57] E. Muschelknautz: Theoretische und experimentelle Untersuchungen über die Druckverluste pneumatischer Förderleitungen unter besonderer Berücksichtigung des Einflusses von Gutreibung und Gutgewicht. *VDI-Forschungsheft* 476 (1959)
- [58] E. Muschelkanutz and W. Krambrock: Vereinfachte Berechnung horizontaler pneumatischer Förderleitungen bei hoher Gutbeladung mit feinkörnigen Produkten. *Chemie Ingenieur Technik* 41, Nr. 21 (1969)
- [59] D. Nemeč and J. Levec: Flow through packed bed reactors: 1. Single-phase flow. *Chemical engineering Science* 60:24, pp. 6947-6957 (2005)

- [60] G. Niederreiter: Untersuchung zur Pfropfenentstehung und Pfropfenstabilität bei der pneumatischen Dichtstromförderung, PhD thesis, Technische Universität München (2005)
- [61] B. Oesterlé and A. Petitjean: Simulation of particle-to-particle interactions in gas–solid flows. *Int. J. Multiphase Flow* 19, pp. 199-211 (1993)
- [62] R. Pan and P.W. Wypych: Pressure drop prediction in single-slug pneumatic conveying. *Powder Handling and Processing* 7 (1), pp. 63-68 (1995)
- [63] P.S. Ramachandran, D.G. Burkhard and B.E. Lauer: Studies of dense phase horizontal flow of solids-gas mixtures. *Indian Journal of Technology* 8, pp. 199-204 (1970)
- [64] T. Ramakrishnan, K. Ramakoteswara Rao, M.A. Parameswaran and S. Sivakumar: Experimental investigation of a dense-phase pneumatic transport system. *Chemical Engineering and Processing*, 32, pp. 141-147 (1993)
- [65] K. Ridgway and K.J. Tarbuck: Radial voidage variation in randomly-packed beds of spheres of different sizes. *J. Pharm, Pharmac.* 18, pp. 168-175, (1966)
- [66] F. Rizk: A comparison between horizontal and vertical pneumatic conveying systems considering the optimal operating conditions. In proceedings of the conference "PNEUMATECH 1", 3-5 May (1982)
- [67] K. Rottschäfer: Geschwindigkeitsverteilungen in durchströmten Füllkörperschüttungen, PhD thesis, Technische Universität München, 1997
- [68] H. Rumpf and A.R. Gupte: Einflüsse der Porosität und Korngrößenverteilung im Widerstandsgesetz der Porenströmung. *Chemie Ingenieur Technik* 43, pp. 367–375 (1971)
- [69] L. Sanchez, N. Vasquez, G.E. Klinzing and S. Dhodapkar: Characterization of bulk solids to assess dense phase pneumatic conveying. *Powder Technology* 138, 93-117 (2003)
- [70] L. Sanchez, N.A. Vasquez, G.E. Klinzing and S. Dhodapkar: Evaluation of models and correlations for pressure drop estimation in dense phase pneumatic conveying and an experimental analysis. *Powder Technology* 153, pp. 142-147 (2005).
- [71] D. Schulze: *Powders and bulk solids - Behavior, characterization, storage and flow.* Springer-Verlag Berlin Heidelberg New York, 511 pages (2008)
- [72] E. Schürfer: *Elektrische Messtechnik*, 8. Auflage, Carl Hanser Verlag, München (2004)
- [73] G. Segler: *Untersuchungen an Körnergebläsen und Grundlagen für ihre Berechnung.* R.K.T.L (1934)
- [74] G.W. Segler and W. Hutt: *Grundlagen der Landtechnik* 29(1), pp. 13-19 (1979)

- [75] C.E. Shannon: Communication in the presence of noise, Proc. Institute of Radio Engineers, Vol. 37, No.1, pp. 10-21 (1949). Reprint as classic paper in: Proc. IEEE, Vol. 86, No. 2 (1998)
- [76] W. Siegel: VDI-Forschungsheft 532 (1969)
- [77] W. Siegel: VDI-Forschungsheft 538 (1970)
- [78] W. Siegel: Grundlagen der pneumatischen Pfröpfenförderung. Schüttgut 1, Nr. 1 (1995)
- [79] M. Sommerfeld: Analysis of collision effects for turbulent gas-particle flow in a horizontal channel: Part I. Particle transport. International Journal of Multiphase Flow 29, pp. 675-699 (2003)
- [80] M. Sommerfeld and G. Zivkovic: Recent advances in the numerical simulation of pneumatic conveying through pipe systems. Computational Methods in Applied Science, Invited Lectures and Special Technological Sessions of the First European Computational Fluid Dynamics Conference and the First European Conference on Numerical Methods in Engineering. Ch. Hirsch, J. Periaux and E. Onate (Eds), Brussels. pp. 201-212 (1992)
- [81] M. Sperl: Experiments on corn pressure in silo cells - translation and comment of Janssen's paper from 1895. Granular Matter 8, pp. 59-65 (2006)
- [82] S. Tan, K.C. Williams and M.G. Jones: Tracing system pressure of dense phase pneumatic conveying for industrial application. In: Proceedings of the Conference World Congress of Particle Technology WCPT6, Nuernberg, Germany (2010)
- [83] Y. Tomita and K. Tateishi: Pneumatic slug conveying in a horizontal pipeline. Powder Technology 94, pp. 229-233 (1997)
- [84] R.D. Toomey and H.F. Johnstone: Gaseous fluidization of solid particles. Chemical Engineering Progress 48, p. 200 (1952)
- [85] N. Vasquez, L. Sanchez and G.E. Klinzing: Dense-phase plug flow analysis: Experimental findings. In: Proceedings of the Conference World Congress of Particle Technology WCPT4, Sydney, Australia (2002)
- [86] VDI-Wärmeatlas. VDI Gesellschaft (Ed.), 1500 pages, 10th Edition (2006)
- [87] W. Wang and Y. Li: Hydrodynamic simulation of fluidization by using a modified kinetic theory. Ind. Eng. Chem. Res. 40, pp. 5066-5073 (2001)
- [88] M. Weber: Correlation analysis in the design of pneumatic transport plant. Bulk Solids Handling 2, pp. 231-233 (1982)

- [89] M. Weber: Friction of the air and the air/solid mixture in pneumatic conveying. *Bulk solids handling* 11:1, p. 99-102 (1991)
- [90] G. Welschhof: Pneumatische Förderung bei grossen Fördergutkonzentrationen. *VDI-Forschungsheft* 492, Duesseldorf (1962)
- [91] C.Y. Wen. In: *Fluidization*. J.F. Davidson and D. Harrison (Eds.), Academic Press, London, pp. 675 (1971)
- [92] C.Y. Wen and H.P. Simons: Flow characteristics in horizontal fluidized solids transport, *AIChE Journal* 5, p. 263 (1959)
- [93] K.C. Williams, M.G. Jones, B. Singh and T. Olszewski: Electrical Capacitance tomography of dense-phase pneumatic conveying of fly ash. In: *Proceedings of Bulk Europe 2008*, Prague, Czech Republic (2008)
- [94] K.C. Wilson, M. Streat and R.A. Bantin: Slip-model correlation of dense two-phase flow. In: *Proceedings of the Conference Hydrotransport 2*, Paper B1. BHRA Fluid Engineering, U.K. (1972)
- [95] M. Winterburg and E. Tsotsas: Impact of tube-to-particle-diameter ratio on the pressure drop in packed beds. *A.I.Ch.E. Journal* 46, pp. 1084-1088 (2000)
- [96] K.-E. Wirth: PhD thesis, University of Erlangen-Nürnberg (1980)
- [97] K.-E. Wirth: Die Grundlagen der pneumatischen Förderung. *Chemie Ingenieur Technik* 55 (2), pp. 110-122 (1983)
- [98] K.-E. Wirth and O. Molerus: Critical solids transport velocity with horizontal pneumatic conveying. *Journal of Powder & Bulk Solids Technology* 9 (1), pp. 17-24 (1985)
- [99] P.W. Wypych and J. Yi: Minimum transport boundary for horizontal dense-phase pneumatic conveying of granular materials. *Powder Technology* 129, pp. 111-121 (2003)
- [100] J. Yi: Transport boundaries for pneumatic conveying. PhD thesis, University of Wollongong (2001)
- [101] F.A. Zenz and D.F. Othmer: *Fluidization and fluid-particle systems*, Rheinhold, New-York (1960)
- [102] E.E. Zukoski: Influence of viscosity, surface tension, and inclination angle on motion of long bubbles in closed tubes. *Journal of Fluid Mechanics* 25 (4), pp. 821-837 (1966)

## List of own publications

### Articles in Journals and research report:

- I. Lecreps, K. Wolz, K. Sommer: Stress states and porosity within horizontal slug in dense-phase pneumatic conveying. In: *Particulate Science and Technology*, 27(4), 297-313, 2009.
- I. Lecreps, K. Sommer: Spannungen und Porosität innerhalb eines Pfropfens bei der pneumatischen Dichtstromförderung. In: *Chemie Ingenieur Technik*, 80(9), 1417, 2008
- I. Lecreps, K. Sommer: Horizontal dense-phase pneumatic conveying of granular material. In: *Bulk Solids & Powder – Science & Technology*, Vol. 2, 2007
- G. Niederreiter, I. Lecreps, K. Sommer: Untersuchung zur Pfropfenentstehung und Pfropfenstabilität bei der pneumatischen Dichtstromförderung – Experiment und mathematische Modellierung. In: *Final Presentation of the Research program “Behavior of Granular Media”*, Shaker Verlag Aachen, 2006

### Conference papers:

#### Oral presentations:

- I. Lecreps, K. Sommer: Investigations of the physical mechanisms leading to high pressure loss by horizontal slug flow pneumatic conveying. Conference “PARTEC 2010”, Nürnberg, Germany, April 26-29, 2010
- I. Lecreps, K. Sommer: Investigations on single slugs to explain high pressure loss by horizontal slug flow pneumatic conveying. “6th International Conference for Conveying and Handling of Particulate Solids – CHOPS 2009”, Brisbane, Australia, August 3-7, 2009
- I. Lecreps, K. Sommer: Spannungen und Porosität innerhalb eines Pfropfens bei der pneumatischen Dichtstromförderung. ProcessNet-Jahrestagung, Karlsruhe, Germany, Oct. 7-9, 2008
- I. Lecreps, K. Sommer: Investigations on single slugs to explain high pressure loss in horizontal dense-phase pneumatic conveying. Conference “BulkEurope 2008”, Prague, Czech Republic, Sept. 11-12, 2008
- I. Lecreps, K. Sommer: Spannungszustände und Porosität innerhalb eines Pfropfens bei der pneumatischen Dichtstromförderung von Granulaten. Interne VDI-GVC-Fachausschusssitzung „Agglomerations- und Schüttguttechnik“, Freising, Germany, March 10-12, 2008
- I. Lecreps, K. Sommer: Horizontal dense-phase pneumatic conveying. Conference “Particulate Processes in the Pharmaceutical Industry II”, San Juan, Puerto Rico, Feb. 3-8, 2008

- I. Lecreps, K. Sommer: Horizontal dense-phase pneumatic conveying of granular material. "9th International Conference on Bulk Materials Storage, Handling and Transportation – ICBMH 2007", Newcastle, Australia, Oct. 9-11, 2007
- I. Lecreps, K. Sommer: Horizontal dense-phase pneumatic conveying of granular material. "6th International Conference on Multiphase Flow – ICMF07", Leipzig, July 9-13, 2007
- I. Lecreps, K. Sommer: Horizontal dense-phase pneumatic conveying of granular material. Conference "PARTEC 2007", S23-1, Nürnberg, Germany, March 27-29, 2007
- I. Lecreps, K. Sommer: Horizontale pneumatische Dichtstromförderung von Granulaten. Interne VDI-GVC-Fachausschusssitzung „Agglomerations- und Schüttguttechnik“, Dresden, Germany, March 12-14, 2007
- I. Lecreps, K. Sommer: Horizontal dense-phase pneumatic conveying of bulk solids. Conference "Bulk Europe 2006", Barcelona, Spain, Oct. 16-17, 2006
- I. Lecreps, K. Sommer: Horizontale pneumatische Dichtstromförderung. Interne VDI-GVC-Fachausschusssitzung „Agglomerations- und Schüttguttechnik“, Reinbek, Germany, March 20-22, 2006

**Posters:**

- I. Lecreps, K. Sommer: Untersuchungen an Einzelpropfen bei der horizontalen pneumatischen Dichtstromförderung. Interne VDI-GVC-Fachausschusssitzung „Lebensmittel-Verfahrenstechnik“, Lausanne, Switzerland, March 23-24, 2009
- I. Lecreps, K. Sommer: Untersuchungen an Einzelpropfen bei der horizontalen pneumatischen Dichtstromförderung. Interne VDI-GVC-Fachausschusssitzung „Agglomerations- und Schüttguttechnik“, Bad Dürkheim, Germany, March 11-12, 2009
- I. Lecreps, K. Sommer: Stress and porosity within a slug of granular material in slug-flow pneumatic conveying. Conference "International Symposium Reliable Flow of Particulate Solids IV (RELPOWFLOW IV)", Tromsø, Norway, June 10-12, 2008
- I. Lecreps, K. Sommer: Horizontal dense-phase pneumatic conveying of granular material. Conference "Science et Technologie des Poudres 2007", Albi, France, Mai 23-25, 2007



## List of Figures

2.1. The three basic flow types in pneumatic conveying . . . . .	22
2.2. State-diagram for pneumatic conveying of Polypropylene granules ( $d_{eq} = 3.0$ mm) in a 50 mm i.d. pipeline [60] . . . . .	22
2.3. Schematical representation of slug flow as it usually occurs in the reality . . . . .	23
2.4. Schematical state-diagram and terminology as used in this work . . . . .	25
2.5. Pressure loss in gas-particles flow . . . . .	33
2.6. Stresses acting on a compressed slug horizontally conveyed . . . . .	39
2.7. Volume element with the three principal stresses acting perpendicular to each other (on the left hand side); Stress circles corresponding to the three principal stress planes (on the right hand side) . . . . .	40
2.8. Two-dimensional stress state on a volume element . . . . .	40
2.9. Possible states of stress on an element P, represented by a series of Mohr's circles . . . . .	41
2.10. Examples of Mohr circles corresponding to the stress state occurring by slug flow . . . . .	42
2.11. The two Mohr circles corresponding to active and passive stress state for a given couple of values $\tau_w / \sigma_{r/w}$ . . . . .	43
2.12. 3-layer-model proposed by Wypych [99] . . . . .	44
2.13. Example of dimensionless state-diagram for dense-phase pneumatic conveying . . . . .	46
3.1. Force balance on a moving slug . . . . .	57
3.2. Section of the pipe illustrating the hydrostatic pressure . . . . .	58
3.3. Particle balance at the front end of a slug as proposed by Konrad [38] . . . . .	60
3.4. Slug element and acting stresses [100] . . . . .	69
3.5. Height $H$ over which particles of the stationary layer have to be lifted [100] . . . . .	70
3.6. Part of each stress in the total pressure loss according to Yi for $K_w = 1$ . . . . .	73
3.7. $\alpha$ calculated according to the two equations found in the literature . . . . .	74
3.8. Effect of the choice of the expression of $\alpha$ on the calculation of the front stress (on the left hand side) and the total length of slug (on the right hand side) . . . . .	74
3.9. Comparison of the slug velocity obtained by applying different models for slug flow pneumatic conveying . . . . .	75
3.10. Effect of the $K_w$ -value on the pressure loss predicted by applying the models of Konrad, Mi, Pan and Yi . . . . .	76
3.11. Pressure drop prediction by applying the Muschelknautz model . . . . .	79
3.12. Pressure drop prediction with assumption of an active stress case - $K_w = 0.4$ . . . . .	80
3.13. Pressure drop prediction with assumption of a passive stress case - $K_w = 2.3$ . . . . .	80
3.14. Pressure drop prediction with $K_w = 1.0$ . . . . .	81
3.15. Pressure drop prediction with the $K_w$ -value calculated by applying Mi's model - $K_w = 0.8$ . . . . .	81
3.16. Pressure drop prediction with $K_w = 1.0$ for a pipeline of $L = 10$ m length . . . . .	82
3.17. Particle velocity calculated by applying the cubic equation proposed by Konrad $L = 10$ m - $K_w = 1.0$ . . . . .	82
3.18. Influence of the slug porosity on the calculation results . . . . .	84

4.1. Industrial-scale pilot plant: 1. pressure transducer, 2. Plexiglas pipes, 3. probe for force and pressure measurements, 4. CCD camera, 5. slug-catcher, 6. storage silo, 7. pressure tank . . . . .	86
4.2. a) Reference image of a Plexiglas pipe with net; b) Marked points reflecting the net scale	88
4.3. Two successive camera images with superposition of the net used to determine the particle velocity within a slug . . . . .	88
4.4. Image and construction scheme of the probe for the simultaneous detection of wall shear stress, normal stress and pressure inside a slug [60] . . . . .	89
4.5. Perpendicular arrangement of the force sensors in the measurement chamber [60] . . . .	90
4.6. Impulse response of the radial force sensor to the impact of a 3 g heavy steel bullet, $f_{sampling} = 20.000$ Hz . . . . .	91
4.7. Aliasing: The signal reconstructed from samples is different from the original continuous signal . . . . .	93
4.8. Raw signal detected with $f_{sampling} = 100,000$ Hz during the passage of a slug conveyed with 7.4 m/s air velocity . . . . .	94
4.9. Raw signal detected with $f_{sampling} = 100,000$ Hz during the passage of a slug conveyed with 8.0 m/s air velocity . . . . .	95
4.10. Raw signal detected with $f_{sampling} = 40,000$ Hz during the passage of a slug conveyed with 7.4 m/s air velocity . . . . .	95
4.11. Raw signal detected with $f_{sampling} = 10,000$ Hz during the passage of a slug conveyed with 7.4 m/s air velocity . . . . .	96
4.12. Response of the radial force sensor to an impulse before and after application of a Bessel low-pass filter; $f_{sampling} = 10,000$ Hz, $f_g = 25$ Hz . . . . .	97
4.13. Theoretical increase of the estimated frequency of particle impulse on the measurement plate with the increase of the slug velocity . . . . .	98
4.14. Superposition of oscillations - Detail from Fig. 4.8 - $f_{sampling} = 100,000$ Hz, $v_f = 7.4$ m/s . . . . .	99
4.15. Schematic processing of the pressure and force signals . . . . .	100
4.16. Scaling of axial and radial stress sensors using weights [60] . . . . .	101
4.17. Linear correlation between strain and signal detected for both axial and radial force sensors	102
4.18. Rectangular function illustrating schematically the stress behaviour by passage of a slug on the measurement plate . . . . .	103
4.19. Damping behaviour of a Bessel filter of second order . . . . .	103
4.20. Discharge of both radial and axial force sensors by radial loading . . . . .	104
4.21. Stress signal of the radial sensor by activated pressure correction . . . . .	106
4.22. Repeated axial stress on the measurement plate by activated correction of the signal interdependence . . . . .	107
4.23. Stress induced by a slug conveyed with 7.7 m/s air velocity - $f_{sampling} = 100$ Hz . . . .	108
4.24. Stress induced by a slug conveyed with 7.7 m/s air velocity - $f_{sampling} = 10,000$ Hz . .	108

4.25. Schematic procedure for the porosity determination based on the semi-empirical equation of Ergun . . . . .	110
4.26. Mathematical description of the radial porosity distribution using the method of Rottschäfer [60] . . . . .	111
4.27. On the left hand side: Fraction of the pipe cross-section area covered by a layer of particles according to the porosity of this layer for mean porosities of 0.41 and 0.60 and given suspension porosities of 0.60, 0.80 and 1.00. On the right hand side: Mean porosity across the pipe cross-section calculated by applying the Ergun equation for the same mean porosities and suspension porosities . . . . .	113
4.28. Top view of the slug-catcher mounted in the pipeline . . . . .	116
4.29. Exploded assembly drawing of the slug-catcher. 1. Shaft axle, 2. Aluminum component, 3. Separating metal sheets, 4. Stop position for the separating sheets, 5. Plexiglas component for process control, 6. Connection with the conveying pipeline . . . . .	117
4.30. The three states of the operating slug-catcher . . . . .	118
4.31. Schematic illustration of the three regions composing a slug. 1. Front end, 2. Core, 3. Rear . . . . .	118
5.1. Pressure measured at seven locations along the pipeline - $v_f = 7.4$ m/s . . . . .	119
5.2. Agreement between the experimental pressure loss measured between the points $P_1$ and $P_6$ and the pressure loss predicted by applying Yi's method [100] . . . . .	120
5.3. Agreement between the experimental pressure loss and the pressure loss predicted by applying Yi's method [100] for the horizontal sections located between the points $P_1$ and $P_6$ . . . . .	121
5.4. Solids mass flow rate and slug velocity experimentally measured . . . . .	122
5.5. Effect of the air velocity on the slug frequency . . . . .	122
5.6. Influence of the air supply velocity on the fraction $\alpha$ of the pipe area covered by the stationary layer . . . . .	123
5.7. Influence of the air velocity on the total slug length . . . . .	124
5.8. The two main types of front face displayed by slugs - $v_f = 6.8$ m/s. . . . .	125
5.9. The two main types of rear displayed by slugs - $v_f = 6.8$ m/s. The images belong to the slugs whose fronts are presented in Fig. 5.8 . . . . .	126
5.10. Particle velocity along the two slugs illustrating type 1 and 2 of slug front and rear . . . . .	126
5.11. Correlation between the fraction of the pipe area covered by the stationary layer and the velocity of the slug arriving . . . . .	127
5.12. Correlation between the velocity of a slug and the fraction of the pipe area covered by the particles left behind . . . . .	127
5.13. Pressure and stress signals measured at the side of the pipe - $v_f = 7.2$ m/s. a) 15-seconds-recording; b) Segment of the signals corresponding to Slug 1 . . . . .	128
5.14. Pressure and stress signals detected at the side of the pipe - $v_f = 8.5$ m/s . . . . .	129
5.15. Four slugs of the same conveying process - $v_f = 6.8$ m/s . . . . .	130
5.16. Effect of the conveying velocity on the slug porosity for $v_f = 6.8$ m/s and $v_f = 7.2$ m/s . . . . .	131

5.17. Effect of the conveying velocity on the slug porosity for $v_f = 7.5$ m/s and $v_f = 8.5$ m/s	132
5.18. Influence of the air supply velocity on the slug porosity. a) Total mass of granules caught in the sample chamber, b) Porosity displayed by the slugs at the time when the catching mechanism was triggered	133
5.19. 20-seconds-recording of pressure and force signals detected at the pipeline bottom. a) $v_f = 7.0$ m/s; b) $v_f = 7.5$ m/s	135
5.20. Air cavity at the top of a slug - $v_f = 7.5$ m/s	135
5.21. Wave of particles - $v_f = 7.5$ m/s	136
5.22. Signals of pressure and stresses measured at the side of the pipe a) $v_f = 7.0$ m/s, b) $v_f = 7.5$ m/s	136
5.23. Layer of particles covering 2/3 of the pipe cross-section	137
5.24. Wave of particles - $v_f = 7.5$ m/s	138
5.25. Signals of pressure and stresses detected at the pipeline top. a) $v_f = 7.0$ m/s, b) $v_f = 7.5$ m/s	139
5.26. 20-seconds-recording of pressure, radial and wall shear stress for air supply velocities covering the entire area of slug flow - Measurement position: pipeline side	140
5.27. Stresses induced by horizontal moving slugs pneumatically conveyed. a) Radial stress, b) Wall shear stress	141
5.28. Velocity gradient according to the position over the pipeline height. $f = 30$ images/s	143
5.29. Example of irregular stress signals measured at the top of a slug - $v_f = 7.0$ m/s	143
5.30. Behaviour of the ratio wall shear stress to radial stress	144
5.31. Stresses induced at the pipe wall by pushing of a model-slug through the pipeline	145
5.32. Pressure, radial and wall shear stress measured within a slug blocked in the pipeline - $v_f = 8.5$ m/s	147
5.33. Velocity gradient at the wall calculated from radial and wall shear stress measurements	149
5.34. Experimental wall shear stress and wall shear stress calculated by applying the kinetic theory for slugs conveyed with $v_f = 6.8$ m/s. a and b) Wall shear stress at the top of the pipe, c and d) Wall shear stress at the pipe side, e and f) Wall shear stress at the pipe bottom	151
5.35. Experimental wall shear stress and wall shear stress calculated by applying kinetic theory for slugs conveyed with velocities covering the whole slug flow area. a and b) $v_f = 7.2$ m/s, c and d) $v_f = 7.5$ m/s, e and f) $v_f = 8.5$ m/s	153
5.36. Low values of wall shear stress at the pipe side correctly predicted by applying the kinetic theory	154
5.37. Correlation between particle velocity, radial and wall shear stress measured over slugs. a) $v_f = 6.8$ m/s - side, b) $v_f = 7.2$ m/s - side, c and d) $v_f = 6.8$ m/s - bottom	154
5.38. Particle velocity, radial and wall shear stresses measured within a slug whose rear remained blocked in the stress measurement probe - $v_f = 6.8$ m/s	155

5.39. Integration of the experimental wall shear stress over the entire pipe circumference. On the left hand side: Schematical integration of the experimental values. On the right hand side: Wall shear stress after integration over the pipe circumference . . . . .	157
5.40. Pressure loss over single slugs calculated by applying the kinetic theory. a and b) By using radial stress values measured at the top, c and d) By using radial stress values measured at the side, e and f) By using radial stress values measured at the pipe bottom	158
5.41. Influence of the fraction of the pipe area covered by settled particles, radial stress, porosity and solids mass flow rate on the pressure loss calculated by applying the kinetic theory . . . . .	160
5.42. Summary of the material characteristics, pipeline layout and flow dependent parameters required for the pressure loss calculation in the horizontal sections of the conveying system . . . . .	161
5.43. Comparison between experimental and calculated pressure loss for the three horizontal sections of the conveying system . . . . .	162
5.44. Influence of the changes in the air density on the superficial air velocity . . . . .	163
5.45. Slug 1: Single slug conveyed with $v_f = 6.8$ m/s - Stress measurement position: pipeline side . . . . .	164
5.46. Air cavity at the top of Slug 1 at $t = 0.64$ s . . . . .	165
5.47. Slug 2: Single slug conveyed with $v_f = 6.8$ m/s - Stress measurement position: pipeline top . . . . .	166
5.48. Scheme illustrating the compression of Slug 2 from the rear towards the front end . . .	167
5.49. Slug 3: Single slug conveyed with $v_f = 6.8$ m/s - Stress measurement position: pipeline top . . . . .	168
5.50. Slug 4: $v_f = 8.5$ m/s - Measurement position of the forces: pipe side . . . . .	170
5.51. Scheme illustrating the expansion of Slug 4 from the rear in the direction of the flow . .	172
5.52. Slug 5: $v_f = 8.5$ m/s - Measurement position of the forces: pipeline side . . . . .	173
5.53. Release of particles at the back of a slug blocked in the pipeline . . . . .	174
5.54. Scheme illustrating the Bernoulli principle applied on slug flow pneumatic conveying . .	178
5.55. Fraction of the particles that can be lifted for $v_f = 6.8$ m/s . . . . .	180
5.56. Fraction of the particles that can be lifted for $v_f = 8.5$ m/s . . . . .	180

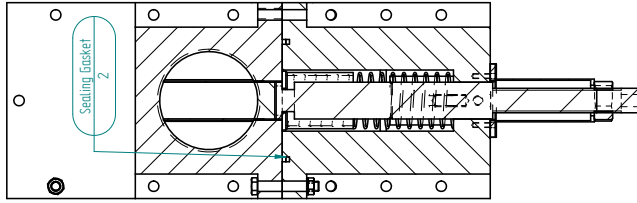
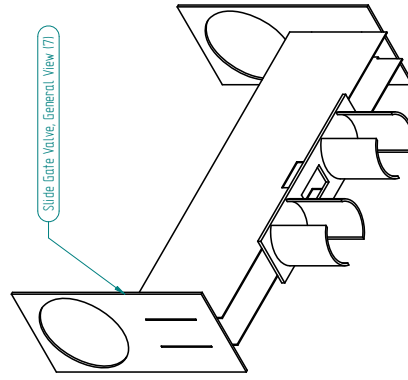
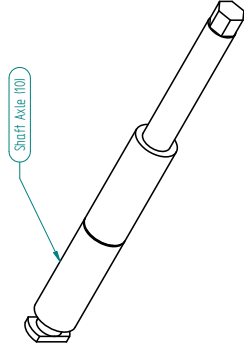
## List of Tables

4.1. Physical characteristics of the test material . . . . .	85
4.2. Length of the different sections of the 80 mm i.d. pipeline . . . . .	87
4.3. Dynamic characteristics of the force measurement system . . . . .	92

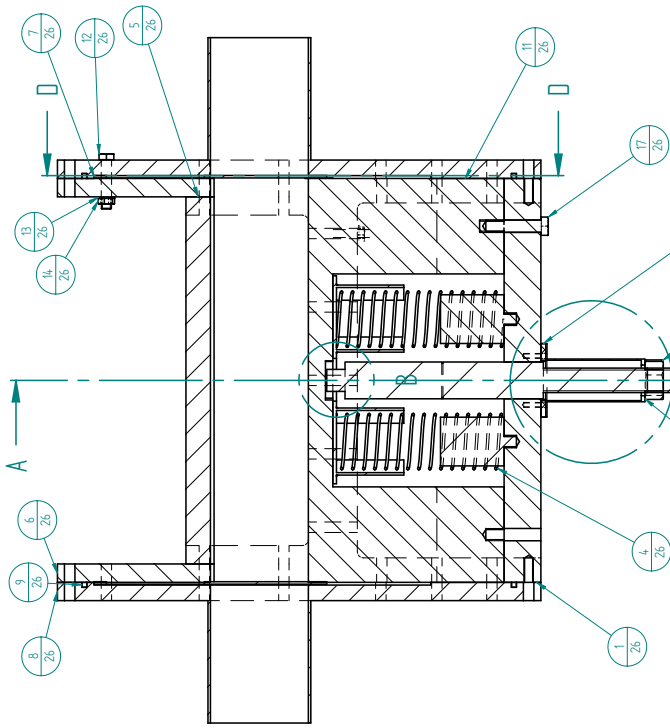
## **A. Annex**

### **A.1. Technical drawings of the slug-catcher**

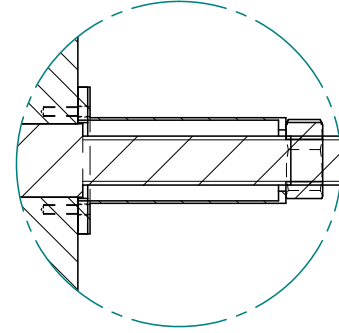
Overall View



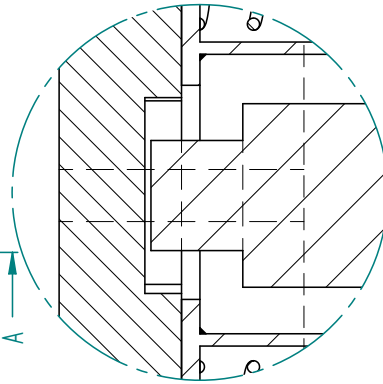
Sectional View A-A



Sectional View D-D



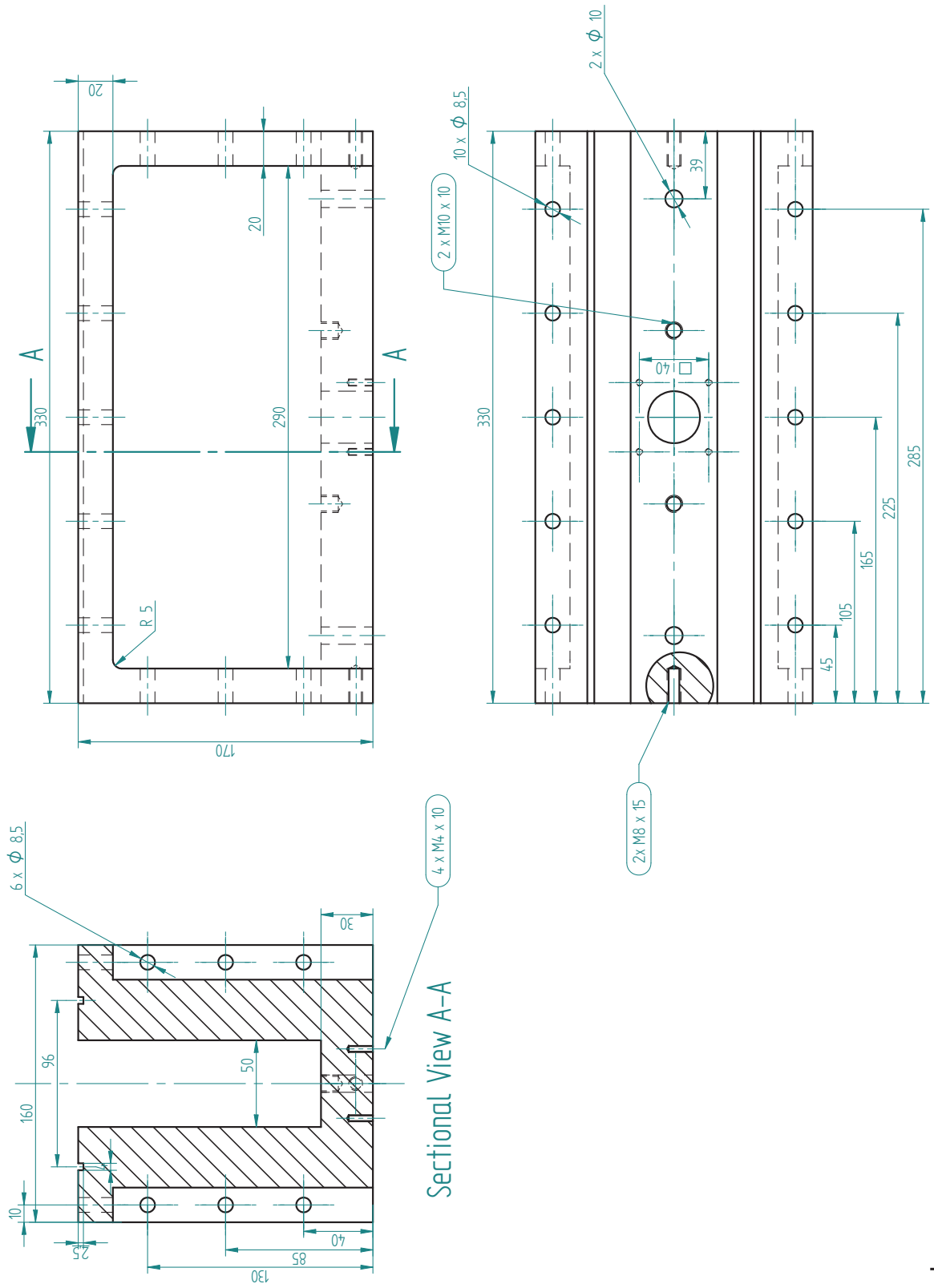
DETAIL C



DETAIL B

Part No.	Description	Material	Quantity
1	Base Part	Aluminium	1
2	Spacer Plate	V2A Steel	1
3	Sealing Gasket	Rubber	2
4	Spring with Locking Pin	Steel	2
5	Measurement Chamber	Perspex	1
6	Guide Plate	Perspex	2
7	Slide Gate Valve	V2A Steel	1
8	Cover Plate	Aluminium	2
9	Sealing Gasket	Rubber	2
10	Clamping Pin	V2A Steel	1
11	End Stop	Aluminium	1
12	Screw M8 40mm	Brass	1
13	Washer	Brass	2
14	Screw Nut M8	Brass	2
15	Spacer	V2A Steel	1
16*	Screw M4 15mm	Brass	1
17	Screw M10 50 mm	Brass	1
18	Screw Nut M24	V2A Steel	1
19*	Screw M8 50mm	Brass	1

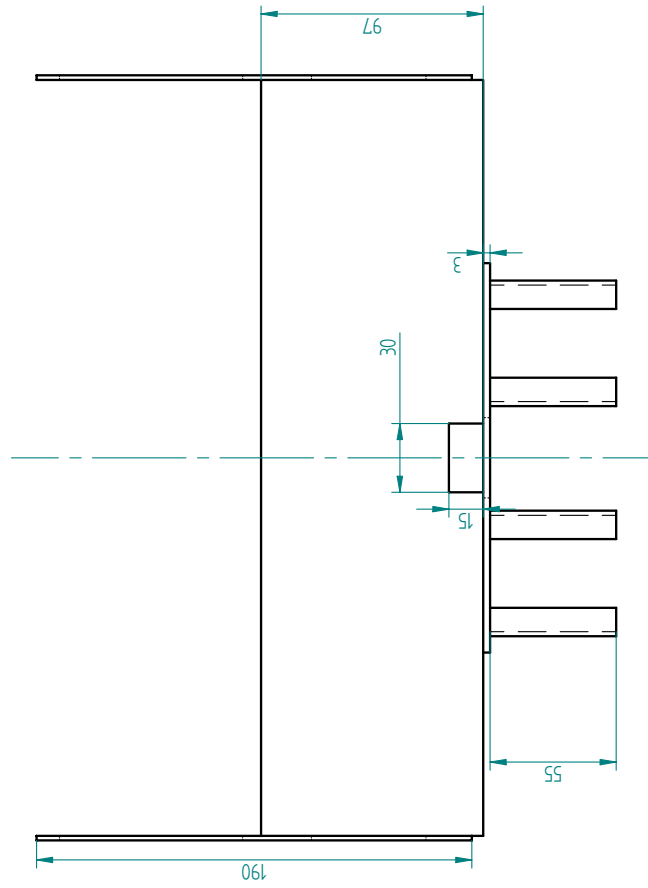
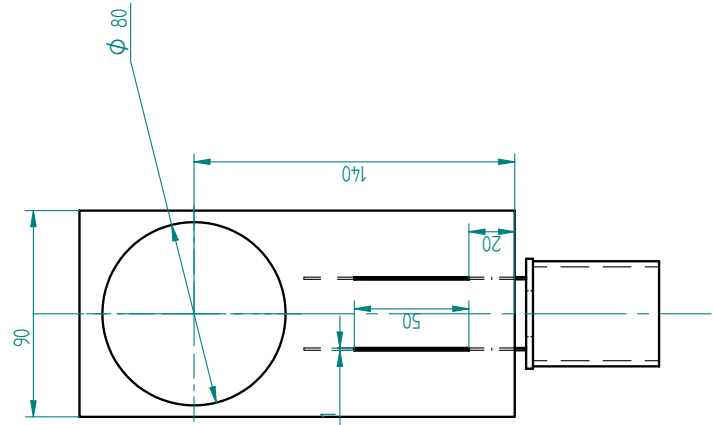
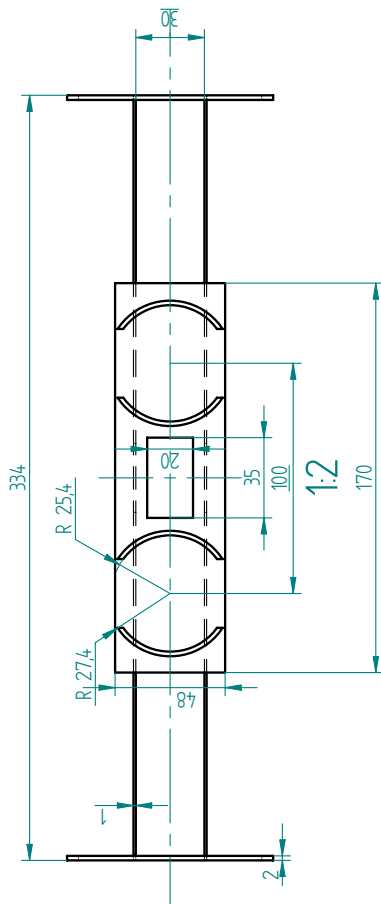




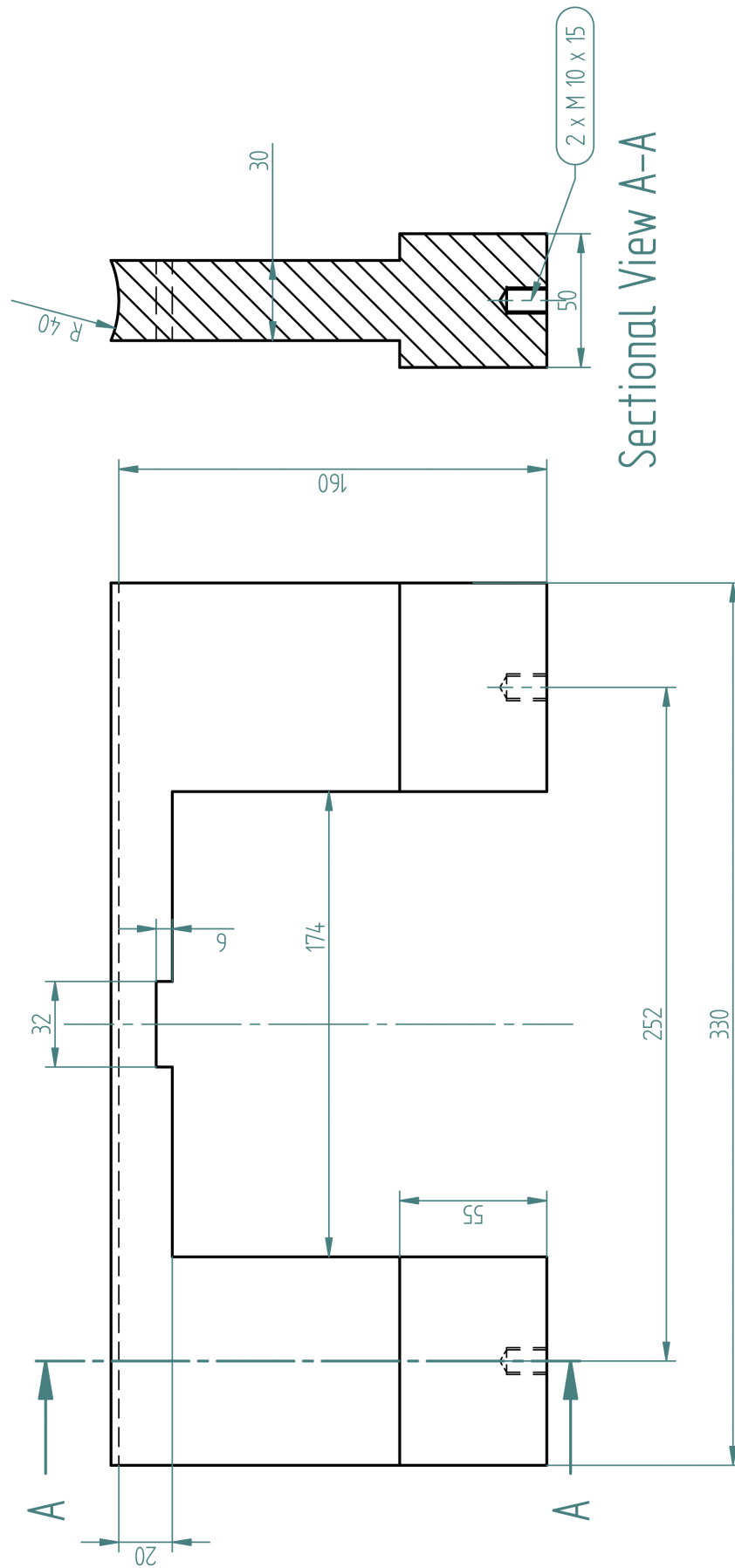
Base Part



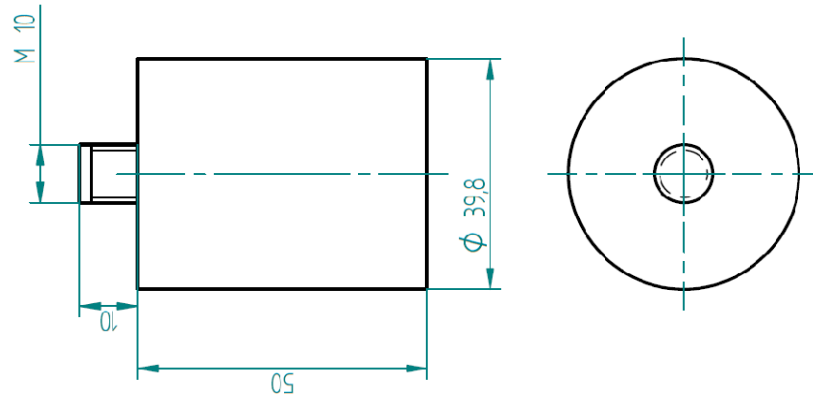
# Slide Gate Valve



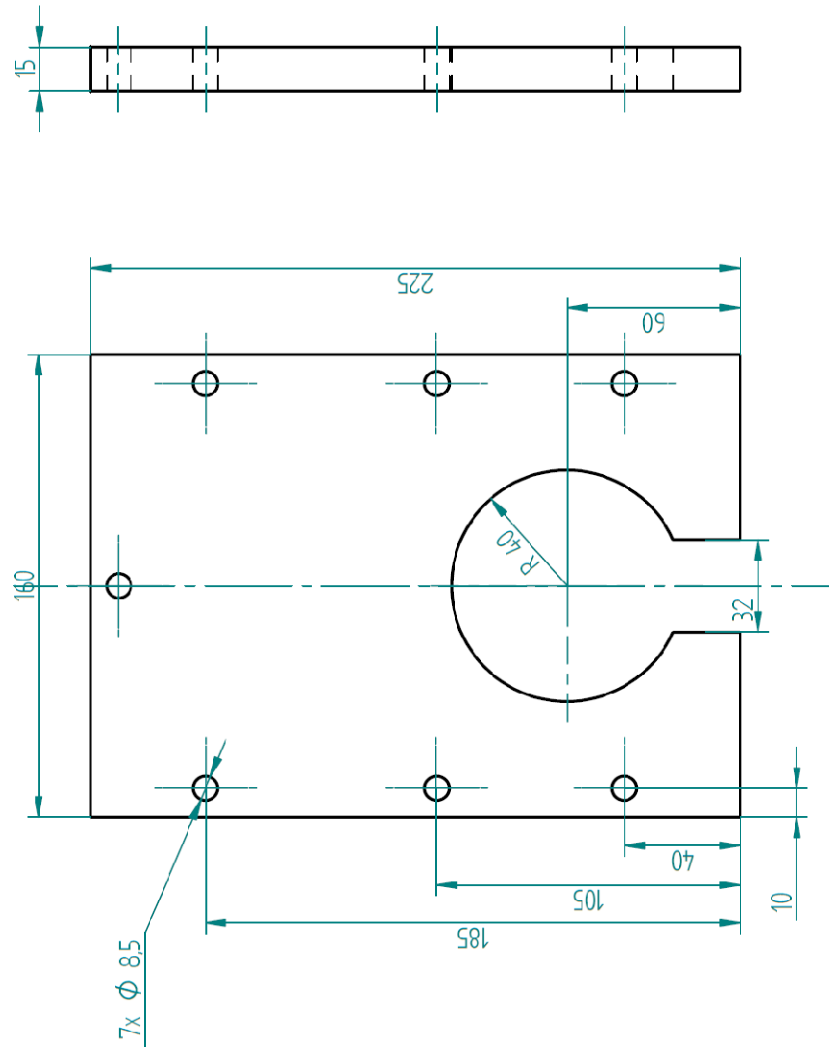
# Spacer



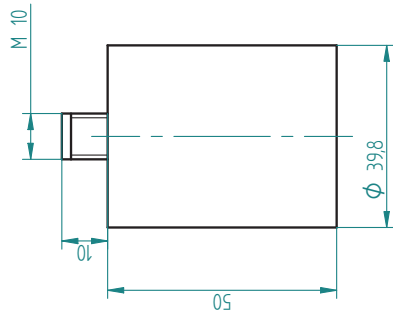
Leading Pin



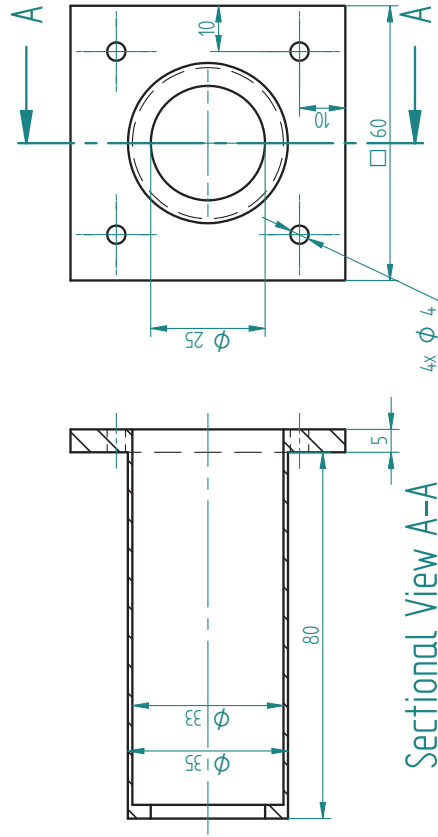
Guide Plate



Guidance Pin

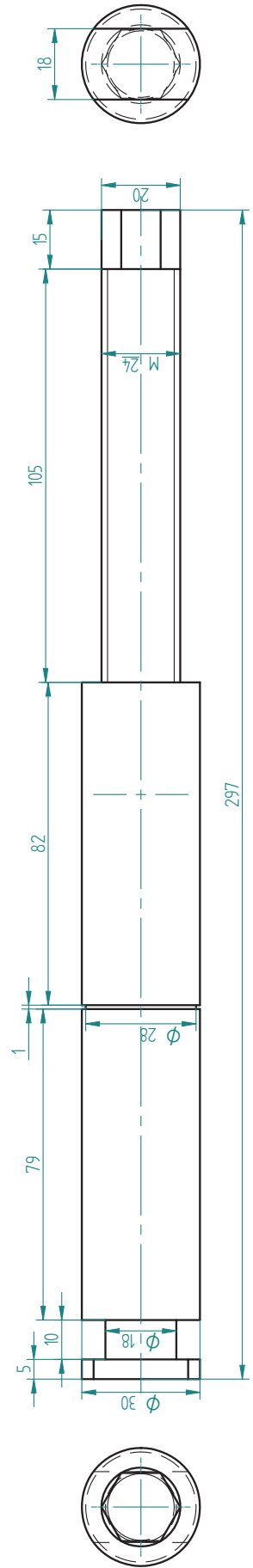


Spacer



Sectional View A-A

Shaft Axle



## A.2. Mathcad® calculation programs

### 1. Konrad's model - Incompressible gas (as published)

The unknown quantity is the pressure loss  $\Delta P_{1K}$ . The gas density is considered to be equal to:

$$\rho_{mK} := 1.2 \text{ kg/m}^3$$

1. Find the mass flow rate of air  $m_{a\_KK}$  to satisfy the following condition:

$$m_{a\_KK} > m_s \cdot \rho_m \cdot \left( \frac{2}{\rho_b} - \frac{1}{\rho_s} \right) + A \cdot \left[ \frac{-a}{2 \cdot b} + \sqrt{\left( \frac{a}{2 \cdot b} \right)^2 + \frac{2 \cdot \rho_b \cdot g \cdot \mu_w \cdot \rho_m}{b}} \right]$$

with  $b_K := b(\rho_{mK})$

Calculation for the minimum mass flow rate:

$$m_{a\_KK} := m_s \cdot \rho_{mK} \cdot \left( \frac{2}{\rho_b} - \frac{1}{\rho_s} \right) + A \cdot \left[ \frac{-a}{2 \cdot b_K} + \sqrt{\left( \frac{a}{2 \cdot b_K} \right)^2 + \frac{2 \cdot \rho_b \cdot g \cdot \mu_w \cdot \rho_{mK}}{b_K}} \right]$$

2. Solve the cubic equation for the particle velocity  $u_{sK}$ .

Calculation:

$$PK(U_{a\_atm}, K_w) := \left[ \frac{-(a + f(K_w))}{b_K \cdot \rho_{mK}} - 2(U_{a\_atm} + U_s) - \frac{m_s}{\rho_b \cdot A} \right]$$

$$qK(U_{a\_atm}, K_w) := \frac{2 \cdot m_s \cdot U_{a\_atm} + U_s}{A \cdot \rho_b} + \frac{m_s \cdot (a + 2 \cdot f(K_w))}{A \cdot b_K \cdot \rho_{mK} \cdot \rho_b} + (U_{a\_atm} + U_s)^2 + \frac{a \cdot (U_{a\_atm} + U_s)}{b_K \cdot \rho_{mK}} - \frac{2 \cdot g \cdot \rho_b \cdot \mu_w}{b_K \cdot \rho_{mK}}$$

$$rK(U_{a\_atm}) := \frac{m_s}{A \cdot \rho_b} \cdot \left[ (U_{a\_atm} + U_s)^2 - \frac{2 \cdot g \cdot \rho_b \cdot \mu_w}{b_K \cdot \rho_{mK}} + \frac{a \cdot (U_{a\_atm} + U_s)}{b_K \cdot \rho_{mK}} \right]$$

solve cubicgleichung $_K(u_{sK}, U_{a\_atm}, K_w) := u_{sK}^3 + u_{sK}^2 \cdot p_K(U_{a\_atm}, K_w) + u_{sK} \cdot q_K(U_{a\_atm}, K_w) - r_K(U_{a\_atm})$

$$\text{koef}_K(U_{a\_atm}, K_w) := \begin{pmatrix} -r_K(U_{a\_atm}) \\ q_K(U_{a\_atm}, K_w) \\ p_K(U_{a\_atm}, K_w) \\ 1 \end{pmatrix}$$

Solution:

$$\text{solution}_K(U_{a\_atm}, K_w) := \text{nullstellen}(\text{koef}_K(U_{a\_atm}, K_w))$$

3. Take the root that lies in the range

$$(U_a + U_s) > u_{sK} > \frac{2 \cdot m_s}{\rho_b \cdot A}$$

i.e. take the value lying between the first and the third positive root.

$$u_{sK}(U_{a\_atm}, K_w) := \text{solution}_K(U_{a\_atm}, K_w)_1$$

4. Calculate the superficial slip velocity

$$U_{sp.K}(U_{a\_atm}, K_w) := U_{a\_atm} + U_s - u_{sK}(U_{a\_atm}, K_w)$$

5. Calculation of the pressure loss  $\Delta P_{1_j}$  by using the Ergun equation

$$\Delta p_{1.K}(U_{a\_atm}, K_w) := \left[ a \cdot U_{sp.K}(U_{a\_atm}, K_w) \right] + b_K \cdot U_{sp.K}(U_{a\_atm}, K_w)^2 \cdot \left( \frac{m_s \cdot L}{A \cdot \rho_b \cdot u_{sK}(U_{a\_atm}, K_w)} \right)$$

$$\Delta P_{1.K}(U_{a\_atm}, K_w) := \Delta p_{1.K}(U_{a\_atm}, K_w)$$



### 1.1. Konrad's model - With additional consideration of the gas expansion

The two unknown quantities are the mean air density  $\rho_m$  and the pressure loss  $\Delta P_{1b}$ .

Consideration of the gas expansion:

$$p_{\text{atm}} := 101300 \text{ Pa}$$

$$U_a(\rho_m, U_{a,\text{atm}}) := \frac{U_{a,\text{atm}} \cdot p_{\text{atm}}}{\rho_m \cdot R_a \cdot T_0 \cdot 1000} \cdot \frac{M_{\text{air}}}{M_{\text{air}}}$$

1. Find the mass flow rate of air  $m_{a,K}$  to satisfy the following condition:

$$m_{a,K} > m_s \cdot \rho_m \cdot \left( \frac{2}{\rho_b} - \frac{1}{\rho_s} \right) + A \cdot \left[ \frac{-a}{2 \cdot b} + \sqrt{\left( \frac{a}{2 \cdot b} \right)^2 + \frac{2 \cdot \rho_b \cdot g \cdot \mu_w \cdot \rho_m}{b}} \right]$$

$$\text{with } a := \frac{150 \cdot \eta \cdot (1 - \epsilon)^2}{d_p^2 \cdot \epsilon^3}$$

$$b(\rho_m) := \frac{1.75 \cdot \rho_m \cdot (1 - \epsilon)}{d_p \cdot \epsilon^3}$$

Calculation of the minimum mass flow rate:

$$m_{a,K}(\rho_m) := m_s \cdot \rho_m \cdot \left( \frac{2}{\rho_b} - \frac{1}{\rho_s} \right) + A \cdot \left[ \frac{-a}{2 \cdot b(\rho_m)} + \sqrt{\left( \frac{a}{2 \cdot b(\rho_m)} \right)^2 + \frac{2 \cdot \rho_b \cdot g \cdot \mu_w \cdot \rho_m}{b(\rho_m)}} \right]$$

2. Solve the cubic equation for the particle velocity  $u_s$ .

$$\text{with } f(K_w) := 2.168 \cdot \rho_b \cdot \mu_w \cdot K_w \cdot \sqrt{\frac{g}{D}}$$

Calculation:

$$p(U_{a\_atm}, \rho_m, K_w) := \left[ \frac{-(a + f(K_w))}{b(\rho_m) \cdot \rho_m} - 2(U_a(\rho_m, U_{a\_atm}) + U_s) - \frac{m_s}{\rho_b \cdot A} \right]$$

$$q(U_{a\_atm}, \rho_m, K_w) := \frac{2 \cdot m_s \cdot (U_a(\rho_m, U_{a\_atm}) + U_s)}{A \cdot \rho_b} + \frac{m_s \cdot (a + 2 \cdot f(K_w))}{A \cdot b(\rho_m) \cdot \rho_m \cdot \rho_b} + (U_a(\rho_m, U_{a\_atm}) + U_s)^2 + \frac{a \cdot (U_a(\rho_m, U_{a\_atm}) + U_s)}{b(\rho_m) \cdot \rho_m} - \frac{2 \cdot g \cdot \rho_b \cdot \mu_w}{b(\rho_m) \cdot \rho_m}$$

$$r(U_{a\_atm}, \rho_m) := \frac{m_s}{A \cdot \rho_b} \cdot \left[ (U_a(\rho_m, U_{a\_atm}) + U_s)^2 - \frac{2 \cdot g \cdot \rho_b \cdot \mu_w}{b(\rho_m) \cdot \rho_m} + \frac{a \cdot (U_a(\rho_m, U_{a\_atm}) + U_s)}{b(\rho_m) \cdot \rho_m} \right]$$

solve cubicgleichungb( $u_s, U_{a\_atm}$ ) = 0

$$\text{cubicgleichungb}(u_s, U_{a\_atm}, \rho_m, K_w) := (u_s^3 + u_s^2 \cdot p(U_a(\rho_m, U_{a\_atm}), \rho_m, K_w) + u_s \cdot q(U_a(\rho_m, U_{a\_atm}), \rho_m, K_w) - r(U_a(\rho_m, U_{a\_atm}), \rho_m))$$

$$\text{koefb}(U_{a\_atm}, \rho_m, K_w) := \begin{pmatrix} -r(U_a(\rho_m, U_{a\_atm}), \rho_m) \\ q(U_a(\rho_m, U_{a\_atm}), \rho_m, K_w) \\ p(U_a(\rho_m, U_{a\_atm}), \rho_m, K_w) \\ 1 \end{pmatrix}$$

Solution:

$$\text{solutionb}(U_{a\_atm}, \rho_m, K_w) := \text{nullstellen}(\text{koefb}(U_{a\_atm}, \rho_m, K_w))$$

3. Take the root in the range

$$(U_a + U_s) > u_s > \frac{2 \cdot m_s}{\rho_b \cdot A}$$

$$u_s(U_{a\_atm}, \rho_m, K_w) := \text{solutionb}(U_{a\_atm}, \rho_m, K_w)[1]$$

4. Calculation of the superficial slip velocity

$$U_{\text{spb}}(U_{\text{a\_atm}}, \rho_m, K_w) := (U_{\text{a}}(\rho_m, U_{\text{a\_atm}}) + U_s - u_s(U_{\text{a}}(\rho_m, U_{\text{a\_atm}}), \rho_m, K_w))$$

5. Calculation of the pressure loss  $\Delta P_{1b}$  using the Ergun equation

$$\Delta p_{1b}(U_{\text{a\_atm}}, \rho_m, K_w) := \left[ (a \cdot U_{\text{spb}}(U_{\text{a}}(\rho_m, U_{\text{a\_atm}}), \rho_m, K_w)) + b(\rho_m) \cdot U_{\text{spb}}(U_{\text{a}}(\rho_m, U_{\text{a\_atm}}), \rho_m, K_w))^2 \right] \cdot \left( \frac{m_s \cdot L}{A \cdot \rho_b \cdot u_s(U_{\text{a}}(\rho_m, U_{\text{a\_atm}}), \rho_m, K_w)} \right)$$

6. Consideration of the mean gas density  $\rho_m$

$$\text{Estimation: } \rho_{\text{a\_estimation}} := 1.2 \text{ kg/m}^3$$

$$\Delta p_2(\rho_m) := \frac{2 \cdot p_{\text{End}} \cdot \rho_m}{\rho_{\text{End}}} - 2 \cdot p_{\text{End}}$$

$$\rho_m(U_{\text{a\_atm}}, K_w) := \text{wurzel}(\Delta p_{1b}(U_{\text{a\_atm}}, \rho_{\text{a\_estimation}}, K_w) - \Delta p_2(\rho_{\text{a\_estimation}}), \rho_{\text{a\_estimation}})$$

7. Total pressure loss:

$$\Delta P_{1b}(U_{\text{a\_atm}}, \rho_m, K_w) := \Delta p_{1b}(U_{\text{a\_atm}}, \rho_m, K_w)$$

## 2. Mi's model - For compressible gas

The two unknown quantities are the mean air density  $\rho_{m3}$  and the pressure loss  $\Delta p_3$ :

Consideration of the gas expansion:

$$U_{a3}(\rho_{m3}, U_{a\_atm}) := \frac{U_{a\_atm} \cdot P_{atm}}{\rho_{m3} \cdot R_a \cdot T_0 \cdot 1000} \cdot \frac{M_{air}}{M_{air}}$$

1. Calculation of the minimum gas velocity  $U_{amin}$

$$U_{amin} := \frac{\rho_s \cdot g \cdot \mu_w \cdot \epsilon^3 \cdot d_p^2}{180(1 - \epsilon)\eta}$$

2. Estimation of the mean slug velocity  $U_{s\_mean}$

$$k := 105 \frac{\epsilon \cdot d_p}{D} \cdot \left( \frac{\mu_w}{f_{s\_Mi}} \right)^{\frac{1}{3}}$$

$$U_{s\_mean}(\rho_{m3}, U_{a\_atm}) := k \cdot (U_{a3}(\rho_{m3}, U_{a\_atm}) - U_{amin})$$

3. Determination of the Froude number

$$Fr(\rho_{m3}, U_{a\_atm}) := \frac{U_{s\_mean}(\rho_{m3}, U_{a\_atm})^2}{g \cdot D}$$

4. Calculate the pressure loss  $\Delta P_3$  and the mean gas density  $\rho_{m3}$  by using the following system of two equations:

$$\Delta p_3(\rho_{m3}, U_{a\_atm}, K_w) := \left( 1 + 1.084 \cdot K_w \cdot Fr(\rho_{m3}, U_{a\_atm})^{0.5} + 0.542 Fr(\rho_{m3}, U_{a\_atm})^{-0.5} \right) \cdot \frac{2g \cdot \mu_w \cdot m_s \cdot L}{A \cdot U_{s\_mean}(\rho_{m3}, U_{a\_atm})}$$

$$\Delta p_4(\rho_{m3}) := \frac{2 \cdot p_{\text{End}} \cdot \rho_{m3}}{\rho_{\text{End}}} - 2 \cdot p_{\text{End}}$$

Solution:

$$\rho_{a\_estimation} := 1.2 \text{ kg/m}^3$$

$$\rho_{m3}(U_{a\_atm}, K_w) := \text{wurzel}(\Delta p_3(\rho_{a\_estimation}, U_{a\_atm}, K_w) - \Delta p_4(\rho_{a\_estimation}, \rho_{a\_estimation}))$$

Calculation:

$$\Delta P_3(\rho_{m3}, U_{a\_atm}, K_w) := \Delta p_3(\rho_{m3}, U_{a\_atm}, K_w)$$

### 3. Pan's model - For compressible gas

The three unknown quantities are the mean air density  $\rho_{m5}$ , the slug velocity  $U_p$  and the pressure loss  $\Delta p_5$ .

Consideration of the gas expansion:

$$U_{a5}(\rho_{m5}, U_{a\_atm}) := \frac{U_{a\_atm} \cdot P_{atm}}{\rho_{m5} \cdot R_a \cdot T_0 \cdot 1000} \cdot \frac{M_{air}}{M_{air}}$$

1. Determine the slug velocity  $U_p$  by solving the following set of equations:

$$a = \frac{150 \cdot \eta \cdot (1 - \epsilon)^2}{d_p^2 \cdot \epsilon^3}$$

$$b_2 := \frac{1.75 \cdot (1 - \epsilon)}{d_p \cdot \epsilon^3}$$

$$A_1(\rho_{m5}) := b_2 \cdot \rho_{m5}$$

$$A_2(\rho_{m5}, U_{a\_atm}, K_w) := - \left( a + 2 \cdot b_2 \cdot \rho_{m5} \cdot U_{a5}(\rho_{m5}, U_{a\_atm}) + 2.168 \cdot \rho_b \cdot \mu_w \cdot K_w \cdot \sqrt{\frac{g}{D}} \right)$$

$$A_3(\rho_{m5}, U_{a\_atm}, K_w) := U_{a5}(\rho_{m5}, U_{a\_atm}) \cdot a + U_{a5}(\rho_{m5}, U_{a\_atm})^2 \cdot \rho_{m5} \cdot b_2 - \rho_b \cdot g \cdot \mu_w \cdot (1 - 1.175 \cdot K_w)$$

$$U_p(\rho_{m5}, U_{a\_atm}, K_w) := \frac{-A_2(\rho_{m5}, U_{a\_atm}, K_w) - \sqrt{A_2(\rho_{m5}, U_{a\_atm}, K_w)^2 - 4 \cdot A_1(\rho_{m5}) \cdot A_3(\rho_{m5}, U_{a\_atm}, K_w)}}{2 \cdot A_1(\rho_{m5})}$$

2. Calculation of pressure loss and mean gas density by using a system of two equations

$$\Delta p_{5g}(\rho_{m5}, U_{a\_atm}, K_w) := 2.168 \cdot \mu_w \cdot \rho_b \cdot K_w \cdot \sqrt{\frac{g}{D}} \cdot U_p(\rho_{m5}, U_{a\_atm}, K_w) + \rho_b \cdot g \cdot \mu_w \cdot (1 - 1.175 \cdot K_w)$$

with    Height of the stationary layer:  $\alpha(\rho_{m5}, U_{a\_atm}, K_w) := \frac{0.542 \cdot \sqrt{g \cdot D}}{U_p(\rho_{m5}, U_{a\_atm}, K_w)} \quad \alpha 2(\rho_{m5}, U_{a\_atm}) := \frac{1}{1 + \frac{U_p(\rho_{m5}, U_{a\_atm})}{0.542 \cdot \sqrt{g \cdot D}}}$

Total length of slugs:  $l_{sT}(\rho_{m5}, U_{a\_atm}, K_w) := \frac{m_s \cdot L}{A \cdot \rho_b \cdot U_p(\rho_{m5}, U_{a\_atm}, K_w) \cdot (1 - \alpha(\rho_{m5}, U_{a\_atm}, K_w))}$

$$\Delta p_5(\rho_{m5}, U_{a\_atm}, K_w) := \Delta p_{5g}(\rho_{m5}, U_{a\_atm}, K_w) \cdot l_{sT}(\rho_{m5}, U_{a\_atm}, K_w)$$

$$\Delta p_6(\rho_{m5}) := \frac{2 \cdot p_{\text{Ende}} \cdot \rho_{m5}}{\rho_{\text{Ende}}} - 2 \cdot p_{\text{Ende}}$$

Calculation of the mean air density:

$$\rho_{m5}(U_{a\_atm}, K_w) := \text{wurzel}(\Delta p_5(\rho_{a\_Schätz}, U_{a\_atm}, K_w) - \Delta p_6(\rho_{a\_Schätz}), \rho_{a\_Schätz})$$

Calculation of the pressure loss:

$$\Delta P_5(\rho_{m5}, U_{a\_atm}, K_w) := \Delta p_5(\rho_{m5}, U_{a\_atm}, K_w)$$

#### 4. Yi's model - For incompressible gas (as proposed by the author)

The two unknown quantities are the slug velocity  $U_{slug2}$  and the pressure loss  $\Delta P_{11}$ .

Characteristic viscosity:  $a_{visc} = 0.542 \cdot \sqrt{g \cdot D}$

Height of the stationary layer:  $\alpha 1(U_{slug2}) := \frac{a_{visc}}{U_{slug2}}$

Width of the layer:  $l_w(U_{slug2}) := \left[ 4 \cdot \alpha 1(U_{slug2}) \cdot (1 - \alpha 1(U_{slug2})) \right]^{\frac{1}{3}} D$

Height of the suspension above the strand:  $H(U_{slug2}) := \begin{cases} H \leftarrow 0.5 \cdot \left( D + \sqrt{D^2 - l_w(U_{slug2})^2} \right) & \text{if } U_{slug2} \geq 2 \cdot a_{visc} \\ H \leftarrow 0.5 \cdot \left( D - \sqrt{D^2 - l_w(U_{slug2})^2} \right) & \text{if } U_{slug2} < 2 \cdot a_{visc} \end{cases}$

Yi and Klinzig:  $c_1(K_w) := \frac{4 \cdot f_w \cdot K_w}{D}$   $c_2(K_w) := \frac{\rho_{sch} \cdot g}{K_w}$   $c_3 := \rho_{sch} \cdot f_w \cdot g$

$$\Delta p_{11}(U_{slug2}, K_w) := \begin{cases} p \leftarrow 0 & \text{if } U_{slug2} \leq a \\ p \leftarrow c_1(K_w) \cdot \left[ c_2(K_w) \cdot H(U_{slug2}) \cdot H(U_{slug2}) + \alpha 1(U_{slug2}) \cdot (1 - \alpha 1(U_{slug2})) \cdot \rho_{sch} \cdot U_{slug2}^2 \right] + c_3 & \text{if } U_{slug2} > a_{visc} \end{cases}$$

Ergun:  $a = \frac{150 \cdot (1 - \epsilon)^2 \cdot \eta}{\epsilon^3 \cdot d_p^2}$   $b4 := 1.75 \cdot \frac{(1 - \epsilon) \cdot \rho_a}{\epsilon^3 \cdot d_p}$

$$\Delta p_{12}(U_{slug2}, U_{a\_atm}) := a \cdot (U_{a\_atm} - U_{slug2}) + b4 \cdot (U_{a\_atm} - U_{slug2})^2$$



### Calculation of slug velocity:

1. Assumption of an initial value for  $U_{\text{slug}}$ :

$$u_{\text{slug}2} := 1 \cdot a_{\text{visc}}$$

2. Find the solution for  $U_{\text{slug}}$  ( $\Delta p_{11} - \Delta p_{12} = 0$ ):

$$U_{\text{slug}2}(U_{\text{a\_atm}}, K_w) := \text{wurzel}(\Delta p_{11}(u_{\text{slug}2}, K_w) - \Delta p_{12}(u_{\text{slug}2}, U_{\text{a\_atm}}, u_{\text{slug}2}))$$

3. Calculation of the pressure loss according to Ergun for  $U_{\text{slug}}$

$$\Delta p_{11s}(U_{\text{a\_atm}}, K_w) := \Delta p_{12}(U_{\text{slug}2}(U_{\text{a\_atm}}, K_w), U_{\text{a\_atm}})$$

4. Calculation of the pressure loss for the entire pipeline

$$\Delta p_{11}(U_{\text{a\_atm}}, K_w) := \Delta p_{11s}(U_{\text{a\_atm}}, K_w) \cdot \frac{m_s \cdot L}{\left( \frac{\pi \cdot D^2}{4} \right) \cdot (1 - \alpha I(U_{\text{slug}2}(U_{\text{a\_atm}}, K_w))) \rho_{\text{sch}} \cdot (U_{\text{slug}2}(U_{\text{a\_atm}}, K_w))}$$

#### 4.1. Yi's model - With additional consideration of gas expansion

The three unknown quantities are the mean air density  $\rho_{m11}$ , the slug velocity  $U_{slug2m}$  and the pressure loss  $\Delta P_{11m}$ .

##### 1. Consideration of the gas expansion:

$$U_{a11}(\rho_{m11}, U_{a\_atm}) := \frac{U_{a\_atm} \cdot P_{atm}}{\rho_{m11} \cdot R_a \cdot T_0 \cdot 1000} \cdot \frac{M_{air}}{M_{air}}$$

Characteristic viscosity  $a_{visc} := 0.542 \cdot \sqrt{g \cdot D}$

Height of the stationary layer:  $\alpha 1m(U_{slug2m}) := \frac{a_{visc}}{U_{slug2m}}$

Width of the layer:  $l_{wm}(U_{slug2m}) := \left[ 4 \cdot \alpha 1m(U_{slug2m}) \cdot (1 - \alpha 1m(U_{slug2m})) \right]^{\frac{1}{3}} \cdot D$

Height of the suspension over the strand:  $Hm(U_{slug2m}) := \begin{cases} H \leftarrow 0.5 \cdot \left( D + \sqrt{D^2 - l_{wm}(U_{slug2m})^2} \right) & \text{if } U_{slug2m} \geq 2 \cdot a_{visc} \\ H \leftarrow 0.5 \cdot \left( D - \sqrt{D^2 - l_{wm}(U_{slug2m})^2} \right) & \text{if } U_{slug2m} < 2 \cdot a_{visc} \end{cases}$

Particle-particle friction coefficient:  $f_w := \mu_w \quad \rho_{sch} := \rho_b$

Yi and Klinzing:  $c_{1m}(K_w) := \frac{4 \cdot f_w \cdot K_w}{D} \quad c_{2m}(K_w) := \frac{\rho_{sch} \cdot g}{K_w} \quad c_3 := \rho_{sch} \cdot f_w \cdot g$

$$\Delta p_{11m}(U_{slug2m}, K_w) := \begin{cases} p \leftarrow 0 & \text{if } U_{slug2m} \leq a \\ p \leftarrow c_{1m}(K_w) \cdot \left[ c_{2m}(K_w) \cdot Hm(U_{slug2m}) + \alpha 1m(U_{slug2m}) \cdot (1 - \alpha 1m(U_{slug2m})) \cdot \rho_{sch} \cdot U_{slug2m}^2 \right] + c_3 & \text{if } U_{slug2m} > a_{visc} \end{cases} \cdot p$$

Ergun:

$$a = \frac{150 \cdot (1 - \epsilon)^2 \cdot \eta}{\epsilon^3 \cdot d_p^2} \quad b3m(\rho_{m11}) := 1.75 \cdot \frac{(1 - \epsilon) \cdot \rho_{m11}}{\epsilon^3 \cdot d_p}$$

$$\Delta p_{12m}(\rho_{m11}, U_{slug2m}, U_{a\_atm}) := a \cdot (U_{a11}(\rho_{m11}, U_{a\_atm}) - U_{slug2m}) + b3m(\rho_{m11}) \cdot (U_{a11}(\rho_{m11}, U_{a\_atm}) - U_{slug2m})^2$$

Calculation of the slug velocity:

1. Assume an initial value for  $U_{slug2}$ :

$$u_{slug2\_estimation} := 1 \cdot a_{visc}$$

2. Find the solution for  $U_{slug2m}$  ( $\Delta p_{11m} = \Delta p_{12m} = 0$ ):

$$U_{slug2m}(\rho_{m11}, U_{a\_atm}, K_w) := \text{wurzel}(\Delta p_{11m}(u_{slug2\_estimation}, K_w) - \Delta p_{12m}(\rho_{m11}, u_{slug2\_estimation}, U_{a\_atm}), u_{slug2\_estimation})$$

Consideration of the air density

$$\Delta p_{13m}(\rho_{m11}) := \frac{2 \cdot p_{Ende} \cdot \rho_{m11}}{\rho_{Ende}} - 2 \cdot p_{Ende}$$

$$\rho_{m11}(U_{a\_atm}, K_w) := \text{wurzel}(\Delta p_{12m}(\rho_{a\_Schätz}, U_{slug2m}(\rho_{a\_Schätz}, U_{a\_atm}, K_w), U_{a\_atm}) - \Delta p_{13m}(\rho_{a\_Schätz}, \rho_{a\_Schätz}))$$

3. Calculation of the pressure loss according to Ergun for  $U_{slug}$ :

$$\Delta p_{11sm}(\rho_{m11}, U_{a\_atm}, K_w) := \Delta p_{12m}(\rho_{m11}(U_{a\_atm}, K_w), U_{slug2m}(\rho_{m11}(U_{a\_atm}, K_w), U_{a\_atm}, K_w), U_{a\_atm}))$$

4. Calculation of the pressure loss for the entire pipeline:

$$\Delta p_{11m}(U_{a\_atm}, K_w) := \Delta p_{11sm}(\rho_{m11}, U_{a\_atm}, K_w) \cdot \frac{m_s \cdot L}{\left( \frac{\pi \cdot D^2}{4} \right) \cdot (1 - \alpha) m(U_{slug2m}(\rho_{m11}(U_{a\_atm}, K_w), U_{a\_atm}, K_w))) \rho_{sch} \cdot U_{slug2m}(\rho_{m11}(U_{a\_atm}, K_w), U_{a\_atm}, K_w)}$$

## 5. Muschelknautz's model

### 1. Definitions

The unknown quantity is the pressure loss  $\Delta P_g$ .

The pressure  $p_9$  at the beginning of the pipeline in relationship to the pressure  $p_2$  at the end of the pipeline is defined as:

$$p_9 = p_{\text{Ende}} \cdot e^{\frac{\mu \cdot g \cdot L \cdot \mu_w}{R \cdot T_0 C(U_a)}}$$

with: R: Gas constant       $T_0$ : Temperature in Kelvin

$$\text{Particle velocity: } U_s(m_s) = \frac{m_s}{A \cdot \rho_s}$$

Ratio of particle velocity to air velocity: C := 0.8

$$\text{Solids ratio: } \mu(U_{a\_atm}) := \frac{m_s}{U_{a\_atm} \cdot A \cdot \rho_a}$$

### 2. Calculations

$$X(U_{a\_atm}) := \frac{\mu_M(U_{a\_atm}) \cdot g \cdot L \cdot \mu_w}{R_a \cdot T_0 \cdot C_0} \quad \text{The term } X(U_{a\_atm}) \text{ should yield a value } < 0.8$$

$$p_9(U_{a\_atm}) := p_{\text{Ende}} \cdot e^{X(U_{a\_atm})}$$

$$\Delta p_9(U_{a\_atm}) := p_9(U_{a\_atm}) - p_{\text{Ende}}$$

# Isabelle Lecreps-Prigge

Geboren am 02.01.1981 in Caen, France



## HOCHSCHULBILDUNG

---

- 2003 **Master in Verfahrenstechnik**  
“Diplôme d’Etude Approfondie” (DEA)  
**Technische Universität Compiègne UTC**, Frankreich
- 2003 **Diplom Ingenieur für Lebensmittelwissenschaft**  
“Diplôme d’Ingenieur en agro-alimentaire”  
**Ecole Polytechnique Universitaire de Lille EPUL**, Frankreich
- 2000 **Diplom in Biologie, Schwerpunkt: Lebensmittelwissenschaft**  
“Diplôme Universitaire de Technologie” (DUT)  
**Technische Universität Caen (IUT)**, Frankreich

## BERUFSERFAHRUNG

---

- Seit 05.2010 **Consulting Engineer im Bereich Schüttguttechnik**  
**TUNRA Bulk Solids Handling Research Associates**  
Newcastle, New South Wales, Australien
- 05.2005 – 12.2009 **Wissenschaftliche Mitarbeiterin am Lehrstuhl für**  
**Verfahrenstechnik disperser Systeme, Prof. Dr.-Ing. Sommer**  
**Technische Universität München**, Deutschland
- Promotionsthema:  
“Physical mechanisms involved in the transport of slugs during horizontal pneumatic conveying”
- Weitere Berufserfahrung:
- 2004 – 2005 *Design und Aufbau einer Filtrationsanlage im Pilot-Maßstab*  
5 Monate **TUM** – Lehrstuhl für Maschinen- und Apparatekunde (Deutschland)
- 2004 *Entwicklung neuer Lebensmittel bestehend aus Lupine-Proteinen*  
3 Monate **Fraunhofer Institut** für Verfahrenstechnik und Verpackung (Deutschland)
- 2003 *Instrumentalanalyse der Textur grüner Erbsen – Anwendung in dem Gefrierverfahren (Diplomarbeit – Industriepartner: Bonduelle)*  
8 Monate **TU Compiègne UTC** – Labor für Verfahrenstechnik (Frankreich)
- 2002 *Erstellung eines Sensoriksystemes*  
4 Monate **GUIOT Sirops**, Sirupfabrik (Frankreich)
- 2002 *Risikoeinschätzung an den Arbeitsplätzen, dem Produktionsband und den Gebäuden - Erstellung einer Datenbank für die Flaschenabfüllung*  
2 Monate **Cidrieres du Calvados** (Frankreich)
- 2002 *Studium des Hygienestatus von Spezialstählen nach Verschmutzung mit Sporen von Bacillus cereus*  
3 Monate **Institut National de la Recherche Agronomique INRA**, Labor für Verfahrenstechnik (Frankreich)
- 2001 Verpackungswerkmeisterin und Produktionsassistentin  
2 Monate **Dupont d’Isigny**, Süßwarenfabrik (Frankreich),
- 2000 *Studie zur Bestimmung von Collagen in Fleischprodukten*  
3 Monate **ADRIA Normandie** (Frankreich)

### SPRACHEN

- Französisch (Muttersprache)
- Deutsch (fließend)
- Englisch (fließend)

### ERGÄNZENDE INFORMATIONEN

Auszeichnung:  
Erster Preis der Region Normandie für den Verdienst junger Frauen in Wissenschaft und Technik (1998)

Persönliche Interessen:  
Piano, New Classics, Reisen, Wandern